

Stress corrosion cracking of steels in industrial process environments

by

Edward Ernest Heaver

submitted in partial fulfilment of the requirements for the degree

Philosophiae Doctor

in

Metallurgy

in the Faculty of Engineering, University of Pretoria

Pretoria

Republic of South Africa

November 1994

STRESS CORROSION CRACKING OF STEELS IN INDUSTRIAL PROCESS ENVIRONMENTS

SYNOPSIS

The interactions between engineering materials and their environment which give rise to stress corrosion cracking are reviewed and industrial examples from the petrochemical industry are described. In one of the examples, cracking took place in carbon steel exposed to pressurised gas containing carbon monoxide, carbon dioxide and water. The crack morphology in this system was studied by metallography of samples from industrial gas processing plants and the crack growth rates were determined using precracked specimens. Constant extension rate tests, U-bend specimens and potentiodynamic studies were used to evaluate alternative materials and inhibitor additions in CO-CO₂-H₂O environments. Electrochemical noise was accessed as a technique to monitor SCC on line.

It was found that the CO-CO₂-H₂O system was characterised by a time dependent adsorption of carbon monoxide at anodic and cathodic sites. The adsorption produced a critical balance between crack tip corrosion rate and the repassivation process comparable to the behaviour at the active-passive transition zone in more conventional systems. The anodic passivation exhibited a breakdown potential near to -400 mV (Ag/AgCl) that defined the zone of SCC susceptibility. Inhibition by CO and hence SCC was virtually independent of CO partial pressure provided there was a sufficient reservoir of CO. The addition of commercial film forming inhibitors did not greatly influence the system and SCC was still observed in CO-CO₂-H₂O environments to which inhibitors had been added. Steels containing alloy additions of more than 9 % chromium were found to be resistant to SCC but austenitic-ferritic weld joints cracked. A low alloy 3½ nickel steel performed well in the constant extension rate tests but was not wholly resistant to SCC.

The morphology of stress corrosion cracks in CO-CO₂-H₂O mixtures was influenced by carbon monoxide partial pressure. More corrosion was observed on the crack walls at low carbon monoxide partial pressure and widened cracks resembling "mesa" corrosion were common. This increased corrosion was probably due to difficulty in maintaining passivity in the crevice formed by the growing crack. Similarly, crevicing in precracked specimens appeared to inhibit SCC and no crack extension was observed. Electrochemical noise proved to be a useful tool for monitoring.

Die interaksies tussen ingenieursmateriale en die omgewing wat aanleiding gee tot spanningskorrosie-kraking word bespreek met spesifieke verwysing na kraking in staal wat aan hoë druk omgewings wat kooldioksied, koolmonoksied en water bevat. Die kraakmorfologie in hierdie sisteem is bestudeer deur middel van metallografie van monsters wat uit industriële prosesse verkry is. Metings van die kraakvoortplantingstempo's is gedoen deur van voorafgekraakte monsters gebruik te maak. Stadige vervormingstempo toetse, U-buigmonsters en potensiodinamiese ondersoek is gebruik om alternatiewe materiale en inhibitore te karakteriseer. Die gebruik van elektrochemiese geruis as 'n moniteringstegniek is onder bedryfstoestande ondersoek.

Daar is gevind dat die CO- CO₂ -H₂O-metaal sisteem gekarakteriseer kan word deur die tydsafhanklike adsorpsie van koolmonoksied by beide anodiese en katodiese gebiede. Die adsorpsie het 'n kritiese balans tussen korrosie en herpassivering by die kraakpunt tot gevolg, soortgelyk aan die aktief-passiewe oorgang in meer konvensionele sisteme. Die anodiese passivering word afgebreek by potensiale meer positief as -400 mV (Ag/AgCl) waar SKK ook dan plaasvind. Inhibering deur die CO was reeds by lae parsiele druk is dus nie prakties nie. Inhibering deur kommersiële filmvormende inhibeerders was nie voldoende om SKK te voorkom nie. Stale met 'n chroominhoud van meer as 9% was bestand teen SKK, maar sweise met autenitiese vullermateriale was wel vatbaar vir kraking. 'n Lae legering 3,5% nikkelstaal het goed presteer in die stadige vervormingstempotoetse, maar was nie volkome bestand teen SKK nie.

Die morfologie van die spanningskorrosie krake in die CO-CO₂-H₂O mengsels was afhanklik van die parsiele druk van koolmonoksied. By lae parsiele drukke was korrosie meer algemeen en het kraakverwyding algemeen voorgekom. Die verhoogde korrosie by die kraakpunt was waarskynlik te wyte aan die probleem van die koolmonoksied om die kraakpunt te bereik en te passiveer. Die verhoogde korrosie in gleuwe was waarskynlik ook die rede waarom kraakvoortplanting nie in die voorafgekraakte monsters voorgekom het nie. Elektrochemiese geruis is 'n nuttige metode om SKK in hierdie sisteem te moniteer.

ACKNOWLEDGEMENTS

The author would like to thank Professor Sandenbergh for his guidance and support during the project and the University of Pretoria for use of their facilities. The assistance of M Tullmin and C Boothroyd at the CSIR, together with that JH Swanepoel is also gratefully acknowledged.

STRESS CORROSION CRACKING OF STEELS IN INDUSTRIAL PROCESS ENVIRONMENTS

TABLE OF CONTENTS

	PAGE
1 INTRODUCTION	1
2 CONTROLLING PARAMETERS AND CHARACTERISTICS OF STRESS CORROSION CRACKING	5
3 MECHANISMS	6
3.1 NATURE OF MATERIALS, CORROSION AND STRESS CORROSION	6
3.2 SCC MECHANISMS UNRAVELLED	10
3.2.1 Pre-existing Active Paths	11
3.2.2 Strain Generated Active Paths	12
3.2.3 Film Rupture	15
3.2.4 Stress-sorption	21
3.2.5 Hydrogen Embrittlement	23
4 TEST METHODS	25
4.1 SMOOTH SPECIMENS	25
4.1.1 Constant Strain	25
4.1.2 Constant Load	26
4.1.3 Slow Strain Rate Tests	26
4.2 PRE-CRACKED SPECIMENS	29
4.3 STANDARD SCC TEST PROCEDURES	32
5 ELECTROCHEMICAL MEASUREMENTS	32
5.1 POTENTIAL MEASUREMENTS	32
5.2 POTENTIODYNAMIC SCANS	33
5.3 FILM DISRUPTION - CURRENT DECAY	33
5.4 ELECTROCHEMICAL NOISE ANALYSIS	34
6 EXAMPLES OF SCC IN MODERN CHEMICAL PLANT	35
6.1 CHLORIDE SCC	36
6.2 POLYTHIONIC SCC	37
6.3 SULPHIDE STRESS CORROSION CRACKING	37
6.4 CAUSTIC SCC	39
6.5 SCC OF BRASS AIR COOLER AND STEAM CONDENSER TUBING	39
	PAGE

6.6	SCC DURING THE	HYDROUS AMMONIA	41
6.6.1	Material		41
6.6.2	Tensile Strength		41
6.6.3	Environment		41
6.6.4	Construction and Inspection of Spheres and Tanks for Storage of Ammonia		43
6.7	HYDROFLUORIC ACID SCC		44
6.8	AMINE SCC		45
6.9	SCC IN COAL GAS LIQUID		46
6.10	SCC IN WET MIXTURES OF CARBON MONOXIDE AND CARBON DIOXIDE		46
6.10.1	General Corrosion in Wet Carbon Dioxide		54
6.10.2	General Corrosion in Carbon Monoxide		56
7	STUDY OF CO-CO₂ SCC AND ITS PREVENTION IN CO-CO₂ GAS MIXTURES		58
8	CHARACTERISATION OF CRACK MORPHOLOGY		62
8.1	LOW PRESSURE LEAN GAS - OPERATING PLANT (PCO 45 kPa PCO ₂ 225 kPa)		62
8.1.1	Compression Gas Line		62
8.1.2	Drum - Operating Plant		64
8.2	LEAN GAS SYSTEM - PILOT PLANT		64
8.3	HIGH PRESSURE LEAN GAS		65
8.4	RICH GAS		65
8.5	MICROHARDNESS TESTING		66
8.6	SUMMARY OF METALLOGRAPHIC RESULTS		66
9	EVALUATION OF STRESS CORROSION CRACK GROWTH RATES FOR CARBON STEEL IN A WET CO/CO₂ ENVIRONMENT		79
9.1	GENERAL DESCRIPTION		79
9.2	APPARATUS		79
9.2.1	Laboratory Tests		79
9.2.2	Plant Bypass Facility		83
9.3	SPECIMEN DESIGN		83
9.4	ELECTROCHEMICAL MONITORING - POTENTIAL NOISE		90
9.5	AUTOCLAVE STARTUP PROCEDURE		90
9.6	BYPASS STARTUP PROCEDURE		91

9.7	RESULTS OF LABORATORY TESTS	92
9.7.1	1000-Hour Interrupted Test in Low Pressure Lean Gas (PCO 40, PCO ₂ 270)	92
9.7.2	1000-Hour Continuous Test - Low Pressure Lean Gas (PCO 40, PCO 270)	94
9.7.3	1000-Hour Continuous Test - Low Pressure Lean Gas, Upper Bound CO Concentration (PCO 80, PCO ₂ 260)	95
9.7.4	1000 Hour Continuous Test in Rich Gas (PCO 210, PCO ₂ 250)	97
10	EVALUATION OF INHIBITOR ADDITIONS TO CO-CO₂-H₂O SYSTEMS USING CERT	101
10.1	EXPERIMENTAL PROCEDURE	101
10.1.1	General	101
10.1.2	Test Chamber	101
10.1.3	Test Procedure	103
10.1.4	Inhibitors	104
10.2	RESULTS	105
10.2.1	CERT - Rich Gas (PCO 210 PCO ₂ 230)	105
10.2.2	CERT Rich gas (PCO 210, PCO ₂ 230) and Additions of Inhibitor	105
10.2.3	CERT Lean Gas (PCO 34 PCO ₂ 266)	106
10.2.4	CERT Lean Gas (PCO 34 PCO ₂ 266) plus Inhibitors	107
11	EVALUATION OF ALTERNATIVE MATERIALS	117
11.1	MATERIALS SELECTION	117
11.2	PLANT BYPASS	119
11.3	U-BEND SPECIMEN PREPARATION	119
11.4	CERT SPECIMEN PREPARATION	120
11.5	RESULTS	120
11.5.1	Results of U-bend Tests	120
11.5.2	Results of CERT	122
12	ASSESSMENT OF THE PERFORMANCE OF POST WELD HEAT TREATED CARBON STEEL IN WET CO-CO₂ GAS MIXTURES	125
12.1	PERFORMANCE OF POST WELD HEAT TREATED PRESSURE VESSELS	125
12.2	PERFORMANCE OF PIPING	126
12.2.1	HP Lean Gas Piping	126
12.2.2	LP Lean Gas Piping	126
12.2.3	Rich Gas	126
12.2.4	Summary of Results	127

13	POTENTIODYNAMIC POLARISATION	130
	13.1 EXPERIMENTAL METHOD	130
	13.2 RESULTS	131
	13.2.1 Carbon Manganese Steel in Rich Gas	131
	13.2.2 Carbon Steel in Lean Gas	132
	13.2.3 Effect of Temperature	132
	13.2.4 3½ Ni Steel In Rich Gas	132
	13.2.5 9Cr-1Mo Steel in Rich Gas	133
	13.2.6 Rich Gas Plus Inhibitors	133
	13.2.7 Effect of Oxygen	134
	13.2.8 Movement of Corrosion Potential after Holding Above the Anodic film Breakdown Potential	134
14	USE OF ELECTROCHEMICAL NOISE MONITORING IN CO-CO₂-H₂O SYSTEMS	148
	14.1 APPLICATION OF ELECTROCHEMICAL NOISE MONITORING TO CO-CO ₂ - H ₂ O SYSTEMS	148
	14.2 ELECTROCHEMICAL NOISE MONITORING SYSTEM	149
	14.3 PROBE DESIGN	151
	14.4 TEST ENVIRONMENTS	153
	14.4.1 Laboratory Tests	153
	14.4.2 Plant Monitoring	153
	14.5 RESULTS	153
	14.5.1 Laboratory Tests	153
	14.5.2 Plant Tests	154
15	DISCUSSION	161
	15.1 CHARACTERISATION OF CRACK MORPHOLOGY	161
	15.2 DETERMINATION OF STRESS CORROSION CRACK GROWTH RATES IN CO-CO ₂ -H ₂ O SYSTEMS USING PRECRACKED SPECIMENS (DCB)	162
	15.3 EVALUATION OF INHIBITOR ADDITIONS TO CO-CO ₂ -H ₂ O SYSTEMS USING CONSTANT EXTENSION RATE TESTS	165
	15.3.1 CERT Without Inhibitor Additions	165
	15.3.2 CERT With Inhibitor Additions	166
	15.4 EVALUATION OF ALTERNATIVE MATERIALS	168
	15.4.1 U-bend Tests	168
	15.4.2 CERT	168
	15.5 POST WELD HEAT TREATED CARBON STEELS	169
	15.6 POTENTIODYNAMIC POLARISATION	170
	15.7 CORROSION MONITORING USING ELECTROCHEMICAL NOISE	173
	15.8 SUMMARY OF SCC IN THE CO-CO ₂ -H ₂ O SYSTEM	174
16	CONCLUSIONS	175

STRESS CORROSION CRACKING OF STEELS IN INDUSTRIAL PROCESS ENVIRONMENTS

1 INTRODUCTION

The intention of proper engineering design and subsequent inspection of fabricated equipment is to ensure reliability in service and in the extreme case guard against sudden unexpected failure. At its most basic, fracture mechanics indicates that final fracture is controlled by applied stress and the geometry of a flaw in the material. Any mechanism therefore that allows the growth of a flaw during normal operation will represent a threat to the integrity of equipment. Fatigue and stress corrosion cracking (SCC) are such mechanisms. The latter, which is the subject of this review, has been long recognised by engineers leading to the text book definition, "stress corrosion cracking is a non-ductile fracture resulting from the simultaneous application of a tensile stress and a specific corrodent" to which might be added, "causing the material to fail at a much lower stress than by the application of stress alone". It is helpful to return to the earlier mentioned fracture mechanics to discover what really happens. The influence of a specific environment on the material allows a "flaw", in this case a crack, to nucleate and grow at stresses below those required by mechanical means alone. The crack continues to grow by stress corrosion until the combination of geometry and applied stress result in purely mechanical failure which may be plastic or brittle depending on the material properties and the nature of the stress.

Since, in general, engineers learn by their mistakes, the level of understanding of a particular phenomenon can be roughly gauged by surveying causes of industrial failures. This has been done in Germany, the United Kingdom and South Africa.⁽¹⁾ Table 1 shows the results.

TABLE 1 CAUSES OF INDUSTRIAL FAILURES IN S.A., GERMANY AND U.K. (AFTER TÜV RHEINLAND)

TYPE OF FAILURE	% OCCURRENCE			
	RSA	GERMANY		UK
		Mixed Process	Petro-Chemical	
Corrosion	29	35	25	54
Fatigue	25	18	22	20
Brittle fracture	16	8	5	6
Overload	11	5	5	5
High temperature corrosion	7	-	-	-
Stress corrosion/Corrosion fatigue/ Hydrogen embrittlement	6	20	28	-
Creep	3	12	14	12
Wear, Abrasion and Erosion	3	2	7	2

Although the UK analysis includes stress corrosion and hydrogen embrittlement in the total corrosion figure it can be concluded that a large number of industrial failures, particularly in the petrochemical process industry are due to stress corrosion. The low figure reported for RSA is probably due to a proportionally lower percentage of sophisticated process plant. Also SCC failures are not always recognised.

Why then, if the phenomena is long known, do failures still occur? For the answer to this it is necessary to look at the ever-growing list of environment-material combinations causing SCC of which the engineer must be aware, (Figure 1) ⁽²⁾; at the diversity of mechanisms proposed for SCC; at the large number of parameters that control cracking and last, but not least, at methods of evaluating the resistance of materials to SCC. This document attempts to do this by reviewing SCC mechanisms, controlling parameters, and test methods and by recounting observed instances of SCC in industrial process environments with particular emphasis on less well-known cracking of carbon steel in wet mixtures of carbon monoxide and carbon dioxide gas.

FIGURE 1 MEDIA CAUSING STRESS CORROSION CRACKING (After Nace)



FERROUS ALLOYS			AUSTENITIC STAINLESS STEELS				Martensitic Stainless 405-410	COPPER BASE ALLOYS			
CAST IRON			Mild Steel	302, 304 321, 347	316, 317	ACI CN-20 20Cr-30Ni		Copper 85-99,9	Brass 70-80 Cu + Zn, Sn or Pb	Brass 59-93 Cu + Al, Zn or As	Cupro-Nickel 66-68 11-33
Grey	Nickel	Silicon									

1 2 3 4 5 6 7 8 9 10 11 12

NICKEL BASE ALLOYS						MISCELLANEOUS METALS AND ALLOYS							
Nickel 99	Ni-Cu 66-32	Ni-Cr-Fe 76-16-7	Ni-Fe-Cr 32-47-20	Ni-Mo 62-28 +Fe, V	Ni-Cr-Mo 54-15-16 +Fe, W	Alumi- nium	Gold	Lead	Plati- num	Silver	Tanta- lum	Tita- nium	Zirco- nium

13 14 15 16 17 18 19 20 21 22 23 24 25 26

CORROSIVE	1	2	4	5	6	7	8	9	10	11	12	13	14	15	16	17	18	19	20	21	25	26
ACETIC ACID - MERCURY SALTS				X			X	X	X								X					
ALKYL ARYL SUPHONATES				X																		
ALUMINIUM CHLORIDE				X	X																	
ALUMINIUM SULPHATE				X																		
AMMONIA				X					X	X												
AMMONIUM BIPHOSPHATE				X	X																	
AMMONIUM CHLORIDE				X	X																	
AMMONIUM FLUOSILICATE				X								X										
AMMONIUM HYDROXIDE				X				X	X	X												
AMMONIUM NITRATE				X																		
ANILINE				X						X												
BARIUM CHLORIDE				X	X																	
BARIUM NITRATE				X																		
BISMUTH				X				X												X		
CALCIUM BROMIDE				X	X																	
CALCIUM CHLORIDE				X		X																
CALCIUM NITRATE				X																		
CARBON TETRACHLORIDE				X	X																	
CHLORINE				X	X																	
CHLORANILINES				X						X												
CHLOROBENZENE				X								X										
CHLOROFORM				X	X																	
CHLOROTOLUIDINES				X						X												
CHROMIC ACID				X						X			X									
COPPER TETRAMINE				X						X												
CRESOL				X																		
CRESYLIC ACID VAPOURS				X																		
CYANOGEN				X																		
DICHLOROPHENOL				X	X																	
EPICHLORHYDRIN				X	X																	
ETANOL				X																		X
ETHYLAMINE				X																		
ETHYL CHLORIDE				X	X					X												X
FERRIC CHLORIDE				X																		
FERROUS CHLORIDE				X	X																	
FLUOSILICIC ACID				X								X	X				X	X				
GASOLINE VAPOUR				X																		
GLUTAMIC ACID				X	X																	
GLYCEROL				X																		
HEXACHLOROETHANE				X	X																	
HYDROCHLORIC ACID (AERATED)				X		X														X		
HYDROCYANIC ACID + HYDROGEN CYANIDE				X		X																
HYDROFLUORIC ACID VAPOURS				X								X										
HYDROFLUORIC ACID (AERATED)				X								X	X	X								
HYDROFLUORIC ACID (NO AIR)				X					X	X		X	X	X								
HYDROGEN				X																		
HYDROGEN CHLORIDE				X	X																	
HYDROGEN SULPHIDE (WET)				X																X		
LEAD ACETATE				X																	X	
LEAD BROMIDE				X																		
LEVULINIC ACID				X	X																	
LITHIUM				X					X	X												
LITHIUM CHLORIDE				X	X				X	X												
MAGNESIUM CHLORIDE				X	X	X	X		X	X			X									
MAGNESIUM CHLORIDE + CALCIUM CHLORIDE				X					X													

FIGURE 1 MEDIA CAUSING STRESS CORROSION CRACKING (After Nace)



FERROUS ALLOYS			AUSTENITIC STAINLESS STEELS					Martensitic Stainless 405-410	COPPER BASE ALLOYS						
CAST IRON			Mild Steel	302, 304 321, 347	316, 317	ACI CN-20 20Cr-30Ni	Copper 85-99.9		Brass 70-80 Cu + Zn, Sn or Pb	Brass 59-93 Cu + Al, Zn or As	Cupro-Nickel 66-68 : 11-33				
Grey	Nickel	Silicon													
1	2	3	4	5	6	7	8	9	10	11	12				
NICKEL BASE ALLOYS						MISCELLANEOUS METALS AND ALLOYS									
Nickel 99	Ni-Cu 66-32	Ni-Cr-Fe 76-16-7	Ni-Fe-Cr 32-47-20	Ni-Mo 62-28 +Fe, V	Ni-Cr-Mo 54-15-16 +Fe, W	Alumi- nium	Gold	Lead	Plati- num	Silver	Tanta- lum	Tita- nium	Zirco- nium		
13	14	15	16	17	18	19	20	21	22	23	24	25	26		

CORROSIVE	1	2	4	5	6	7	8	9	10	11	12	13	14	15	16	17	18	19	20	21	25	26	
MAGNESIUM FLUOSILICATE												X	X				X	X					
MAGNESIUM SULPHATE																							
MANGANESE CHLORIDE				X	X																		
MERCURIC CHLORIDE				X	X			X	X	X	X		X							X			
MERCURIC CYANIDE													X										
MERCURIC NITRATE													X										
MERCUROUS NITRATE				X				X	X	X			X										
MERCURY				X					X	X		X	X	X						X			
METHALLYLAMINE										X													X
METHANOL																							
MONOETHANOLAMINE				X																			
NAPHTHA FEEDSTOCK					X																		
NAPHTHENIC ACIDS					X																		
NICKEL CHLORIDE					X																		
NICKEL NITRATE					X																		
NITRIC ACID				X						X													
PENTACHLOROETHANE					X	X																	X
PERCHLOROETHYLENE																							
PHOSPHORIC ACID					X																		
PHOSPHORIC ACID (AERATED)					X																		
POLYTHIONIC ACID					X																		
POTASSIUM CARBONATE				X																			
POTASSIUM CHLORIDE					X	X			X	X	X												
POTASSIUM CHROMATE										X													
POTASSIUM HYDROXIDE				X	X	X							X										
POTASSIUM PERMANGANATE										X										X			
SILVER NITRATE				X																			
SODIUM ALUMINATE				X																			
SODIUM BISULPHATE					X	X																	
SODIUM BISULPHITE					X	X																	
SODIUM CARBONATE					X	X																	X
SODIUM CHLORIDE					X	X																	
SODIUM FLUORIDE					X	X																	
SODIUM HYDROXIDE	X	X	X	X	X	X	X					X	X	X					X				
SODIUM NITRATE					X							X	X										
SODIUM PHOSPHATE (TRIBASIC)					X	X																	
SODIUM SULPHATE					X																		
SODIUM SULPHIDE																			X				
STEAM																			X				
STEAM, GEOTHERMAL (AERATED)					X	X																	
STRONTIUM NITRATE				X																			
SULPHATE LIQUOR				X	X																		
SULPHONATED OIL																							
SULPHUR												X											
SULPHURIC ACID				X																			
SULPHURIC ACID + CHLORINE					X	X																	
SULPHUROUS ACID						X																	
TOLUENE									X	X													
TRIETHANOLAMINE										X													
TRIMETHYLAMINE									X														
URANYL SULPHATE																							X
WATER + HYDROGEN SULPHIDE + LIGHT HYDROCARBONS						X																	
ZINC CHLORIDE					X	X																	
ZINC FLUOROSILICATE													X										

CONTROLLING PARAMETERS AND CHARACTERISTICS OF STRESS CORROSION CRACKING

Stress corrosion cracking is specific to material-environment combinations. Cracks form at multiple initiation sites, normal to the principal stress. The cracks are multibranching and propagate intergranularly, transgranularly or both, depending on the system and prevailing conditions. Crack propagation occurs without significant plastic deformation. The development of a stress corrosion crack involves an initiation period which may be extremely long, followed by a period of crack growth which is relatively short. The SCC growth behaviour of many material/environment combinations is characterised by a threshold and stage 1, 2 and 3 growth (Figure 2). The threshold stress is the stress or stress intensity below which no significant crack growth can be detected. Stage 1 growth has a marked dependence on stress intensity. In this region a small increase in stress intensity results in a rapid increase in crack growth. Stage 2 growth or plateau velocity is by and large independent of stress intensity, with crack growth controlled by crack tip corrosion mechanisms. At the third region purely mechanical fracture mechanisms prevail and failure is imminent.

Stress corrosion cracking requires the simultaneous presence of a susceptible material, stress and a corrosive environment. The removal of any one of these will prevent cracking. The susceptibility of a material is influenced by microstructure, yield strength, strain hardening exponent, composition and localised micro-chemistry. The stress component can be applied or residual. High stress favours SCC. Stress intensity and strain rate are principal controlling parameters. Important environmental parameters that control SCC include transport to the crack tip, oxidising potential, pH, composition and temperature.

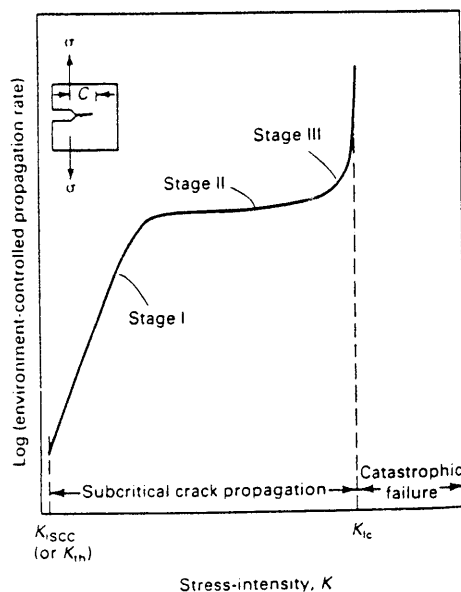


FIGURE 2 Stages of stress corrosion crack growth.

3
MECHANISMS
3.1
NATURE OF MATERIALS, CORROSION AND STRESS CORROSION

Before embarking on a review of SCC mechanisms it is necessary to describe something about the nature of engineering materials.

In the petrochemical process industry the term "materials" most usually refers to metal alloys. Table 2 gives the usage of common metals in petrochemical plant.⁽³⁾

TABLE 2 USAGE OF COMMON METALS IN PETROCHEMICAL PLANT

EQUIPMENT	MATERIALS
Pressure vessels, tanks, structures and heat exchangers	Mostly ferrous alloys comprising of carbon and low alloy steels and stainless steels
Heat exchangers, electrical equipment	Titanium, copper and ferrous alloys
Low temperature equipment	Aluminium alloys and ferrous alloys
Equipment requiring corrosion resistance	Ferrous alloys, nickel alloys and titanium alloys

Any metal alloy consists of an agglomeration of crystals or grains that can be resolved microscopically. Each grain consists of a near perfect array of atoms arranged in a lattice. The most prevalent atomic arrangements found in metals are body centred cubic (BCC), face centred cubic (FCC) and close packed hexagonal (CPH). Table 3 gives the crystal structure of common metals.

TABLE 3 CRYSTAL STRUCTURE OF COMMON METALS

CRYSTAL STRUCTURE	METALS
FCC	Gold, aluminium, silver, beta-cobalt, copper, nickel, gamma-iron (austenite)
BCC	Chromium, alpha-iron (ferrite), molybdenum
CPH	Magnesium, zinc, alpha-titanium and alpha-cobalt

A metal crystal always contains planar defects in the lattice called dislocations. Under tension the movement of dislocations develops dislocation arrays within individual crystals and ultimately steps in the metal surface due to emergent slip planes.⁽⁴⁾

The nature of metal alloys and their deformation mechanisms contribute to SCC by ensuring the presence of localised inhomogeneities in the surface exposed to the environment. Firstly, the agglomeration of crystals in an alloy is not uniform, with differences existing between the grains themselves and between the grains and grain boundaries. Secondly, deformation mechanisms give rise to a sub-atomic imbalance by causing local accumulations of dislocation networks and by disruption of the surface protective films by emergent slip planes. Inhomogeneities due to constitution of the material or resulting from its deformation are potential sites for accelerated localised corrosion which is in most cases a prerequisite for stress corrosion cracking.

To understand how localised corrosion comes about from small differences in the material it is necessary to briefly examine the fundamentals of corrosion. Aqueous corrosion of metals is almost always electrochemical.⁽⁵⁾ Electrochemical reactions are represented as a cell consisting of coupled oxidation and reduction reactions. The reactions are simultaneous and balanced. Oxidation is the removal of electrons from an atom or group of atoms and occurs by definition at the anode ($M \rightarrow M^{2+} + 2e^{-}$). Reduction is the addition of electrons and occurs at the cathode ($M^{2+} + 2e^{-} \rightarrow M$). The electrochemical cell is analogous to a short circuited battery. The movement of electrons and proximity of the oxidation-reduction reactions to the metal/electrolyte interface cause the electrode surface to be charged relative to the electrolyte at a specific electrode potential characteristic of the metal/electrolyte system. The charged interface in turn imposes a narrow electric field extending into the solution with the result that the dipolar water molecules align themselves in the electric field. Similarly, solvated ions align themselves adjacent to the surface layer of water to form a second plane of charge. The electronic double layer at a metal aqueous interface provides an energy barrier that must be overcome for corrosion to proceed (activation polarisation). It follows that microscopic differences or sub-atomic irregularities in the electrode surface will alter the activation polarisation making corrosion easier at some sites than others.

Anodic and cathodic sites occur simultaneously on the same piece of metal and corrosion rate can be gauged by the current flowing according to the equation

$$i_{\text{corr}} t = \frac{nFw}{M}$$

where

- i_{corr} = measured in amperes
- t = time in seconds
- nF = number of coulombs to oxidise 1 mol of metal
- n = number of electrons involved in the reaction
- F = Faraday's constant
- M = molecular weight of the metal in grammes
- w = mass of corroded metal.

The anodic and cathodic currents must be equal; however the area of anodic and cathodic sites may be quite different. If the anodic area is small relative to the cathode then corrosion is focused at a localised site. In a smooth homogeneous material anodic and cathodic sites are separated by only a few nanometers and move around so that the effect of disproportionate electrode areas is equalised. However if the material is inhomogeneous then the anode site can become fixed, at for instance grain boundaries, specific alloy phases, emergent slip planes or dislocation networks. When this happens rapid metal loss occurs at a very localised site. If a tensile stress exists, the flaw caused by corrosion will be an area of stress concentration that in turn encourages further corrosion and so the process becomes autocatalytic culminating in a stress corrosion crack. This is a simplification of what happens but is a reasonable summation of how the interaction between stress and corrosion is able to generate a crack.

The story however is not complete without some mention of passivity and hydrogen. The role of passivity in SCC was hinted at earlier when emergent slip planes were described breaking a passive surface film. Aqueous corrosion is a coupled electrochemical reaction consisting of anodic and cathodic constituents. Anything that retards either of these will retard the overall corrosion rate which will then be either anodically or cathodically controlled depending on which reaction is the slowest. Metal dissolution occurs at the anode. If metal dissolution product is allowed to build up at the surface, supersaturation can occur leading to film formation by precipitation of oxides or hydroxides. If a standard polarisation curve is drawn for potential and log of current a point is reached where the current falls and a region follows where current is independent of potential (Figure 3). The metal is then said to be passivated.

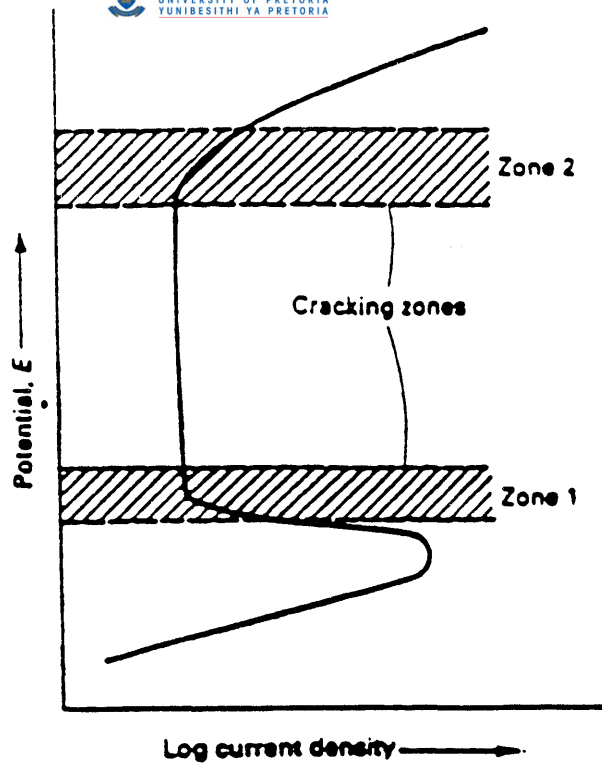


FIGURE 3 POTENTIOKINETIC POLARIZATION CURVE AND ELECTRODE POTENTIAL VALUES at which stress corrosion cracking occurs (After ASM Handbook⁵)

It is characterised by low corrosion and behaviour akin to the more noble metals. The film that gives rise to passive behaviour can be extremely thin and tenacious as in 300 series stainless steels and aluminium alloys or it can be thicker and less resistant as in steels. Most engineering alloys owe their corrosion resistance to film formation. The passive film behaviour is also important in stress corrosion. A rupture in the film will result in localised corrosion (and/or possibly SCC) at the rupture site until the film is satisfactorily repaired. Film thickness, speed of repair and ease of rupture are therefore all important parameters that contribute to the corrosion behaviour.

The embrittling effect of hydrogen on materials and steels in particular has been, like SCC, also known for many years. Hydrogen also has a significant role in stress corrosion but here a reader encounters an overlap of terminology. Atomic hydrogen due to its small size is able to enter and diffuse through the well ordered metal lattice where its interference with certain deformation processes manifests as embrittlement and cracking can result. The crack mechanism is termed hydrogen embrittlement.

The source of atomic hydrogen may be from hydrogen in the operating environment due to physical dissociation of the hydrogen molecule ($H_2 \rightleftharpoons 2H$). Hydrogen may be infused into a metal during electroplating or during welding as a result of the thermally activated decomposition of surface moisture or hydrocarbon contamination. Hydrogen can also be charged into a metal during corrosion which is where SCC comes in and the problem of terminology arises. Cracking where hydrogen is observed to be the culprit is, as earlier stated, referred to as hydrogen embrittlement.

However if the source of hydrogen is corrosion then the resulting cracks are often called stress corrosion cracks. Since hydrogen-induced damage originates from the cathodic reaction ($2H^+ + 2e^- \rightleftharpoons 2H$) it is sometimes described as cathodic SCC as opposed to other "anodic" SCC mechanisms involving dissolution of metal at the crack tip.

Unfortunately the confusion does not end here as some types of SCC undoubtedly progress by anodic dissolution at the crack tip assisted by the embrittling effect of hydrogen generated from the cathodic reaction. Stress corrosion, then, although at first a seemingly simple term describing the combined effect of stress and corrosion does in fact describe a multitude of mechanisms by which a stressed metal, singularly or collectively interacts with its environment to produce a premature failure.

3.2 SCC MECHANISMS UNRAVELLED

The most widely accepted mechanisms for stress corrosion cracking are summarised in Table 4, together with examples of environment-metal combinations to which they mostly closely apply. More often than not the characteristics of a stress corroding system can be explained by more than one of the mechanisms in Table 4 or by a combination of some of them. Stress corrosion of stainless steel in chloride solutions is an example. It may be explained in terms of strain generated active paths or by film rupture while some workers postulate an additional influence of hydrogen.⁽⁶⁾ As this can be very confusing it is easier to examine the mechanisms listed in Table 4 separately.

TABLE 4 ACCEPTED SCC MECHANISMS (After Parkins⁽¹⁸⁾)

PRE-EXISTING ACTIVE PATHS	STRAIN GENERATED ACTIVE PATHS	FILM RUPTURE	STRESS SORPTION	HYDROGEN EMBRITTLE-MENT
Weld decay in SS	Brass in NH_4^+	MgAl in CrO_4^-	Brass in Hg	Carbon steel in wet H_2S
Polythionic acid SCC in SS	Austenitic stainless steel in chloride	Titanium in CH_3OH	Liquid metal embrittlement	High strength steel in water
Carbon steel in NO_3		Carbon steel in wet CO/CO_2 Austenitic stainless steel in chlorides		
Al-Zn-Mg alloys in Cl^-				
Usually intergranular	Intergranular or transgranular, depending on stacking fault energy	Usually transgranular	Usually intergranular	Intergranular or transgranular

3.2.1 Pre-existing Active Paths

The agglomeration of crystals that make up a metal or alloy is not uniform and major differences in microstructure and composition can be found within most engineering materials. Since composition and microstructure influence corrosion behaviour it follows that parts of the material may corrode differently to others and that paths for selective attack by a corrosive agent may arise out of pre-existing inhomogeneity in the material. This form of corrosion due to pre-existing active paths is most often the result of differences between the metal grain and its grain boundary. If the constitution of the grain boundary causes it to be anodic to the grain, the anodic site will be fixed at the grain boundary causing it to be consumed preferentially to the grain. The (anodic) grain boundary is small in comparison to the (cathodic) grain, so a high current density is generated which leads to rapid local dissolution following active paths at the grain boundary. The end result is intergranular corrosion. Grain boundary precipitates and grain boundary segregation are the principal origins of grain boundary active paths.

Examples can be found in the intergranular corrosion of sensitised stainless steels following carbide precipitation and segregation of phosphorous leading to intergranular SCC of carbon steels in nitrate solutions^(7,8). Active paths may also arise from differences in the constitution of the grains themselves, causing one phase to be corroded preferentially. Examples are the selective attack of ferrite in 300 series stainless steel weldments exposed to urea and the selective attack of the lead rich phase in solder by hydrogen sulphide.

Corrosion along pre-existing active paths is able to occur without stress. However stress will often focus the penetration of active path corrosion, forcing it through the cross-section of the material normal to the axis of the principal stress. When this happens the result is stress corrosion cracking. It cannot however be presumed that SCC will always follow from the application of stress to a system that favours active path corrosion. Much depends on the electrochemistry at the base of the penetration formed by selective attack along an active path. The ratio of the corrosion current from the walls relative to the tip must be substantially less than 1 otherwise the penetration (crack) will blunt or the solution will saturate at the crack tip preventing further dissolution of the corroding metal into the electrolyte.

3.2.2 Strain Generated Active Paths

Metal and alloy crystals contain planar defects in the lattice called dislocations. Under tension the movement of dislocations and their subsequent interaction forms arrays within individual crystals. The dislocation arrays show some dependence on the stacking fault energy (SFE) of the material. In high SFE materials the tendency is toward cellular arrangements of dislocations. In low SFE materials, dislocations pile up on stacking faults giving rise to a planar pattern.

Anodic sites are fixed at areas of high dislocation density causing them to be consumed preferentially. The anodic activity of dislocation tangles is enhanced by the tendency of impurities to segregate there, and localised corrosion is exacerbated.

If the dislocation arrangement is cellular then the tendency is for intergranular penetration compared to transgranular attack if the dislocation piles are planar. Crack advance is by preferential dissolution at areas of high dislocation density generated by the accommodation of strain⁽⁹⁾. Additionally, slip step height is increased by a low stacking fault energy such that more anodic dissolution is possible at film ruptures caused by emerging slip. The result is an increased sensitivity to SCC.

There is a strong correlation between anodic current density measured during dynamic strain and crack susceptibility, but the currents measured are insufficient to explain SCC by dissolution alone. Consequently the SCC model for preferential dissolution of metal at areas of high dislocation density has been refined. It has also been modified to explain certain aspects of transgranular stress corrosion cracking (TGSCC). For instance preferential dissolution does not explain discontinuous cracking frequently observed during TGSCC ⁽¹⁰⁾, neither does it explain the observations that TGSCC fracture surfaces are flat, crystallographically orientated and show very little evidence of metal dissolution during crack advance. Several models describing SCC propagation by dissolution plus mechanical fracture have been developed to explain many of these observations. Corrosion tunnelling is the most widely accepted.^(11,12) Swann and Embury proposed that an array of corrosion tunnels is formed by preferential dissolution at emergent slip planes. The tunnels grow in length and diameter until the remaining ligaments fail mechanically (Figure 4).⁽¹³⁾ The process is then repeated so that crack propagation is by alternate dissolution (tunnel growth) and mechanical fracture (failure of remaining ligaments). In order to explain fractographic observations, it was later proposed that the morphology of corrosion tunnels is modified by the application of stress which causes flat slots to form rather than tunnels (Figure 4).⁽¹³⁾ The slots result from preferential dissolution along the high dislocation density plane created by planar slip.

Preferential dissolution in association with planar slip accounts for many features of TGSCC but suffers from fractographic observations that TGSCC is not generally located on the slip planes. Kaufman and Fink⁽¹⁴⁾ proposed that anodic dissolution is able to localise plastic strain leading to very localised ductile fractures that appear macroscopically brittle. They propose that TGSCC occurs by the following steps :

- 1) Anodic dissolution occurs preferentially along slip bands.
- 2) Preferential dissolution causes stress to be concentrated locally leading to increased dislocation density in these regions.
- 3) Following enhanced dislocation activity, the rate of anodic dissolution is accelerated locally resulting in a further increase in stress.

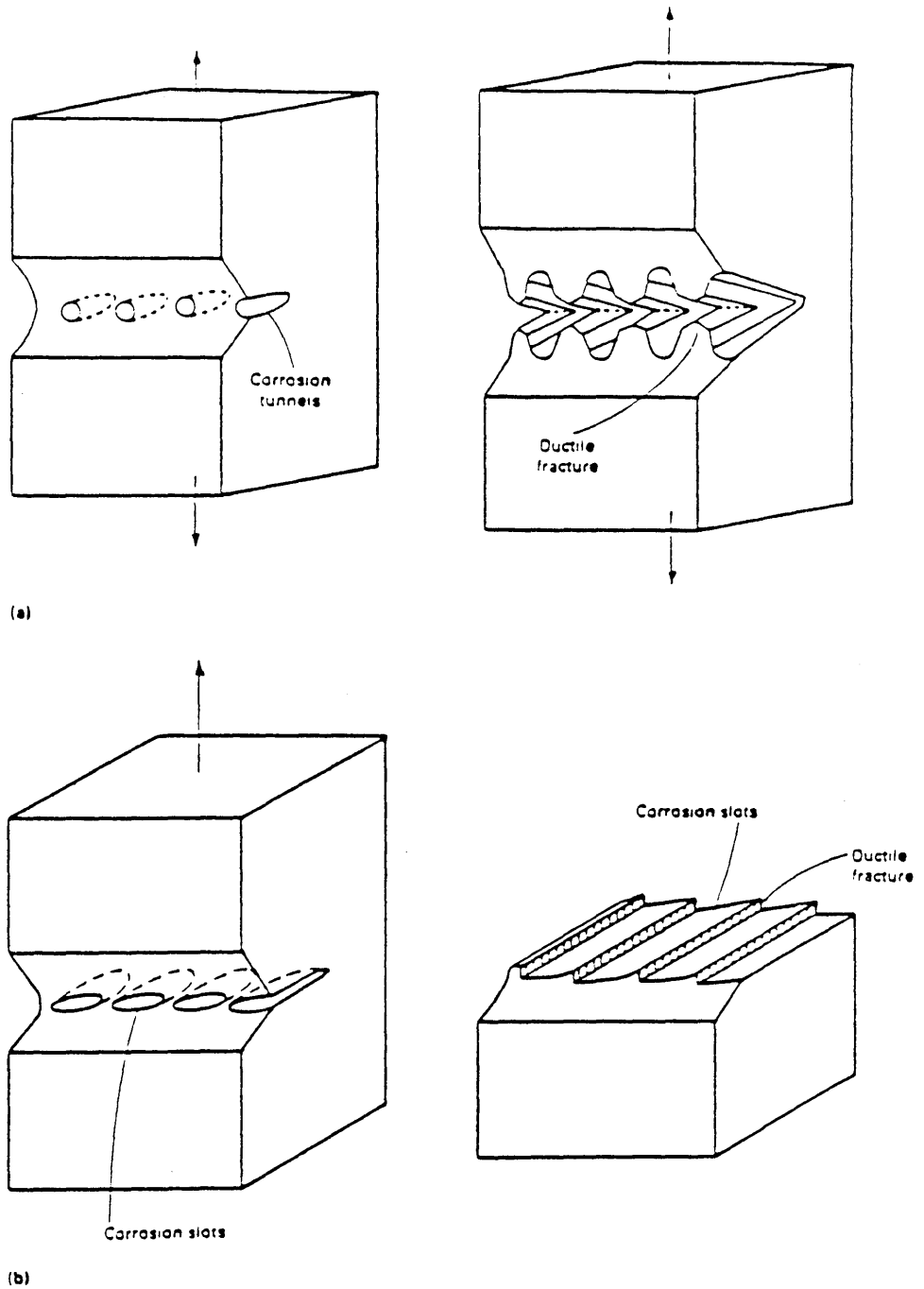


FIGURE 4 CORROSION TUNNEL MODELS (After Silcock and Swann ⁽¹³⁾)

- (a) Schematic of tunnel model showing the initiation of a crack by the formation of corrosion tunnels at slip steps and ductile deformation and fracture of the remaining ligaments.
- (b) Schematic diagram of the tunnel mechanism of SCC and flat slot formation.

- 4) Deformation continues to be localised by anodic dissolution until the material undergoes ductile fracture on a very local scale.
- 5) The combination of localised anodic dissolution and deformation continues, leading ultimately to fractures that appear macroscopically brittle.

In summary, intergranular stress corrosion cracking can be explained by preferential dissolution either at pre-existing anodic sites or by dissolution at strain generated anodic sites. However this mechanism does not fully explain transgranular SCC. There is increasing acceptance that transgranular SCC takes place by alternate dissolution and mechanical fracture. Strain plays a role by generating active sites for preferential, very localised dissolution.⁽¹⁵⁾

3.2.3 Film Rupture

Most engineering materials owe their corrosion resistance to the presence of a surface protective film that prevents further attack. Under tension the movement of dislocations in the base metal results in dislocation arrays and ultimately steps in the metal surface due to emergent slip planes. The steps resulting from slip are small but are sufficient to break the thin protective film and fresh metal is exposed to the environment (Figure 5).^(6,15) Anodic dissolution will take place at the rupture in the film and continues until the film is repaired. If complete repair takes place the alloy is repassivated and no further attack occurs.

If the break is not repaired, material will continue to dissolve resulting in pitting or general corrosion. A third scenario of simultaneous film formation and dissolution is possible so that the walls of the penetration are able to passivate while the tip remains active. This serves to focus selective dissolution at the tip of the film rupture and is the situation which most commonly leads to SCC.

Simultaneous film formation and dissolution occur at potentials which lie either side of the passive range on the anodic polarisation curve allowing critical potentials at the active to passive transition and at the start of the transpassive range (Figure 3) to be identified for TGSCC. Intergranular SCC apparently occurs over a wider range of potentials but it is likely that chemical inhomogeneities at the grain boundary locally change the electrochemical response (anodic polarisation) so that a potential which is in the passive region for the bulk material may in fact be in the active passive transition or transpassive zone for the grain boundary.

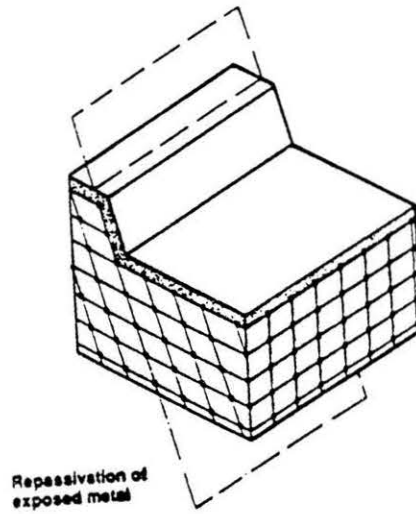
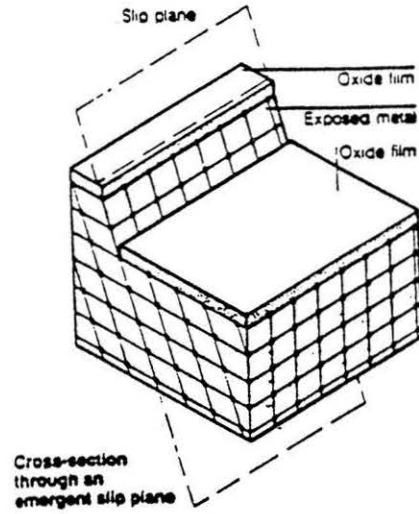
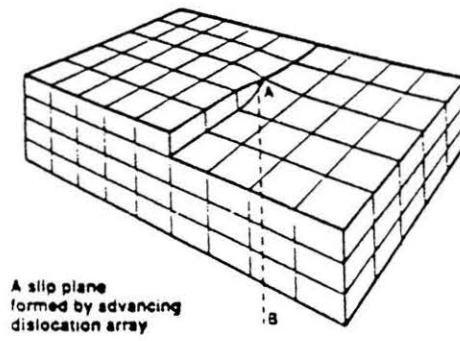


FIGURE 5 Diagram showing surface film disruption and repair by emergent slip plane. (After Turner ⁽⁶⁾)

During simultaneous passivation and oxidation the crack tip is thought to remain active as a result of dynamic strain (strain generated active paths) or due to local composition differences (pre-existing active paths).⁽¹⁶⁾⁽¹⁷⁾ If SCC progresses solely by selective dissolution at film ruptures the total crack advance should be a function of total charge transfer and crack velocity a function of crack tip current density.

For crack advance by pure anodic dissolution, the limiting value is described by the Faradic relationship

$$\frac{da}{dt} = \frac{i_a M}{ZF\rho}$$

where

i_a	is the anodic current density
M	is the atomic weight
Z	is the velocity
F	is Faraday's constant
ρ	is the material density

Several factors can reduce the crack velocity to below that predicted by the equation. The most obvious is that the crack tip may not be bare at all times due to intermittent repair and repassivation. In which case dissolution will be discontinuous and crack velocity will fall below the predicted value. Other factors that can cause a deviation from the predicted growth rate are, transport of ions to the crack tip, a change in crack tip stress concentration, local differences in material chemistry, and only a proportion of the dissolution leads to crack growth.

The relationship however holds moderately well for a fairly wide variety of materials (Figure 6)⁽¹⁸⁾ particularly those that exhibit IGSCC (pre-existing active path SCC) but holds less well for TGSCC. Consequently models describing selective dissolution at film rupture sites have been revised to include aspects of purely mechanical fracture. An example is the corrosion tunnel model described in paragraph 2.2.2. Others describe fracture processes that begin in the surface film. Of these, the tarnish rupture model and the film induced cleavage model have received the most recognition.

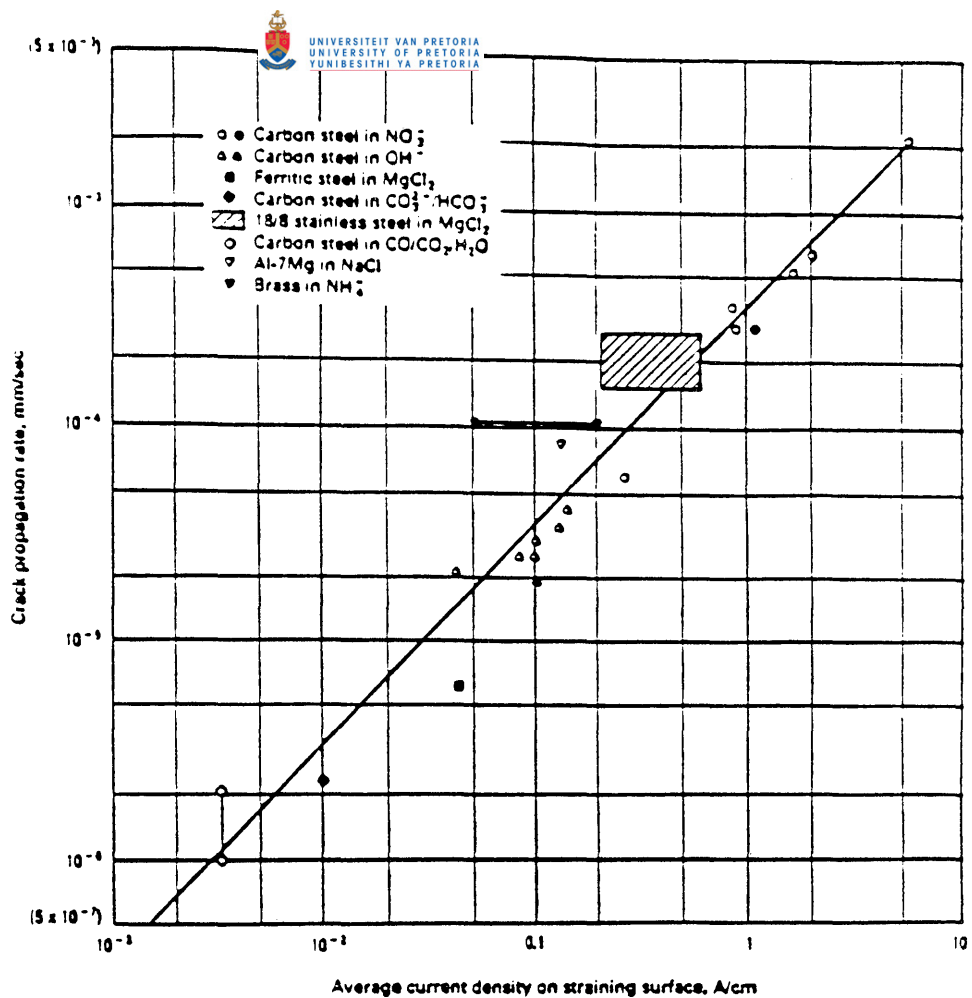


FIGURE 6 Relationship between the average crack propagation rate and the oxidation (that is, dissolution and oxide growth) kinetics on a straining surface for several ductile alloy/aqueous environment systems. (After Parkins ⁽¹⁸⁾)

The tarnish rupture model ⁽¹⁹⁾, simply supposes that an applied stress is able to fracture the brittle protective film. The base metal exposed at the break rapidly repassivates by reacting with the environment. A further application of stress, again ruptures the film and the repassivation process is repeated so that crack growth takes place by alternate film rupture and repair (Figure 7). ⁽²⁰⁾

Film induced cleavage has been proposed as a mechanism for TGSCC. ⁽²¹⁾ It differs from the tarnish rupture model by supposing that cracking occurs in the substrate rather than being confined to the film. Cracking is considered to propagate by discontinuous cleavage, induced in the otherwise ductile base metal by an interaction with the environment. Crack propagation by cleavage in the base metal is based on evidence from fractographic, crack trace and acoustic emission studies of TGSCC.

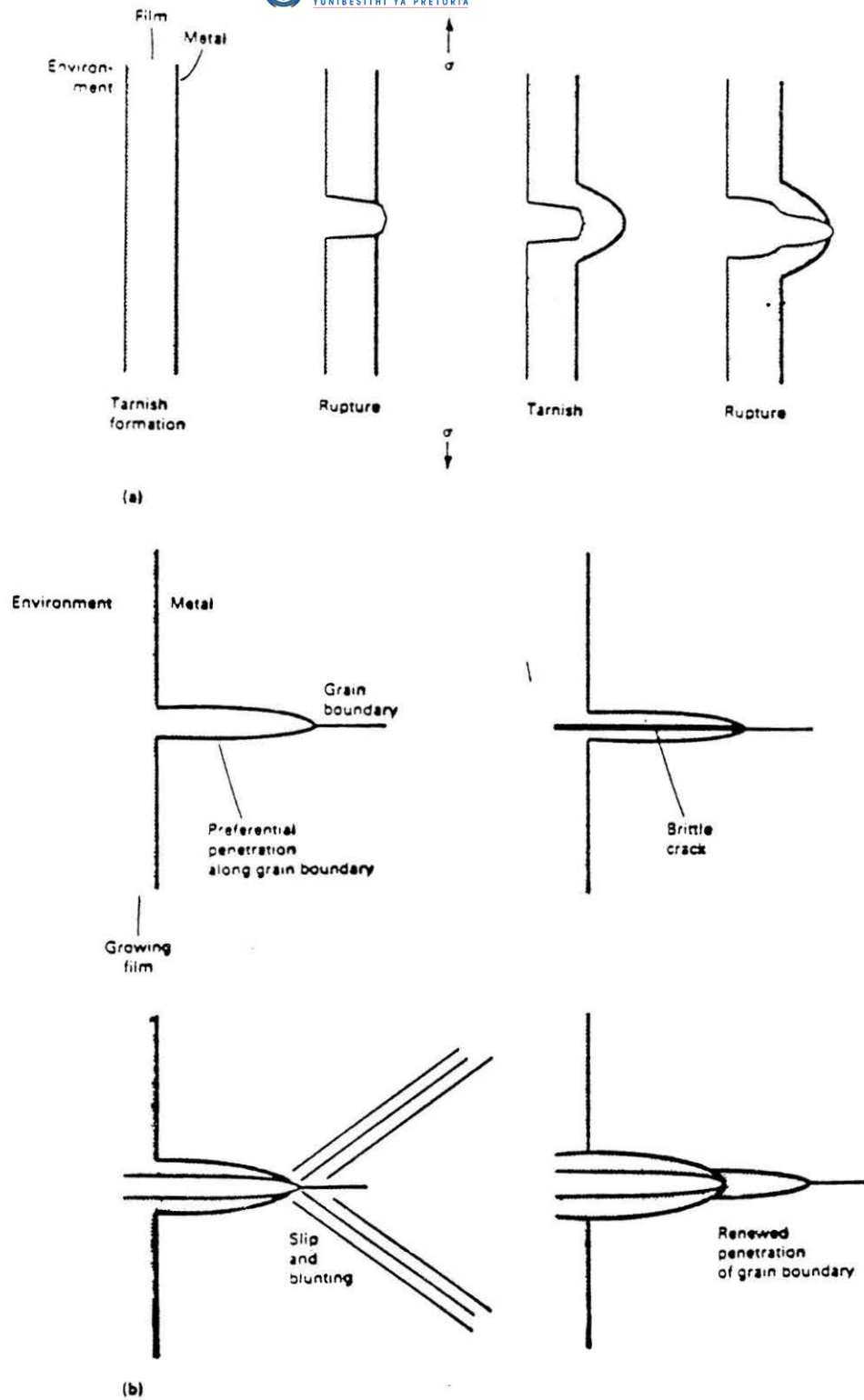


FIGURE 7 TARNISH RUPTURE MODELS (After Pugh ⁽²⁰⁾)

- (a) Schematic of tarnish rupture model for SCC.
- (b) Modified tarnish rupture model of SCC for systems with intergranular oxide film penetration.

Fractographic studies in particular have shown many similarities between the fracture surfaces of TGSCC and cleavage fractures.⁽¹⁴⁾ These are as follows :

- 1) The fracture appearance is crystallographic, consisting of parallel, but displaced primary facets separated by steps.
- 2) The opposite fracture faces often match and interlock.
- 3) The steps between facets are approximately perpendicular to the crack front and hence approximately parallel to the crack direction.
- 4) The steps radiate from initiation sites.
- 5) River patterns are formed when cracks cross grain boundaries.
- 6) Undercutting occurs at steps.

The fracture surfaces of transgranular stress corrosion cracks clearly resemble conventional cleavage surfaces, however there remains controversy over how the environment is able to induce (brittle) cleavage in a material that is normally ductile. For a while it was believed that de-alloying was responsible for the embrittlement. Forty,⁽²⁴⁾ who observed de-alloying during SCC of alpha brass, suggested that embrittlement occurred as a result of a vacancy dislocation interaction. Vacancies generated ahead of the SCC crack by selective dissolution of zinc atoms were thought to inhibit glide, favouring brittle fracture. The computer model of Paskin, et al⁽²²⁾ showed that generation of dislocations at a crack ceased in the presence of a thin coherent film if its lattice parameter was less than the substrate. It was supposed that dislocation emission was prevented by a compressive stress induced in the base metal by the film. The result was crack growth by bond rupture (cleavage) when the film was present, instead of by shear when it was absent. Alternatively it was suggested that film ruptures proceed rapidly enough to capture and annihilate dislocations generated at the crack tip, favouring cleavage as a result of dynamic embrittlement.

Environment-alloy systems produce brittle films by a number of mechanisms that include oxidation, de-alloying and hydride formation, however they do not all result in SCC. In the film induced cleavage model the specificity of SCC is explained by the necessity for a suitable relationship between the film and the substrate in terms of atomic spacing and epitaxial arrangement.⁽²³⁾ Once these conditions are met the film can be a de-alloyed layer, or an oxide or any other film type.

The process of film induced cleavage is described in Figure 8. It assumes that :

- a thin film forms on the surface (a);
- a crack initiated in the film advances into the substrate by cleavage for a limited distance (b);
- after arrest the crack is progressively blunted (c);
- the film reforms and the procedure is repeated;
- limited regions of the crack front advance and then spread laterally as shown in plan view in Figure 8 (d to f).

The crack advance distance Δx (Figure 8) is specific to the system. The crack velocity is the same as normal cleavage cracks proceeding at the speed of elastic waves in the solid. The total propagation time of the SCC crack is believed to correspond to the arrest periods during which the environmental reactions are proceeding.⁽²³⁾

3.2.4 Stress-sorption

The stress-sorption theory of stress corrosion cracking hypothesises that specific ionic species from the environment absorb onto metal exposed at the crack tip.⁽²⁵⁾ The absorbed species lowers the interatomic bond of the metal substrate making crack growth by bond rupture (cleavage) easier. Similar models have been proposed for hydrogen embrittlement⁽²⁶⁾ supposing that the cohesive strength of the matrix is reduced by dissolved hydrogen. Stress-sorption predicts that cracks should propagate at a continuous rate determined by the arrival of the embrittling species at a crack tip.

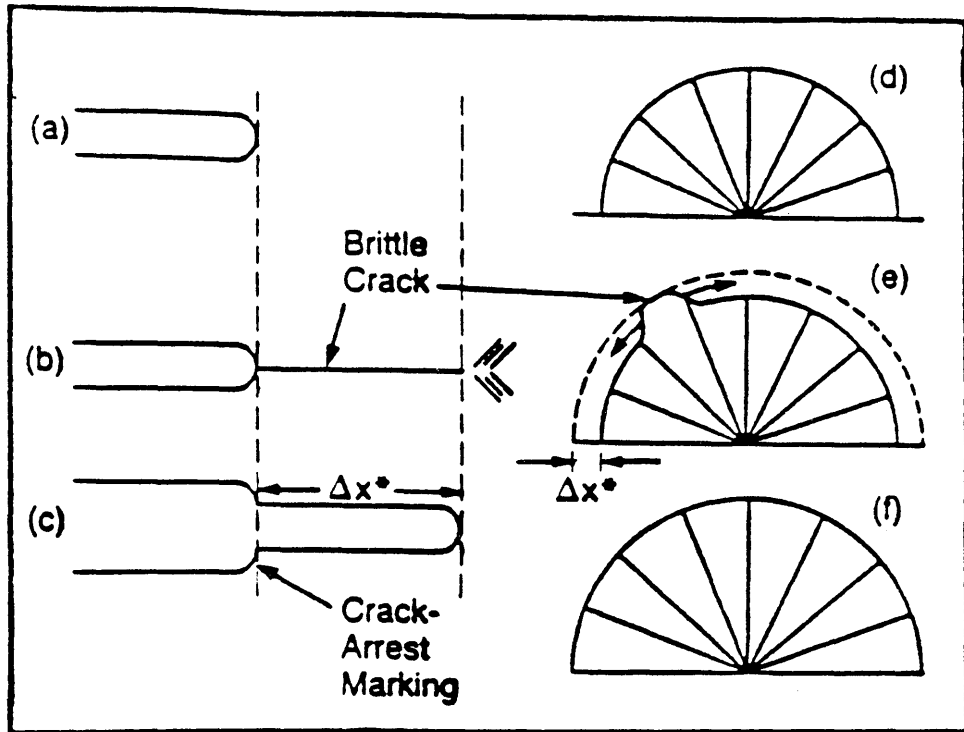


FIGURE 8 Schematic illustration of successive events during the propagation of transgranular stress corrosion cracks:

- (a) through (c) represent a section at the crack tip;
- (d) through (f) represent a plan view of a semicircular crack, showing cleavage steps radiating from the initiation site;
- (c) and (e) indicate the crack advance distance per event. After Pugh⁽²³⁾

A modification was proposed by Uhlig⁽²⁵⁾ suggesting that stress-sorption acts conjointly with electrochemical dissolution to produce a dual mechanism in which bond rupture along paths of low surface energy alternates with electrochemical dissolution along active paths.

The stress-sorption model suffers from a lack of independent evidence for bond strength reduction by absorbed ions. It does however describe liquid metal embrittlement reasonably well.

3.2.5 Hydrogen Embrittlement

Aqueous corrosion is a coupled electrochemical reaction consisting of anodic and cathodic reactions. The metal dissolution reaction occurs at the anode. Its corresponding cathodic reaction is most commonly the reduction of oxygen ($O_2 + 2H_2O + 4e^- \rightarrow 4OH$) or the reduction of hydrogen ($2H^+ + 2e^- \rightarrow H_2$). The latter is more usual in, but not limited to acidic media. The reduction of hydrogen ion proceeds by the addition of two electrons to form atomic hydrogen ($2H^+ + 2e^- \rightarrow 2H$) which is evolved at the cathode. Atomic hydrogen is very reactive and rapidly absorbs onto the metal surface where it recombines to form molecular hydrogen ($H + H \rightarrow H_2$). The former can enter the metal lattice, the latter cannot and usually bubbles off harmlessly at the cathode. Some chemicals poison the hydrogen recombination reaction ($H + H \rightarrow H_2$) and cause atomic hydrogen to be charged into the metal lattice where it has an embrittling effect. Common recombination poisons are hydrogen sulphide, cyanide and arsenic. Certain grain boundary impurity elements have also been identified as poisons; these include tin and antimony. If hydrogen charging due to a poisoned cathodic reaction takes place, hydrogen-induced subcritical crack growth can be the dominant growth process for some stress corrosion systems. Once the cathodically charged hydrogen enters the metal lattice its damaging effect is similar to hydrogen charged by other mechanisms. A detailed description of hydrogen embrittlement models is beyond the scope of this review but as certain of them are analogous to some of the SCC mechanisms proposed earlier they merit brief discussion.

The surface absorption theory described by Petch and Stables⁽²⁷⁾ supposes that hydrogen absorption onto fresh metal reduces the surface free energy of the metal. The fracture stress given by the Griffith⁽²⁸⁾ criterion is therefore lowered so that a smaller stress is needed for crack advance when the surfaces are coated with hydrogen than when they are not.

Oriani⁽²⁹⁾ considered that dissolved hydrogen reduces the interatomic cohesive force in the iron lattice and that crack growth occurs when the crack tip stress exceeds the local cohesive force as reduced by an accumulation of hydrogen.

Embrittlement mechanisms due to interactions of hydrogen with dislocations are popular. Beacham⁽³⁰⁾ proposed that high concentrations of hydrogen ahead of the crack tip aid deformation processes by easing dislocation motion, or generation, or both. The result is fracture at lower applied loads.

Conversely, Tien et al ⁽³¹⁾ proposed that hydrogen swept along by dislocations either limits their movement causing embrittlement of the metal or leads to localised accumulations of hydrogen with a similar effect. Hydrogen accumulation at microstructural traps⁽³²⁾ such as grain boundaries, voids, precipitate interfaces or inclusions can locally enhance the effect of dissolved hydrogen. If recombination takes place high internal pressures result from the evolution of molecular hydrogen which is insoluble in the metal lattice. The pressure can be sufficient to create fissures in the metal. These are usually associated with inclusions or precipitates. This mechanism predominates in the formation of step-wise cracking.

Hydride formation has a role to play in hydrogen embrittlement of several metals such as magnesium, titanium and zirconium. When sufficient hydrogen is present a brittle hydride is precipitated at the crack tip. Cleavage fracture of the hydride film occurs and is followed by crack arrest in the base metal. The stress concentration at the crack tip enhances formation of further hydrides⁽³³⁾ after which the process is repeated. Alternatively crack growth can proceed between brittle hydrides by ductile rupture of the remaining ligaments.

A well-known example of cathodic (hydrogen induced) SCC is that of carbon and low alloy steels in moist hydrogen sulphide atmospheres. Other examples include stress corrosion cracking of steels in wet hydrogen cyanide and cracking of high strength steels in acid chloride solutions.

4 TEST METHODS

Stress corrosion tests are most often used to provide a ranking of materials resistance to a particular environment or to pre-screen candidate materials. Alternatively they can be used to evaluate the relative severity of particular environments. Test methods can be chosen to examine crack initiation and growth or just crack growth. In the case of the latter pre-cracked specimens are usually used. In both cases either constant load or constant stress can be applied. Strain rates are controlled.

4.1 SMOOTH SPECIMENS

Smooth specimens can be used to examine crack initiation and growth. They suffer from the disadvantage that the initiation period can sometimes be quite long requiring that long exposures are used. This however can in part be overcome by subjecting the specimens to high loads in what amounts to a go-no go test for the environment material combination. Any threshold stress values determined are not reliable enough to be used in subsequent engineering design of equipment. They merely give an indication of relative susceptibility of the materials tested.

4.1.1 Constant Strain

Constant strain test specimens are easy to fabricate and use, however the results are not always reproducible. The geometry of the specimen allows the initial stress level to be calculated so that threshold stresses can be determined. As the crack penetrates through a constant strain specimen the load is decreased so that crack arrest can occur and the specimen may not break. This is more likely if numerous cracks initiate as their interaction will relax the applied stress. If bent specimens are used the fibre stress reduces through the thickness reaching zero at the neutral axis where it changes to a compressive stress. The severity of the test therefore decreases as the crack penetrates. This does not happen in uniaxial tension specimens so their choice provides better control of the applied stress and a more severe test; however the jig arrangement is more complicated.

Figures 9 and 10 show common test arrangements for bent-beam specimens, C-rings, uniaxial tension specimens and U-bend specimens all of which apply a constant load. Their geometry and methods of calculating the applied stress levels are described in the relevant ASTM standards which are G39 - 79⁽³⁴⁾, G38 - 73⁽³⁵⁾, G49 - 85⁽³⁶⁾ and G30 - 79⁽³⁷⁾ respectively. Most of these specimens are also suitable for testing weldments, however there are certain requirements for preparation and orientation; these are described in ASTM Standard G58 - 83.⁽³⁸⁾

4.1.2 Constant Load

The application of a constant load results in increased stress as the crack progresses. The constant load test is therefore a more severe test than the constant strain method leading to earlier failure and lower estimates of threshold stress. The jigs required however can be complicated so it is frequently necessary to reduce the specimen size to quite small dimensions so that the required load can be applied. This can sometimes lead to mechanical failure of the specimen following pitting or general corrosion making interpretation of the results difficult.

Some of the constant strain specimen configurations can be adapted, usually by the inclusion of a spring, to apply constant load (Figures 9 and 10). Circular uniaxial tension specimens can be tapered. The resulting axial variation in stress can be used to estimate threshold stress levels.

4.1.3 Slow Strain Rate Tests

SCC initiation is assisted by applying a slow dynamic strain above the elastic limit of the material. Consequently the process of SCC is accelerated which provides a rapid test that can be applied to most materials and product forms. Slow strain rate tests can be used to provide an order of ranking of materials or to compare severity of environments. Testing is carried out using standard tensile machines capable of applying loads at the required strain rate.

Standard tension specimens are used, contained in a corrosion cell and load is applied at a constant rate until the specimen fails.^(39,40,41) The evaluation is made by metallurgical examination of the fracture and by comparing the stress-strain curve produced in a corrosive to that obtained in an inert environment. A SCC index is usually reported as the ratio between the result in the corrodent divided by the result in an inert environment. Elongation or reduction of area are convenient for this calculation. The most critical variable in a slow strain rate test is the magnitude of the strain rate. If it is too high there is insufficient time for the environment to influence fracture. If it is too low repassivation or film repair can prevent SCC damage when the SCC mechanism is anodic. This is not the case if cracking is due to hydrogen charging (cathodic SCC) which allows the slow strain rate test to be used to distinguish between the two. The difference is shown in Figure 11. Strain rate regimes for promoting SCC in various metal/environment systems are given in Table 5.

TABLE 5 CRITICAL STRAIN RATE REGIMES PROMOTING SCC IN VARIOUS METAL/ENVIRONMENT SYSTEMS (After ASM Handbook⁽⁵⁾)

S Y S T E M	APPLIED STRAIN RATE, S⁻¹
Aluminium alloys in chloride solution	10 ⁻⁴ and 10 ⁻⁷
Copper alloys in ammoniacal and nitrite solutions	10 ⁻⁶
Steels in carbonate, hydroxide, or nitrate solutions and liquefied ammonia	10 ⁻⁶
Magnesium alloys in chromate/chloride solutions	10 ⁻⁵
Stainless steels in chloride solutions	10 ⁻⁶
Stainless steels in high-temperature solutions	10 ⁻⁷
Titanium alloys in chloride solutions	10 ⁻⁵

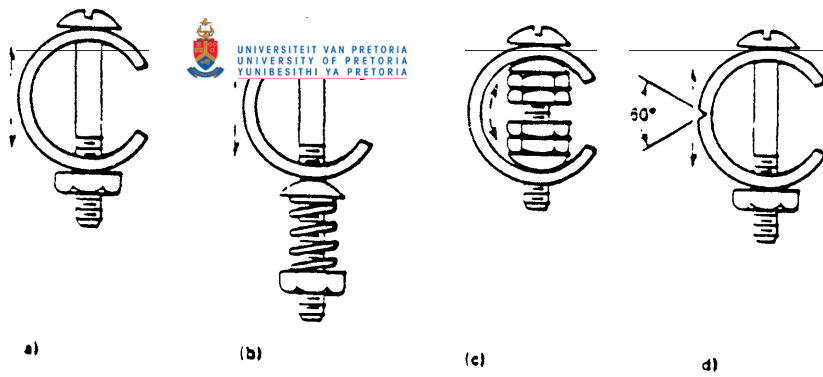


FIGURE 9A METHODS OF STRESSING C-RINGS

- (a) Constant strain. (b) Constant load.
 (c) Constant load. (d) Notched C-ring; a similar notch could be used on the side of (a), (b) or (c).

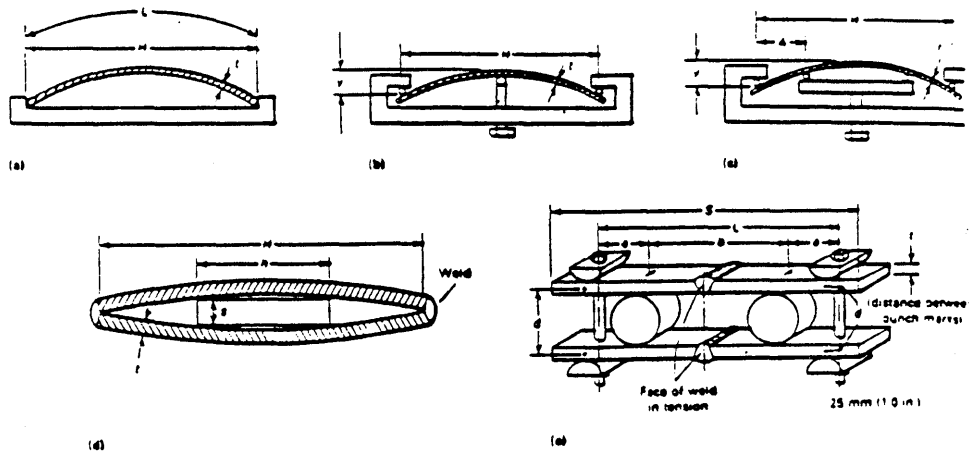


FIGURE 9B SCHEMATIC SPECIMEN AND HOLDER CONFIGURATIONS FOR BENT-BEAM STRESSING

- (a) Two-point loaded specimen. (b) Three-point loaded specimen.
 (c) Four-point loaded specimen. (d) Welded double-beam specimen.
 (e) Bolt-loaded double-beam specimen.

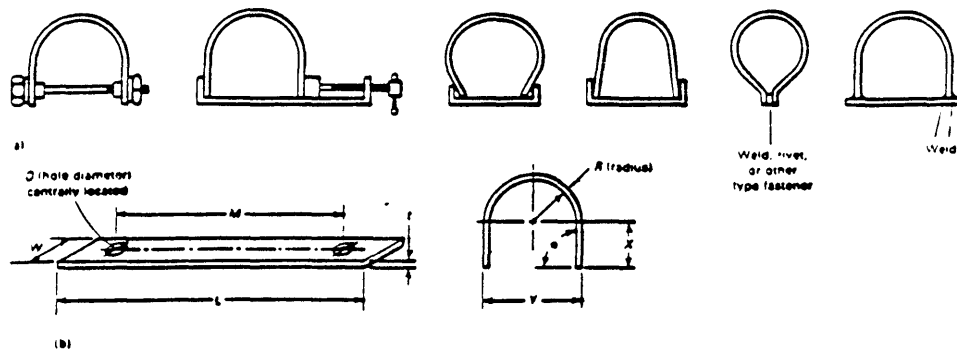


FIGURE 9C TYPICAL U-BEND SCC SPECIMENS

- (a) Various methods of stressing U-bends.
 (b) Typical U-bend specimen dimensions.

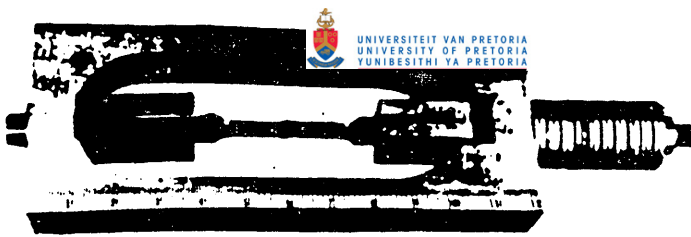


FIGURE 10 SPRING-LOADED STRESSING FRAME

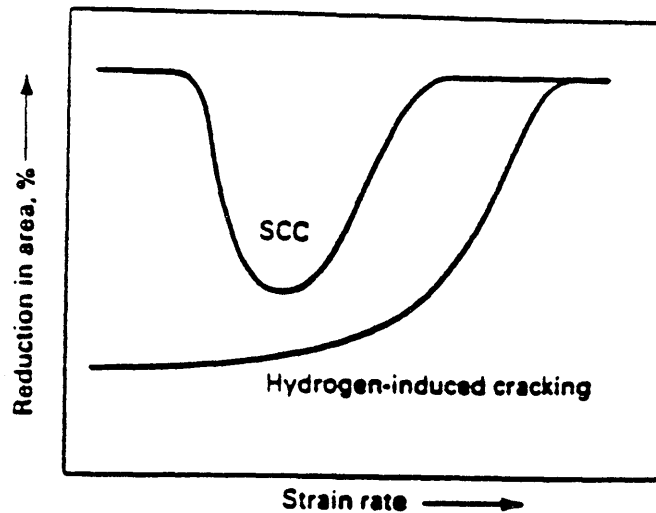


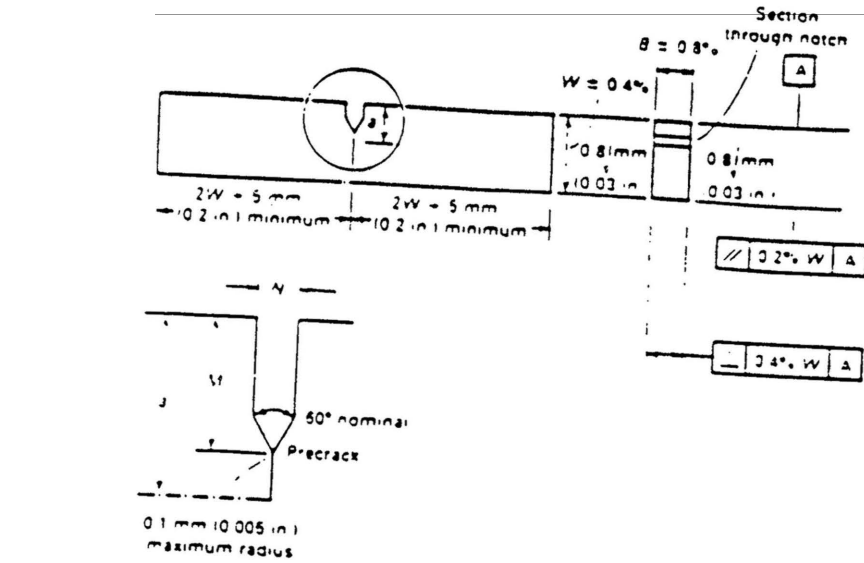
FIGURE 11 SCHEMATIC SHOWING THE EFFECT OF STRAIN RATE ON SCC AND HYDROGEN-INDUCED CRACKING (After ASM Handbook⁽⁵¹⁾)

4.2 PRE-CRACKED SPECIMENS

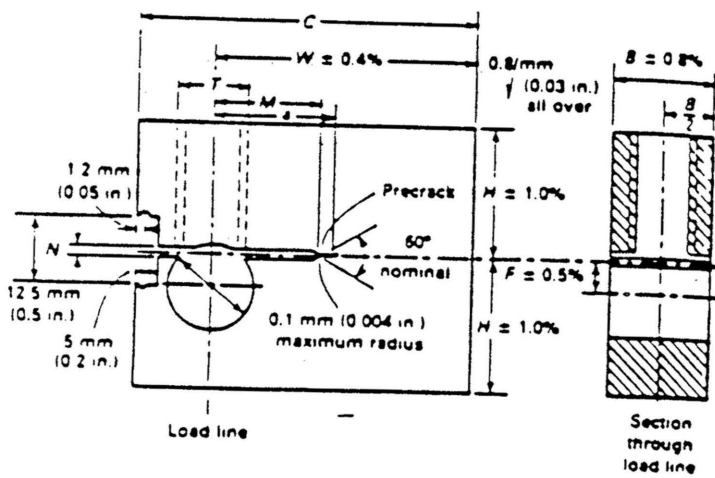
Engineering materials contain flaws; consequently fracture is governed by the intensity of the stress at the tip of the flaw and not simply by the applied stress. The stress intensity (K_I) is dependent on the magnitude of the applied stress and the geometry of the flaw. When the stress intensity exceeds a critical value (K_{Ic}) which is a material characteristic, fracture occurs.

Similarly a stress corrosion crack will grow if the stress intensity (K_I) exceeds a critical threshold value (K_{ISCC})⁽⁴²⁾⁽⁴⁵⁾ for the material-environment combination. The rate of advance of the crack is related to the stress intensity at the crack tip. The growth characteristics of a stress corrosion crack are described by plotting da/dt versus K_I (Figure 8). Plain-strain fracture toughness specimens which allow calculation of the crack tip stress intensity are also used for SCC testing. The pre-cracked specimens most commonly chosen are the cantilever beam, the wedge opening loaded (WOL) and the double cantilever beam (DCB) specimens shown in Figure 12.

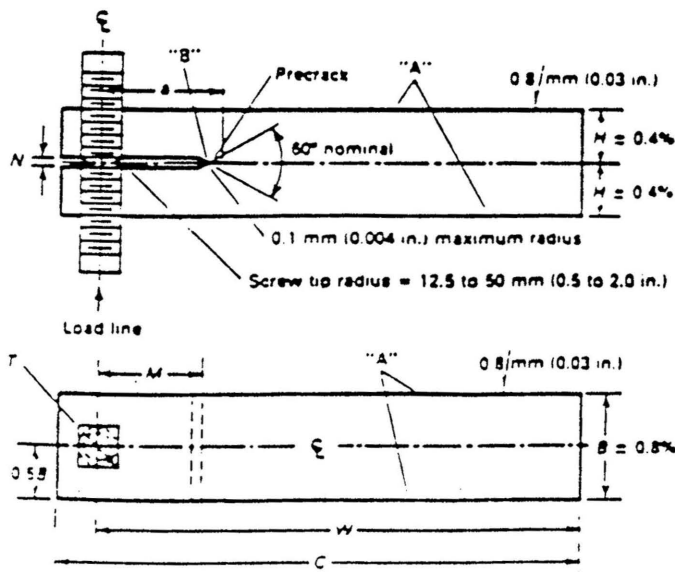
FIGURE 12 DIMENSIONS OF FRACTURE TOUGHNESS SPECIMENS



a) Proportional dimensions and tolerances for cantilever bend test specimens.



b) Proportional dimensions and tolerances for modified compact specimens.



c) Proportional dimensions and tolerances for double-beam specimens.

(c)

Cantilever beam specimens are tested by applying a constant load.⁽⁴²⁾ Consequently their use requires loading frames or a tensile machine and containment of the specimens in a corrosion cell. The crack tip stress intensity can be determined from displacement measurements once a compliance calibration has been done for the material and geometry. Alternatively K_I can be calculated from an expression describing stress intensity for a rectangular beam in pure bending. The specimen is usually face notched to 5 to 10% of the thickness and the notch is extended by fatigue-cracking the specimens at low stress intensity. The specimens are first tested in air to establish K_{Ic} values. Subsequently specimens are immersed in the environment and loaded to successively lower initial stress intensity levels. If the material is susceptible to SCC in the environment the crack will propagate under increasing stress intensity due to the application of a constant load. When the stress intensity reaches K_{Ic} the specimen will fail. The threshold level for stress corrosion (K_{ISCC}) is the highest stress intensity value which does not result in crack extension. Usually at least ten specimens are required to establish K_{ISCC} for a particular material environment. The method is not suitable for testing materials in which the time to failure is long. Crack growth rates can be established but constant monitoring is required.

Wedge opening loaded (WOL) specimens⁽⁴³⁾ can be used in constant load tests but are more frequently used with constant displacement. Self stressed WOL specimens are easily portable and can be used to study SCC behaviour of materials under actual operating conditions. The stress intensity factor at the crack tip (K_I) is calculated from

$$K_I = \frac{C_3 P}{B \sqrt{a}}$$

where

P	=	applied load
B	=	specimen thickness
a	=	crack length measured from the loading plane
C_3	=	a constant determined from a/w
W	=	the specimen length.

The crack tip stress intensity decreases as the crack advances. K_{ISCC} for the material-environment corresponds to the stress intensity at crack arrest.

Double Cantilever Beam (DCB) specimens⁽⁴⁴⁾ are similar in principle to WOL specimens but their greater length makes them more suited to SCC tests. They can be used in either constant load or constant displacement tests. When growth rate determinations are to be made using the latter, two of the three testing variables must be measured - crack depth, load or crack opening displacement. It is desirable to obtain crack length measurements within a precision of 0,127mm (0,005 inches). Compared to the modified WOL geometry the DCB provides for a greater extent of crack extension and for a given growth rate the decrease in stress intensity is much less than the modified WOL specimen. Furthermore, bolt loading is easier to control and reproduce than wedge loading. These advantages must be considered against problems with compliance and arm breakage associated with bolt loaded DCB specimens.

4.3 STANDARD SCC TEST PROCEDURES

Standard procedures have been developed for testing the suitability of materials for certain environments which include polythionic acids, magnesium chloride, salt, sodium chloride and sour service (wet H₂S). These are respectively ASTM G35 - 73,⁽⁴⁶⁾ G36 - 73,⁽⁴⁷⁾ G41-8,⁽⁴⁸⁾ G44 - 75⁽⁴⁹⁾ and NACE TM-01-77.⁽⁵⁰⁾ Similar procedures exist for testing the SCC resistance of certain groups of materials. ASTM G37 - 85⁽⁵¹⁾, G47 - 79⁽⁵²⁾ and G64 - 85⁽⁵³⁾ describe procedures for assessing the SCC resistance of copper-zinc and high strength aluminium alloys.

5 ELECTROCHEMICAL MEASUREMENTS

5.1 POTENTIAL MEASUREMENTS

Corrosion of metal can be simulated by control of electrode potential⁽⁵⁵⁾. Similarly stress corrosion cracking can be studied by measuring potential and identifying potential regimes in which cracking occurs. A method of achieving this is to conduct slow strain rate tests at different values of applied potential.

5.2 POTENTIODYNAMIC SCANS

Anodic stress corrosion cracking requires a critical balance between active and passive behaviour. The active material at the crack tip must undergo a transition to passive as the crack advances. This implies that there will be a time-related decay in current density. The region can be identified by conducting fast and slow potentiodynamic scans.⁽⁵⁴⁾ During the fast scan (~ 1000 mV/min) the sample is polarised anodically at a high rate which does not allow sufficient time for passive film formation. At the slower scan rate (~ 10 mV/min) the passive film can readily form. SCC is predicted where there is a large difference between anodic currents so recorded and the range of SCC susceptible potentials can be identified (Figure 13).

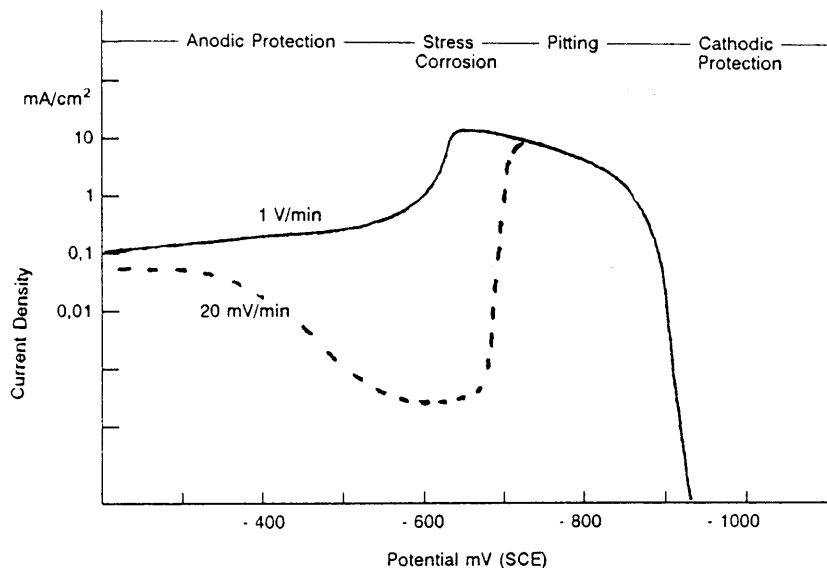


FIGURE 13 POTENTIODYNAMIC POLARISATION CURVES

for C-Mn steel in 1 N Na_2CO_3 + 1 N NaHCO_3 at 90°C showing the domains of behaviour predicated from the curves. (After Parkins⁽¹⁸⁾)

5.3 FILM DISRUPTION - CURRENT DECAY

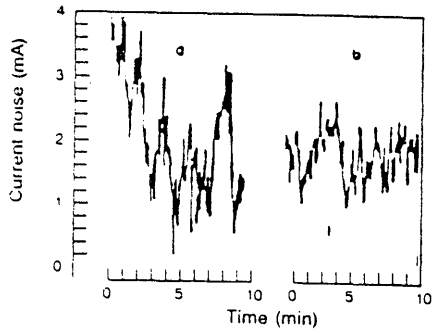
In some systems it is not possible to obtain the film free condition necessary at the start of potentiodynamic scanning and the film has to be disrupted by scratching or by rapid straining.^(56,57) Subsequent measurement of the current response can reveal areas of SCC susceptibility. Rapid current decay indicates repassivation, slow decay signifies active corrosion. An intermediate response identifies the likelihood of stress corrosion cracking.

ELECTROCHEMICAL NOISE ANALYSIS

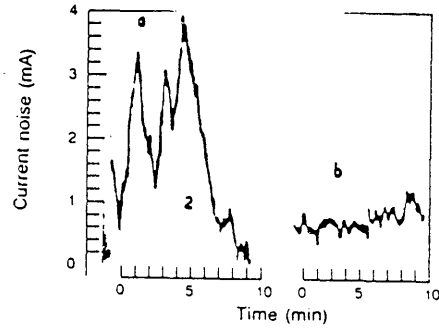
Electrochemical (EC) noise is the term used to describe spontaneous transients in the current or potential time record of an electrochemical reaction. There is debate over the source and significance of the transients but Dawson et al ⁽⁵⁸⁾⁽⁵⁹⁾ are of the opinion that they result from stochastic film rupture events which locally expose the underlying metal. Metal dissolution occurs but typically results in a fairly rapid repassivation process, hence the short-lived current transients.

EC noise is usually measured using a three element probe. Two of the elements are fabricated from similar material and are coupled so that the current flowing between them (coupling current) can be measured. An inert material is chosen for the third element which is made the reference electrode, against which the potential of the working electrode is measured.

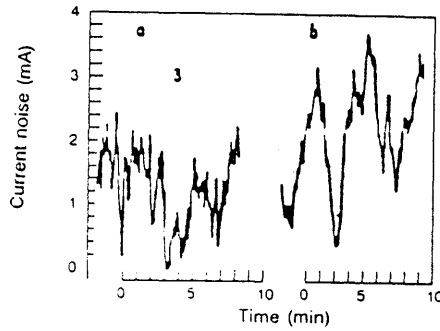
EC noise has been characterised from research and plant observations. It has been noted that the amplitude of low frequency potential or current noise is related to the rate of the corrosion process and that the frequency range as measured by the shape of the power spectrum is influenced by the nature of the process.⁽⁶⁰⁾ Metals exhibiting passivity give low coupling currents and noise levels. Initiation of localised events increases the potential noise level whilst propagation of localised types of corrosion increases the mean current and current noise. General corrosion has a high mean current but a more random noise signal with little evidence of individual transients (Figure 14).^(63,64) The ability of the noise technique to distinguish corrosion processes has led to an interest in its use to identify SCC. It might be expected that SCC would give a characteristic EC noise spectrum especially if cracking is occurring by film rupture and anodic dissolution. Lotto and Cottis report that the noise technique can be used to monitor SCC processes in alpha-brass⁽⁶²⁾ and high strength aluminium alloys.⁽⁶¹⁾ In most cases cracking gave the highest noise amplitude. Cracking was also indicated by the highest standard deviation peaks. The source of the EC noise was believed to be repassivation transients resulting from the exposure of fresh metal surface following rupture of the passive film by cracking. Similar tests carried out on high strength steel in an environment where the SCC mechanism is almost certainly hydrogen embrittlement resulted in characteristic noise only when the specimens actually broke.⁽⁶³⁾ It might have been expected that noise would be generated by intermittent exposure of fresh metal to the solution following discontinuous cracking induced by hydrogen.



Noise behaviour in 3 % NaCl (a) after 2 h (b) after 72 h



Noise behaviour in 3 % NaCl plus inhibitor (a) after 2 h (b) after 72 h



Noise behaviour in 3 % NaCl in the case of crevice corrosion (a) after 2 h (b) after 72 h

FIGURE 14 CHARACTERISTIC NOISE FOR PITTING, PASSIVE AND CREVICE CORROSION (After PR Roberge et al⁽⁶⁴⁾)

6 EXAMPLES OF SCC IN MODERN CHEMICAL PLANT

A modern chemical plant can incorporate a number of processes including - coal gasification, power plant (steam generation), air separation, hydrogen sulphide and carbon dioxide removal, ammonia recovery, fuel synthesis and a refinery. Consequently a wide spectrum of material-environment combinations are encountered which promote SCC. The more important are summarised in the following paragraphs and represent industrial examples of most of the stress corrosion crack propagation mechanisms described earlier.

6.1 CHLORIDE SCC

It is well known that chloride solutions promote SCC in stainless steels. The phenomena is temperature dependent, seldom occurring below 60°C. Cracking is influenced by the amount of chloride present; however it is not possible to present reliable threshold limits as SCC invariably occurs where chlorides are able to concentrate out of the bulk solution. For heat exchangers with water on the tube side below 60°C, a level of 1000 ppm chloride has been mentioned as a limiting concentration for type 316 at a neutral pH and assuming no scale, sedimentation or crevices, and with a continuous flow above 1,5 m/s. A chloride concentration of 250 ppm is a more conservative limit.⁽³⁾ Susceptibility to chloride SCC is highest in ferrous materials containing additions of between 7% and 20% Ni.⁽⁶⁵⁾ Chloride SCC can be overcome by selecting ferritic or duplex stainless steels or by austenitic stainless steels containing more than 30% Ni.

The service problems that arise due to chlorides most usually happen when the medium contains trace levels of chlorides that subsequently concentrate. Wet/dry, evaporating or condensing services, under deposits, under lagging or at crevices are typical examples.

Chloride SCC has been found at ring joints, at tube-tubesheet joints, in impellers, piping bellows and flanges where one or other of the above concentrating mechanisms was operative. It was overcome by design or process changes to prevent chloride concentration or, in extreme cases by a material change to duplex or high nickel stainless steels.

Chloride SCC has been found on the outside of austenitic stainless steel piping beneath insulation. Cracking under insulation mostly occurs in the temperature range 55°C to 260°C but cannot be ruled out below 540°C.^(67,68) Insulating materials containing only 10 ppm chlorides may cause cracking. It is important to provide an efficient weather barrier to keep the insulation dry since moisture containing chlorides will evaporate at the hot pipe surface causing the chlorides to concentrate.⁽⁶⁸⁾ Chlorides are present in normal rainfall, particularly at the coast; an alternative source is by leaching from the insulation material. Cracking can be prevented by wrapping the stainless steel with aluminium foil before applying the insulation.

6.2 POLYTHIONIC SCC

Polythionic acid promotes intergranular SCC in sensitised austenitic grades of stainless steel.⁽⁶⁹⁾ Polythionic acid is generated in petrochemical process units during shutdown periods when vessels are opened to air. Moisture and oxygen react with iron sulphide scale on the vessel wall to form a family of polythionic acids of the type $H_2S_xO_8$.^(70,71)

Fully solution annealed 300 series stainless steel is totally resistant to SCC by polythionic acids. Stress relieving heat treatments or prolonged service in the temperature range 550°C to 850°C will cause standard grades of austenitic stainless steels to sensitise, rendering them susceptible to attack by polythionic acids.⁽⁶⁹⁻⁷³⁾ This can be overcome by using stabilised grades 321 and 347 to prevent sensitisation. The performance of 321 and 347 can be further improved by a stabilising heat treatment. Sensitising can also be reduced or prevented by using the low carbon grades (316L or 304L). Where sensitisation cannot be avoided; NACE recommended practice RP-01-70⁽⁷⁴⁾ should be used to minimise polythionic attack.

6.3 SULPHIDE STRESS CORROSION CRACKING

At low temperatures (< 200°C), moist hydrogen sulphide or aqueous solutions of hydrogen sulphide (sour service) are responsible for spontaneous failures of steels and other high strength alloys.^(75,78) The phenomena is referred to by a number of names, the most common of which are, sulphide stress corrosion cracking (SSCC) or hydrogen induced stress corrosion cracking. As the name implies cracking is a form of hydrogen embrittlement caused by the hydrogen generated during corrosion entering the metal.

When the environment is identified as sour, selection of materials is based on NACE MR-01-75.⁽⁷⁶⁾ The underlying principle for materials selection lies with the relationship between material strength (or hardness) and susceptibility to SCC (Figure 15). In general chemistry and heat treatment of materials should be selected so that the hardness does not exceed 240 Hv10. By and large adherence to NACE MR-01-75 is successful in preventing SSCC but some failures have been encountered where either the presence of H_2S was not anticipated or the metallurgy of the components deviated from the NACE requirements.

In the air separation plant sulphide stress corrosion due to the presence of traces of hydrogen sulphide in the air has been found in 12% chromium steel blades in the second compression stage of the main air compressor. Similar cracks have also been found in the third stage impeller. The problem was overcome by ensuring that the replacement parts were properly heat treated to meet the requirements of NACE standard MR-01-75.^(76,77)

Ferrite base metals welded with austenitic filler were found to be highly susceptible to SSCC when exposed to sour conditions. Disbonding occurred along the fusion line where admixture between the high alloyed filler and the parent metal resulted in a susceptible microstructure (hardness >240 Hv). The performance was worsened by post weld heat treatment which increased the fusion line hardness by precipitating alloy carbides. Dissimilar welded joints are no longer permitted in sour service.

Welds exposed to the vapour space in storage tanks are a common site for SSCC if the stored medium contains H₂S. Cracking is caused by a H₂S rich condensate although the H₂S concentration in the stored medium might actually be quite low. The problem can be overcome by ensuring that weld hardnesses are below 240 Hv or by post weld heat treatment. Neither are practical for an existing tank and the only option is to keep the tank filled.

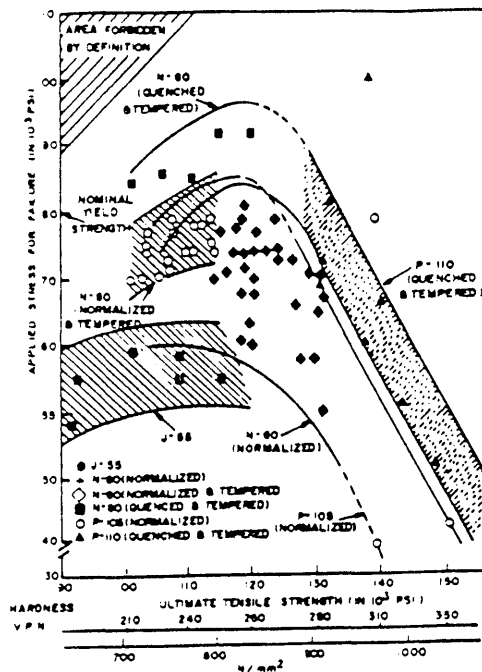


FIGURE 15 Effects of heat treatment, hardness and tensile strength on the resistance of steels to sulphide stress corrosion cracking (After Beirne⁽⁷⁵⁾)

Caustic promotes stress corrosion cracking in a wide variety of materials in the chemical industry. Carbon steel is subject to SCC at elevated temperatures in solutions of caustic. Cracking is controlled by stress relieving welded and cold worked areas. Figure 16 shows the conditions where a stress relief heat treatment is necessary. At elevated temperatures 300 series stainless steels and Inconels are susceptible to SCC in concentrated solutions of caustic. The range of susceptibility is shown in Figure 17 for stainless steels. Incolloy 800 shows a greater susceptibility than Inconel 600 but both suffer SCC in concentrated caustic between 190°C and 450°C. The resistance of Inconel 600 is reported to be improved by several heat treatments, principally stress relieving at 900°C, or 770°C or 630°C.

Caustic as a principal process constituent can usually be handled without too much trouble. Difficulties arise when caustic is present as an impurity in condensing or evaporating services which allow it to concentrate at levels and at temperatures that will promote SCC. The phenomenon has been encountered in steam service^(79,80) where, by and large downstream problems could be traced to carry over from the boiler.

Environmentally assisted cracking in steam service due to the presence of caustic has been encountered in carbon steel blowdown lines, Inconel 625 and 300 series stainless steel expansion bellows and in low alloy steam turbine blading. In all cases the observed cracks were intergranular although caustic SCC of austenitic steel can sometimes be transgranular. On carbon steel, caustic SCC can be solved by a stress relief heat treatment or by design to eliminate crevices. For more onerous services such as steam turbines or expansion bellows improvement in process control to eliminate caustic carryover is often the only solution.

6.5 SCC OF BRASS AIR COOLER AND STEAM CONDENSER TUBING

Trace levels of ammonia are able to promote SCC of stressed copper alloys if water and oxygen are also present. Cracking has been observed in aluminium brass intercooler and steam condenser tubing. Cracking is predominantly transgranular. Performance is improved by choosing copper-nickel in preference to brass tubes. Steam condenser tubes fabricated from brass are ordered in the annealed condition to minimise the risk of SCC and restrictions are placed on expansion when rolling the tube into the tubesheet.

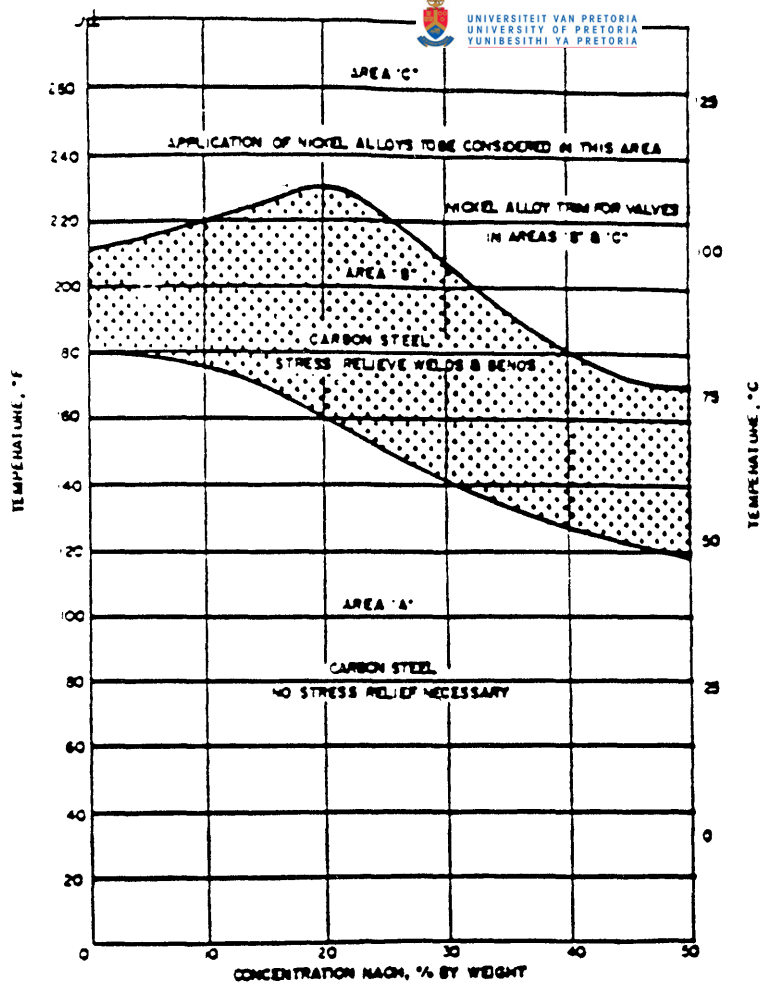


FIGURE 16
Caustic soda service graph.
(After NACE⁽¹¹⁶⁾)

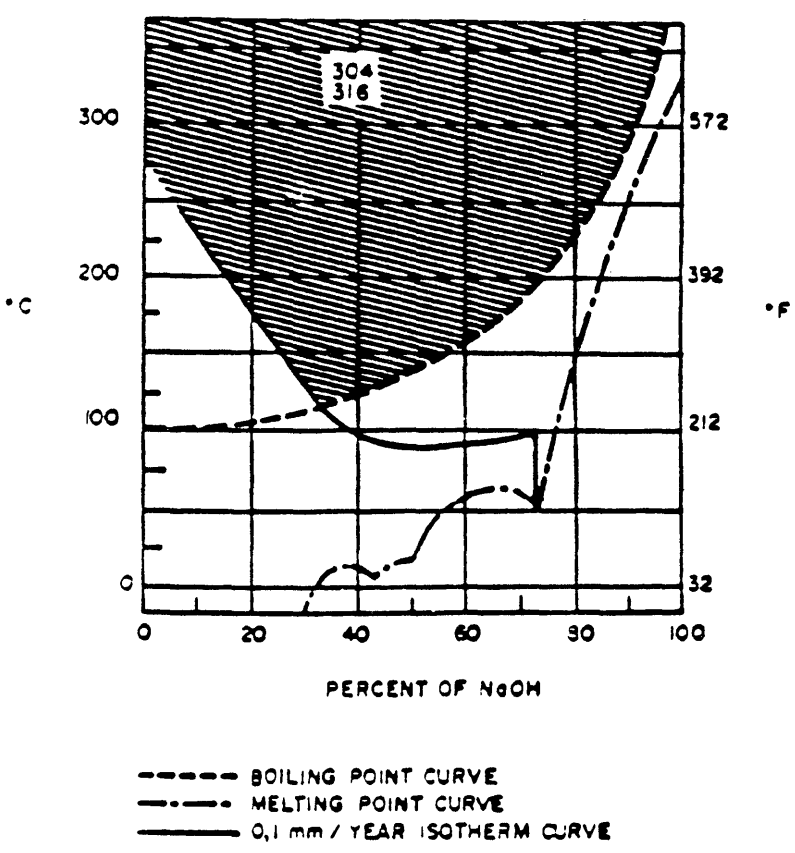


FIGURE 17
Iso-corrosion curves 0,1 mm/year, for 314 and 316 steels, in pure sodium hydroxide at different concentrations and temperatures. The shaded field represents application areas in which the risk of stress corrosion cracking is present.
(After La Que and Copson⁽¹¹⁷⁾)

6.6 SCC DURING THE STORAGE OF ANHYDROUS AMMONIA

Transgranular stress corrosion cracks have been observed in carbon steel used to store anhydrous ammonia.^(81,82,83) Stress corrosion requires the simultaneous presence of a susceptible material, tensile stress and a promoting environment. These have been characterised for the carbon steel-anhydrous ammonia system.^(82,83)

6.6.1 Material

High strength carbon steels are more vulnerable to ammonia stress corrosion cracking. The risk of SCC in ammonia storage vessels is therefore minimised if they are fabricated from low strength materials with a specified minimum yield strength below 350 MPa.

6.6.2 Tensile Strength

The principal source of tensile stress giving rise to SCC is from residual stresses after welding. These can be substantially reduced by an appropriate post weld heat treatment (PWHT). In existing as-welded tanks or spheres where PWHT is impractical shot peening might be considered. The peening imparts a thin layer of compressive stress in the metal surface which retards the initiation of SCC. Shot peening is reported to reduce the incidence of ammonia SCC temporarily but not prevent it. To be fully effective welds must be ground smooth before peening and any cracks removed.

6.6.3 Environment

The occurrence of SCC in liquid anhydrous ammonia is dependent upon the water, and oxygen content of the liquid. Water contents greater than 0,2% have been found to inhibit cracking but the water concentration must always be maintained, as irreversible damage can result from water free ammonia contacting the metal surface even for a short time. Less water is required to inhibit cracking if the ammonia has a low oxygen content. The interdependence of oxygen and water concentration is described by Figure 18.⁽⁸⁴⁾ The inhibiting effect of water is not necessarily realised in the vapour space. The equilibrium content of oxygen in ammonia vapour is typically 60 times higher than the corresponding concentration in the liquid.

Conversely the equilibrium concentration of water in the vapour phase is about 500 times less than in the liquid ammonia. Consequently the water and oxygen contents of liquid condensing on the roof and walls from the vapour space will not necessarily have the same water and oxygen contents as the bulk liquid and full inhibition might not be achieved. Similar conditions occur at the liquid meniscus.

Cracking due to liquid condensation in the vapour space can be minimised by maintaining the liquid ammonia temperature below the vapour space metal temperature.

In addition to the effects of chemical composition, ammonia SCC also shows a temperature dependence. Cracking is less prevalent at low temperature.

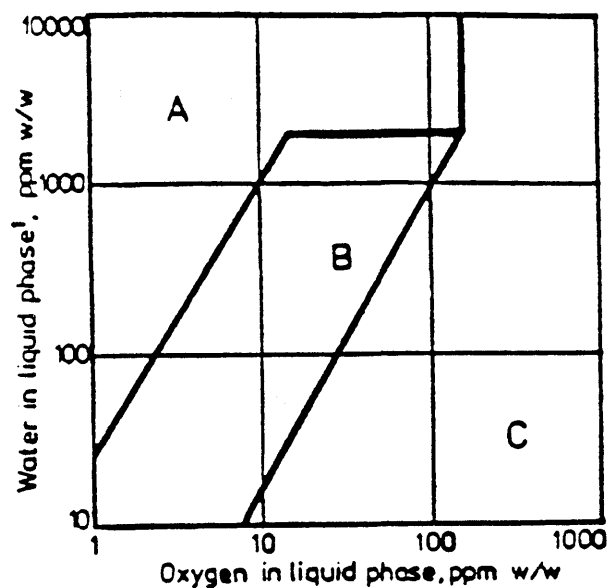


FIGURE 18 Advice given regarding inspection frequency for as-welded spheres with material yield strengths $<350 \text{ N/mm}^2$: (After Cracknell⁽⁸¹⁾)

A - inspect at normal frequency²;

B - inspect at least twice normal frequency²;

C - do not operate in this area - either reduce oxygen level or add water to bring operating conditions into zone B A or B.

NOTES:

1. When water is added deliberately it should be either distilled water, or plant condensate of equivalent quality.
2. To the code of practice for spheres, the first in-service inspection shall take place after not more than two years service, followed by periodic inspections at intervals determined by the results of the first service examination, but in no case to exceed six years. (After Cracknell⁽⁸⁵⁾)

6.6.4 Construction and Inspection of Spheres and Tanks for Storage of Ammonia

Cracknell suggested tentative rules for the construction, inspection and operation of spheres, vessels and tanks for the storage and transport of ammonia to prevent SCC. These are quoted directly from Cracknell's paper⁽⁸⁵⁾ as follows :

- i) Water additions: For certain steels, detailed in Table 6 the addition of 0,2% minimum water should be mandatory. It is strongly recommended in all other cases except where precluded by the end use of the ammonia.

- ii) Choice of steel: The choice of steel must meet any local regulations for the handling of ammonia and design rules for the avoidance of brittle fracture. It should in addition meet the requirements of the Table 6 depending on the strength and operating temperature.

- iii) As-welded vessels: (i.e. specified minimum yield strength 350 N/mm² or less): Where as-welded vessels are used additional precautions shall be taken. The vessels shall either
 - a) be used only for ammonia containing at least 0,2% water;
or
 - b) operate at substantially 1 atm pressure (= -33°C); or
or
 - c) be used only with ammonia on which the analysis of the liquid phase for oxygen and water is regularly monitored and judged against the criteria of Figure 18."

TABLE 6 TENTATIVE RULES FOR STEEL YIELD STRENGTH AND ADDITIONS OF WATER TO BE USED FOR STORAGE OF ANHYDROUS AMMONIA (After Cracknell ⁽⁸⁵⁾).

SPECIFIED MINIMUM YIELD STRENGTH, N/mm ² (ksi)	MAXIMUM OPERATING TEMPERATURE	REQUIREMENTS
>460 (67) °*	Any	The vessel shall be stress relief heat treated and 0,2% water added
350 to 460 ⁽⁵¹⁻⁶⁷⁾	Any	Shall be stress relief heat treated
<350 ⁽⁵¹⁾	-5°C (+23°F) and above	Strongly recommended that if vessel will go in a furnace it should be stress relief heat treated
<350 ⁽⁵¹⁾	Below -5°C (+23°F)	Stress relief not mandatory but recommended

- * Note that many countries ban use of high strength steels for transport of ammonia.
- ° The dividing line is not necessarily at 460 N/mm².

Since Cracknell's recommendations were formulated SCC has been identified in refrigerated tanks operating at -33°C and 1 atmosphere pressure. These should now be included in any inspection schedule. Additionally the liquid ammonia temperature should be maintained below the vapour space metal temperature to prevent condensation.

6.7 HYDROFLUORIC ACID SCC

Hydrofluoric acid is used in the alkylation plant where it can cause SCC of several corrosion resistant alloys.⁽⁸⁶⁾ Monel 600 is used where hydrofluoric acid containing feed includes water. Above 200°C Monel suffers intergranular attack by sulphur compounds. Inconel 600 is the preferred material if sulphur compounds are anticipated. In moist aerated hydrofluoric acid vapours Monel, Inconel 600 and Nickel 400 are susceptible to SCC. SCC can be minimised by controlling the environment to exclude oxygen or by a stress relief heat treatment (540°C for 1 hr). In hydrofluoric acid services where Monel 400 is used, the welding electrodes must not contain niobium as this element promotes SCC in the weld metal.

6.8 AMINE SCC

Over a period of years stress corrosion cracking has been detected in a number of units utilising amine solutions to remove H₂S and/or CO₂ from refined product streams.⁽⁸⁷⁾ The process involves absorption of H₂S and CO₂ in a water-based solution of either Monoethanolamine (MEA) or Diethanolamine (DEA) at high pressure, with stripping taking place in another vessel aided by low pressures and increased temperature.

The cracking is intergranular and usually located in high stress areas, generally adjacent to welds.^(88,89,90) The cracking tends to be transverse in the welds and longitudinal in the HAZ's whilst both transverse and longitudinal cracking may occur in the parent material adjacent to the weld.

A recently conducted Japanese survey indicated that cracking had been detected in 6% of DEA plants, 3% of Benfield and 21% of MEA plants. Cracking has been detected in almost all items of equipment within MEA plants⁽⁹⁰⁾ but predominantly within the absorbers, regenerators and interconnecting piping. The Japanese survey indicated that absorbers were more susceptible to cracking than regenerators with a failure ratio of 27 to 15 respectively. It also appears that cracking is most likely to occur in the lower part of the absorber.⁽⁸⁹⁾

In amine service SCC is limited to carbon steels. Higher strength materials are more susceptible than lower strength materials. In MEA service, SCC has only been detected in un-stress relieved material. However in DEA service, cracking has been found in PWHT'ed welds.

Several environmental influences have been observed. Temperature may have some effect on the speed or severity of cracking; however cracking occurs at all temperatures present within MEA plants, which may range from ambient up to 150°C.^(87,88,89)

Cracking is not believed to occur with fresh (as delivered) MEA solution and it is not clear precisely which component in the operating solution causes cracking. A typical operating solution would contain

H ₂ S and/or CO ₂ in solution			
MEA in water	-	20%	(22,5% max)
Heat stable salts	-	1,5%	(3.0% max)
Cl ⁻	-	40ppm	(300ppm max)
CN ⁻ + CNS	-	250ppm	(1000ppm max)

It is reported that the presence of CN is not required for cracking and that cracking occurs in both rich (saturated with H₂S, CO₂) and lean (after H₂S/CO₂ is stripped out) solutions. More cracking is found associated with lean solutions.

Cracking is prevented by requiring PWHT of all vessels and piping in amine service, regardless of strength of material or environmental conditions such as temperature or MEA solution concentration. An alternative approach where PWHT is not feasible is to fabricate from a non-susceptible material such as 304L stainless steel.

6.9 SCC IN COAL GAS LIQUID

Stress corrosion cracking has been encountered in carbon steel lines carrying gas liquor. The cracks are restricted to the weld area and are intergranular and branched. Post weld heat treatment has not proved successful in preventing the re-occurrence of SCC. The equipment that has been affected is mostly in the ammonia recovery plant. The agent responsible for SCC is thought to be an aqueous solution of NH₃, CO, CO₂, H₂S and CN.^(91,92) The affected equipment operates in the temperature range 35 to 120°C at a pH greater than 7. The hardness of the material is below 200 BHN.

It has been suggested that SCC in gas liquor is associated with ammonia stripping and that cracking can be prevented by maintaining the ammonia concentration above certain critical levels.⁽⁹³⁾

6.10 SCC IN WET MIXTURES OF CARBON MONOXIDE AND CARBON DIOXIDE

Transgranular stress corrosion cracking has been observed in as-welded carbon steel lines carrying wet mixtures of CO and CO₂ gas.⁽⁹⁴⁻¹⁰⁰⁾ Cracking is supported over a wide range of CO/CO₂ gas mixtures, however lowering of the CO partial pressure is reported to increase the stress needed to cause CO/CO₂ SCC and lengthen the time necessary to initiate cracks.

Stress corrosion cracks have been produced at carbon monoxide partial pressures (PCO) as low as 6,9 kPa, but is reported to be slow below 12,6 kPa PCO.⁽⁹⁴⁾⁽⁹⁶⁾ Published test results and service experience have been reviewed to determine the range of CO and CO₂ partial pressures that support SCC. These are summarised in Table 7 and Figure 19. Stress corrosion cracking has been recorded in all the gas mixtures listed. The figure illustrates a potential for cracking in almost any wet mixture of CO and CO₂ gas.

The agent responsible for cracking is water into which CO and CO₂ gas has been dissolved. Dry gas mixtures of CO and CO₂ do not support SCC. The severest cracking occurs in the gas phase on surfaces wetted by condensate. Cracking is less prevalent on immersed surfaces. Splash zones are highly susceptible.⁽⁹⁹⁾

CO/CO₂ stress corrosion cracking is strongly influenced by temperature. It is most prevalent in the temperature range 20°C to 60°C. Cracks have been produced in four CO/CO₂ environments at temperatures up to 150°C but cracks are unlikely above 75°C due to lowering of carbon monoxide solubility in water and reduced CO absorption onto the metal surface. In the absence of oxygen, cracking is slow below 40°C and is rare below 20°C due to a lowering of the aqueous CO₂ corrosion rate.

Experiments in wet CO/CO₂ environments to identify materials that are immune to SCC have revealed that alloy additions of at least 9% chromium are required to prevent cracking.⁽¹⁰⁰⁾ No test results are reported for the performance of welds. Steels with high alloy additions of chromium (>9%) are difficult to fabricate and are not available in all product forms. Consequently type 304 austenitic stainless steel is the cheapest material that is immune to this type of SCC and is at the same time a practical choice for construction of complicated pressurised piping and vessel systems.

For every material/environment combination causing SCC there is a particular level of stress that must be exceeded before cracking will take place. The source of stress most usually responsible for SCC is residual stress remaining in weldments after welding. These stresses are typically near to the yield point of the material and can be reduced by applying a stress relief heat treatment. Provided the total stress is maintained below the threshold level for SCC, cracking can be prevented by post weld heat treatment. Threshold stresses as low as one third of yield have been reported for carbon steels in wet CO/CO₂ mixtures. This would suggest that a stress relief would not be totally successful in removing SCC from this particular system.

TABLE 7 CARBON MONOXIDE AND CARBON DIOXIDE MIXTURES THAT HAVE CAUSED SCC

SOURCE	PCO (kPa)	PCO ₂ (kPa)
INDUSTRIAL PROCESS PLANT		
Total Feed	200	240
Fresh Feed	420	100
INDUSTRIAL PROCESS PLANT		
Separator Drum	30	250
Lean gas inlet	55	400
PILOT PLANT		
Rich gas	380	180
PILOT PLANT		
Lean gas	48	260
KOWAKA and NAGATA ⁽¹⁰⁰⁾	1200	245
TANIMURA ⁽¹⁰⁶⁾	130 263 530 1053	70 141 283 567
WATERVLIET ARSENAL ⁽¹⁰⁵⁾	137	689
SHELL ⁽⁹⁹⁾	70 280 520	860 1700 1500
KOWATA and NAGATA ⁽¹⁰⁰⁾	260 100 50 10 260 260	140 160 180 170 10 10
K DUNLOP ⁽⁹⁸⁾	75	Not stated
BROWN and HARRISON ⁽⁹⁴⁾	13	Not stated
BRITISH GAS ⁽⁹⁴⁾	6,9 138	Not stated Not stated

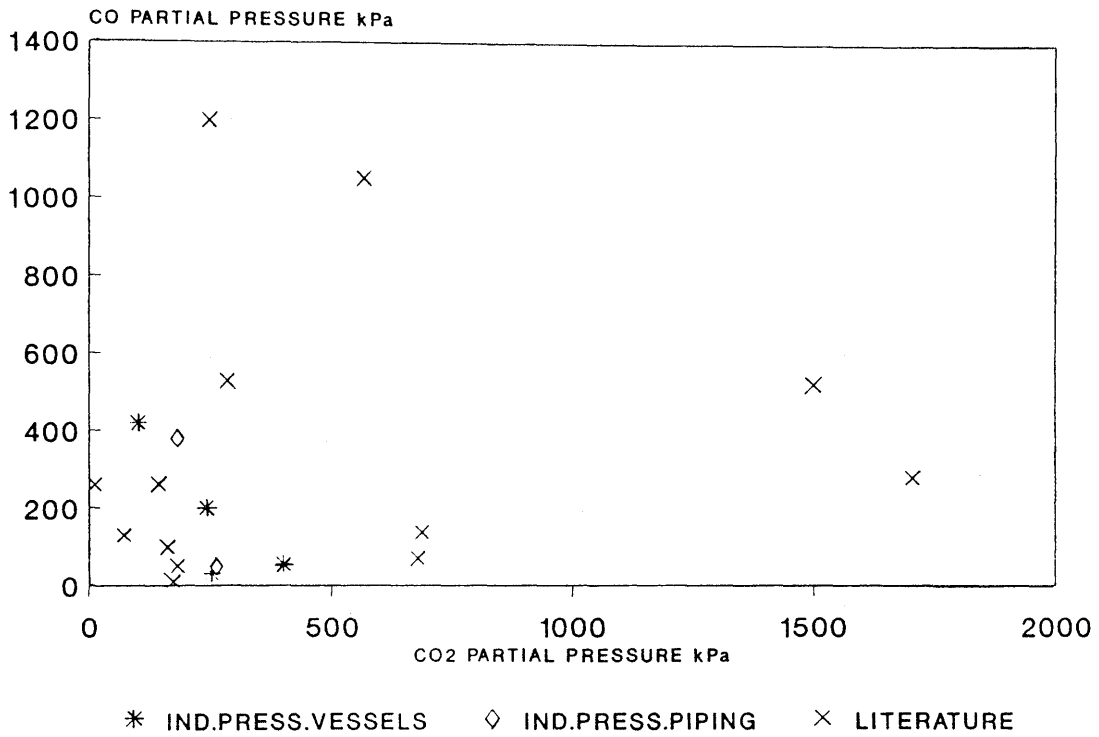


FIGURE 19 CO and CO₂ mixtures which have caused SCC in carbon steel (from Table 7).

The mechanism for CO/CO₂ is reported to be one of anodic dissolution at ruptures in the passive surface film. In CO/CO₂ gas systems an aqueous solution of CO₂ is the principal corroding agent, and surface absorption of CO provides passivation. The application of stress disrupts the surface passive layer of absorbed CO allowing localised aqueous corrosion to take place at the film breakage. Propagation of an anodic SCC crack requires the existence of a critical balance between corrosion and passivation so that the walls of the crack re-passivate whilst the crack tip remains active. Complete re-passivation results in crack arrest. In contrast, failure to re-passivate the crack walls will result in less harmful general corrosion or pitting corrosion. The range of SCC susceptibility is therefore narrowed to a band of corrosion potentials within which the steel exhibits transpassive behaviour. Dunlop and Olson⁽⁹⁸⁾ report cracking in the range -475 to -575 mV SCE. This is supported by results obtained by Harrison⁽⁹⁴⁾ who reports cracking at a similar range of potentials with maximum crack growth at -475 mV SCE. Berry and Page⁽⁹⁶⁾ found SCC at potentials between -510 and -685 mV. Intergranular SCC in carbonate has been recorded between -450 and -625 mV SCE. The schematic in Table 8 reflects the corrosion behaviour of carbon steel in aqueous solutions of CO and CO₂ gas. Species other than CO and CO₂ may play a supporting role by promoting either corrosion or passivity.

TABLE 8 CORROSION BEHAVIOUR OF CARBON STEELS IN AQUEOUS SOLUTIONS OF CO AND CO₂ GAS

Material performance	Severe general corrosion	Corrosion and SCC	Severe SCC	Moderate SCC	Shallow Surface Cracks	Shallow Pits	
Behaviour	Corrosive	Transpassive				Passive	
Description	A passive film is not formed	A passive film is formed but is ruptured by the application of stress. Material exposed at film ruptures is slow to re-passivate and localised metal loss by anodic dissolution results in SCC				A passive surface is formed and full passivity is maintained	
Environmental condition	← Increasing corrosivity promoted by: Higher PCO ₂ Higher PO ₂ Higher total acids			→ Increasing passivity promoted by: Higher PCO and some organic compounds			

Carbon monoxide is able to poison the hydrogen recombination reaction ($H + H \rightarrow H_2$) in much the same way as H_2S in sour gas systems and cathodic stress corrosion cracking (hydrogen induced) has been reported in wet CO/CO_2 gas systems under certain conditions. High pressure carbon dioxide gas with carbon monoxide absent has also promoted similar cracking in contact with susceptible material.⁽⁹⁷⁾ Materials susceptible to hydrogen induced cracking are usually recognised as high strength carbon and low alloy steels having hardnesses greater than 240 Hv10 although cracking can occur in lower strength (softer materials) if the environment is severe.

Hannah, Newman and Proctor⁽¹⁰¹⁾ carried out slow strain rate tests in pressurised $CO-CO_2$ mixtures. They found that at atmospheric pressure cracking was promoted in all environments that contained CO_2 regardless of the presence of CO . Cracking was increased by cathodic polarisation but was reduced by anodic polarisation, suggesting that the cracking mechanism was hydrogen embrittlement. Additionally cracking on the slow strain rate test specimens was restricted to the necked region, a result typical of hydrogen embrittlement in low strength carbon steels.

At elevated pressures cracking was promoted by both anodic and cathodic polarisation. Under cathodic polarisation the cracks were again restricted to the necked region and the failures were attributed to hydrogen embrittlement. When anodic polarisation was applied the cracks occurred along the whole of the gauge length suggesting stress corrosion rather than hydrogen embrittlement. At the free corrosion potential the mechanism was also stress corrosion. However Hannah et al⁽¹⁰¹⁾ rejected the theory of Brown⁽⁹⁴⁾ that the mechanism was one of anodic dissolution by wet CO_2 corrosion at ruptures in a passive film produced by CO absorption. As an alternative, it was suggested that crack advance was by discontinuous cleavage nucleated in a thin surface film. It was believed that in the C-Mn steel/ $CO-CO_2-H_2O$ system cleavage occurred in a thin, carbon-hardened film produced by electrochemical reduction of CO . The system was considered analogous to the C-Mn steel/anhydrous ammonia system.

Historically some interest was shown in CO/CO_2 SCC when cracking was encountered in town gas systems supplemented with high pressure reformed gas but waned when natural gas was introduced as an alternative energy source. Further studies were conducted when interest in synthetic fuel was high in the 1970's and a comprehensive investigation was made in Japan following failure of high pressure CO/CO_2 gas cylinders.⁽¹⁰⁰⁾ Industrial experience of CO/CO_2 is otherwise very limited.

Town gas systems operated for many years with gas mixtures of CO and CO₂. However the early systems were low pressure (water gauge) and were contained in flanged cast iron lines. No cracks (SCC) were recorded. Later high pressure systems were introduced (approximately 20 bar) utilising reformed gas. The pipes were mainly 4 to 6 inch but sometimes up to 16 inch and were fabricated from API 5L grades x45 and x52, medium strength carbon steels. Stress corrosion cracks were found associated with welds in non stress-relieved pipe after 5 to 6 years' service. The presence of cracks in the high pressure piping, but not in low, was attributed to higher stresses and higher gas partial pressures. Cracking could be reproduced in the laboratory and some of the parameters were evaluated.

Service experience of palliative measures was not gained as the problem was solved by the discovery of natural gas which does not contain CO and which made the high pressure reformed gas systems redundant.

In the chemical industry SCC was encountered in a CO/CO₂/H₂ regenerated gas compression and wash system (see Figure 20) within six months of startup. Leaks were detected in the vicinity of weldments in carbon steel lines. To prevent cracking stress-relief was specified and an upper limit of 500 MPa was placed on the tensile strength of the material. The plant has operated since 1959 without further significant problems.

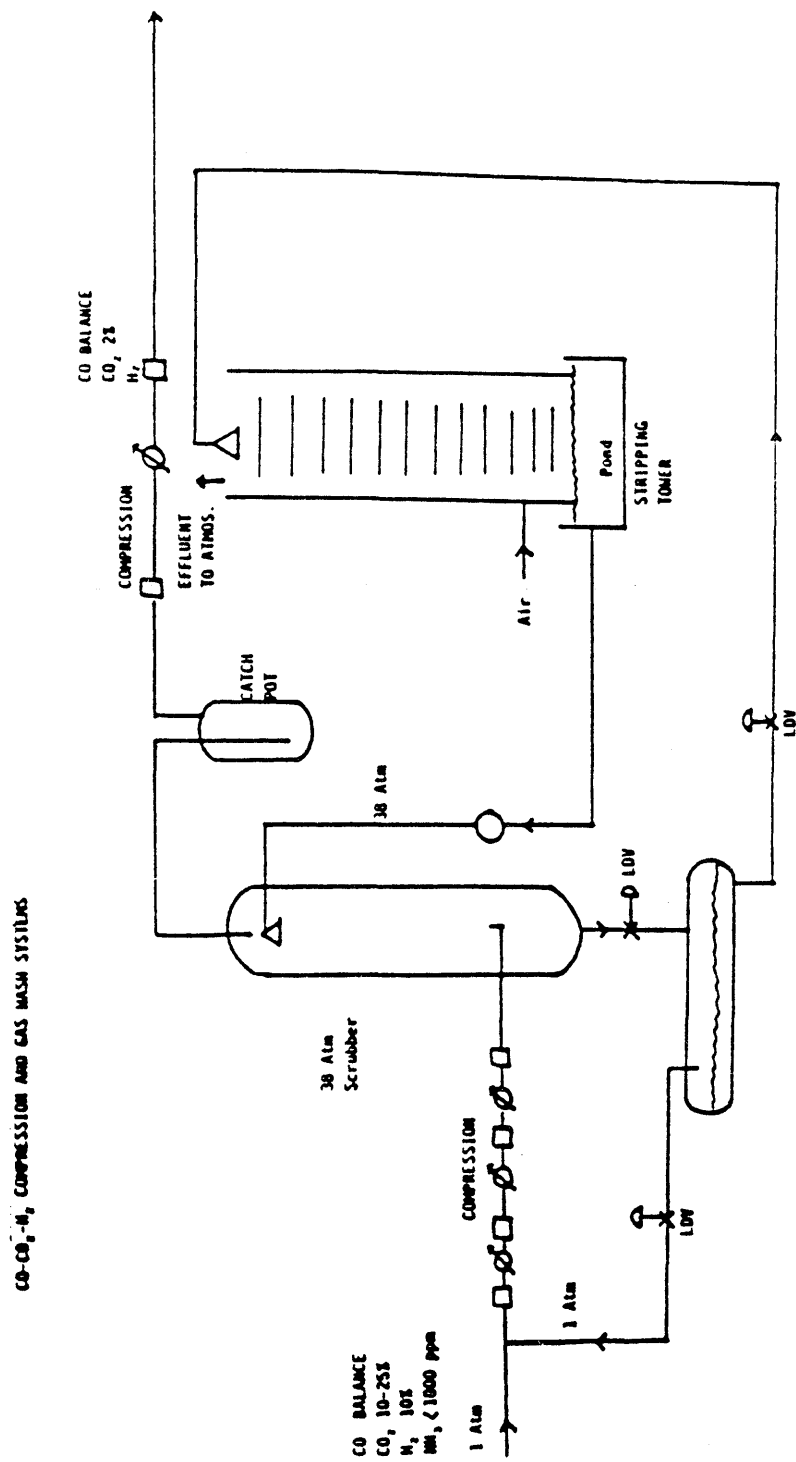


FIGURE 20 Process flow diagram for CO/CO₂/H₂ regenerated gas compressions and wash system

A German industrial gas compression system suffered CO/CO₂ stress corrosion cracking. The gas composition, pressure and temperature varied through the plant within the following ranges :

CO ≈ 75%; CO₂ 2,5 to 3,5%; acetylene 17 to 20%;

water ppm pressure 4 to 110 bar; temperature 35 to 150°C.

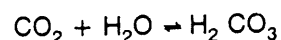
Cracks were found in welds and in parent metal where the mechanical stress was high (elbows). The original St 42,2 carbon steel cracked after 2 to 5 years and was replaced with a lower strength material, St 35,8 post weld heat treated. The replacement cracked again after two years' service. The presence of chlorides prevented the use of austenitic stainless steel. The current practice is to regularly crack-detect using magnetic particle testing. If the cracks are 1 mm to 2 mm deep they are run for six months and retested.

Although industrial experience of CO/CO₂ stress corrosion cracking is limited some support for the use of stress relief to mitigate cracking was found. One user however found little improvement after stress relief. It was not unusual for there to be a long period between startup and the incidence of stress corrosion cracking if cracking was initiation controlled. However once started the crack growth is fairly rapid. Cyclic loading accelerates crack growth and should be minimised.

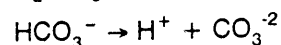
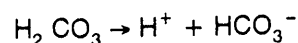
6.10.1 General Corrosion in Wet Carbon Dioxide

The CO-CO₂-H₂O system is in effect an inhibited wet carbon dioxide environment, some of the parameters that affect wet CO₂ corrosion might therefore be expected to influence CO-CO₂-H₂O stress corrosion cracking, particularly if the mechanism is one of anodic dissolution at film ruptures. Cracking by hydrogen embrittlement would also be expected to show some dependence on the rate of CO₂ corrosion as presumably more hydrogen will be charged at higher corrosion rates. It is perhaps useful then to review general corrosion in wet carbon dioxide.

Briefly, carbon dioxide in solution forms carbonic acid by carbon dioxide hydration. ⁽¹⁰⁷⁾



Carbonic acid undergoes two dissociations, firstly to bicarbonate and then to carbonate in the following sequence: ^(101,109)



The corrosion rate in wet carbon dioxide service is predominantly controlled by the pH of the condensate.⁽¹¹⁰⁾ This is in turn related to the partial pressure of carbon dioxide (PCO_2) since this determines how much carbonic acid is formed by controlling the amount of gas dissolved in the liquid ⁽¹⁰⁹⁾ (Figure 21). Temperature also affects the corrosion rate through its influence on the kinetics of the corrosion reactions and carbon dioxide solubility. The relationships between carbon dioxide partial pressure and corrosion rate are described in Figures 22 and 23. A rule of thumb emerges for corrosion of carbon steel ^(111,112)

- $PCO_2 > 2 \text{ bar}$ severe corrosion
- $PCO_2 \text{ 0,5 to 2,0 bar}$ may corrode
- $PCO_2 < 0,5 \text{ bar}$ not corrosive.

Except at very high partial pressures the corrosion rate of carbon steel below 40°C is also quite low.

Three hundred series austenitic stainless steels (type 304, 304L, 321 and 347) are fully resistant to corrosion by wet carbon dioxide. Certain ferritic grades containing more than 12% chromium have useful resistance to wet carbon dioxide but can be difficult to fabricate. ⁽¹¹⁴⁾

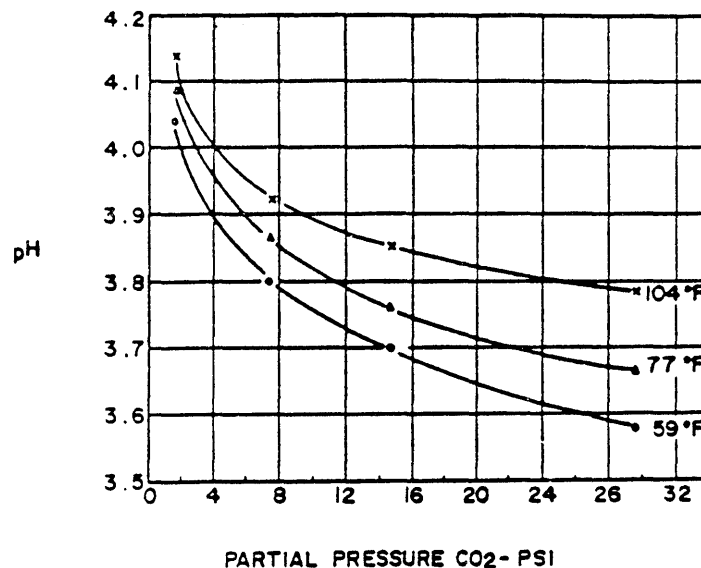


FIGURE 21 Influence of CO_2 partial pressure on the pH of condensate. (After De Berry ⁽¹⁰⁷⁾)

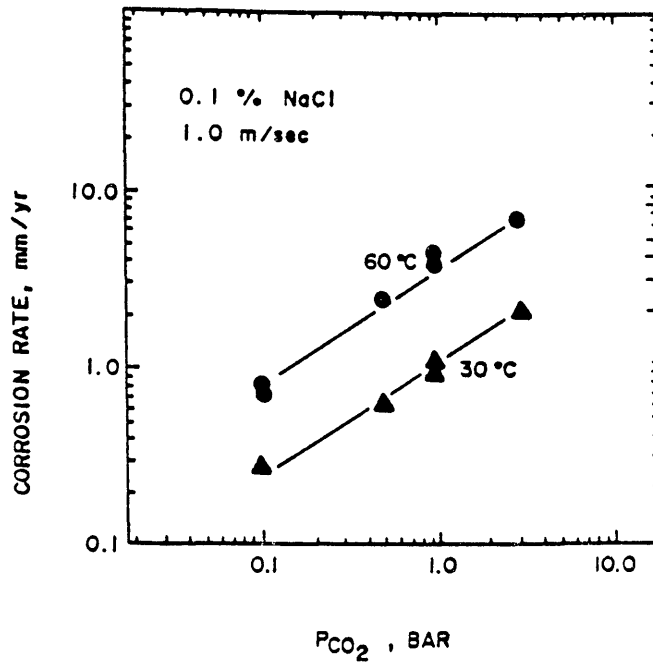


FIGURE 22 Influence of temperature of the corrosion rate of carbon steel and various stainless steels in wet carbon dioxide PCO_2 , 1 bar. (After Sato⁽¹⁰⁶⁾)

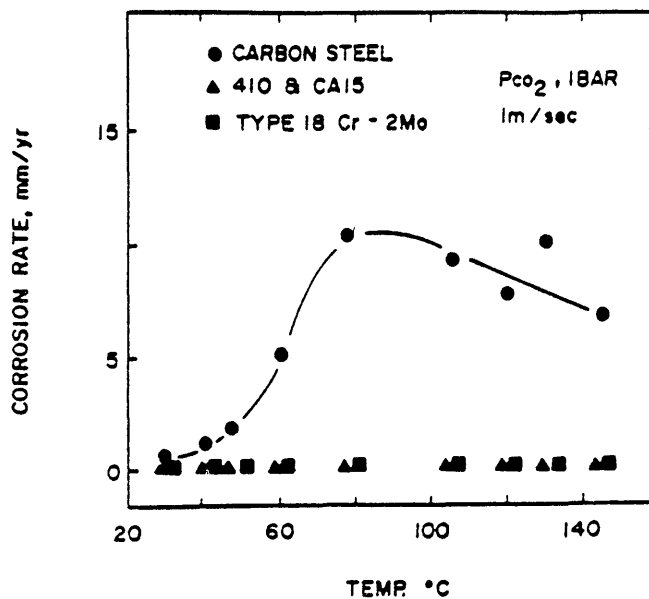


FIGURE 23 Influence of the partial pressure of carbon dioxide on the corrosion rate of steel in wet CO_2 environments. (After Sato⁽¹⁰⁶⁾)

6.10.2 General Corrosion in Carbon Monoxide

Carbon monoxide is not corrosive to carbon steels at low pressures, however at high pressure corrosion is severe even at low temperature.

Corrosion is controlled by pressure and temperature. It appears that steel is corroded by conversion of iron into carbonyls. Resistance to corrosion by carbon monoxide is achieved by alloy additions of chromium. Figure 24 gives details of the reported corrosion rates of various materials in high pressure carbon monoxide.

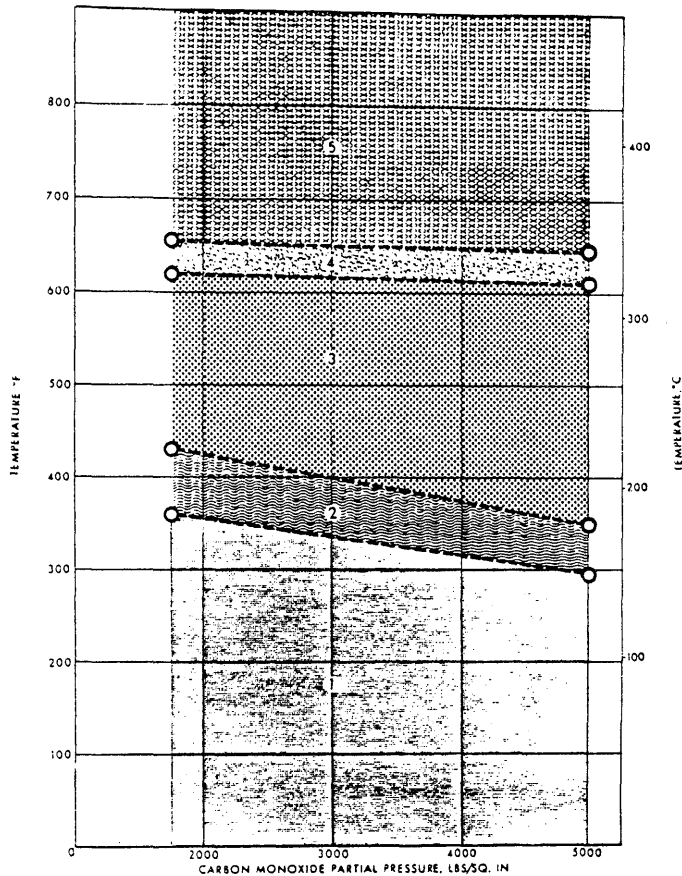


FIGURE 24 Resistance of Materials to carbon monoxide corrosion. ⁽¹¹⁶⁾

LEGEND FOR CARBON MONOXIDE GRAPH

Materials in a particular shaded zone have reported corrosion rates of 20 mpy or less

ZONE 1	ZONE 2	ZONE 3	ZONE 4	ZONE 5
5Cr-½Mo steel				5Cr-½Mo
12Cr Types 405,410	12Cr Types 405,410		12Cr Types 405,410	12Cr Types 405,410
17Cr Type 430	17Cr Type 430		17Cr Type 430	17Cr Type 430
18Cr-8Ni Types 321,347	18Cr-8Ni Types 321,347	18Cr-8Ni Types 321,347	18Cr-8Ni Types 321,347	18Cr-8Ni Types 321,347
25Cr-20Ni Type 310	25Cr-20Ni Type 310	25Cr-20Ni Type 310	25Cr-20Ni Type 310	25Cr-20Ni Type 310
	27Cr Type 446	27Cr Type 446	27Cr Type 446	27Cr Type 446
5Mn Bronze	5% Manganese	5Mn Bronze	5Mn Bronze	5Mn Bronze
Carbon Steel	Bronze			Carbon Steel

STUDY OF CO-CO₂ SCC AND ITS PREVENTION IN CO-CO₂ GAS MIXTURES

Stress corrosion cracking has been observed in carbon steel piping and vessels at a pilot plant and two industrial gas processing plants. Cracking took place in two principal gas systems, having nominal gas compositions of 36% H₂, 1,7% CO, 12% CO₂, 36% CH₄, and 69% H₂, 10% CO, 11% CO₂, 3% CH₄ respectively. The gas systems are referred to as lean and rich gas, identified by their CO content. For SCC to take place it is necessary to have three factors present. These are :

1. a high tensile stress;
2. a susceptible material;
3. a promoting (SCC) environment.

Removal of any one of these will prevent cracking, and forms the basis for solutions to SCC problems. With this in mind the options to negate stress corrosion cracking in CO-CO₂-H₂O systems were reviewed and are summarised in Decision Tree 1 (Figure 25).

The cause of cracking was identified as wet mixtures of carbon monoxide and carbon dioxide gas, non of which can be removed from the process environment. Coatings were not considered to be a viable long term solution for a complicated process plant where the high number of bends and fittings gives rise to installation and maintenance problems. It was also considered that the longterm effectiveness of coatings could not be guaranteed in an environment that was predominantly gaseous. Once these options had been eliminated, four areas for further study were identified from the decision tree. These were:

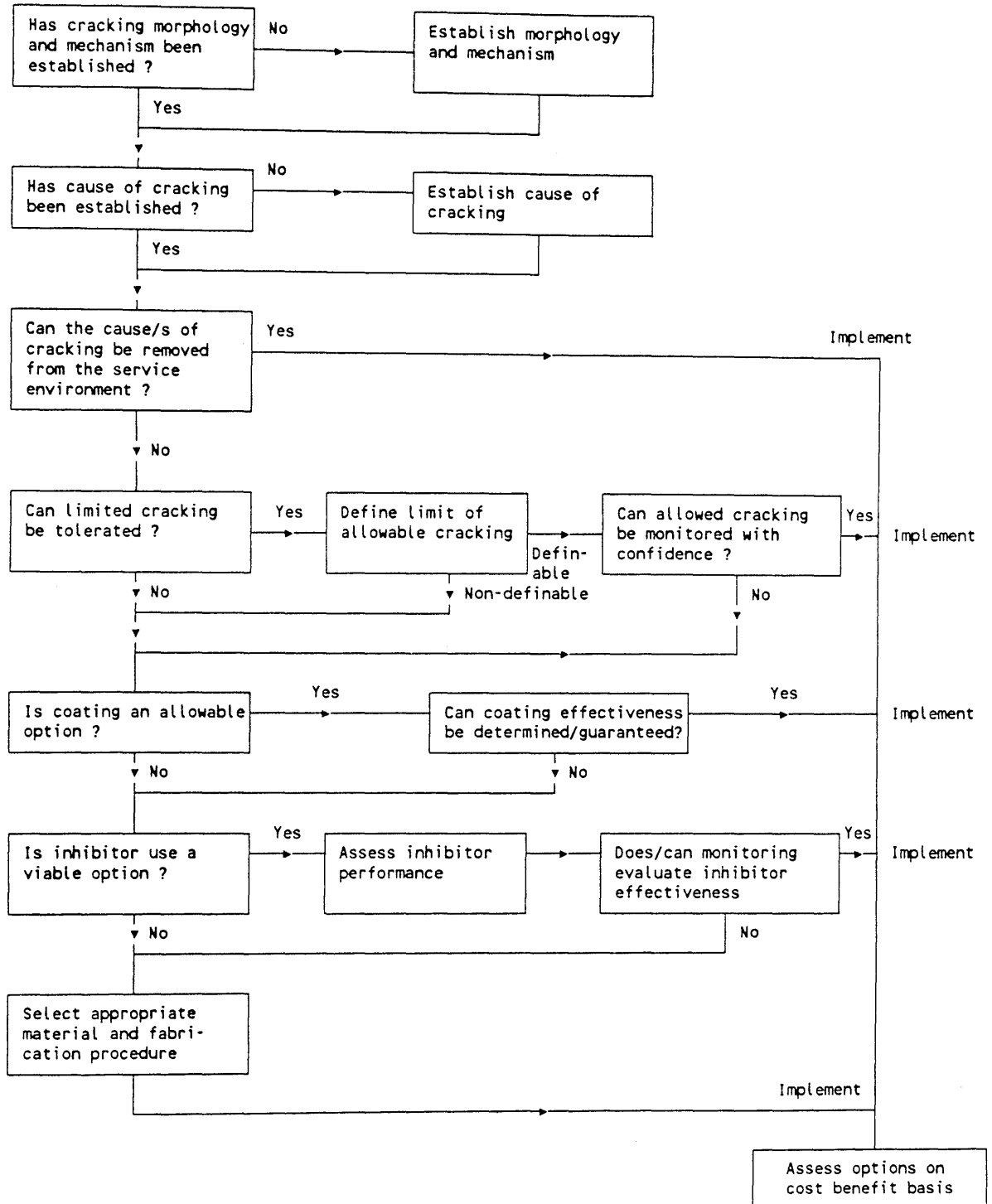
1. Characterisation of crack morphology.
2. Determine the tolerance for limited cracking by establishing crack growth rates.
3. Evaluate inhibitor additions.
4. Evaluate alternative materials and fabrication procedures.

It was also recognised that cracking occurred in a narrow potential range of about 150 mV. It was therefore feasible that fluctuations in operating parameters might cause the process environment to move in and out of the cracking regime. If this was the case then an opportunity would exist to prevent SCC by adjustment to the process. There was therefore a need to firstly understand the electrochemistry leading to SCC in wet CO-CO₂ and then monitor the system on line.

FIGURE 25

DECISION TREE - CRACKING OF PIPING AND VESSELS
USED TO CONTAIN MIXTURES OF CO AND CO₂

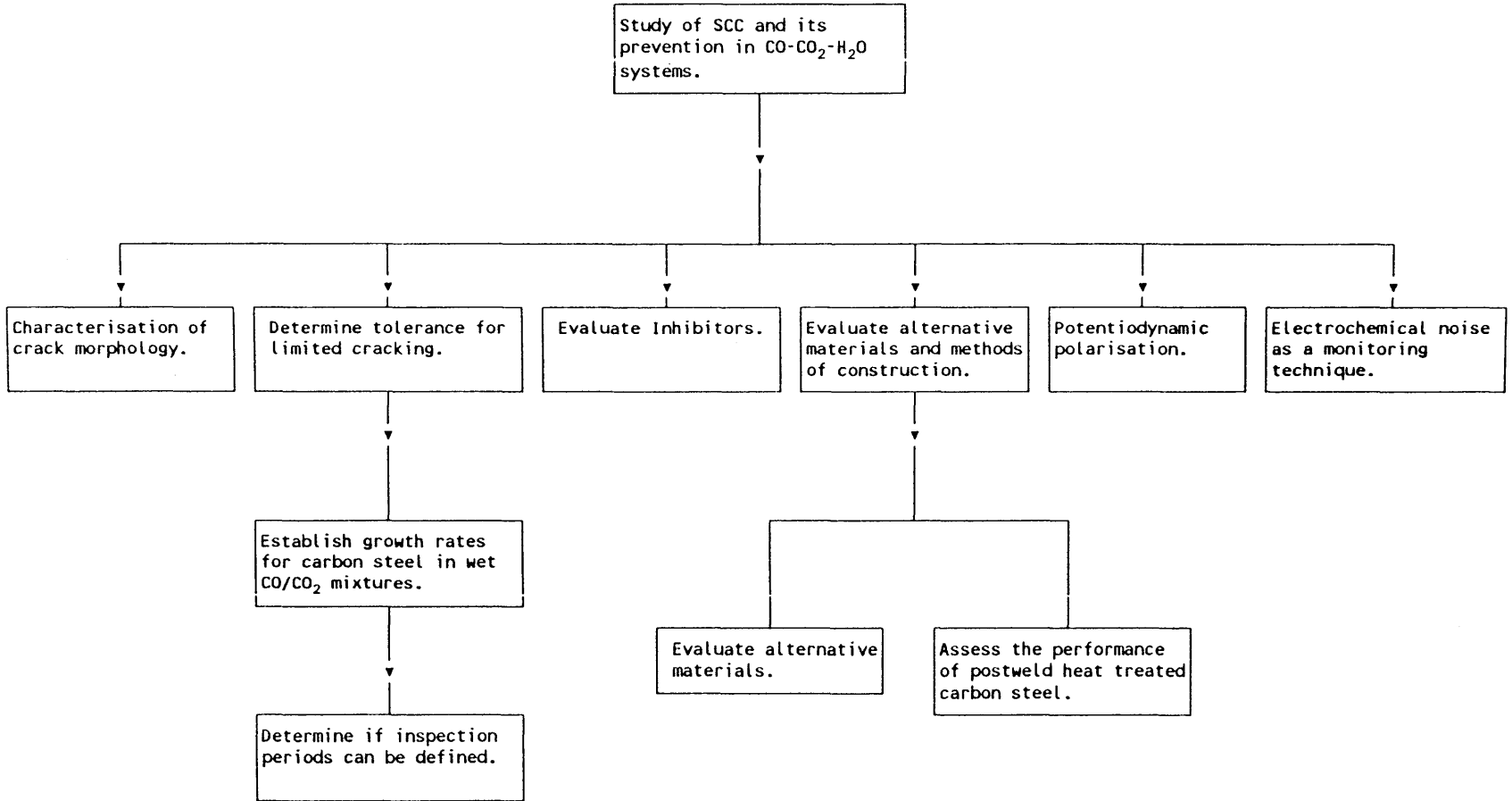
CURRENT STATUS



On-line monitoring would also be important to support any inhibitor dosing programme. Electrochemical noise (ECN) monitoring was the most attractive technique for monitoring on line condensing systems and it was added, together with potentiodynamic polarisation studies to the list of topics for further investigation.

In this way seven areas of research were defined. These are shown in Figure 26 as a development of the decision tree (Figure 25) and were;

1. Characterisation of crack morphology.
2. Determination of stress corrosion crack growth rates in CO-CO₂-H₂O systems.
3. Evaluation of inhibitor additions to CO-CO₂-H₂O systems.
4. Evaluation of alternative materials.
5. Assessment of the performance of post weld heat treated carbon steel.
6. Potentiodynamic polarisation studies in the CO-CO₂-H₂O system.
7. Assessment of electrochemical noise as a technique for on line monitoring SCC in wet CO/CO₂ gas systems.



8 CHARACTERISATION OF CRACK MORPHOLOGY

It has been indicated that a wide variety of wet CO/CO₂ gas mixtures are able to promote SCC in stressed carbon steel. The piping and vessels at a pilot plant and two operating plants were opened and after first magnetic particle testing to identify cracked areas, samples were removed for metallography. From this exercise it proved possible to characterise the morphology of cracks found at various locations in the plant depending upon the prevailing operating conditions. Table 9 summarises the samples examined and the nominal operating conditions. Unless otherwise stated the materials were SA106 Gr B carbon steel in the as welded condition that had been in operation for approximately 10 years. The carbon steel filler used to make the welds was E7018.

8.1 LOW PRESSURE LEAN GAS - OPERATING PLANT (PCO 45 kPa PCO₂ 225 kPa)

8.1.1 Compression Gas Line

The gas line saw environmental conditions typical of the low pressure lean gas system (PCO 45 kPa, PCO₂ 225 kPa). Shallow transverse cracks were found in the weld area of the 8" SA106 Gr B piping. Sectioning revealed steep sided pits giving rise to a saw toothed appearance. The walls of cracks often showed significant corrosion with corrosion sometimes growing laterally as if following the material texture. Narrow cracks typical of stress corrosion were often found at the base of the pits (Figures 27 and 28).

TABLE 9 SAMPLES EXAMINED AND THE NOMINAL OPERATING CONDITIONS

SYSTEM	NOMINAL OPERATING CONDITION Vol%	PCO kPa	DESCRIPTION
Low pressure lean gas, Industrial plant	H ₂ - 36 CO - 1,7 CO ₂ - 12,0 CH ₄ - 36 kPa - 1880 °C - 38°C	31	Compression gas line SA106
Lean gas, Pilot plant	H ₂ - 35 CO - 2,5 CO ₂ - 13,5 CH ₄ - 36 kPa - 2400 °C - 38-60°C	59	Carbon steel SA106
High pressure lean gas, Industrial plant	H ₂ - 36 CO - 1,7 CO ₂ - 12 CH ₄ - 36 kPa - 3000 °C - 40-50°C	51	Carbon steel lines SA106B Carbon steel A516 Gr.70 Drum
Rich gas, Industrial plant	H ₂ - 69 CO - 10 CO ₂ - 11 CH ₄ - 3 kPa - 1990 °C - 40-50°C	199	Main header, carbon steel Line SA106

Balance Argon, Nitrogen, Ethylene, Ethane, Propylene

8.1.2 Drum - Operating Plant

The drum was fabricated from SA516 Gr 70 carbon steel and operated at 55°C and 1880 kPa with a nominal lean gas composition consisting of CO 1,7%, CO₂ 12%, H₂ 36,0% and CH₄ 36,0%. Three-phase separation into gas, water and hydrocarbon was achieved in the drum. The nominal partial pressures of CO and CO₂ gas at the inlet were 45 kPa and 225 kPa respectively. The gas was saturated with both water and hydrocarbon. The vessel had been stress relieved.

The vessel welds suffered extensive cracking both transverse and longitudinal to the weld axis. The parent metal exhibited environmental damage which, viewed from the surface, resembled elongated pits of the order of 6mm long and roughly orientated normal to the principal stress. A cross-section revealed the presence of transgranular stress corrosion cracks several of which exhibited corroded walls and rounded tips which accounted for the erroneous pitting appearance when viewed from the surface (Figures 29, 30 and 31). Once again cavities were occasionally found spreading laterally from the crack wall (Figures 26 and 27). The depth of cracks after ten years service measured 1,0 to 1,5 mm.

8.2 LEAN GAS SYSTEM - PILOT PLANT

The pilot plant lean gas system was originally fabricated by oxy-acetylene welding which has a high heat input and can be expected to result in lower residual stress in the weld. In 1983 all welds in the lean gas system were X-rayed and 85% were found to suffer from "lack of penetration" which was not surprising as the practice at the time was to use a straight butt joint. Defective welds were replaced using present-day arc welding processes. In 1989 it was necessary to cut out some of the welds when random X-rays revealed "welding defects". It was possible to retrieve some of these sections. The nominal CO and CO₂ partial pressures at the Pilot plant are 59 kPa and 324 kPa respectively. Figure 32 shows the results of a magnetic particle inspection of the inside of the pipe showing multiple craze cracking. This form of attack is often termed etch corrosion at the plant. Cross-sections through the cracked areas are shown in Figures 33 to 37. A cross-section revealed a saw-toothed surface appearance similar to that found in the aeration gas line operating at slightly lower PCO and PCO₂ (Figure 33). The walls of the cracks had undergone significant corrosion and frequently resembled pits (Figure 35).

Occasionally narrow cracks more typical of stress corrosion were found at the root of pits (Figure 36).

In some cases cavities due to localised corrosion extended laterally from the walls of cracks or pits (Figure 35). Figure 37 shows a cavity at the base of a crack. This phenomenon was observed elsewhere in CO-CO₂-H₂O gas systems.

8.3 HIGH PRESSURE LEAN GAS

Samples were cut from field welds in a carbon steel line after ca 12 years' service at an industrial plant. Figure 38 shows typical crack indications transverse to the root of a girth weld. Similar cracks are just visible in the parent metal near to the weld. Sections removed through cracks in the weld metal are shown in Figure 39. The cracks are wide at the top, reminiscent of pitting described in previous paragraphs, however significant crack extension due to stress corrosion has taken place. The cracks were transgranular and reached depths up to 5 mm.

Cross-sections were taken through MPI crack indications found in the parent metal. The results are in Figure 40. Sub-surface linkage of corrosion pits has resulted in the porous appearance shown.

8.4 RICH GAS

The carbon monoxide partial pressure in the rich gas system is much higher than the lean gas systems (PCO 199 kPa compared with PCO ca 45 kPa). Cracks were more often found parallel to the weld axis but were also present transverse to the weld (Figures 41 and 42). Cross-sections through the cracks revealed that they penetrated deeply and occasionally extended through the wall thickness. The cracks were transgranular and extremely fine and multi-branched (Figures 43 and 44).

At one location shallow mesa corrosion characteristic of wet CO₂ corrosion was observed adjacent to a weld. Numerous small cracks were present within the corroded zones, contrasting with the main weld and the rest of the pipe material which was otherwise crack free (Figure 45). A cross-section through the localised corrosion revealed that it had occurred at a weld repair. The cracks were fine and branched and resembled other cracks found in the lean gas system.

8.5 MICROHARDNESS TESTING

The microhardnesses adjacent to the observed stress corrosion cracks were determined. The results are in Table 10.

TABLE 10 MICROHARDNESS RESULTS (100g LOAD)

SAMPLE	DPN HARDNESS Hv 0,01	AVG	MAX
Compression line HAZ	195, 189, 174, 171 *	177	189
Compression line weld metal	189, 163 *	176	189
Drum, parent metal	142, 212, 182, 222, 193, 188	189	222
Lean gas line HAZ	170, 179, 169, 179, 169	173	179
High pressure lean gas weld metal	269, 254, 256, 240, 247	249	256
Rich gas piping HAZ	173, 172, 180, 155, 175	171	180
Rich gas piping locally corroded weld repairs	260, 249, 251, 247, 270	255	270

* 50 g load.

A hardness of Rc 22 or 240 Hv10 is recognised as the value below which most ferrous materials have a low sensitivity to hydrogen induced cracking. With the possible exception of the repair welds in rich gas piping, none of the hardnesses of the materials examined indicated a particular sensitivity to hydrogen embrittlement. This result suggested that the cracking mechanism was anodic rather than cathodic.

8.6 SUMMARY OF METALLOGRAPHIC RESULTS

Figure 46 summarises the results of the metallographic examination by showing how the crack appearance changed as the carbon monoxide partial pressure increased. Pitting and general corrosion are favoured at low carbon monoxide partial pressures.

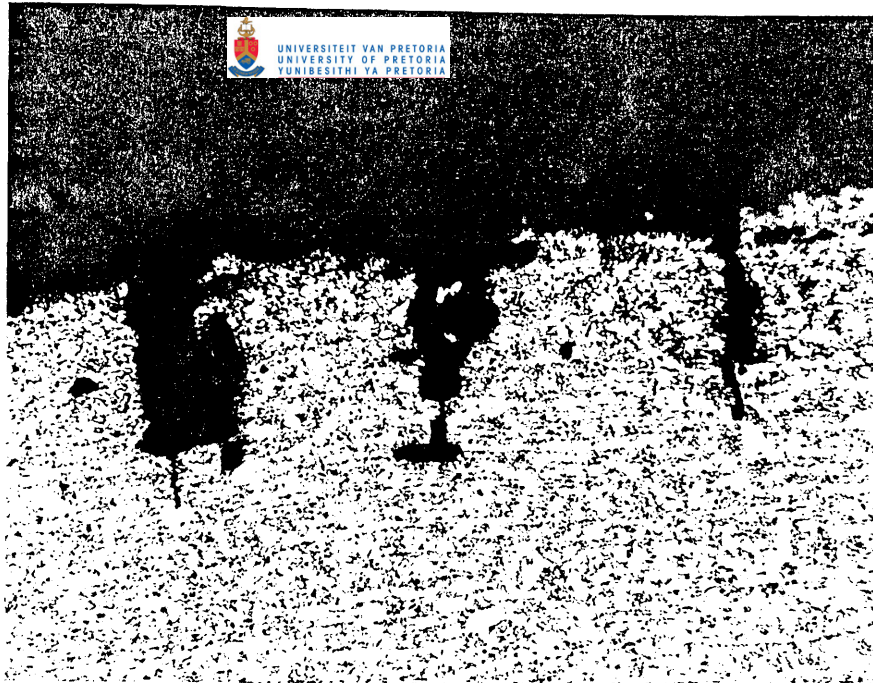


FIGURE 27 Magnification x100 Etch Nital

FIGURES 27 AND.28

Samples removed from carbon steel compression gas lines showing steep sided pits with small stress corrosion cracks initiating from the base of the pits.

The depth of the damage measured ca 0,5mm.
Total pressure 1880 kPa, 40°C.
PCO 45 kPa, PCO₂ 225 kPa.
Hardness 177 Av, 189 Max., Hv 0,01.

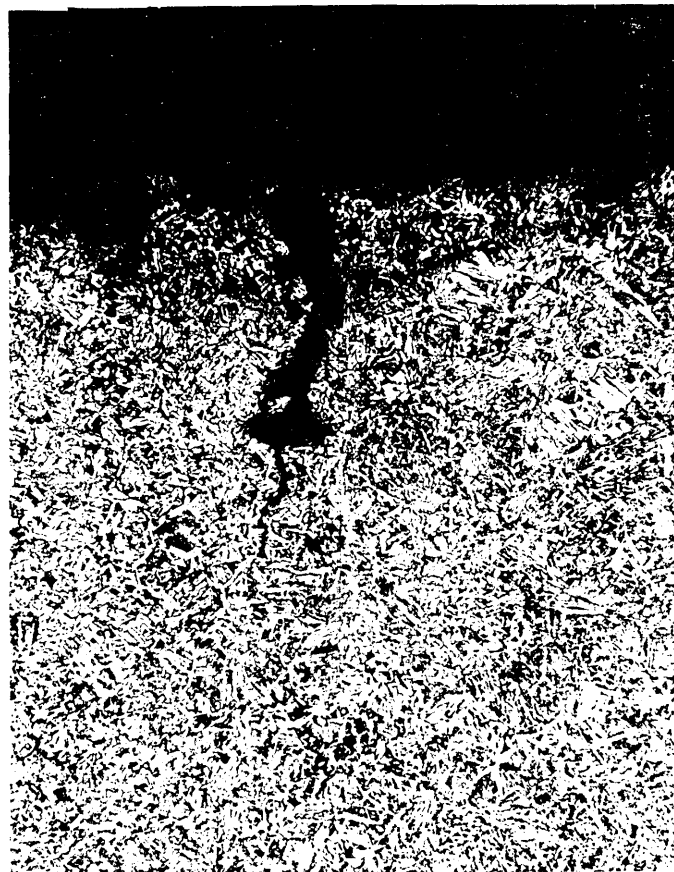


FIGURE 28 Magnification x100 Etch Nital

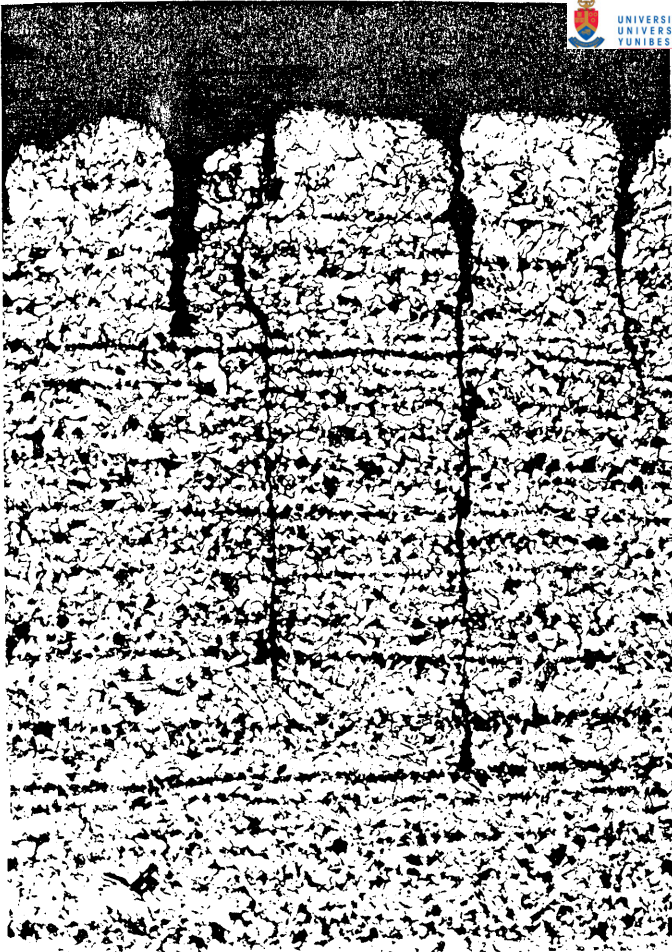


FIGURE 29 Magnification x100 Etch Nital

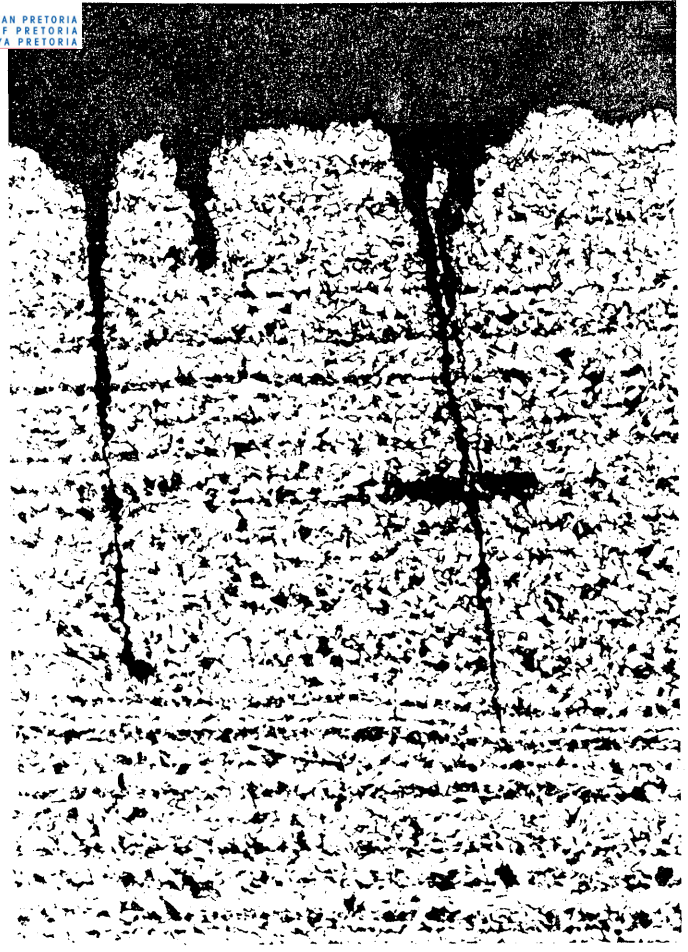


FIGURE 30 Magnification x100 Etch Nital

FIGURES 29 to 31 show stress corrosion cracks found in the parent metal of a drum. Widening of the crack due to corrosion of the crack wall had taken place. Cavities had been formed by corrosion spreading laterally from the crack wall.

Total pressure 1880 kPa, 55°C
PCO 45 kPa, PCO₂ 225 kPa
Hardness 189 Av 222 Max.

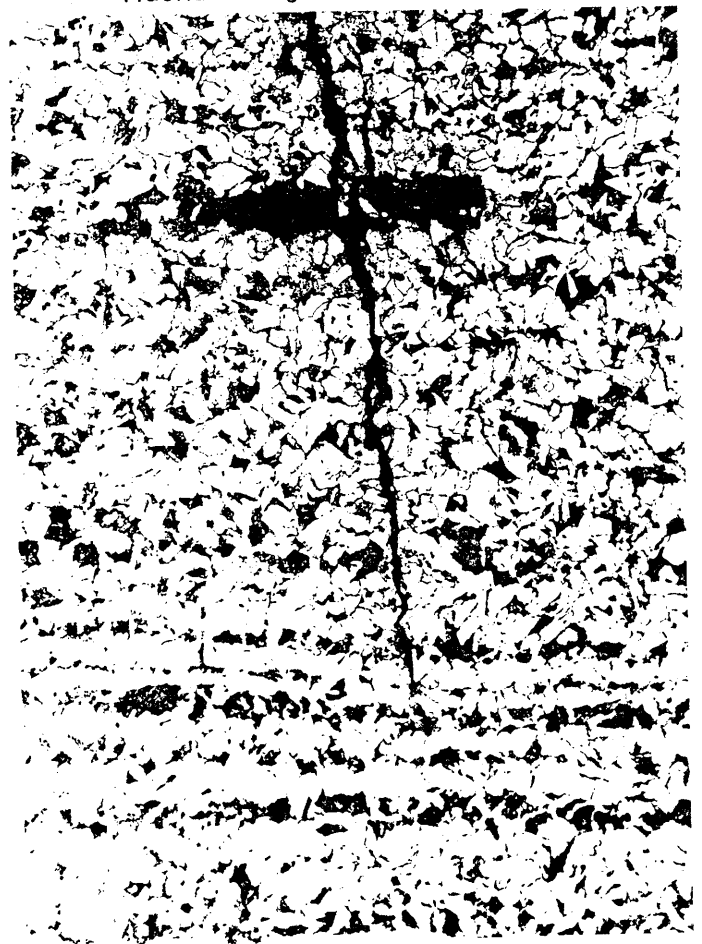


FIGURE 31 Magnification x200 Etch Nital



FIGURE 32 The results of magnetic particle inspection of the inside of a lean gas pipe removed from the industrial plant.

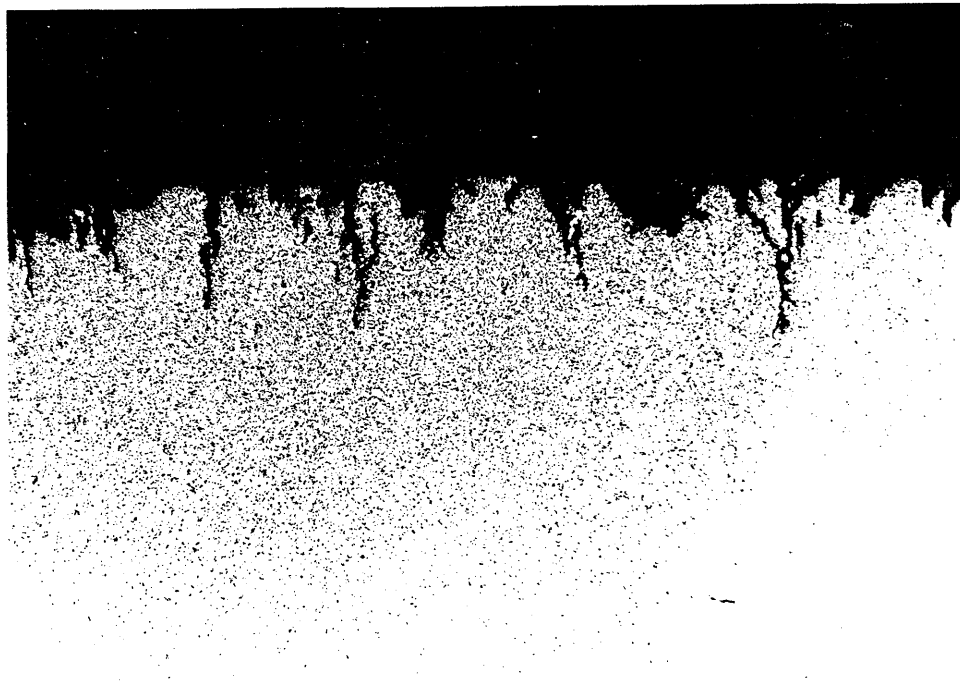


FIGURE 33 Cross-section through the cracks showing a saw-toothed appearance

Magnification x25 Etch Nital
Total pressure 2400 kPa, 40°C, PCO 59, PCO₂ 324 kPa
Hardness 173 Av., 179 Max., Hv 0,01

FIGURES 34 and 35 show cracks from the lean gas system at the industrial plant. Considerable corrosion has taken place at the crack wall resulting in the wide appearance of the cracks. Further corrosion led to an appearance that resembled pitting (Figure 35). Internal cavities due to lateral corrosion are also visible in Figure 34.

Total pressure 2400 kPa 40°C
PCO 59, PCO₂ 324 kPa
Hardness 173 Av., 179 Max., Hv 0,01

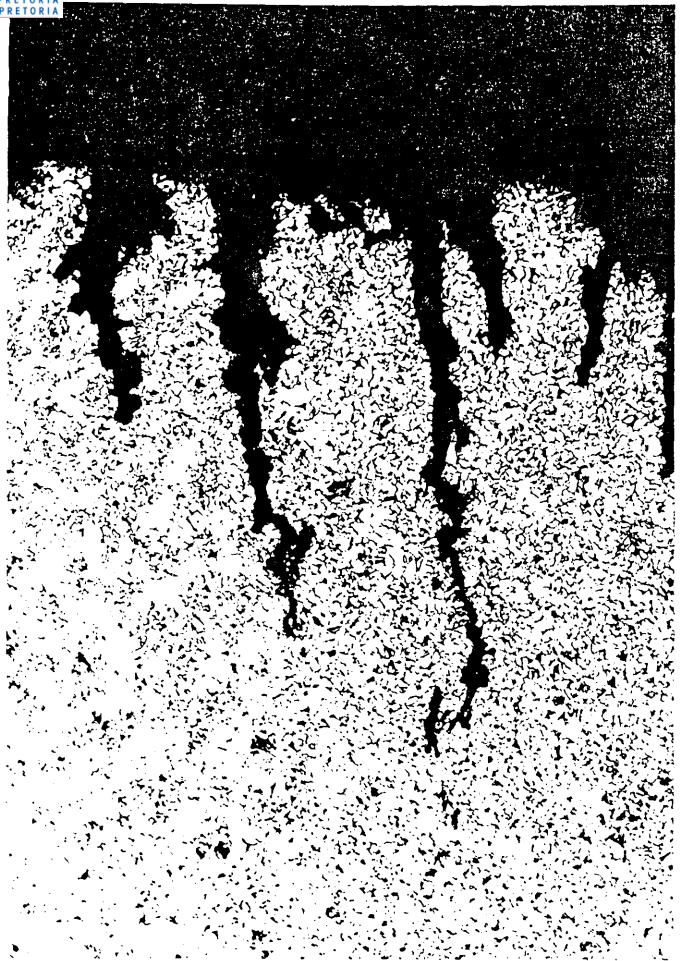


FIGURE 34 Magnification x100 Etch Nital



FIGURE 35 Magnification x100 Etch Nital



FIGURE 36 Fine crack more typical of SCC found at the base of corroded cracks found in the Pilot plant lean gas system.
Magnification x200 Etch Nital.

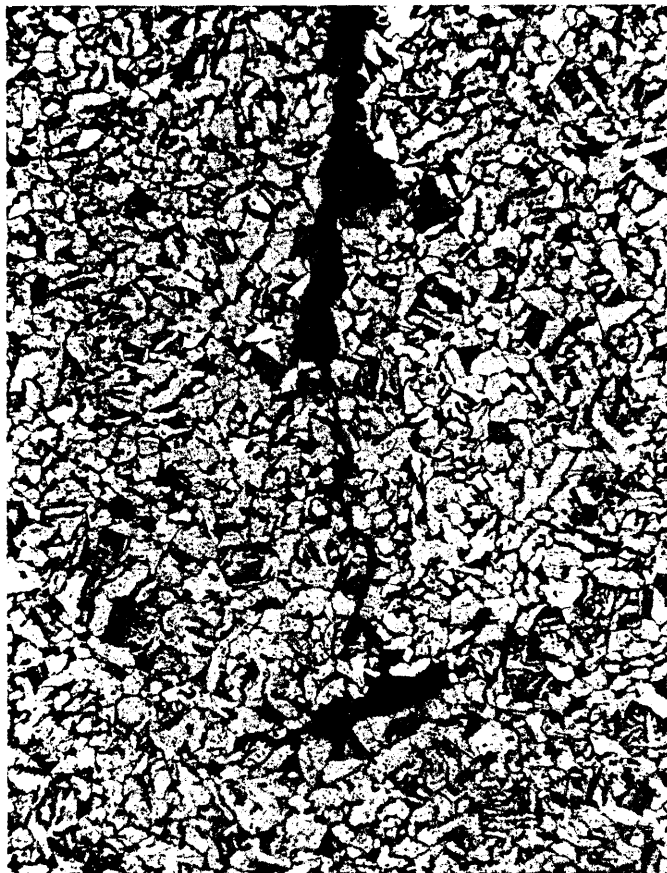


FIGURE 37 Cavity at the base of a crack in the same system.
Magnification x200 Etch Nital. PCO_2 59, PCO 324 kPa 60°C.

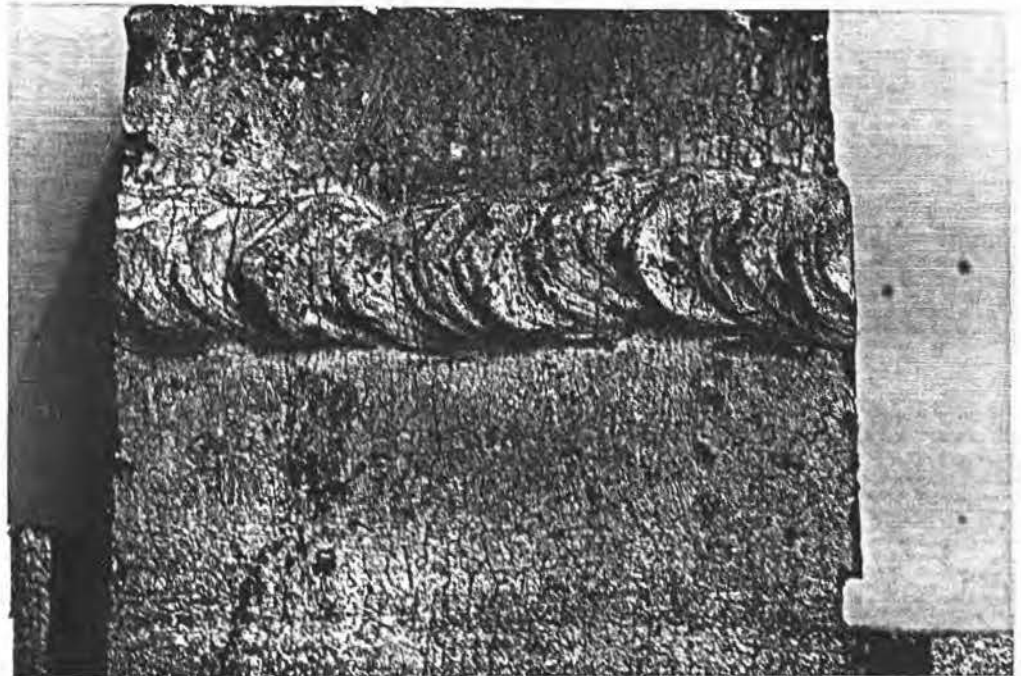


FIGURE 38 Typical crack indications transverse to the root of a girth weld in the high pressure lean gas system at the operating plant. Similar cracks are just visible in the parent metal next to the weld.

Magnification x100 Etch Nital.
Total pressure 3000 kPa 40 to 50°C
PCO 51 PCO₂
Hardness 249 Av., 256 Max.



FIGURE 39 A cross-section through cracks found in welds in the high pressure lean gas system at the operating plant. The cracks are wide at the top due to corrosion but are sharp and branched at the base, typical of SCC.

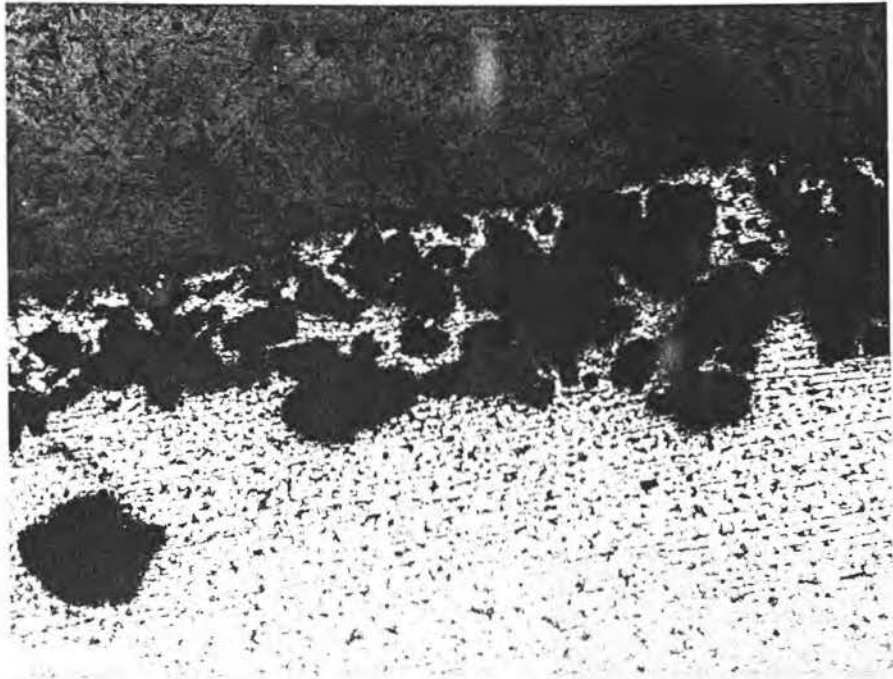


FIGURE 40

Cross-section through the crack indications adjacent to the weld shown in Figure 38. The damage was found to consist almost entirely of pits or cavities, giving rise to a rather spongy appearance. Magnification x100 Etch Nital

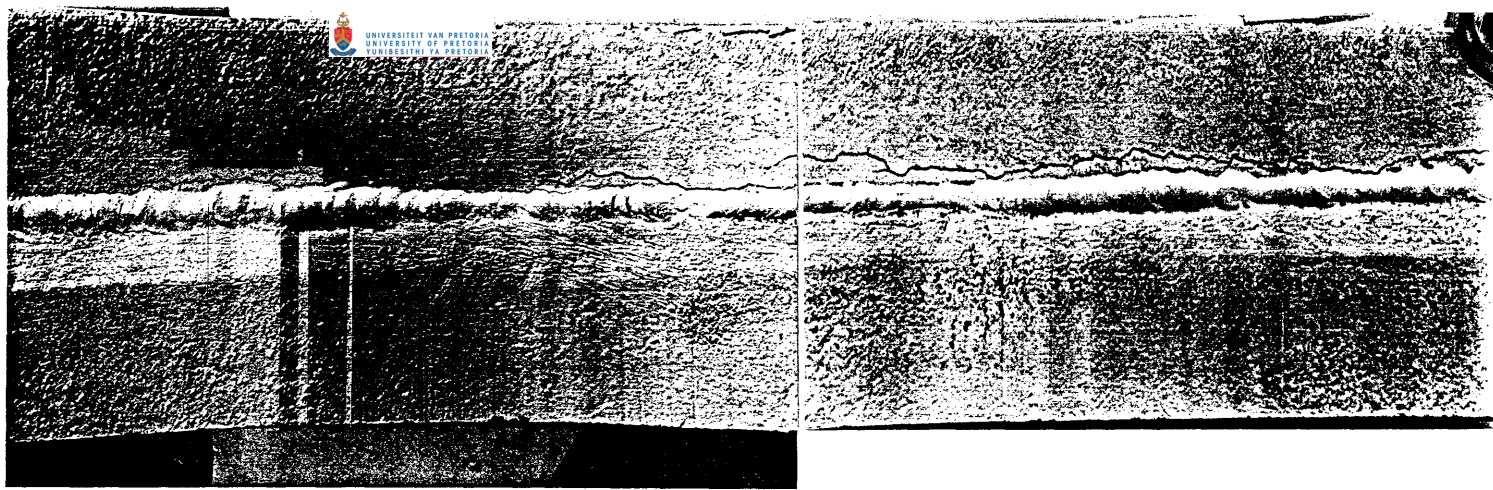


FIGURE 41 Inside surface of a pipe removed from service in rich gas, showing stress corrosion cracks parallel to a girth weld.

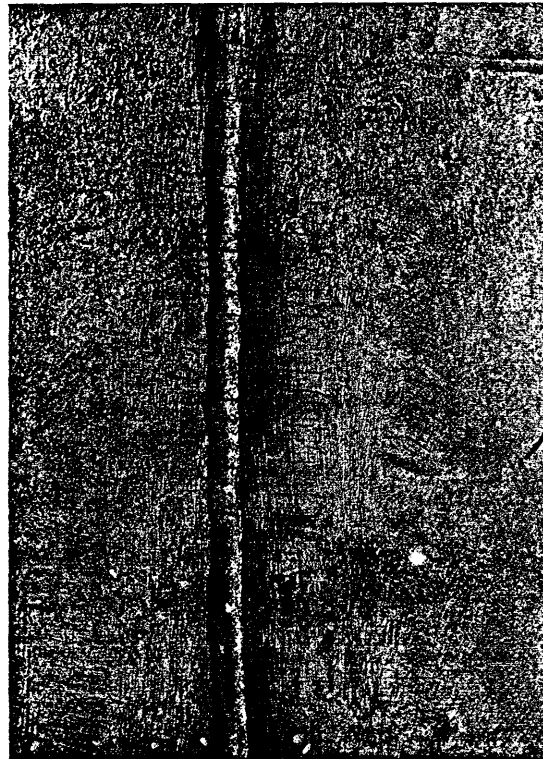


FIGURE 42 Stress corrosion cracks found transverse to a girth weld in the rich gas system at an operating plant.

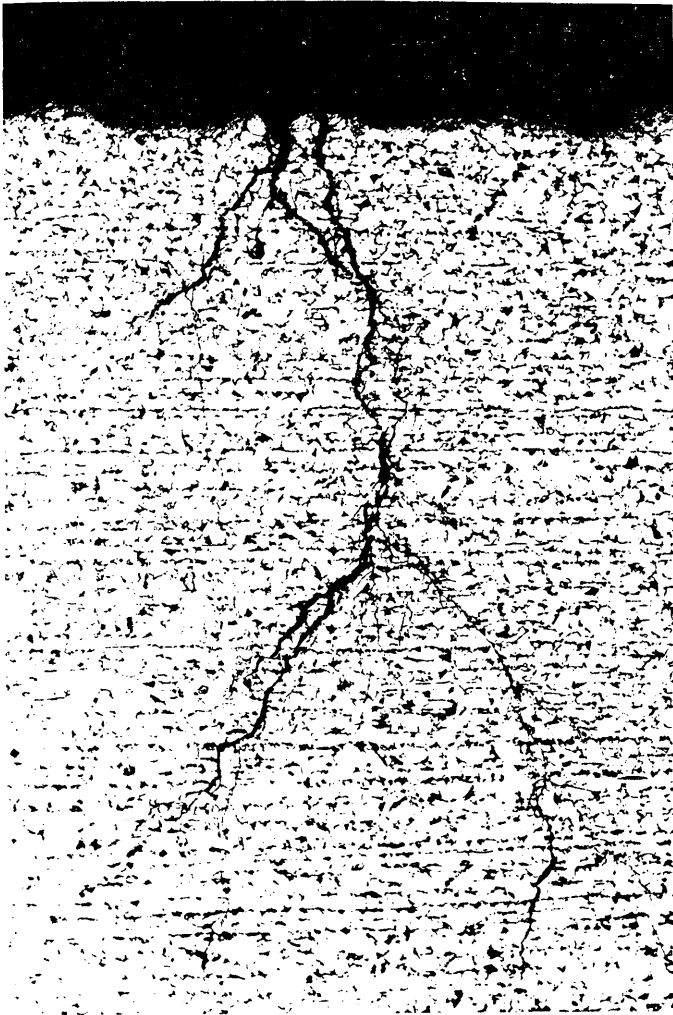


FIGURE 43 Magnification x100 Etch Nital

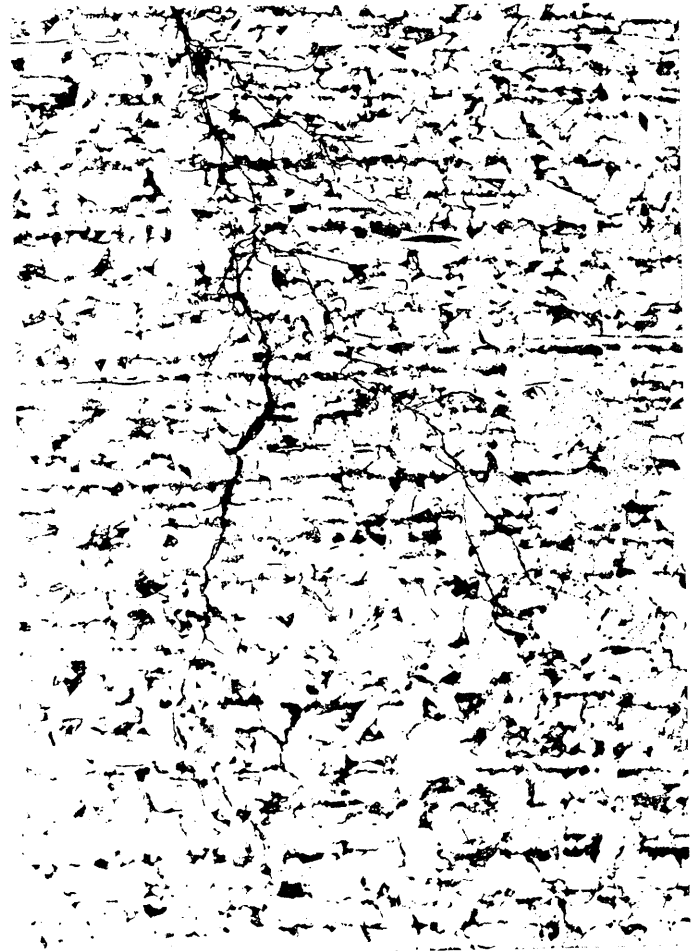


FIGURE 44 Magnification x200 Etch Nital

FIGURES 43 and 44 show the fine multi-branched nature of cracks found in the rich gas system.

Total pressure 1990 kPa 40 to 50°C.
PCO 199 kPa PCO₂
Hardness 171 Av., 180 Max., Hv 0,01

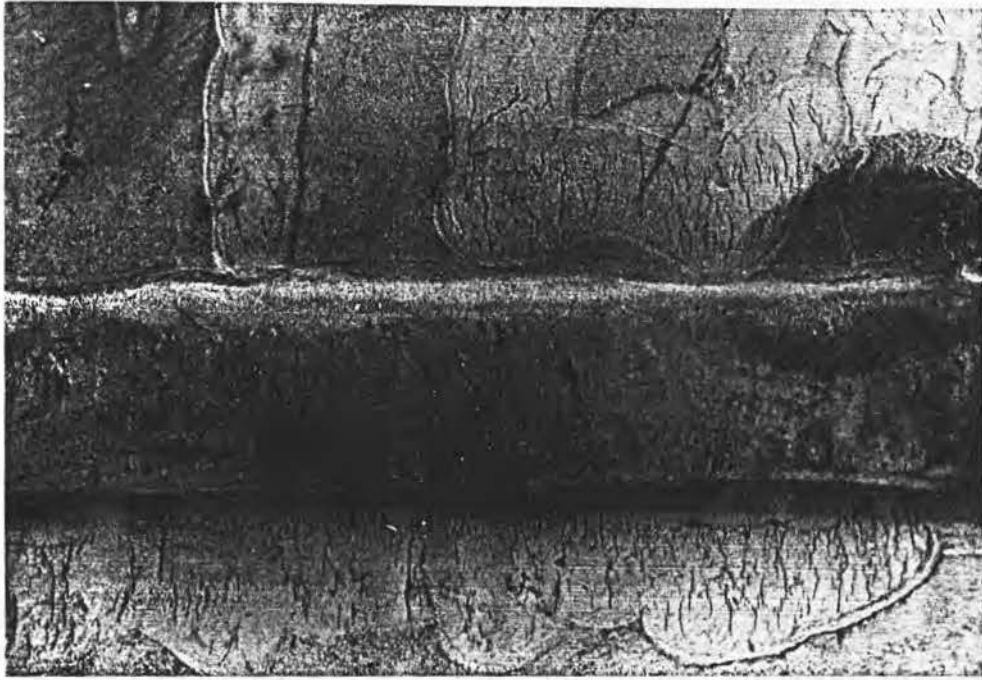
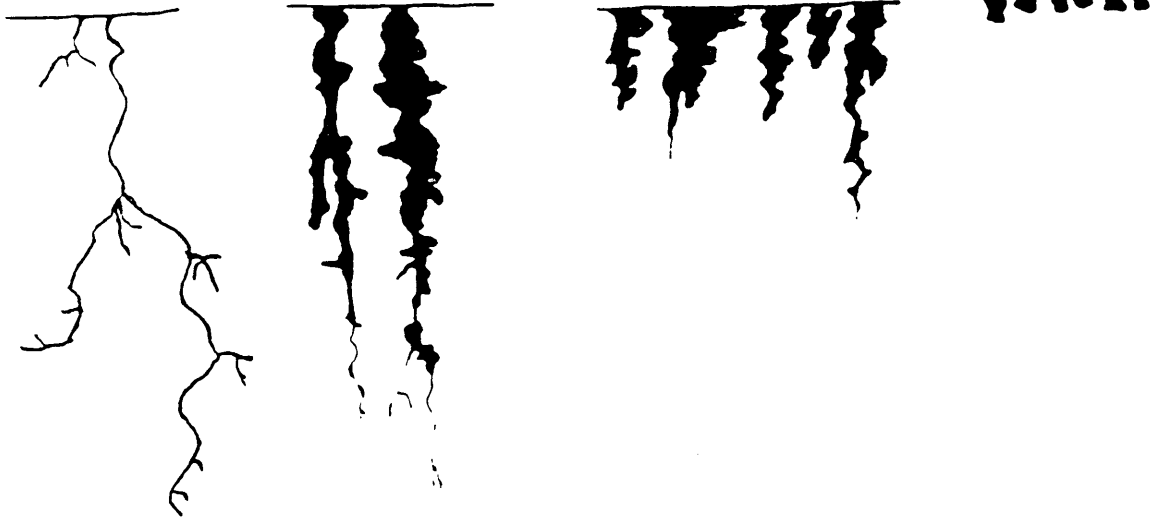


FIGURE 45 Cracking in localised areas of parent metal adjacent to a girth weld in rich gas service.
Hardness 225 Av., 270 Max., Hv 0,01

FIGURE 46

SKETCH SHOWING HOW CRACK APPEARANCE
CHANGES WITH INCREASING CARBON
MONOXIDE PARTIAL PRESSURE

H ₂	69	H ₂	36	H ₂	35	H ₂	36
CO	10	CO	1,5	CO	2,5	CO	1,5
CO ₂	11	CO ₂	12	CO ₂	13,5	CO ₂	12,0
CH ₄	2,4	CH ₄	36	CH ₄	36	CH ₄	36
°C	40-50	°C	40-50	°C	39-42	°C	38-50
1990	kPa	3000	kPa	1850	kPa	1990	kPa
PCO	199 kPa	PCO	45 kPa	PCO	46 kPa	PCO	29 kPa



9 EVALUATION OF STRESS CORROSION CRACK GROWTH RATES FOR CARBON STEEL IN A WET CO/CO₂ ENVIRONMENT

9.1 GENERAL DESCRIPTION

In order to determine if limited cracking could be tolerated it was necessary to establish crack extension rates for carbon steel exposed to the wet CO/CO₂ mixtures. A test programme was developed to measure crack growth rates using a laboratory set-up and consequently validate the results using a side stream facility in the plant.

Laboratory tests were carried out in a stainless steel autoclave situated at the CSIR Metallurgical and Corrosion Services Division, Cottesloe.

The plant tests were made in two side stream facilities at one of the operating plants where SCC was experienced.. The test programme and the method are described in the following paragraphs. All tests unless otherwise stated were carried out in the liquid phase.

9.2 APPARATUS

9.2.1 Laboratory Tests

The laboratory tests were carried out in a stainless steel autoclave capable of retaining the lean gas and rich gas service pressure (30 bar) - Figure 47. The autoclave was fitted with a temperature control to allow testing in the range ambient to 60°C, representative of lean gas and rich gas service temperatures. Suitable Conax access fittings were installed to facilitate instrumentation. The specimens were stacked to ensure isolation from the shell of the autoclave. The arrangement is shown in Figures 48 and 49. The specimens were immersed in condensate which was taken periodically from the operating plant. Similarly the system was pressurised using gas samples taken from the relevant gas systems in the operating plant circuit and contained in stainless steel sample bottles. Supplementary commercial carbon monoxide was used to adjust the carbon monoxide partial pressure in the autoclave as required. A full analysis of gas and condensate used in the experiment is given in Tables 11 and 12.



FIGURE 47 PARR AUTOCLAVE USED FOR LABORATORY TESTS

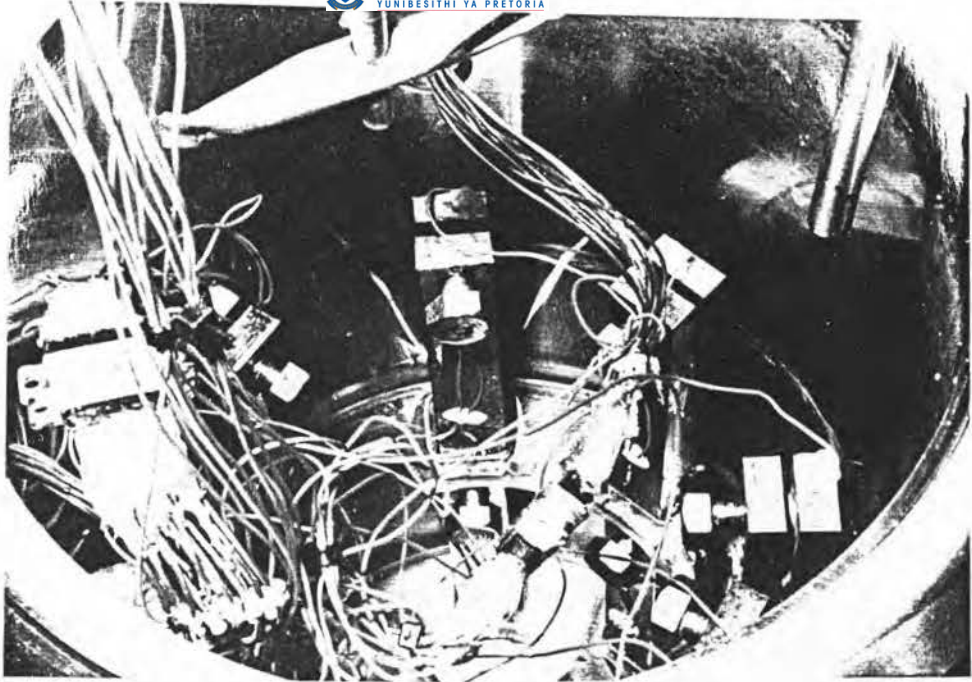


FIGURE 48 ARRANGEMENT OF SPECIMENS INSIDE THE AUTOCLAVE

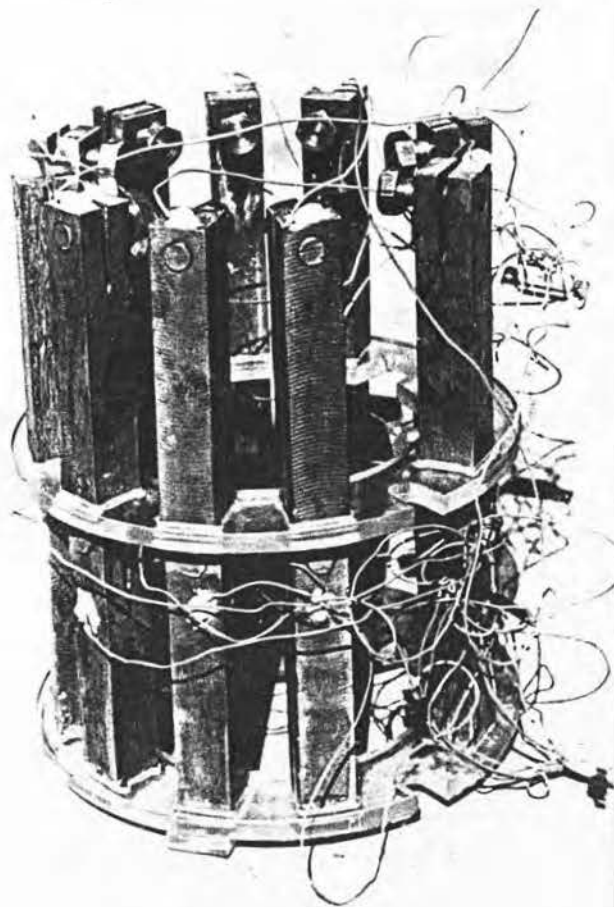


FIGURE 49 ARRANGEMENT OF SPECIMENS

TABLE 11 RICH AND LEAN GAS CONDENSATE ANALYSIS

COMPONENT	WEIGHT %
ETHANOL	0,097
PROPANOL	0,042
2m-PROPANOL	0,005
ACETONE	0,005
BUTANOL	0,015
BENZENE	0,062
3m-BUTANE	0,004
3-BUTANE	0,001
TOLUENE	0,002
2-PROPANOL	<0,001
ETHANOL	<0,001
UNKNOWN ALIPHATICS	<0,001
UNKNOWN CARBONYLS	0,001
UNKNOWN ALCOHOLS	<0,001
ACID NUMBER	0,006
WATER	BALANCE

TABLE 12 GAS ANALYSIS

COMPONENT	LEAN GAS	RICH GAS
HYDROGEN	38,80	69
CARBON MONOXIDE	2,59	10
CARBON DIOXIDE	14,49	11
ARGON	2,18	4,03
NITROGEN	1,09	1,10
METHANE	31,50	4,0
ETHYLENE	1,90	0,02
ETHANE	1,05	-
PROPYLENE	2,64	-
PROPANE	0,18	-
BUTYLENE	0,08	-
BUTANE	0,20	-
C ₅ +	1,56	-

Two side stream facilities were constructed to enable on-line installation and retrieval of stress corrosion test coupons. Each construction consisted of a small pressure vessel fabricated from stress-relieved SA 106 Gr B pipe plus accompanying pipework and isolation valves. A drawing of one of the vessels is included as Figure 50. The piping layout is shown in Figure 51. Basically, the systems consisted of specimen holders through which the respective gases (one for lean gas and one for rich gas) were circulated at controlled flow rates and pressures. Allowance was made for specimens to be tested in direct contact with the flowing gas or submerged in process condensate. This was achieved by placing the gas outlet at the mid point of the vessel. Each pressure vessel was supplied with a sample holder (Figure 52) which could easily be withdrawn from the vessel once the top flange was opened. Figures 53 and 54 are photographs taken from above and below the plant installation.

9.3

SPECIMEN DESIGN

Stress corrosion cracking of smooth specimens includes an initiation period. This can be considerably shortened by using pre-cracked specimens. Constant load testing necessitates stressing equipment and is complicated by the need to test at pressure. Additionally an important requirement of the growth rate determination is that key rates of crack extension are verified by site testing. This required that a relatively simple specimen and test arrangement was selected. Bolt loaded cantilever beam (DCB) specimens were chosen (Figure 55). Compared to the modified WOL geometry the DCB provides for a greater extent of crack extension and for a given growth rate the decrease in stress intensity is much less than the modified WOL specimen. Furthermore, bolt loading is easier to control and reproduce than wedge loading. These advantages were considered against problems with compliance and arm breakage associated with bolt loaded DCB specimens.

The DCB specimens were prepared in accordance with the requirements of ISO 7539-6 : 1989 (E) "Corrosion of metals and alloys - stress corrosion testing" Part 6: Preparation and use of pre-cracked specimens". The specimens were pre-fatigued under constant load conditions at a frequency of 5 Hz in a universal servo-hydraulic test machine. The maximum load in the final 2 mm was kept below 6 kN for all specimens. In most cases the maximum load in the final 2 mm of crack growth was 5 kN but for a few specimens it was 4 kN. The pre-crack was grown to a length where the notch geometry would no longer influence crack growth and the fatigue crack was checked on each side of the specimen to ensure it was uniform (difference in lengths <5% W) (Figure 12).

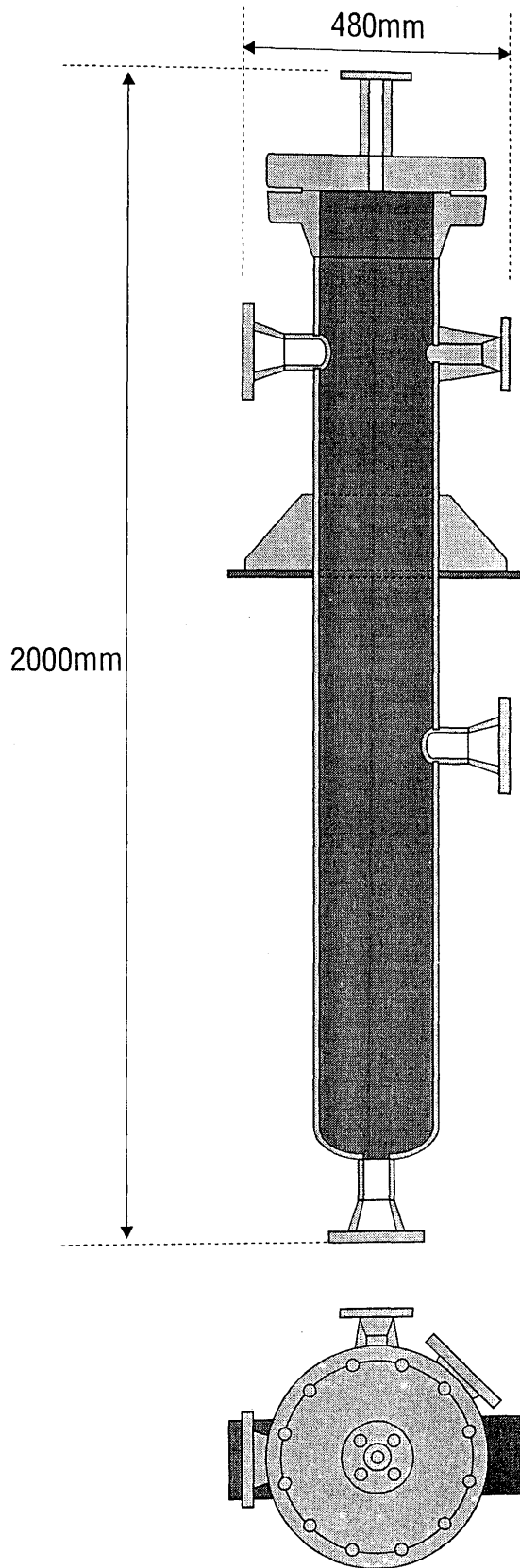
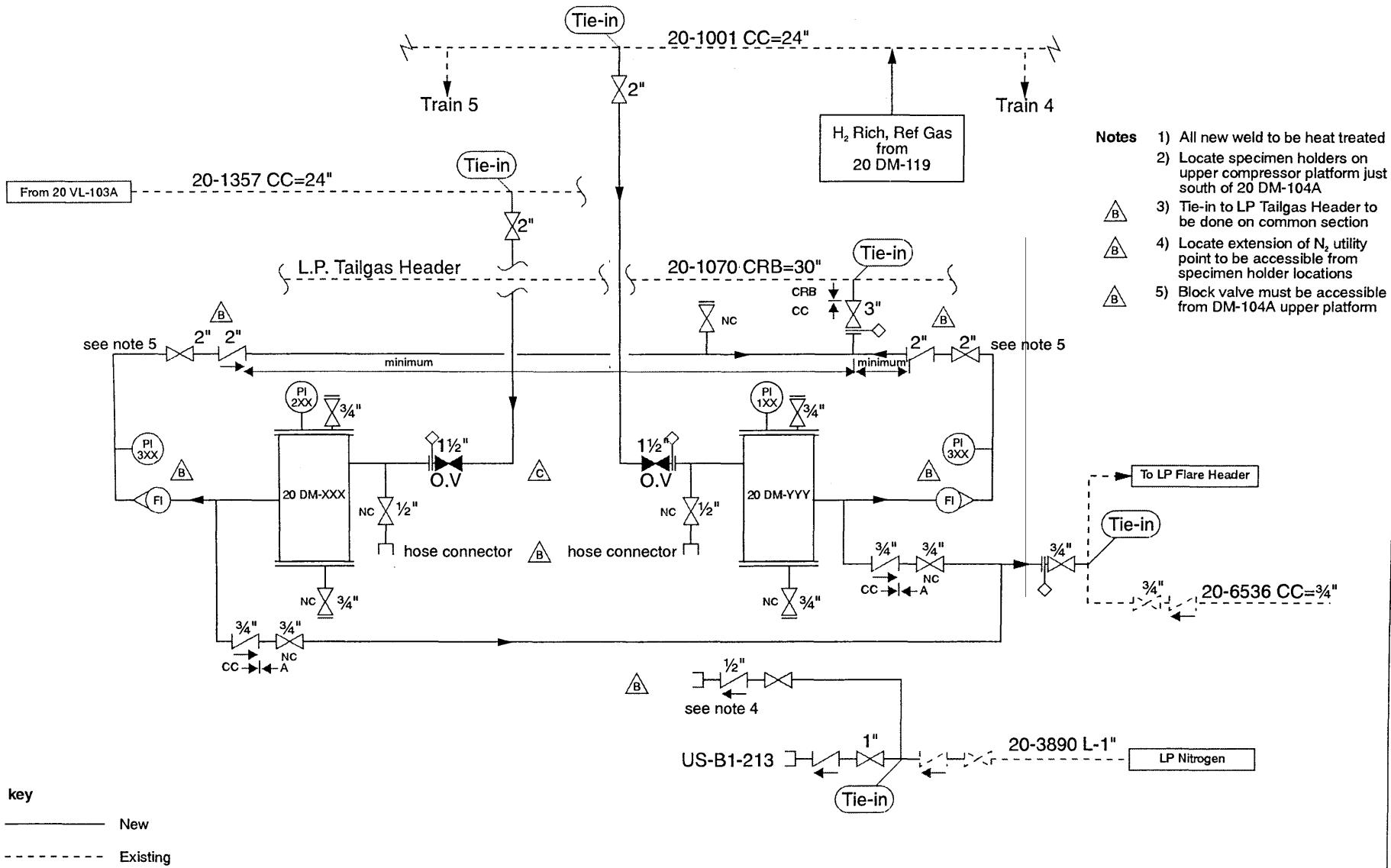


Figure 50: Drawing of the small pressure vessel in which bypass samples were exposed



Page 85

Figure 51: Piping layout for plant bypass

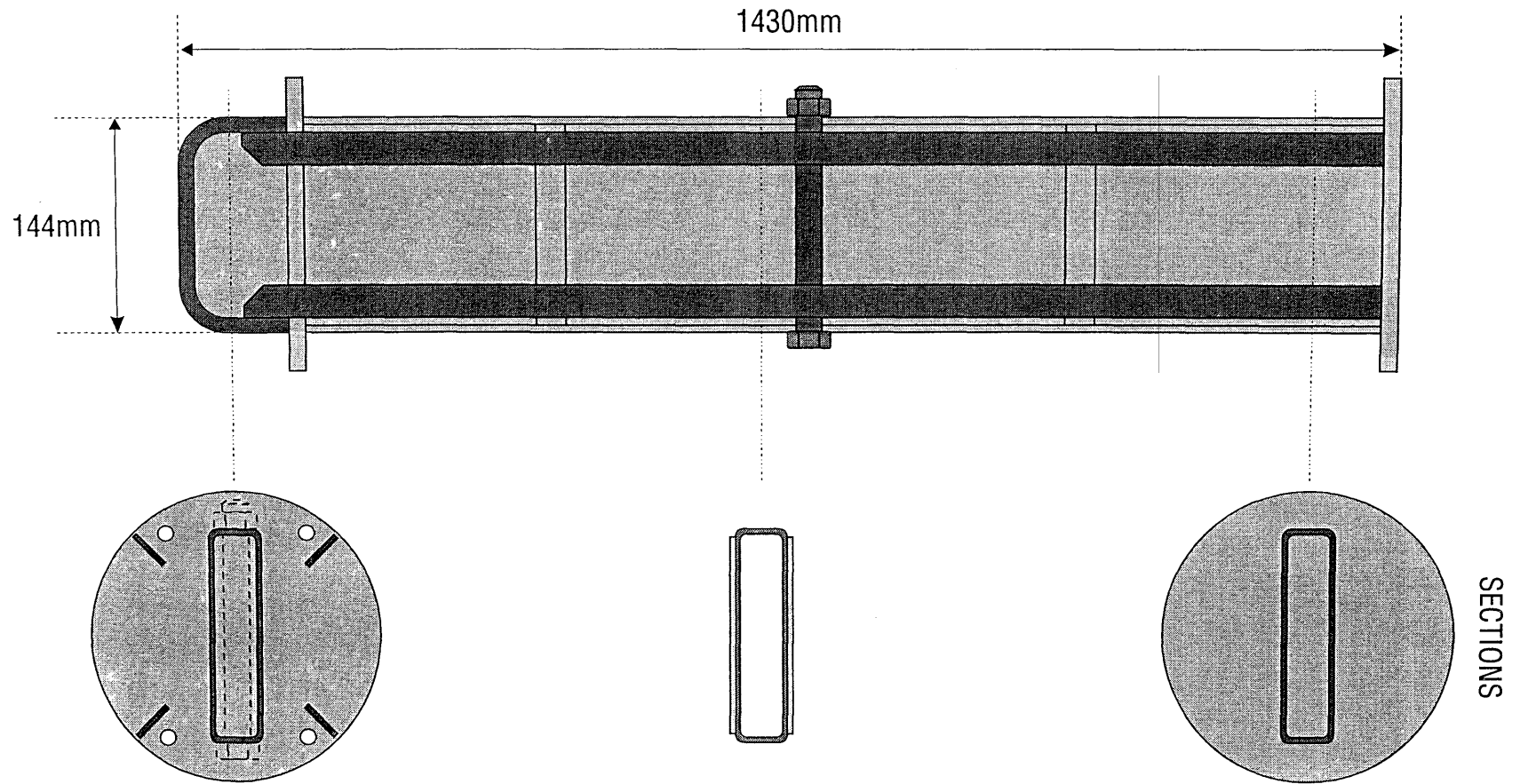


Figure 52: Drawing of the sample basket inserted in the bypass vessel

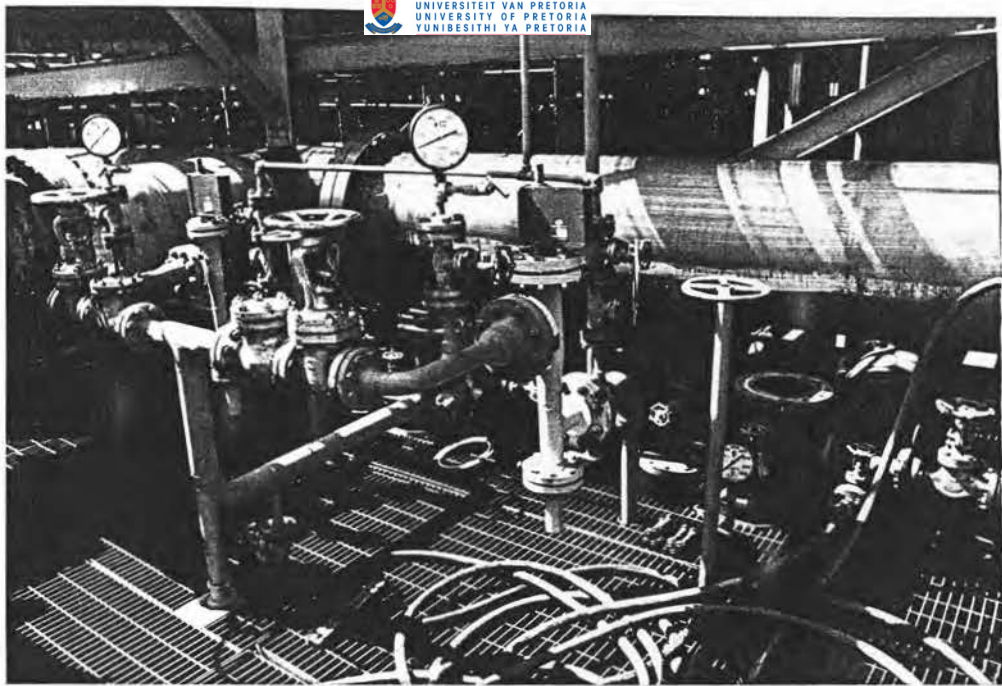


FIGURE 53 PLANT BYPASS INSTALLATION VIEWED FROM THE TOP

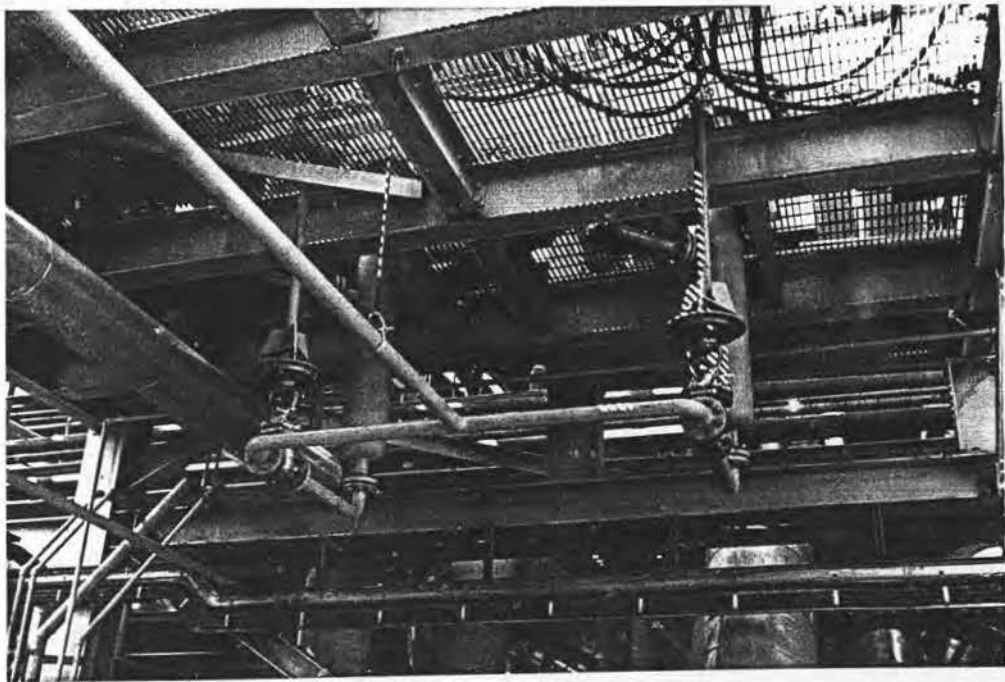


FIGURE 54 PLANT BYPASS INSTALLATION VIEWED FROM THE BOTTOM

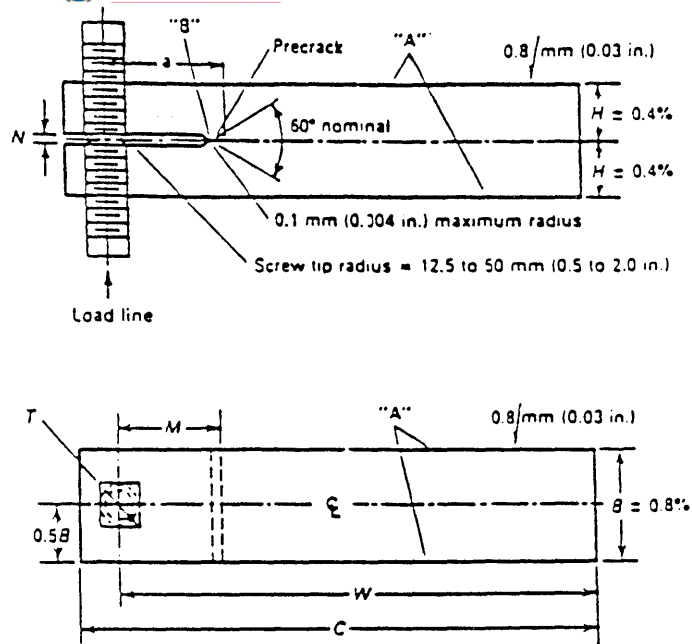


FIGURE 55 Proportional dimensions and tolerance used for the double cantilever beam (DCB) specimens.

- B = 50 mm
- H = 12,5 mm
- W = 125 mm
- C = 137,5 mm
- M = 25 mm

After pre-fatiguing the effective crack length (from the load line to the crack tip) was measured in each specimen. Reference photomicrographs were taken of the crack tips at magnifications x7 and x45. Immediately before stacking in the autoclave the bolt loading arrangement was torqued to give a pre-determined stress at the crack tip. The applied load was monitored via a strain gauge mounted on each specimen. The strain gauge output had been previously calibrated by loading pre-cracked specimens in a servo-hydraulic machine. The calibration is in Figure 56.

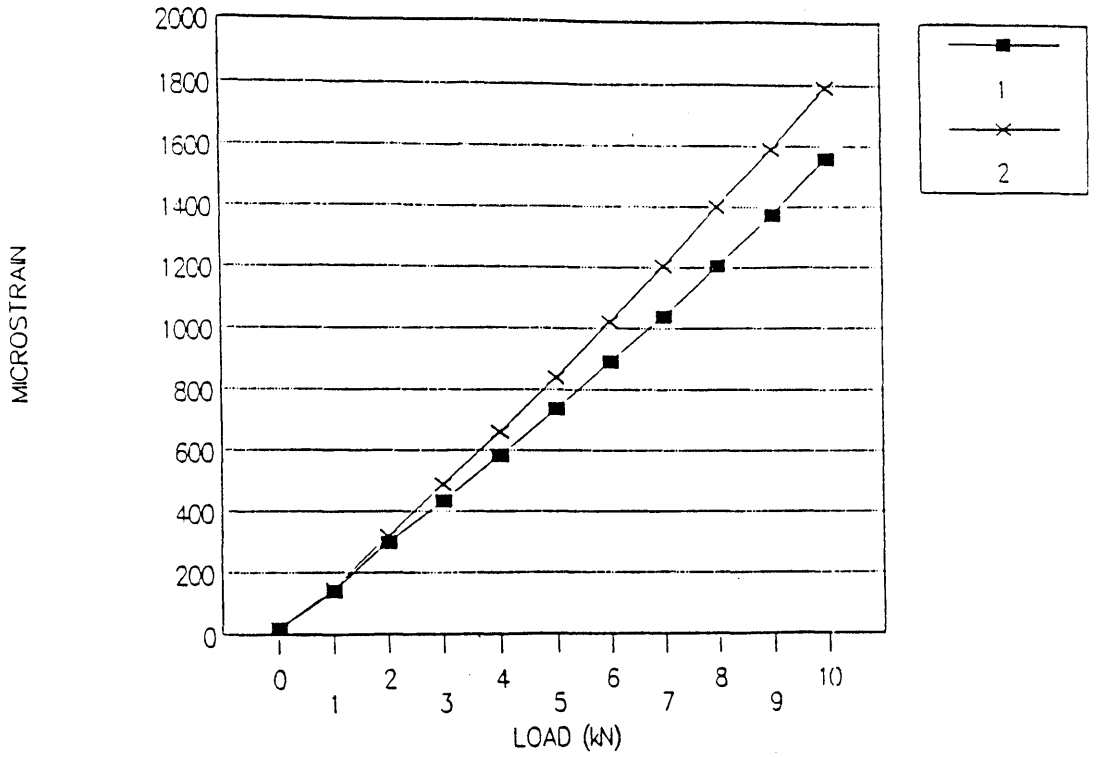


FIGURE 56

CALIBRATION OF A STRAIN GAUGED DCB

Strain gauge output as a function of applied load.

(Crack length in specimen 1 was 30mm and in specimen 2, 40 mm)

The crack tip intensity in each specimen was calculated using : ⁽¹¹⁵⁾

$$K_5 = \frac{P\sqrt{12}}{\sqrt{h}} \left(\frac{a}{h} + 0,6728 + 0,0377 \frac{h^2}{a^2} \right)$$

which for this specimen geometry reduced to :

$$K = 1239,4 P \left(\frac{a}{h} + 0,6728 + 0,0377 \frac{h^2}{a^2} \right)$$

where P = applied load

a = initial crack length

h = half height of the specimen.

9.4 ELECTROCHEMICAL MONITORING - POTENTIAL NOISE

Potential noise was monitored on specimens placed in the autoclave to determine the onset of SCC and to establish if there was a correlation between anodic events (number and magnitude of transients) and crack growth rate.

The system initially used to monitor potential noise consisted of a digital multi-meter interfaced to an IBM compatible PC by means of a IEEE interface card. The multi-meter was equipped with an eight-channel multiplexer, to facilitate simultaneous noise monitoring on eight specimens, each at a sampling frequency of 1 Hz. A potential resolution of 1 μ V was achieved using the 5,5 digit precision setting of the multi-meter.

The leads on the DCB specimens were attached close to the crack tip and the soldered contact points of the electronic leads were protected by a thick multilayer coating of Stopoff 45 lacquer that was subsequently covered by a cold setting resin followed by two further layers of lacquer. The specimen leads were attached to the Conax leads in a similar fashion and exited the vessel. Potential crevice sites on the DCB's were similarly coated.

9.5 AUTOCLAVE STARTUP PROCEDURE

The pre-loaded specimens were stacked in the Parr autoclave following the arrangement shown in figures 48 and 49. The stirrer, thermowell and gas inlet are all attached to the vessel lid which was lowered into the body to allow closure.

After closing up and torquing all twelve clamping bolts, the vessel was flushed with high purity nitrogen gas and then filled with the condensate. The gas sampling valve on the vessel lid was kept open during filling and condensate was gravity-fed into the vessel through the bottom drain valve. When the vessel was full (as indicated by condensate discharging from the gas sample valve) the filling procedure was reversed so that 500 ml of condensate were removed from the vessel. At this point the noise data collection was started. (This also served to ensure that before starting the test none of the channels were short-circuited.) The bottom drain valve was then closed and the vessel purged with high purity nitrogen for about 30 minutes, after a preliminary leak test had been carried out by pressurising with nitrogen at 30 bar.

After purging with nitrogen, the sample of gas was bled into the reactor from the gas cylinder and the PID temperature controller activated. The set point of 50°C was reached after approximately 45 minutes. This generally resulted in an increase in the pressure in the vessel. Repressurising with gas was required within 12 hours of startup due to dissolution of the gas into the condensate.

9.6 BYPASS STARTUP PROCEDURE

The DCB specimens were stacked into the sample holder using the pre-stressing bolts on the DCB's as convenient spacers to allow free circulation of the gas. Once the sample holders were in place the holders were carefully placed inside the vessels and the vessel was filled with condensate up to the outlet nozzle. This allowed the DCB's to be exposed to either gas or condensate depending upon their position in the holder. The DCB's were positioned so that they were exposed to the liquid phase. The vessel lid was bolted up and the vessel was pressurised with low pressure nitrogen while all connections were soap tested. The nitrogen purge was continued until the vessels were oxygen free. The blanks on the gas inlets were then swung and the outlet to the low pressure header valve was set to open. The system was slowly pressurised using the globe valves on the inlets while intermittently soap testing until full pressure was achieved. At this time the block valve to the low pressure header was still closed. At full pressure the inlet globe valves were closed and the block valve opened. The flow rate was then set to between 500 to 1000 m³/h using the globe valve in conjunction with the flow meters.

To open the vessels, the appropriate gas supply valves were closed and the pressure indicators were viewed to ensure positive isolation. The system was depressurised to flare using ¾" flare line, and was subsequently purged with low pressure nitrogen until gas free. After purging, the bypass was depressurised and all spectacle blinds were swung to the closed position. Condensate was drained from the vessels and the vessel lids were removed to allow the sample holders to be withdrawn from the vessels.

9.7 RESULTS OF LABORATORY TESTS

9.7.1 1000-Hour Interrupted Test in Low Pressure Lean Gas (PCO 40, PCO₂ 270)

Twenty DCB specimens were fabricated from SA516 Gr 70. The chemistry and mechanical properties are given in Table 13. The specimens were pre-stressed so that the stress intensities ranged from 15,3 to 32,9 MPa \sqrt{m} (Table 14). Two notch orientations (DCB) were used as described by Figure 57. Orientations X-Y and Z-X were used.

TABLE 13 CHEMICAL COMPOSITION AND MECHANICAL PROPERTIES

CARBON	MANGANESE	PHOSPHOROUS	SULPHUR	SILICON	TENSILE STRENGTH (MPa)	YIELD STRENGTH (MPa)
0,22	1,05	0,008	0,005	0,334	525	297

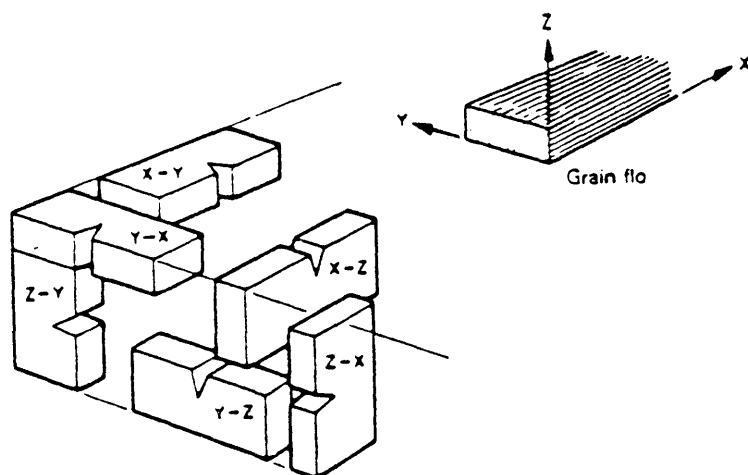


FIGURE 57 BASIC FRACTURE PLANE IDENTIFICATION: RECTANGULAR SECTION

TABLE 14 INITIAL CRACK LENGTHS AND CRACK TIP STRESS INTENSITIES FOR 1000-HOUR INTERRUPTED TEST IN LOW PRESSURE LEAN GAS. (PCO 40, PCO₂ 270).

SPECIMEN	CRACK LENGTH (mm)	APPLIED LOAD (kN)	CRACK TIP STRESS INTENSITY (MP√m)
S1	10,5	6,0	26,2
S2	11,2	7,1	31,4
S3	12,2	5,5	24,9
S4	12,4	7,25	32,9
S5	7,2	4,77	19,2
S6	9,7	3,57	15,3
S10	8,5	4,17	17,4
S12	10,9	7,0	30,8
S14	8,0	5,17	21,3
S16	8,0	5,33	22,0
S17	10,2	5,0	21,6
S20	8,5	4,17	17,4
F1	13,25	5,0	23,2
F2	10,5	6,0	26,2
F3	10,9	6,5	28,6
F4	11,2	6,2	27,4
F5	13,2	3,57	18,8
F8	13,9	4,75	22,3
F9	12,5	5,5	25,1
F10	12,4	6,2	28,2

NOTE: The effective crack length corresponds to the values quoted + 25 mm for the depth of the notch

The twenty specimens were loaded into the autoclave following the procedure described in the previous paragraph. Each specimen was connected to the electrochemical monitoring set and each was strain gauged.

The autoclave was pressurised to 2000 kPa using lean gas from the industrial plant to simulate the low pressure lean gas service condition with a nominal carbon monoxide partial pressure of 40 kPa. The test temperature was controlled at 55°C.

The autoclave was left closed for two weeks and subsequently opened to check for crack extension using a binocular travelling microscope at x50 magnification. No crack growth was observed. At this time it was found that the strain gauges had disbonded from the specimens so it was decided to modify the specimens so that pre-loading could be determined by clip gauge displacement.

The specimens were returned to the vessel and testing was continued for a further two weeks. Once again there was no measurable crack extension.

After the final test period lasting 20 days there was still no measurable crack extension, a result which was verified by sectioning two high stress intensity specimens and subjecting them to close scrutiny by scanning electron microscopy and optical microscopy. Although no crack extension was found, the surface of the pre-fatigue crack showed evidence of pitting corrosion.

Electrochemical noise was monitored for the duration of the test, however since no crack extension was recorded the relevance of the potential transients recorded to SCC could not be established. During the first two-week test period a change in rest potential occurred on all channels from ca -480 mV to -160 mV independent of crack tip stress intensity. This was not observed in any subsequent tests although initial rest potentials after repressurisation were the same at around -120 mV. The stainless steel autoclave body was used as the reference electrode for all potential measurements.

During the second two-week test period there were some significant fluctuations from the rest potential but the transients could not be correlated to stress intensity level.

9.7.2 1000-Hour Continuous Test - Low Pressure Lean Gas (PCO 40, PCO 270)

On completion of the 1000-hour interrupted test the DCB's were returned to the autoclave for a period of six weeks.

A ring welded test coupon was added to the specimens exposed in the autoclave. The ring welded coupon is a severe test for stress corrosion cracking and can be destructively examined for cracks. It was chosen to enable the autoclave environment to be tested for the ability to support SCC without needlessly destroying further DCB's.

The ring welded specimen was prepared by welding a single bead GTAW circular deposit, 80 mm outside diameter, onto a 100 x 100 SA516 Gr 70 carbon steel plate, 12 mm thick. Type E70S-6, 2,4 mm wire was deposited using 50 A, 13 V shielded by 7 l/min gas flow. No preheat or post weld heat treatment was applied. The weld was crack detected using magnetic particle inspection. Leads were attached to the weld to allow monitoring of electrochemical activity.

With all the test coupons in place the autoclave was pressurised to the test conditions, which were kept the same as for the previous test. The gas was replaced every two weeks.

At the end of the test all specimens were examined for crack extension. Once again no crack extension was detectable in the DCB. The ring welded specimen did however show evidence of cracking which was later confirmed by a micro section. The deepest crack found was 0,5 mm representing a growth rate of 4,3 mm/year. The cracks were extremely fine and multibranched, an appearance which resembled cracks found in rich gas (PCO 199 kPa) rather than lean gas (PCO 40). Microhardness determinations in the vicinity of the cracks gave values of 183, 222, 260, 247 and 247 indicating that the ring weld was not excessively hard. From this result it was concluded that it was unlikely that the cracks occurred during welding due to hydrogen.

9.7.3 1000-Hour Continuous Test - Low Pressure Lean Gas, Upper Bound CO Concentration (PCO 80, PCO₂ 260)

Following the failure to produce crack extension in a laboratory simulation of the nominal low pressure lean gas concentration a simulation was done of the upper bound CO concentration found during normal plant fluctuations in low pressure lean gas. This entailed increasing the PCO used in previous tests from around 40 kPa to 80 kPa. A ring welded specimen and four C-rings stressed to 100% of yield were also placed in the autoclave. Two C-rings had a bright surface finish, the others were scaled by a short heat treatment at 600°C prior to stressing.

In order to improve the accuracy of the crack length readings, the areas surrounding the crack tips on each side of the DCB specimens were diamond polished and the end of each pre-fatigue crack was marked by two adjacent 200 g diamond impressions.

The stress intensities and average crack lengths used in the test are listed in Table 15. All the specimens were notched and pre-fatigued parallel to the rolling direction. The stress intensities of specimens FH, FJ, FK, FL and FN corresponded to loads above yield.

The samples were installed in the autoclave following the procedure described previously and were exposed to the test environment for an uninterrupted period of 1000 hours. As before the gas was replenished regularly at two-week intervals.

Upon retrieval from the autoclave once again no crack extension was observed in the pre-cracked DCB specimens, even after examining each microscopically at x400 and breaking open selected high stress intensity specimens for SEM examination. By contrast evidence of cracking was found in each of the smooth C-ring specimens. Shallow stress corrosion cracks measuring 0,2 mm were found. In this test no cracks were observed in the ring welded specimen.

The potentials of the C-ring, ring weld and DCB specimens were all close to that of the autoclave reference potential. The noise traces obtained from cracked C-ring specimens could not be distinguished from DCB and ring weld specimens that did not crack. Each showed positive and negative transients of the order of 30 μ V.

TABLE 15 INITIAL CRACK LENGTHS AND CRACK TIP STRESS INTENSITIES FOR 1000-HOUR CONTINUOUS TEST - LOW PRESSURE LEAN GAS, UPPER BOUND CO CONCENTRATION (PCO 80, PCO₂ 260)

SPECIMEN	CRACK LENGTH (mm)	STRESS INTENSITY (MPa√m)
FA	12,39	29,55
FB	10,83	26,35
FC	12,43	29,58
FD	12,27	27,21
FE	10,82	25,47
FF	12,42	31,85
FG	11,97	24,78
FH	12,91	34,48
FI	12,19	23,99
FJ	13,84	37,52
FK	14,24	42,56
FL	12,88	34,46
FM	11,65	22,37
FN	13,78	37,47
FO	12,21	20,38
FP	12,78	32,09
FQ	11,73	20,17

NOTE: The effective crack length corresponds to values quoted + 25 mm.

9.7.4 1000 Hour Continuous Test in Rich Gas (PCO 210, PCO₂ 250)

Following the failure of the previous tests to develop any detectable crack extension in pre-cracked DCB specimens, an uninterrupted test was made in rich gas which, from the literature and plant experience, was thought to be a more severe SCC promoting media than low pressure lean gas, due to its higher carbon monoxide partial pressure.

Seventeen DCB specimens were pre-stressed to the stress intensities listed in Table 16. The crack length measurements were made using a travelling microscope at x50 magnification. The results were verified by using a moving stage in conjunction with an optical microscope at x400. Since a variation below 0,1mm (Table 17) was recorded it was concluded the measurement of crack length was of sufficient accuracy to detect crack extensions to the magnitude found previously in C-rings (approximately 0,1 mm).

The following specimens were wired for potential noise measurements.

Channel 1	C-ring, 100% yield, scaled surface finish
Channel 2	C-ring, 100% yield, bright surface finish
Channel 3	DCB specimen F11
Channel 4	Ring weld specimen
Channel 5	DCB specimen F15
Channel 6	DCB specimen F14
Channel 7	DCB specimen - no stress
Channel 8	C-ring 100% yield, surface finish

The potential transients were measured initially against an unnotched ASTM A516 Gr 70 specimen and later against the 316 autoclave wall.

Following a 1000-hour uninterrupted exposure in the autoclave the DCB specimens were all examined using the travelling binocular microscope at x50. Selected DCB specimens with high, intermediate and low stress were subjected to more intense scrutiny by careful microscopic examination at x400 magnification following local metallographic preparation of the crack tip area. The C-rings and ring welds were subjected to dye penetrant testing followed by sectioning and metallography.

No crack extension was detected in any of the DCB specimens examined. The pre-fatigue crack however was found to contain corrosion product. Shallow stress corrosion cracks up to a depth of 0,1 mm were found in the C-rings regardless of surface finish. The appearance of the cracks was similar to that detected previously in the lean gas environment. No cracks were detected in the ring welded specimen.

Once again the potential noise traces were similar for all specimens regardless of whether or not cracking was observed. Transients were around 60 μ V.

TABLE 16 AVERAGE PRE-CRACK LENGTHS OF DCB SPECIMENS AND STRESS INTENSITIES FOR 1000-HOUR CONTINUOUS TEST IN RICH GAS (PCO 210, PCO₂ 250)

SPECIMEN	LOAD	CRACK LENGTH (mm)	STRESS INTENSITY (MPa√m)
F1	4,5	12,90	20,69
F3	4,5	11,88	20,23
F2	5,0	13,54	23,30
F18	5,0	11,80	23,44
F4	5,5	12,09	24,84
F19	5,5	12,14	24,87
F5	6,0	13,55	27,97
F6	6,0	12,19	27,16
F7	6,5	12,27	29,47
F8	6,5	12,40	29,56
F9	7,0	13,77	32,78
F10	7,0	12,37	31,81
F11	7,5	13,16	34,67
F12	7,5	14,09	35,36
F13	8,0	15,13	38,54
F14	8,0	12,03	36,09
F15	9,0	12,32	40,86
F16	Unstressed		

NOTE: The effective crack length corresponds to the values quoted + 25 mm for the depth of the notch.

TABLE 17 PRE-CRACK LENGTHS OF DCB SPECIMENS FOR 1000-HOUR CONTINUOUS TEST IN RICH GAS (PCO 210, PCO₂ 250)

SPECIMEN	SIDE 1 (mm)	SIDE 1 (mm)	DIFFERENCE	SIDE 2 (mm)	SIDE 2 (mm)	DIFFERENCE
F1	12,91	13,015	0,105	12,58	12,808	0,228
F2	13,76	13,796	0,036	13,34	13,290	0,050
F3	11,50	11,449	0,051	12,38	12,313	0,067
F4	11,93	11,837	0,093	12,49	12,377	0,113
F5	13,84	13,676	0,164	13,71	13,459	0,251
F6	11,93	11,899	0,031	12,82	12,504	0,316
F7	12,16	12,109	0,051	12,53	12,437	0,093
F8	12,26	12,181	0,079	12,65	12,611	0,039
F9	13,68	13,660	0,020	13,92	13,870	0,050
F10	12,71	12,465	0,245	12,30	12,282	0,018
F11	13,12	13,441	0,321	13,14	13,031	0,109
F12	14,06	13,984	0,076	14,28	14,020	0,080
F13	15,38	15,354	0,026	15,23	15,109	0,121
F14	12,59	12,430	0,160	12,20	12,046	0,154
F15	12,82	12,567	0,253	12,71	12,396	0,314
F18	12,12	12,066	0,054	11,53	11,525	0,005
F19	11,46	11,371	0,089	12,90	-	-

* CSIR

* SASTECH

EVALUATION OF INHIBITOR ADDITIONS TO CO-CO₂-H₂O SYSTEMS USING CERT

Constant extension rate tests were used to determine if stress corrosion cracking in the CO-CO₂-H₂O system could be prevented by inhibitor additions. The effect of reducing the temperature on the severity of SCC was also tested. Since evaluations were made in two gas environments some information was also obtained on the effect of CO partial pressure.

10.1 EXPERIMENTAL PROCEDURE

10.1.1 General

A hydraulic tensile testing machine capable of testing at constant strain rates in the range of 10⁻³ s⁻¹ to 10⁻⁷ s⁻¹ was used to tensile test standard uniaxial tensile specimens (Figure 58) at a controlled strain rate in an environmental chamber.

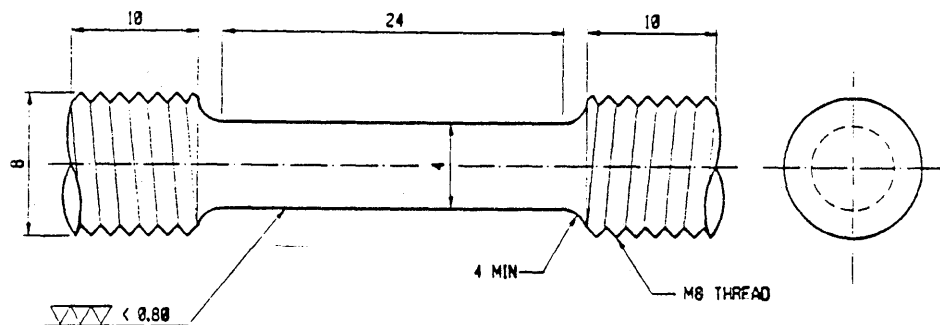


FIGURE 58 STANDARD UNIAXIAL TENSILE SPECIMEN

10.1.2 Test Chamber

A cylindrical environmental chamber capable of withstanding the test pressure was constructed of type 316L austenitic stainless steel. Teflon seals were used to create a pressure seal between the chamber and the extension arms. Type 316 stainless steel 1/8" tubing was used to conduct gas from a portable type 316L stainless steel cylinder to the test vessel. An arrangement of a pressure gauge and pressure valves on the gas outlet was used to control the gas flow until it bubbled through water at a rate of ca 1 bubble per second. The outside of the chamber was heated by a spiral electric element and the temperature was controlled by a thermocouple which passed through the vessel wall into the environmental chamber.

A Luggin probe was also passed into the chamber until it was adjacent to the specimen, so that corrosion potential could be monitored for the duration of the experiment. The Luggin probe arrangement included a pressure reducer so that potential could be recorded against a standard silver, silver chloride electrode outside the pressure chamber at one atmosphere. The test facility is sketched in Figure 59.

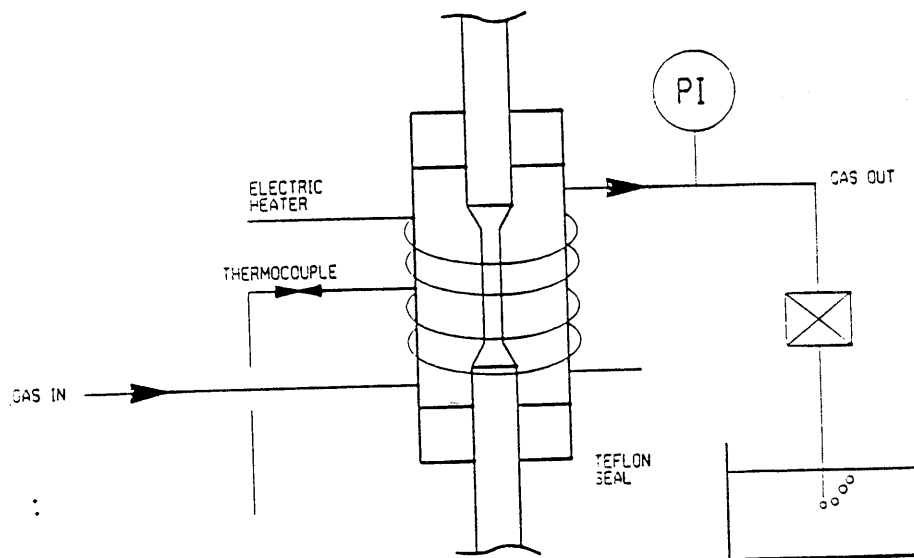


FIGURE 59 SKETCH SHOWING THE TEST FACILITY USED TO DO THE CERT

10.1.3 Test Procedure

The uniaxial tensile test piece was first screwed into the bottom extension arm. The arm was then pushed into the bottom of the chamber until the tensile test piece was correctly positioned between the gas inlet and outlet so that the thermocouple and Luggin probe were approximately adjacent to the centre of the test piece. The chamber was then filled from the top with condensate taken from the plant. The top arm was pushed into the chamber and screwed tight onto the top of the test piece. The gas outlet valve was then closed, and the valve on the gas bottle opened to pass gas into the chamber, pressurising it. The gas contained in the bottle had previously been sampled from a pressure point on the relevant stream in the plant. Once the chamber was up to pressure as read from the pressure indicator (PI) on the gas outlet, the outlet valve was slowly opened and regulated until a constant stream of gas bubbles was achieved. The gas was allowed to flow for at least 40 minutes to de-oxygenate the condensate before the test was started. The heater was also switched on during this period and the temperature was slowly raised until it reached the set point of 50°C.

After the initial test, the partly emptied cylinder was used for degassing before it was subsequently swapped with a new full cylinder prior to starting the next test. Once the chamber was re-pressurised using the full cylinder the gas flow was regulated until it flowed at a rate of ca 1 bubble per second.

Two strain rates were chosen. The sample was initially strained at $3 \times 10^{-5} \text{ s}^{-1}$ until an extension of 0,4 mm was recorded, which represented approximately 60% of yield and took ten minutes to achieve. The strain rate was then dropped to $7 \times 10^{-7} \text{ s}^{-1}$ which was maintained for the duration of the test. The strain rate chosen was based on the work of Berry and Payer⁽⁴¹⁾ which indicated that the lowest reduction of area was recorded in CO-CO₂-H₂O systems when the strain rate was between $2 \times 10^{-7} \text{ s}^{-1}$ and $1 \times 10^{-6} \text{ s}^{-1}$. Strain was recorded using a linear voltage differential transformer that measured cross-head movement up to 1 μm . A chart recorder was used to draw load extension curves. The variation in potential was also recorded and superimposed on the curve.

At the end of each test the reduction of area was recorded and the gauge length of the specimens was examined for corrosion products, pitting and secondary cracking. Certain specimens were longitudinally sectioned and examined microscopically. Some fractography was also done.

Initial tests were performed in condensate pressurised with rich gas. In later tests lean gas was used to pressurise the condensate. All testes were carried out in the liquid phase. Gas analyses were performed by gas chromatography. The nominal composition and deviations are given in Table 18. When inhibitors were tested, they were added to the condensate immediately before it was placed into the test chamber prior to pressurising with gas. Usually only one test was made for each condition although some duplicates were performed to examine the reproducibility of the results.

TABLE 18 NOMINAL COMPOSITION OF GAS USED FOR CERT

	LEAN GAS mol %		RICH GAS	
	MEAN	RANGE	MEAN	RANGE
Hydrogen	34	31 - 37	69	65 - 71
Carbon monoxide	2,0	2,2 - 2,4	11	10 - 12
Carbon dioxide	13	11 - 14	11	10 - 12
Methane	38	35 - 41	4	3,8 - 5

10.1.4 Inhibitors

The inhibitors were chosen on the basis of the observation by Parkins ⁽⁴⁰⁾ that inhibitors against SCC work in two ways, either by moving the potential out of the zone of susceptibility thereby preventing SCC or alternatively preventing SCC by inhibiting attack while the potential remains in the susceptible range. The latter is considered safe and the former unsafe, since the potential may move back into the susceptible range at certain localities. For this reason the inhibitors tested were mostly filmers. Inorganic substances that shift the corrosion potential were avoided. The inhibitors tested were also mostly commercial inhibitors that had been successfully used in oil and gas production and in crude refineries to prevent corrosion by wet carbon dioxide gas. The exception was Reomet 42 which is a general purpose inhibitor. The following paragraphs contain a brief description of the inhibitors evaluated.

Ranomet 42 - A multimetal inhibitor supplied in an aqueous preparation. The active chemical ingredient is a triazole derivative.

Petrotec 1420 - A water dispersible inhibitor neutraliser designed to control corrosion caused by hydrogen sulphide and carbon dioxide or mixtures of both. It contains a mixture of thiophosphates (30-60). Fatty amine quaternary salts and an acid phosphate ester, in aromatic hydrocarbons (30-60).

Petrotec 1430 - Designed for corrosion control in refinery overhead systems and is a filming inhibitor with neutralising abilities. Also contains thiophosphates (10-30), fatty amine quaternary (5-10) and acid phosphate esters (5-10).

AO-0003 - A mixture of thiophosphates and diethylene ether.

KXO-63 - A formulation of acid phosphate esters (30-60) phosphoric acid and thiophosphates (10-30) in water.

KD-40 - Consists of salts of phosphate esters of oxyalkylated polyols in water and is effective against corrosion due to carbon dioxide and hydrogen sulphide gases. KD-40 is selectively absorbed at active corrosion sites.

10.2 RESULTS

10.2.1 CERT - Rich Gas (PCO 210 PCO₂ 230)

The influence of rich gas on the fracture of carbon steel tested at 50°C was quite marked. The reduction of area fell to 22% compared with 66% in air, representing a ductility ratio of 0,33. This was reflected by the load extension curves (Figure 60) which showed a marked reduction in ductility. There was some variation in results, with higher reduction of areas up to 35% sometimes recorded in rich gas at 50°C. The ductility ratio calculated from this higher value was 0,53. Little change was measured due to lowering the test temperature to 20°C. The reduction of area measured and the ductility ratios calculated were 20% to 36% and 0,30 to 0,54 respectively. The load extension curves however indicated a small benefit from the lower test temperature (Figure 61).

10.2.2 CERT Rich gas (PCO 210, PCO₂ 230) and Additions of Inhibitor

Reductions in area from 19 to 59% were recorded depending on the inhibitor and concentration used. Mostly the reduction of areas measured after inhibitor additions were around 35% which did not represent a significant improvement over the uninhibited environments. The respective ductility ratio range was 0,78 to 0,89.

The frequently recorded, 35% reduction of area represented a ductility ratio of 0,53 indicative of a still strong influence of the environment on crack propagation. Figures 61 to 67 show the load extension curves for various inhibitor additions. Table 19 summarises the reductions of area and ductility ratios recorded.

A large addition of Petrolite 1420 (5000 ppm) was the only condition that resulted in a suppression of stress corrosion. The other results of note were those obtained after additions of Ranomet 42. At low and high dosage rates very low reductions of area were measured. Values of 25% and 19% were recorded for 10 and 1000 ppm respectively. However as addition of 100 ppm gave fairly good inhibition with little evidence of secondary cracking on the specimen. The reduction of area and the ductility ratios were 40% and 0,60 respectively.

Metallography and fractography were performed on the broken samples. All showed similar features. Transgranular stress corrosion cracks at varying depths up to 0,3 mm were observed along the gauge length (Figure 68). Some pitting was usually present on the surface of the samples (Figure 69) but was minor to almost non-existent on inhibited samples (Figure 70). The fracture surfaces had a feathery appearance with few distinct features (Figure 71). This result was typical of the fracture appearance of transgranular stress corrosion cracks in BCC metals.

Figure 72 compares the fracture appearance of specimens broken in air, rich gas and in rich gas plus various additions of inhibitor. The effect on reduction of area and fracture appearance is clearly evident.

10.2.3 CERT Lean Gas (PCO 34 PCO₂ 266)

The influence of the environment on the fracture behaviour in lean gas was reflected by the load reductions of area recorded for tests made at 50°C. Reductions of area of 20 and 25% were measured compared with 65% in air. This result gave a ductility ratio of 0,30. Testing carried out at 20°C gave larger reductions of area but also more scatter with reductions of area from 37 to 54% recorded. Table 19 and Figure 73 show the reductions of area and load-extension graphs. The load-extension graphs for lean gas and rich gas are compared in Figure 74.

10.2.4 CERT Lean Gas (PCO 34 PCO₂ 266) plus Inhibitors

The results of inhibitor additions to lean gas were very similar to those obtained when inhibitor was added to rich gas. Reductions in area ca 36 % were generally recorded (Table 19), representing an improvement over the uninhibited environment at 50°C but stress corrosion cracking was not prevented. The best result in lean gas was achieved by an addition of KXO-63 which achieved a reduction of area of 49% and a 0,75 ductility ratio.

The load-extension curves for the tests are in Figure 75.

TABLE 19

INHIBITOR		RICH GAS		LEAN GAS	
		Reduction of area %	Ductility Ratio RA _g /RA air	Reduction of area %	Ductility Ratio RA _g /RA air
Uninhibited	50°C	22	0,33	20	0,30
		35	0,53	25	0,38
Uninhibited	20°C	20	0,30	27	0,41
		36	0,50	54	0,83
Petrotec 1420	10	26	0,39	NT	-
	100	25	0,37	48	0,73
	5000 ppm	59	0,89	NT	-
Petrotec 1430	10	35	0,53	NT	-
	100 ppm	32	0,48	36	0,55
Reomet 42	10	25	0,38	NT	-
	100	40	0,60	NT	-
	1000 ppm	44	0,66	NT	-
		19	0,28		
KD-40	100	39	0,59	36	0,55
	1000	35	0,53	NT	-
KXO-63	100	39	0,53	49	0,75
	1000	39	0,53	NT	-
A-0003	100	32	0,48	NT	-
	1000	35	0,53	NT	-

NT - Not Tested

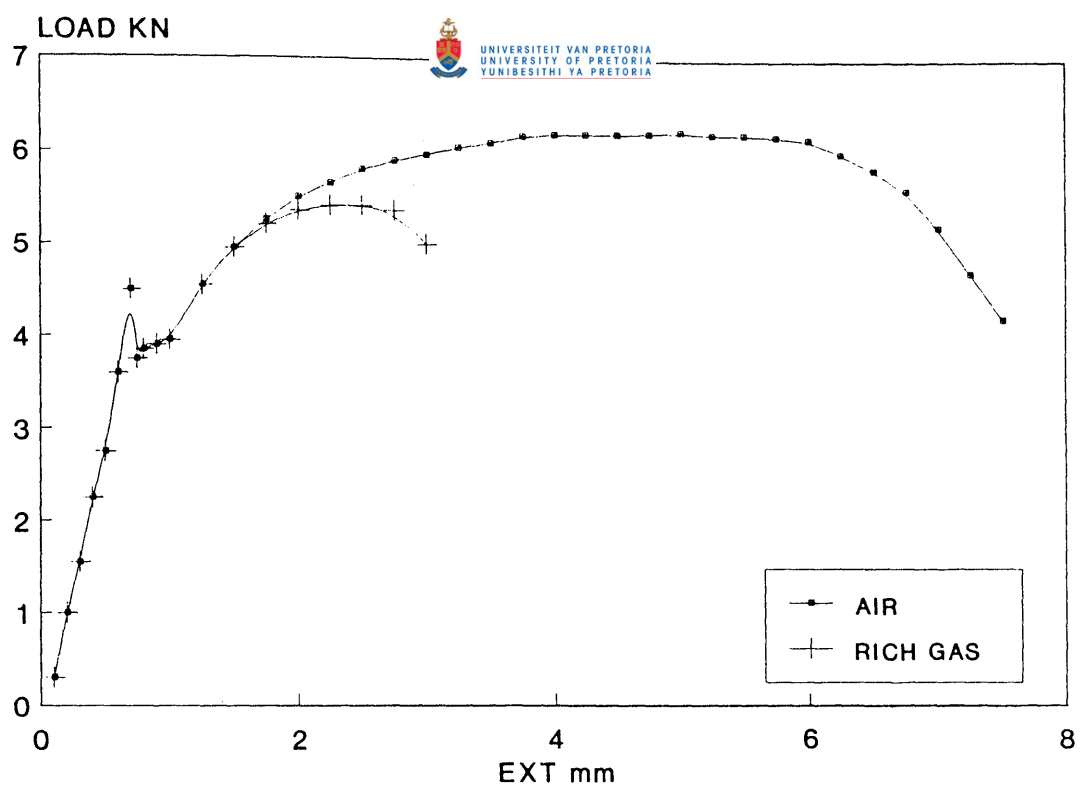


FIGURE 60 LOAD EXTENSION CURVES FOR CARBON STEEL IN AIR AND RICH GAS

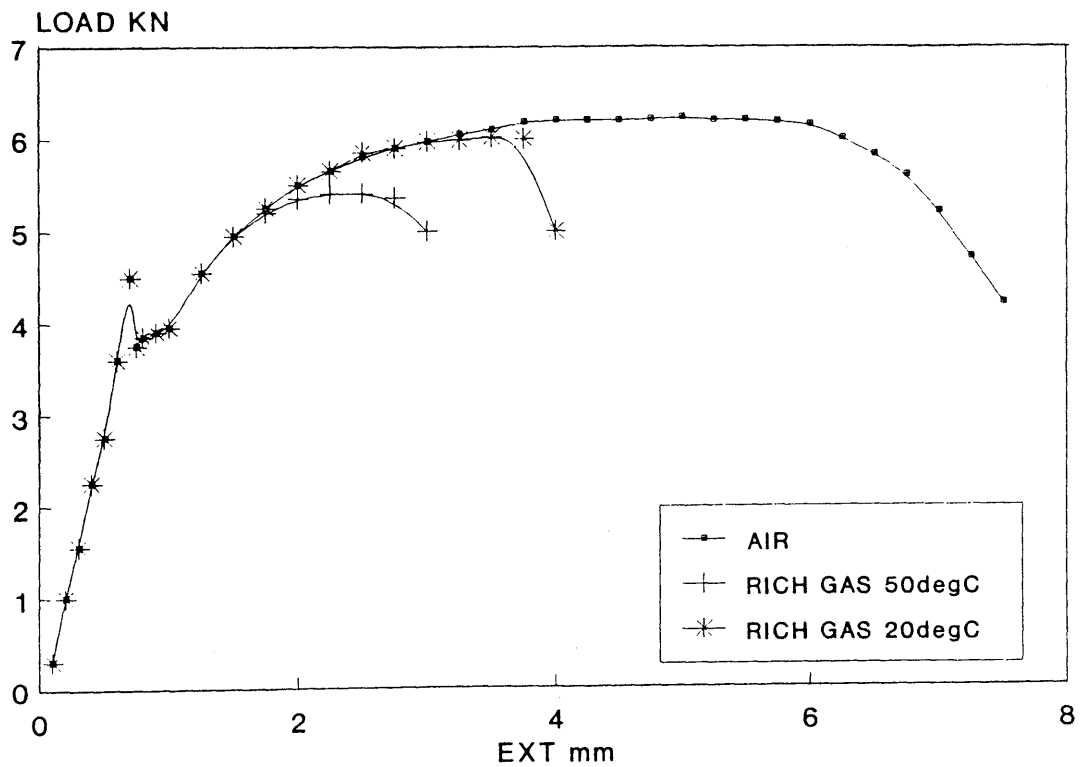


FIGURE 61 LOAD EXTENSION CURVES FOR CARBON STEEL TESTED IN RICH GAS AT 20 AND 50°C

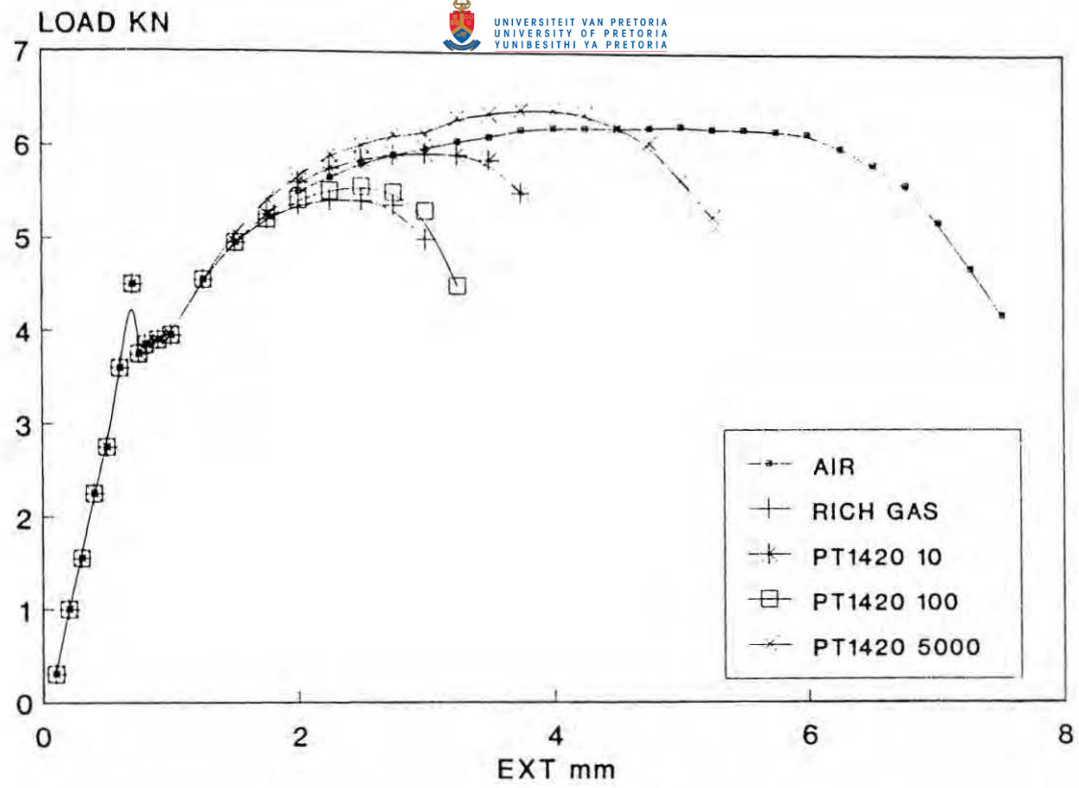


FIGURE 62 CHANGE IN LOAD EXTENSION CURVES RESULTING FROM THE ADDITION OF INHIBITOR PT 1420 TO RICH GAS

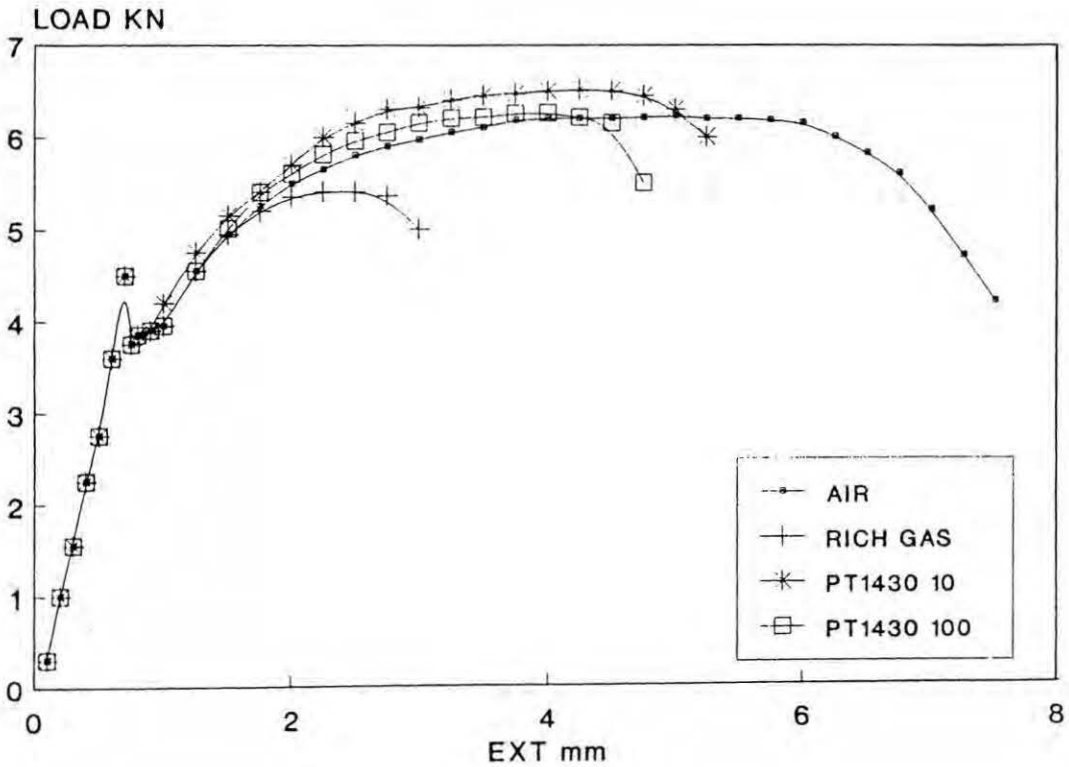


FIGURE 63 CHANGE IN LOAD EXTENSION CURVES RESULTING FROM THE ADDITION OF INHIBITOR PT 1430 TO RICH GAS

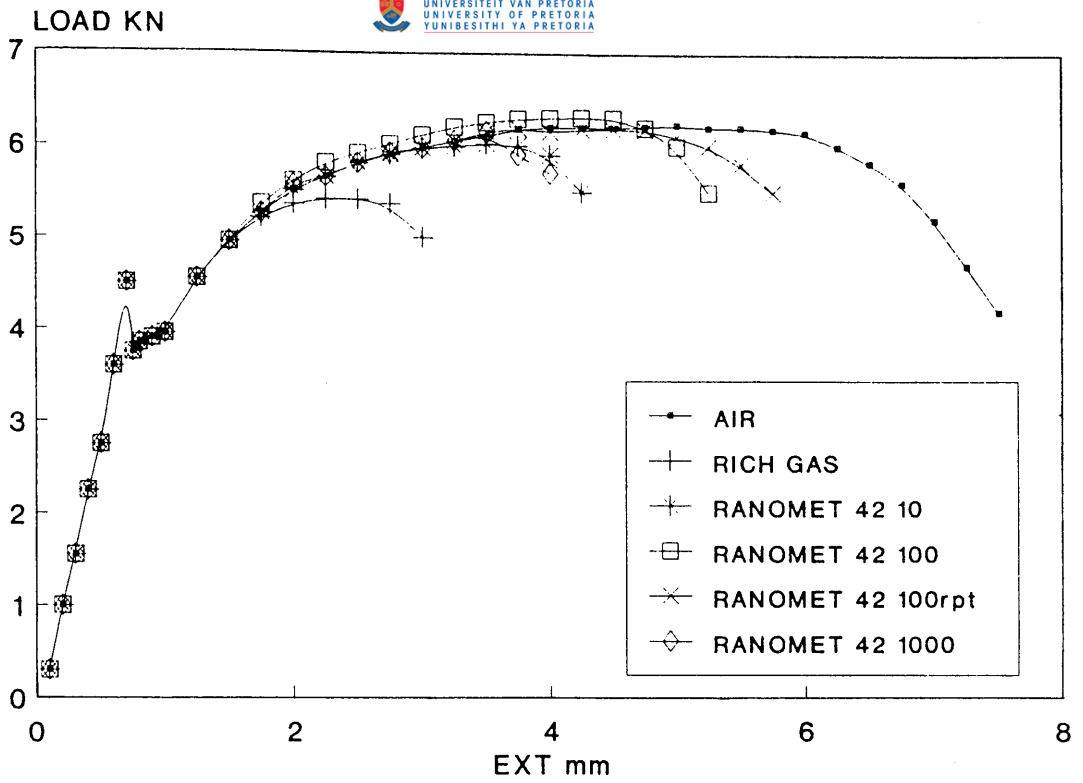


FIGURE 64 CHANGE IN LOAD EXTENSION CURVES RESULTING FROM THE ADDITION OF INHIBITOR RANOMET 42 TO RICH GAS

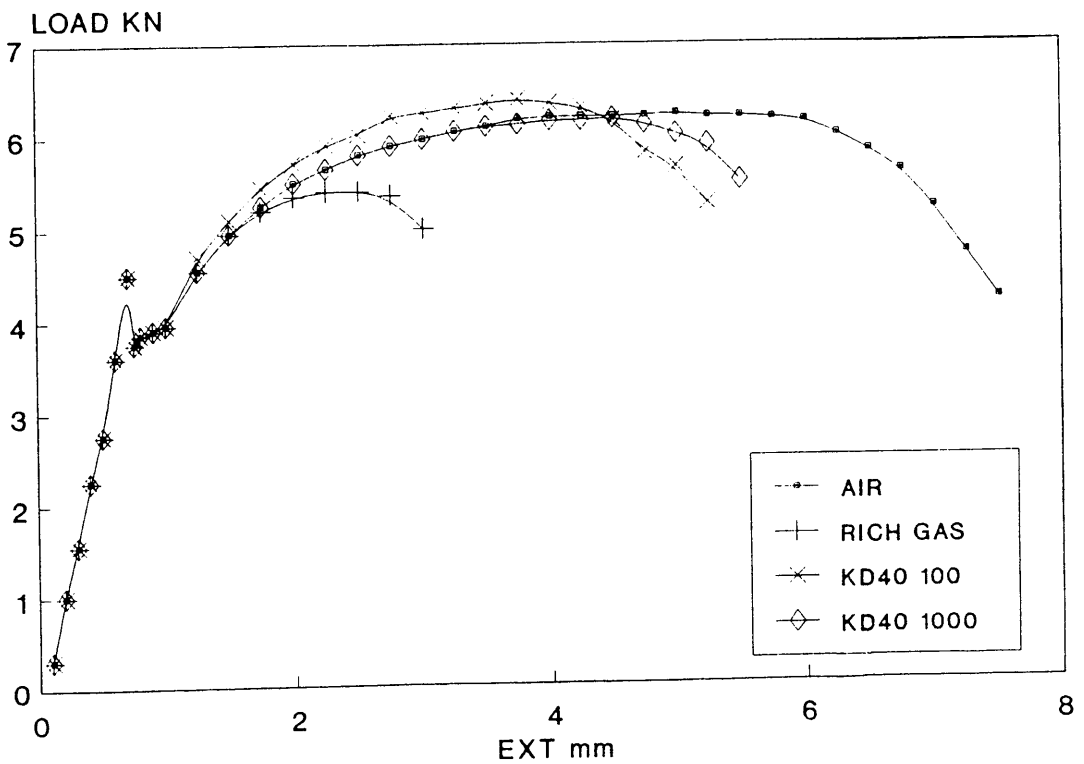


FIGURE 65 CHANGE IN LOAD EXTENSION CURVES RESULTING FROM THE ADDITION OF INHIBITOR KD 40 TO RICH GAS

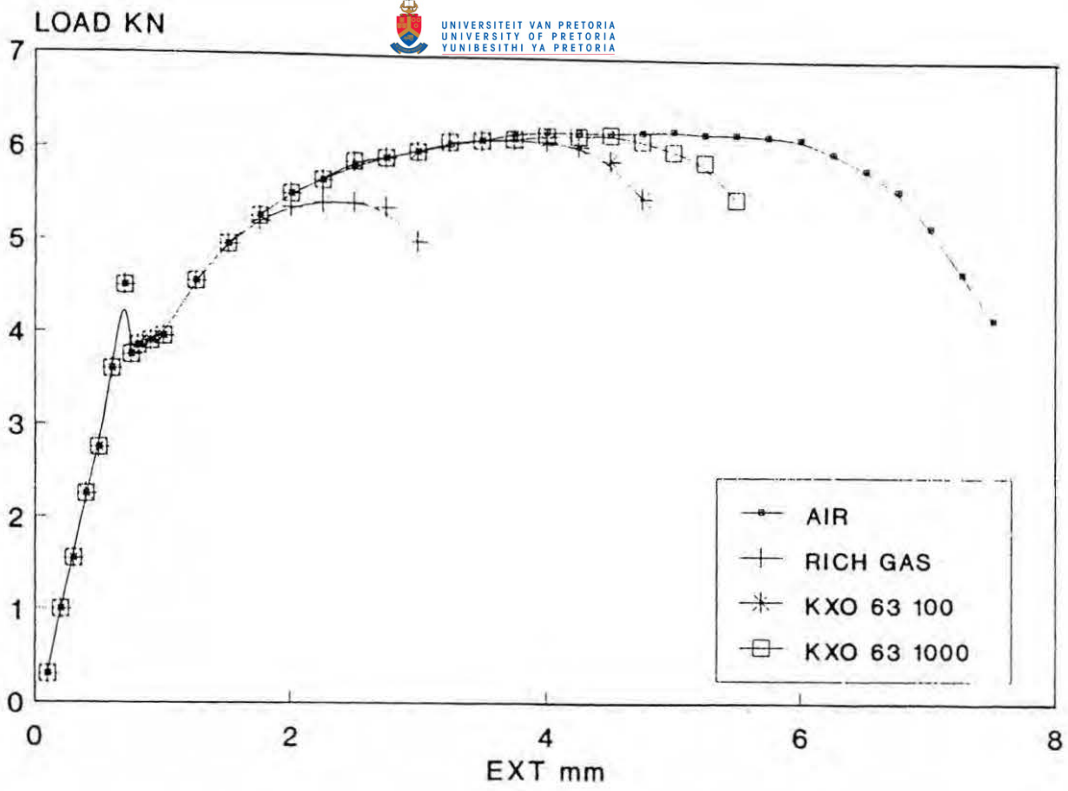


FIGURE 66 CHANGE IN LOAD EXTENSION CURVES RESULTING FROM THE ADDITION OF INHIBITOR KXO 63 TO RICH GAS

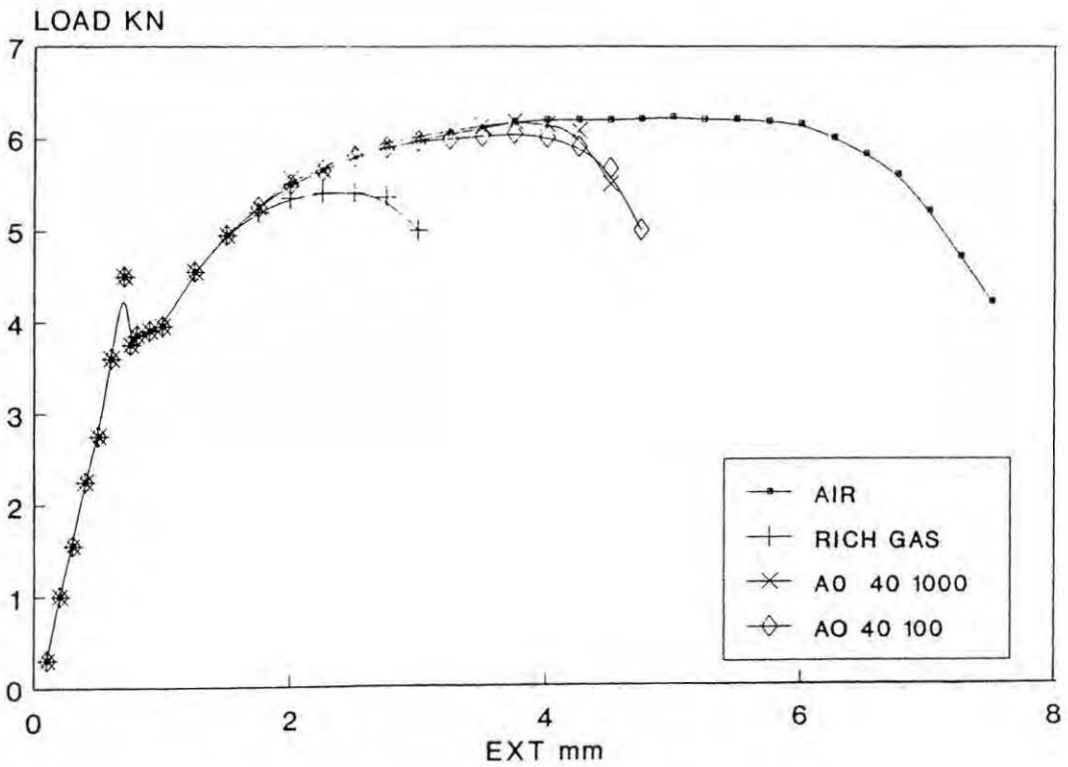


FIGURE 67 CHANGE IN LOAD EXTENSION CURVES RESULTING FROM THE ADDITION OF INHIBITOR AO 40 TO RICH GAS

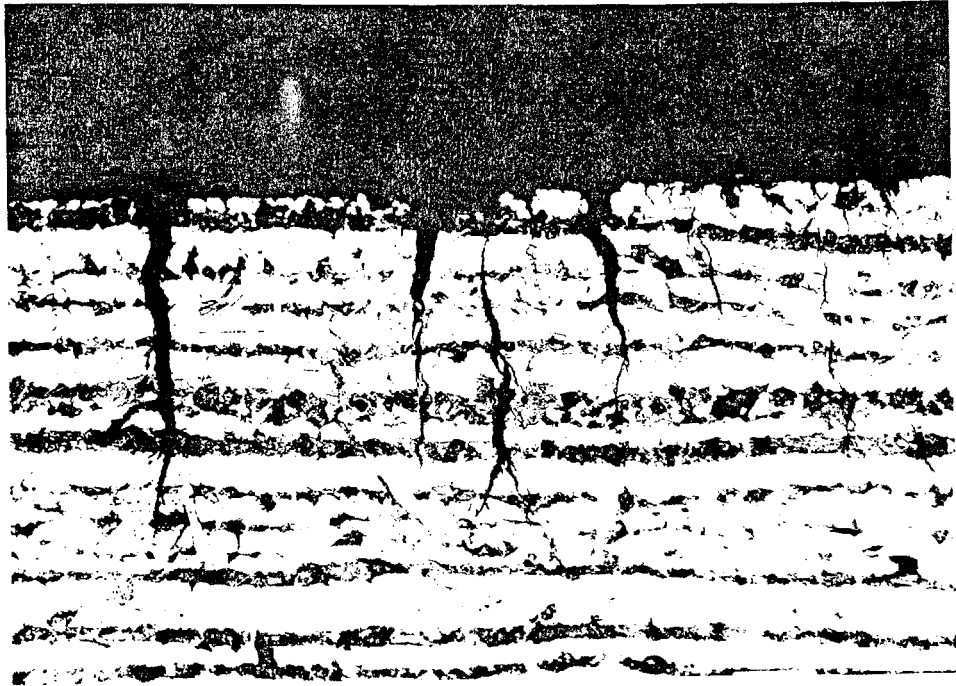


FIGURE 68 Transgranular stress corrosion cracks found in the gauge length of CERT specimens, tested in rich gas
Magnification x100 Etch Nital

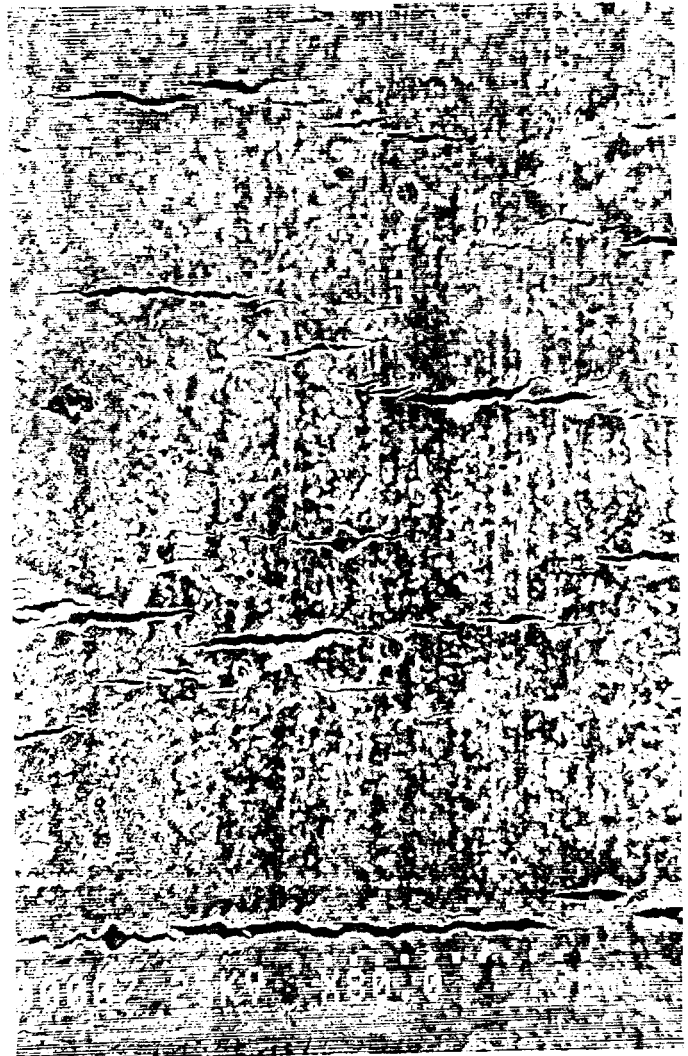


FIGURE 69 Secondary cracks and slight pitting found in the gauge length of CERT specimens tested in rich gas.

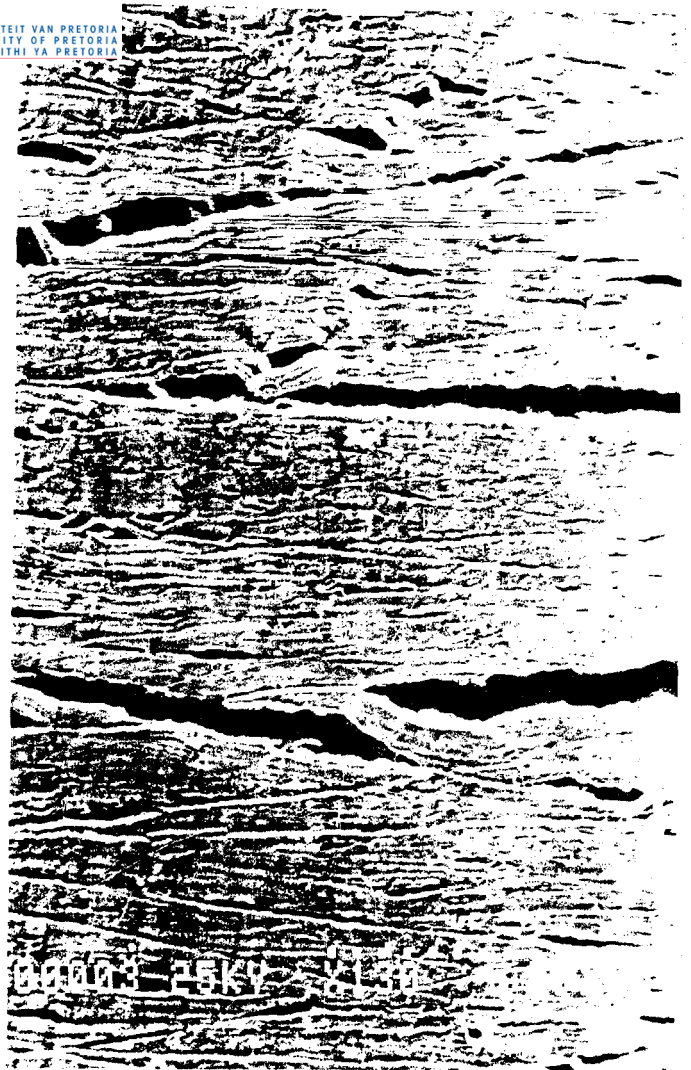


FIGURE 70 Secondary cracks present in the gauge length of inhibited rich gas (100 ppm Petrotec 1420). There is little evidence of other forms of localised corrosion.



FIGURE 71 Fracture surface of CERT specimens tested in rich gas.

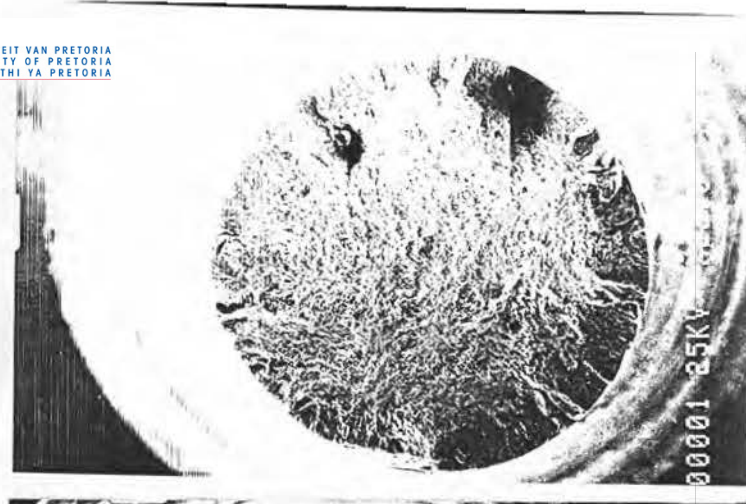
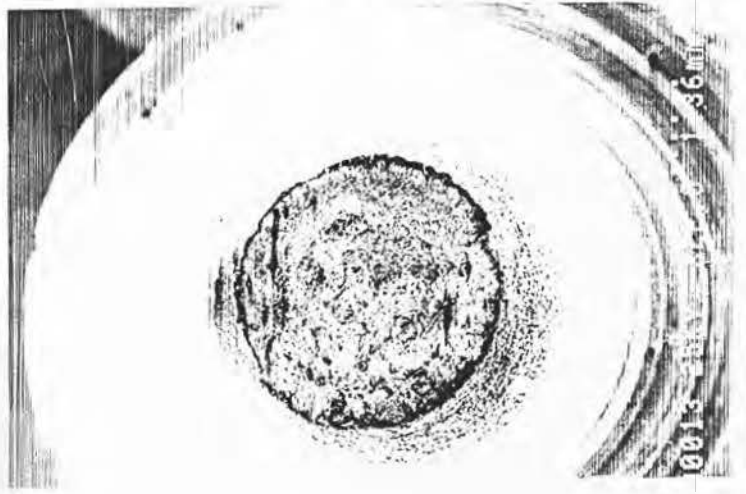
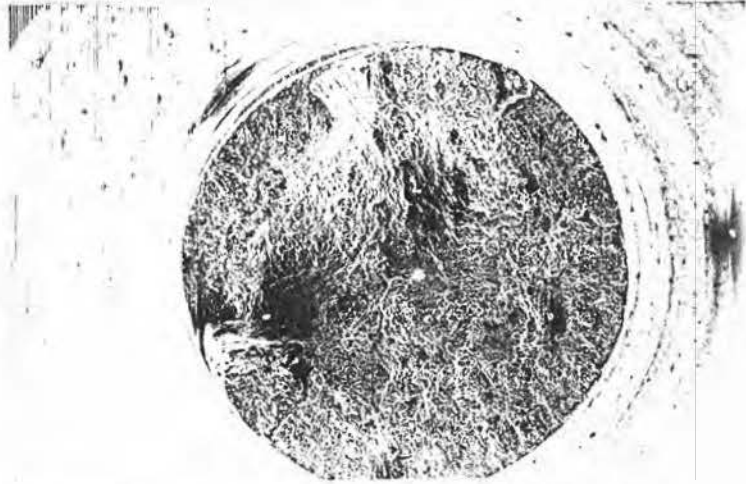
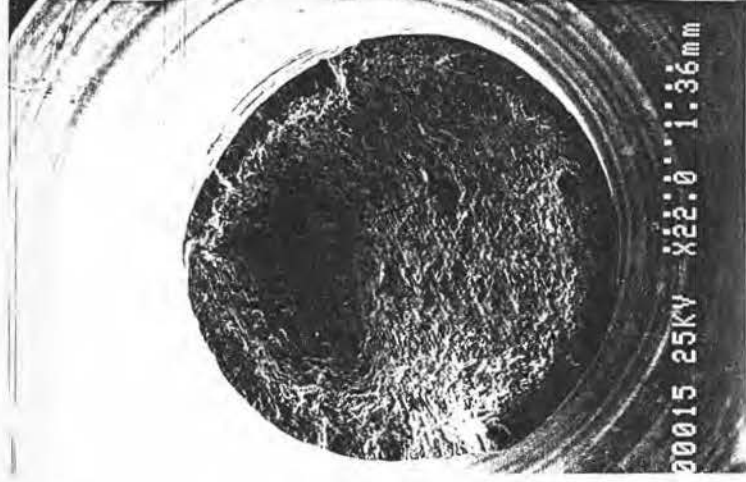
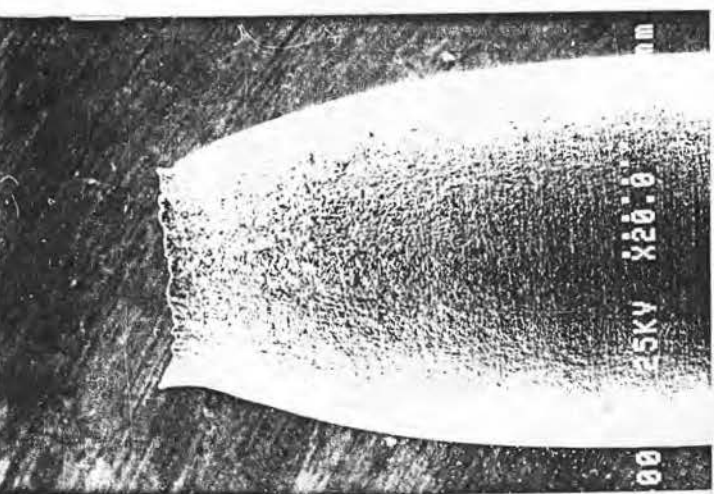
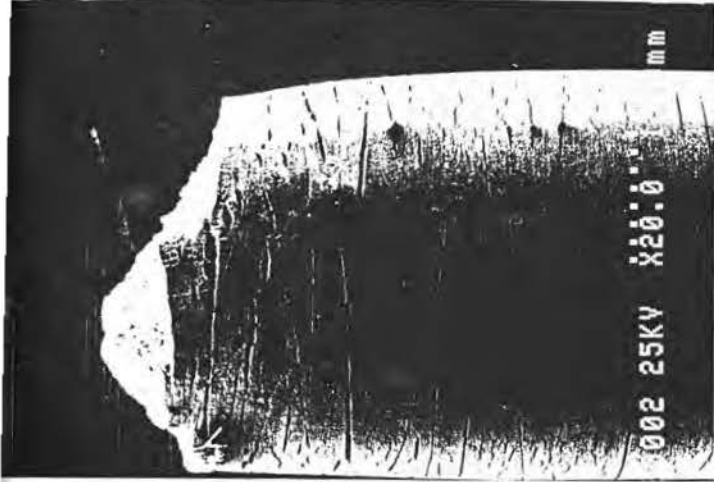




FIGURE 72 Comparison of the fracture appearance of specimens broken in air rich gas and inhibited rich gas.



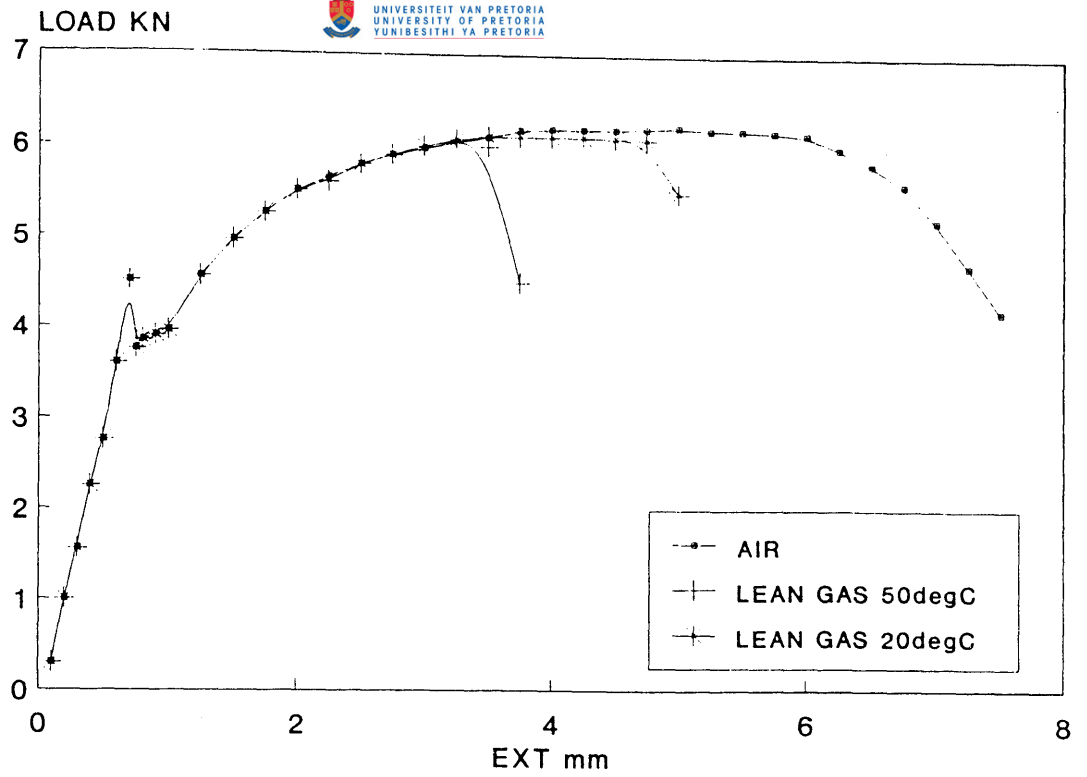


FIGURE 73 LOAD EXTENSION CURVES FOR CARBON STEEL IN AIR AND LEAN GAS AT 20°C AND 50°C

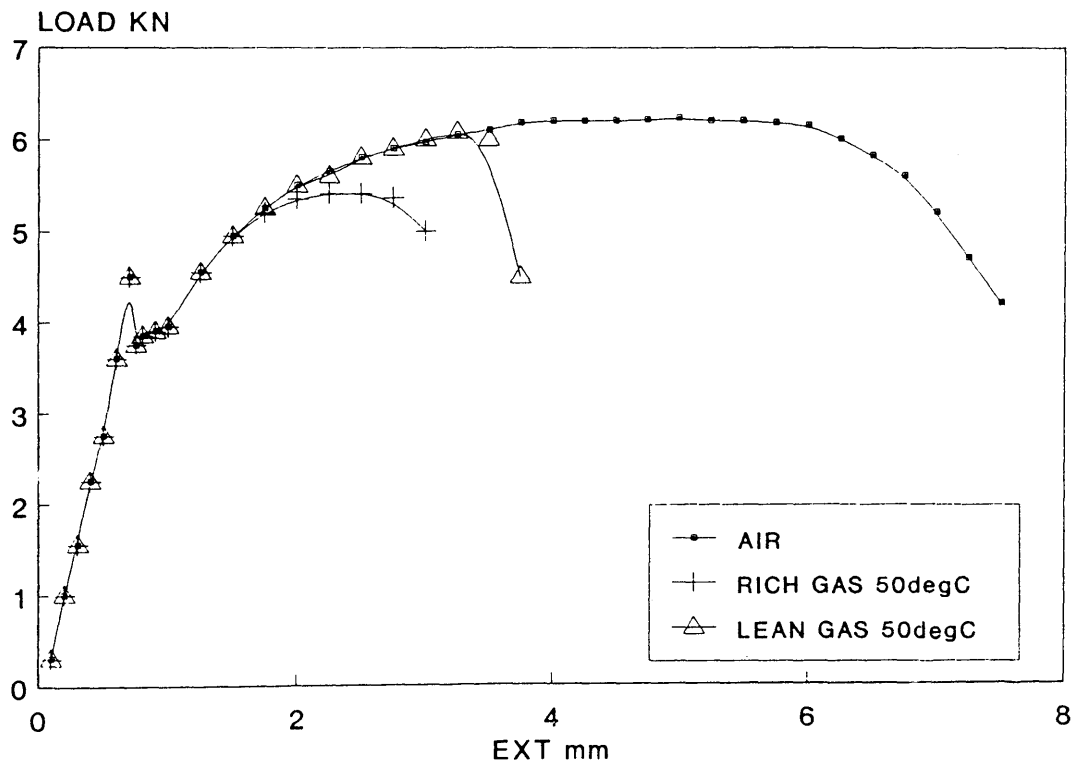


FIGURE 74 LOAD EXTENSION CURVES FOR CARBON STEEL IN AIR, RICH GAS AND LEAN GAS AT 50°C

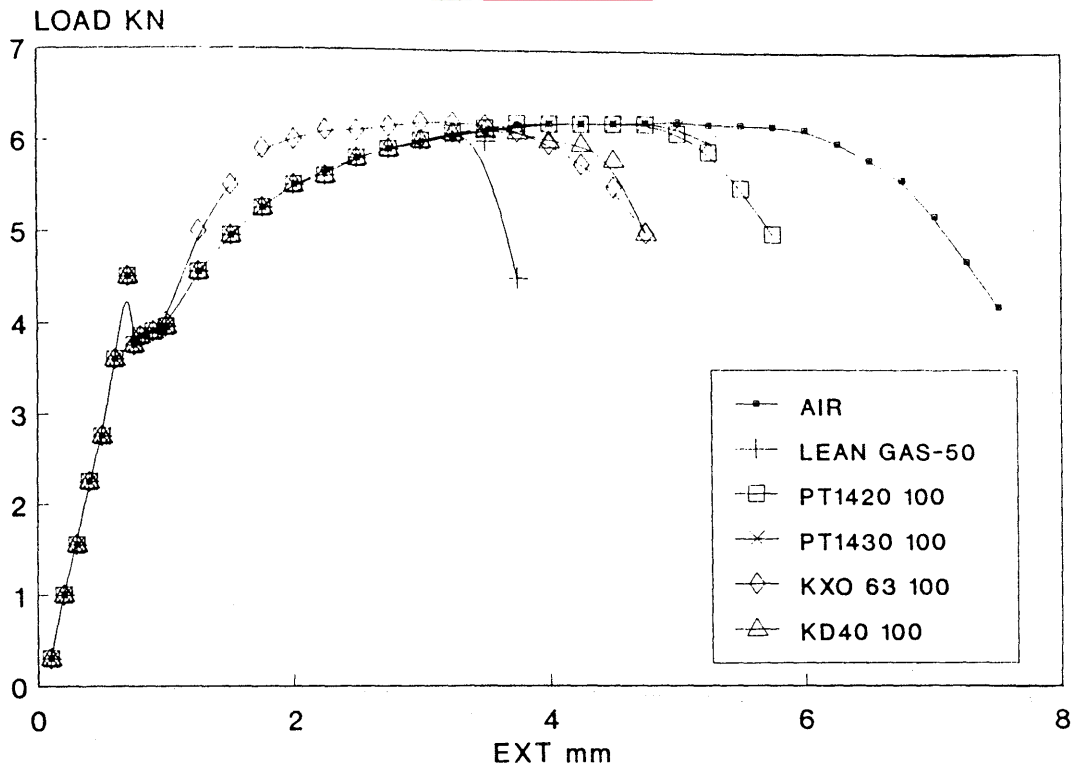


FIGURE 75 LOAD EXTENSION CURVES COMPARING THE EFFECT OF VARIOUS INHIBITOR ADDITIONS TO LEAN GAS, AIR AND LEAN GAS AT 20°C AND 50°C.

11.1 MATERIALS SELECTION

Selection of materials for pressure applications is a two-step procedure. The first step is to select the generic type of material based on principal requirements, in this case resistance to CO-CO₂-H₂O SCC. Once this has been accomplished the specific material specifications can be chosen. This is done on the basis of strength from allowable stress tables in the design code taking into account cost, weldability, form, thickness and availability.

For resistance to CO-CO₂-H₂O SCC it has been shown that ferrous materials require an alloy addition of at least 9% Chromium. Table 20 lists specifications for engineering materials that are within this category.

TABLE 20 MATERIALS FROM ANSI/ASME B31.3 AND ASME VIII ALLOWABLE STRESS TABLES THAT CONTAIN MORE THAN 9% CHROME

DESCRIPTION	SPECIFICATION	GENERIC TYPE
Ferritic and Martensitic	A335 Gr P91 A731 S41500 A731 S44400 A731 S43035	9Cr-4Ni 13Cr-4Ni 18Cr-2Mo-Ti 18Cr-Ti
Duplex	A790 S31500 A790 S31803 A790 S32304	18Cr-5Ni-3Mo 22Cr-5Ni-3Mo 23Cr-4Ni-N
Austenitic	A358 S20100 A312/A358 S21904 A312/A358 S24000 A312 S30403	17Cr-4Ni-6Mn 20Cr-6Ni-9Mn 18Cr-3Ni-12Mn 18Cr-8Ni

Availability, cost and weldability narrow this group to three materials, ferritic 9Cr-1Mo, Duplex 22Cr-5Ni-3Mo and type 304 austenitic stainless steel. A 12% chromium steel manufactured in South Africa, 3CR12 was also of interest because it is easily available and has a relatively low price. Consequently it was added to the list. Also added was a 3½ Ni low alloy steel. The reason here was that low alloy additions of nickel have been used to successfully combat preferential CO₂ corrosion of weldments and additionally nickel readily forms carbonyls so its presence might influence CO absorption at the crack tip. Each candidate material has certain disadvantages which are summarised in Table 21.

TABLE 21 CONSIDERATIONS FOR SELECTION OF LEAN GAS AND RICH GAS PIPING

MATERIAL	TYPE	DISADVANTAGES
A312 S30403	18Cr-8Ni Austenitic stainless steel	High cost
A790 S31803	22Cr-5Ni-3Mo Duplex stainless steel	High cost. Piping fittings not readily available. Welding not straight forward.
3CR12	12Cr Low alloy	It is not a recognised material for pressure parts and piping. It is welded using austenitic filler giving rise to design and metallurgical difficulties. The weld heat affected zones are hard and have poor notch toughness. Piping and fittings are not readily available. Data on resistance of 3CR12 welds to CO-CO ₂ -H ₂ O SCC does not exist.
SA335 Gr P91	9Cr-1Mo Low alloy	Welds and heat affected zones have high hardness and poor notch toughness. Piping and fittings are not readily available. Little data on the resistance of 9Cr-1Mo to CO-CO ₂ H ₂ O environments exists.

Although the low alloy materials have several disadvantages the difference in unit cost compared to stainless steel is large enough to motivate considerable investment in development should a large scale piping replacement be required. It was therefore decided to verify their suitability for the service by exposing U-bend test specimens in a plant bypass and by CERT's.

The procedure recommended by the manufacturer for welding 3CR12 requires the use of an austenitic filler, otherwise the higher heat input utilised for matched fillers results in low toughness heat affected zones, due to rapid grain growth in this region. The fusion line of an austenitic-ferritic joint is extremely sensitive to hydrogen charging which can ultimately result in disbonding. Wet high pressure carbon dioxide is a moderate hydrogen charging medium and can cause stress corrosion cracking of high strength (hard) materials. At least one case is documented where hydrogen charging, following wet CO₂ corrosion, was claimed to be responsible for fusion line disbonding of a dissimilar weld.

For these reasons it was decided to include welded 3CR12 in the test programme and to also test carbon steel - 304L welded joints to further investigate the possibility of fusion line disbonding in rich gas and lean gas environments.

The resistance of materials to wet CO₂ corrosion and to CO-CO₂-H₂O stress corrosion shows a dependence on alloy content, particularly alloy additions of chromium with at least 12% needed for immunity to wet CO₂ corrosion. It is therefore conceivable that chromium depletion at the grain boundaries of type 304 austenitic stainless steel due to sensitising may lead to stress corrosion cracking in rich gas and lean gas environments. To test this, type 304 stainless steel was subjected to furnace heat treatments of different durations in the sensitising temperature range and U-bend specimens were prepared for stress corrosion testing.

11.2 PLANT BYPASS

The lean gas and rich gas plant bypass installations described in Paragraph 10 were used to test U-bend specimens at the operating temperature of 50°C

11.3 U-BEND SPECIMEN PREPARATION

U-bend specimens were prepared from the various materials in accordance with the requirements of ASTM G30-79 specification. Welded specimens were made to the requirements of ASTM standard G58-83. Details of the materials exposed and relevant heat treatments and welding procedures are given in Table 22. After pre-stressing, the U-bend specimens were bolted on to specimen holders which were installed in the plant bypass. The specimens were isolated from the holders by using teflon washers and exposed to the test environment for 90 days. For each gas environment specimens were placed in the gas phase and in the liquid phase. Figure 76 shows the arrangement of specimens on the specimen holders.

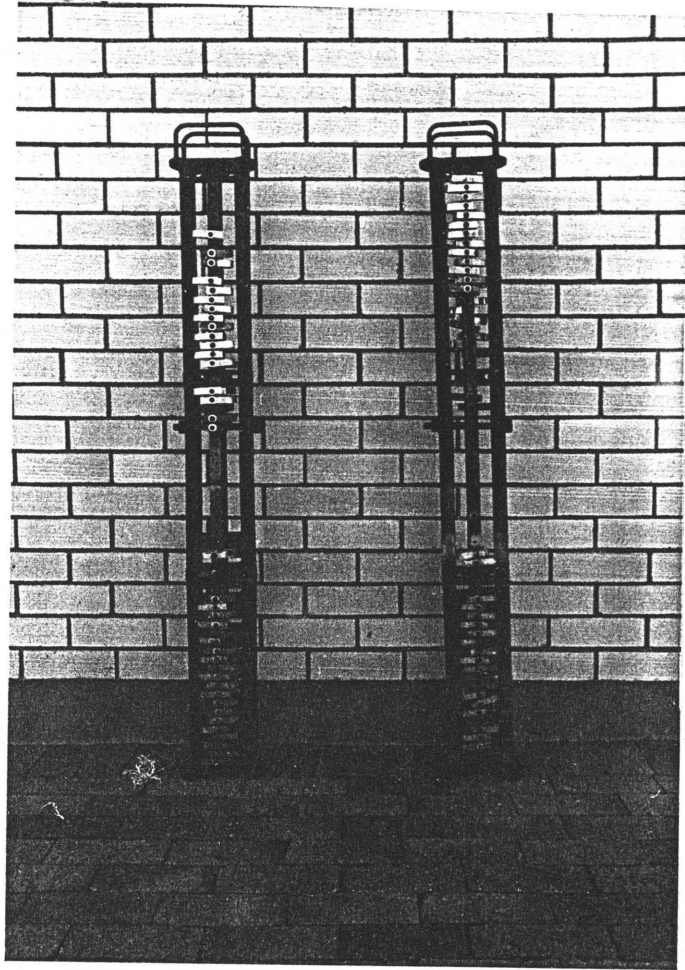


FIGURE 76 ARRANGEMENT OF U-BENDS ON THE SPECIMEN HOLDERS

11.4 CERT SPECIMEN PREPARATION

Standard tensile test specimens were machined from plate and were subjected to CERT, using the procedure described in Paragraph 11.

11.5 RESULTS

11.5.1 Results of U-bend Tests

Table 22 summarises the results of U-bend tests after a 90 day exposure in the lean gas and rich gas bypass facilities. Carbon steel specimens cracked in all conditions exposed, regardless of surface finish. None of the high alloy materials tested suffered SCC. The type 304 stainless steel was fully resistant to the test environment even after a severe sensitising heat treatment.

Dissimilar joints between carbon steel and stainless steel suffered disbonding along the fusion line of the joint. The cracks were intergranular and propagated through a region of high local hardness (460 to 500 Hv 0,10) at the high alloy side of the fusion line. Cracks were found in samples exposed to both lean gas and rich gas. Samples which had not been stress relieved did not crack. No cracks were found in welded 3CR12 specimens although this joint was also an austenite/ferrite combination.

TABLE 22 SUMMARY OF RESULTS OF U-BEND TESTS IN PLANT BYPASS

MATERIAL	DESCRIPTION	RICH GAS		LEAN GAS	
		Liquid Phase	Gas Phase	Liquid Phase	Gas Phase
Carbon steel	Bright surface finish	C	C	C	C
Carbon steel	Heat treated 600°C - Scaled surface finish	C	NT	C	NT
Type 410 s		N	N	N	N
SAF 2205		N	N	N	N
3CR12		N	N	N	N
3CR12 welded	Welded using 309L consumables	N	N	N	N
304/CS weld	As welded	N	NT	N	NT
304/CS weld	PWHT 2 hours 650°C	C	N	N	C
Type 304		N	N	N	N
Type 304	PWHT 2 hours 675°C	N	N	N	N
Type 304	PWHT 4 hours 675°C	N	N	N	N
Type 304	PWHT 8 hours 675°C	N	N	N	N
Type 304	PWHT 20 hours 675°C	N	N	N	N

LEGEND:

- C - SCC cracks
- N - No cracks
- NT - Not tested

11.5.2 Results of CERT

The results of constant extension rate tests made in simulated rich gas and lean gas environments are summarised in Table 23. Carbon steel is included in the table for comparison.

All of the low alloy steels tested showed a marked improvement over carbon steels exhibiting ductility ratios of the order of 0,72 compared with 0,30 shown by carbon steel. When fracture appearance and ductility was used as the assessment criteria the most resistant material was 3CR12 followed by 9Cr-1Mo and 3½ Ni low alloy steel. However in rich gas this result is not supported by ductility ratio. Figures 77 to 80 show the load extension graphs for carbon steel, 3½ Ni steel, 9Cr-1Mo and 3CR12 respectively.

TABLE 23 RESULTS OF CERT TO DETERMINE THE RESISTANCE OF MATERIALS TO CO-CO₂-H₂O

MATERIAL	RICH GAS			LEAN GAS		
	% RA	Ductility Ratio	Presence of Secondary Cracks	% RA	Ductility Ratio	Presence of Secondary Cracks
Carbon steel	22	0,33	Secondary cracks all along the gauge length	20	0,30	Secondary cracks all along the gauge length
3½ Ni low alloy steel	52	0,65	Secondary cracks limited to necked region	59	0,73	Secondary cracks limited to necked region
9Cr-1Mo low alloy steel	55	0,74	Few secondary cracks. Only in the necked region	49	0,74	Few secondary cracks. Only in the necked region
3CR12	27	0,56	No secondary cracks	35	0,75	No secondary cracks

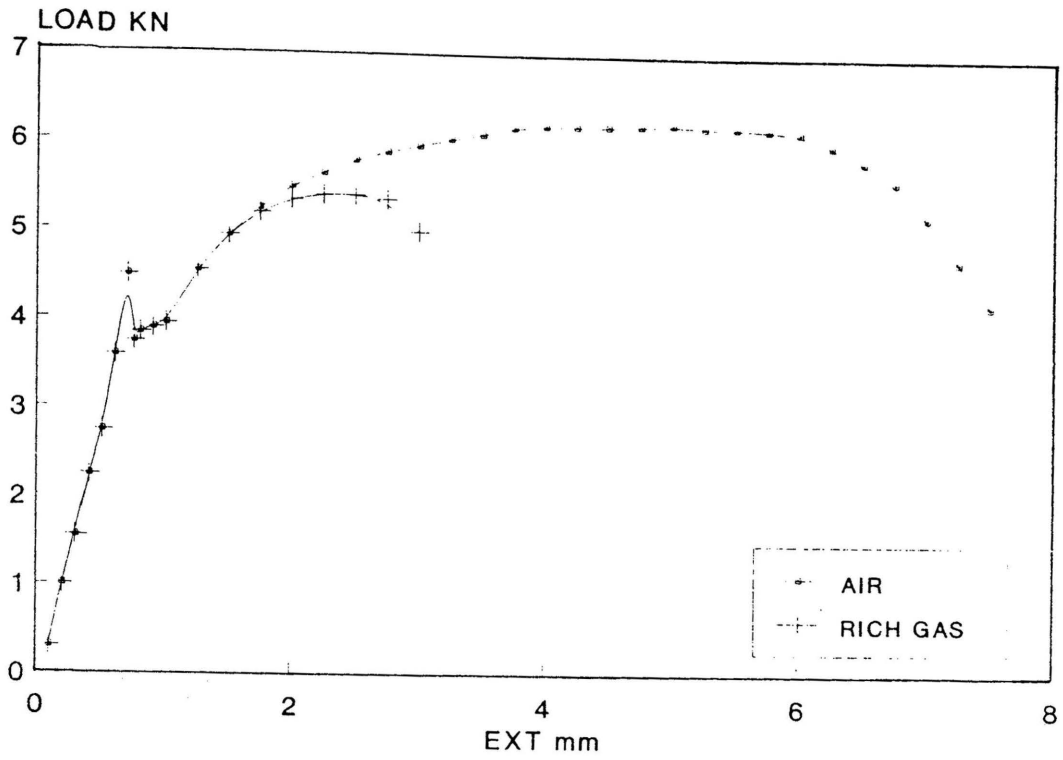


FIGURE 77 LOAD EXTENSION CURVES FOR CARBON STEEL IN RICH GAS AND AIR

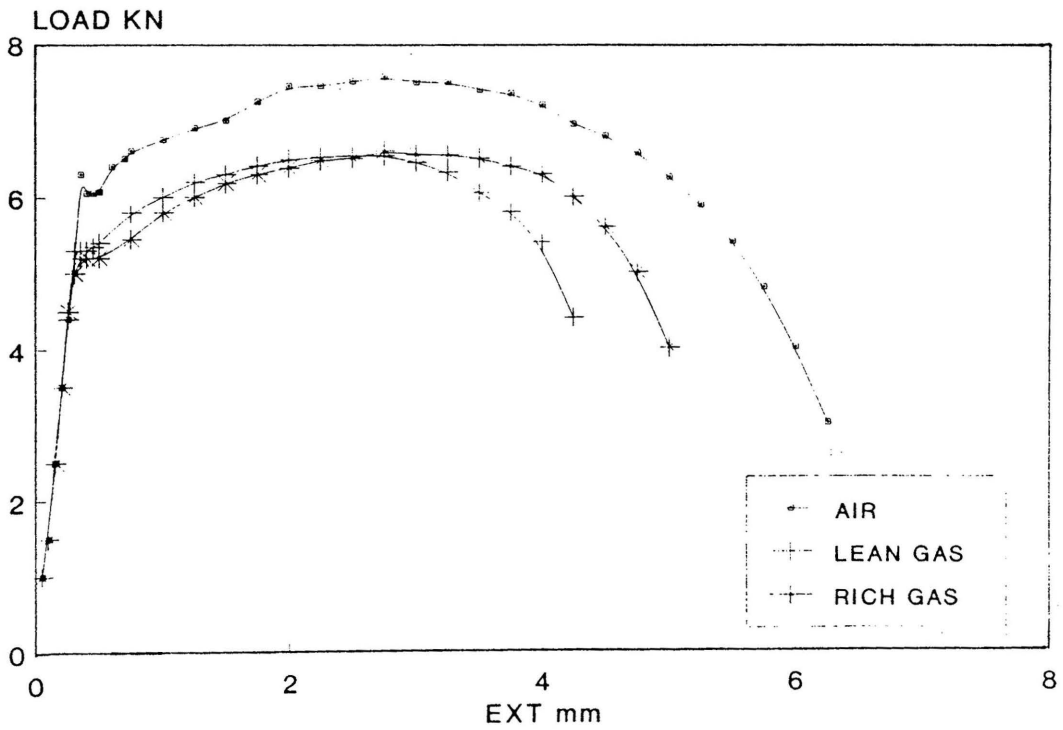


FIGURE 78 LOAD EXTENSION CURVES FOR 3 1/2 Ni STEEL TESTED IN AIR

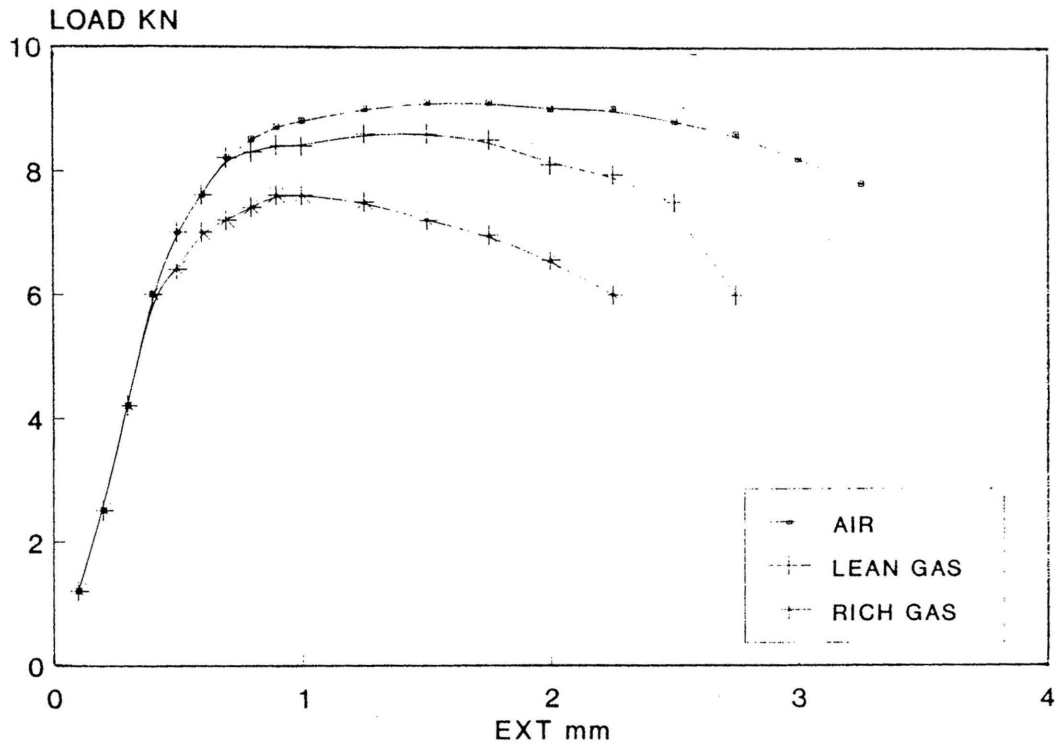


FIGURE 79 LOAD EXTENSION CURVES FOR 9Cr-1Mo STEEL TEST IN AIR, LEAN GAS AND RICH GAS

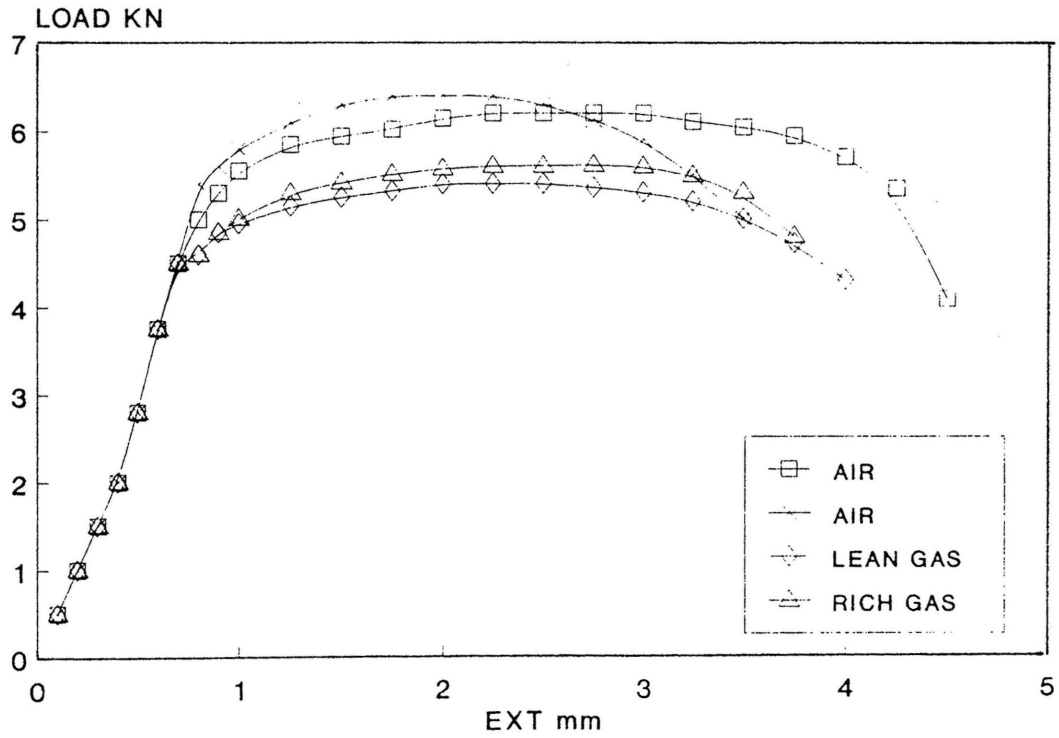


FIGURE 80 LOAD EXTENSION CURVES FOR 3CR12 STEEL TESTED IN AIR, LEAN GAS AND RICH GAS

12 ASSESSMENT OF THE PERFORMANCE OF POST WELD HEAT TREATED CARBON STEEL IN WET CO-CO₂ GAS MIXTURES

The performance of post weld heat treated carbon steel piping and equipment was assessed in industrial environments containing wet mixtures of CO and CO₂ gas. Unless otherwise stated the pressure vessels were fabricated to SA 516 Gr 70 and the piping to SA 108 Gr B. The specified compositions are in Table 24.

TABLE 24 SPECIFIED COMPOSITIONS FOR SA 516 Gr 70 AND SA 106 Gr B

Specification	Carbon	Manganese	Phosphorous	Sulphur	Silicon	Yield Strength	UTS
SA 516 Gr 70	0,27	0,79-1,30	0,35 max	0,04	0,13-0,45	205 min	485-620
SA 106 Gr B	0,30	0,29-1,60	0,098	0,058	0,10 min	240 min	415 min

The pressure vessels were heat treated in the temperature range 590°C to 630°C with a minimum holding time of 1 hour and 2½ minutes per millimetre thereafter, in accordance with the ASME and pressure vessel code and the petrochemical companies' own specifications. The piping was heat treated at a slightly higher temperature of 600 to 650°C in accordance with API 945 recommended practice in order to optimise stress relief. The reason the vessels were not stress relieved at the higher temperature is, at the time of fabrication SCC was not anticipated in the service environment.

12.1 PERFORMANCE OF POST WELD HEAT TREATED PRESSURE VESSELS

Sixteen large pressure vessels operating at 50°C, 1890 kPa total pressure, in a lean gas service environment were assessed after 10 years service. The vessels were, without exception, designed to Division 2 of the ASME pressure vessel code.

All of the vessels suffered extensive stress corrosion cracking with deep cracks present in the vicinity of main and attachment welds. The parent metal suffered extensive craze cracking. The typical appearance of the cracks is shown in Section 9 Figures 29 to 31.

Severe SCC was occasionally observed in the parent metal remote from the main welding seams. Its uniform shape suggested it was due to welding temporary attachments during construction.

12.2 PERFORMANCE OF PIPING

Following a service life of approximately two years welds in HP lean gas, in LP lean gas and welds in rich gas service were examined by wet magnetic particle testing (MT). The operating temperature of the piping was around 50°C with a total pressure near to 2000 kPa. The pipe sizes were between 12 and 16 inch. Any welds which gave an indication of the presence of stress corrosion cracks were sectioned and examined more closely by metallography.

12.2.1 HP Lean Gas Piping

The MT did not reveal cracks in any of the weldments examined, however craze cracking was found on the parent metal adjacent to the welds. A microscopic examination of sections through the worst crack indications did not reveal any cracks. The welds examined were in service for one year.

12.2.2 LP Lean Gas Piping

A MT examination of lean gas piping after three years' service also did not reveal any weld metal cracking. However, half of the welds examined exhibited craze cracking in the parent metal. The cracks were roughly orientated perpendicular to the principal hoop stress. Figure 81 shows a typical example of craze cracking. Sectioning revealed stress corrosion cracks up to 0,5 mm deep. Most had corroded out to form sub-surface cavities. Examples are shown in Figure 82 to Figure 84.

12.2.3 Rich Gas

Only one of the welds examined by magnetic particle testing (MT) showed any evidence of cracking. A cross-section through the cracked area revealed multi-branched stress corrosion cracks (Figure 85). The cracking had taken place in a repair weld. Micro hardness tests made adjacent to the stress corrosion crack revealed that the average hardness was 280 Hv 0,01.

12.2.4 Summary of Results

The survey carried out on post weld heat treated carbon steel piping and equipment revealed that stress relief did not prevent SCC of vessels operating in lean gas. In contrast piping operating in lean and rich gas showed no evidence of stress corrosion cracking at weldments following stress relief. Shallow parent metal craze cracking was however observed in lean gas service. The cracks showed a marked tendency to corrode, eventually forming subsurface corrosion cavities. Craze cracking was multi-directional SCC resembling elephant skin and was due to shallow surface residue stresses remaining after fabrication of the plate.

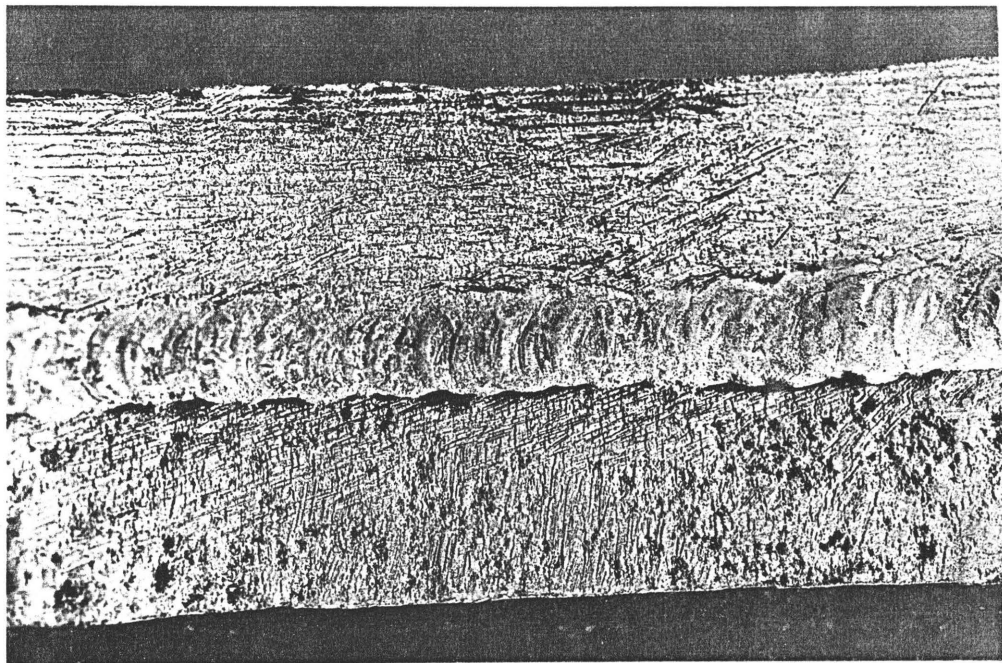


FIGURE 81 Typical appearance of postweld heat treated carbon steel piping after three years service in lean gas. The magnetic particle examination revealed craze cracking roughly aligned perpendicular to the hoop stress.

FIGURES 82 to 84 show the typical appearance of craze cracking after sectioning. The majority, although not all of the cracks had corroded out to form subsurface cavities.

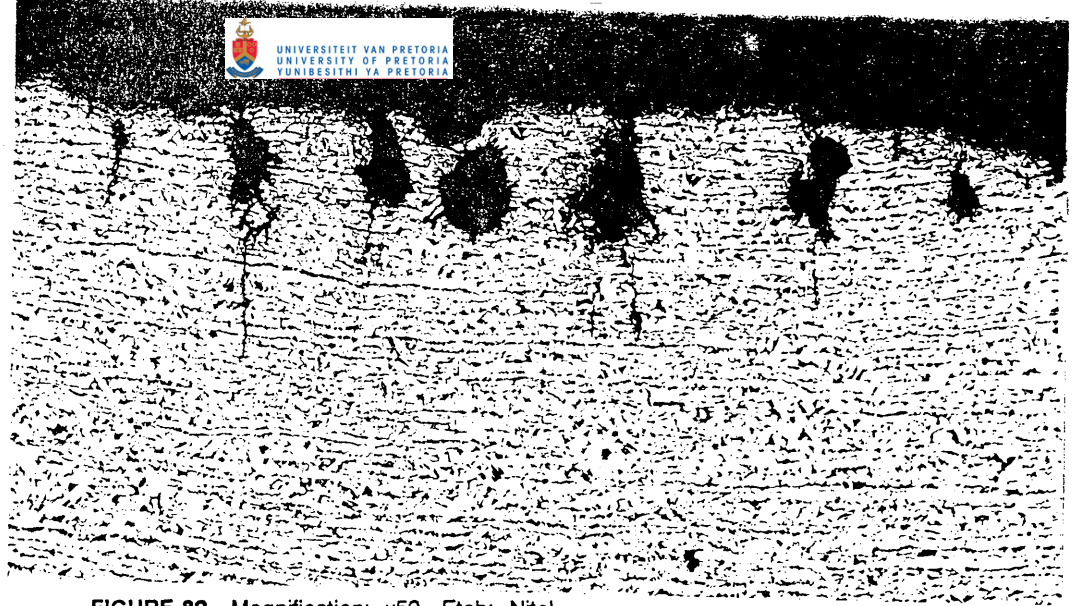


FIGURE 82 Magnification: x50, Etch: Nital



FIGURE 83 Magnification: x100, Etch: Nital



FIGURE 84 Magnification: x100, Etch: Nital



FIGURE 85 Multi-branched stress corrosion cracking found at a hard weld repair in rich gas

13 POTENTIODYNAMIC POLARISATION

13.1 EXPERIMENTAL METHOD

Cylindrical electrodes prepared from SA 516 Gr 70 carbon steel were used in a conventional three electrode cell that was placed inside a stainless steel autoclave. The area of the working electrode was 5 sq cm. Silver/silver chloride, in a saturated chloride solution was used as the reference electrode and the cell was isolated from the autoclave body by a glass container opened to the gas space so that the pressure could equalise. The reference electrode was placed inside the autoclave at the experimental temperature. A conventional potentiodynamic polarisation technique was used to study the anodic and cathodic polarisation characteristics of carbon steel in various aqueous solutions pressurised with gas mixtures containing carbon monoxide and carbon dioxide gas. So that plant conditions could be simulated a technique similar to that described in Section 9 was adopted. Aqueous condensate was drawn from the plant and repressurised in the autoclave with gas taken from the relevant process streams. Prior to pressurising, the condensate was degassed with pure nitrogen to remove any oxygen that might have been absorbed during transport from the plant.

The autoclave pressure was controlled by the inlet and outlet needle valves and the pressure was measured by a standard pressure gauge. The same valves were used to control the gas flow until it steadily bubbled through the autoclave. The cell temperature was regulated by a thermocouple via a controller to an electric heating mantle on the outside of the autoclave. Exposure time, gas partial pressure and temperature were initially adjusted to examine their influence on the polarisation characteristics of carbon manganese steel in aqueous solutions of carbon monoxide and carbon dioxide gas. The same equipment was then used to draw polarisation curves following the addition of various inhibitors. Additional polarisation curves were drawn for a 3½ Ni low alloy steel and a 9Cr-1Mo alloy steel in condensate saturated with rich gas.

The anodic and cathodic curves for key conditions were drawn, individually starting each time at the open circuit potential (E_{CORR}). The polarisation curve for the film free condition was achieved by a reverse scan. Typically, the electrode was stabilised after pressurising and scanned at 20 mV/min in the negative direction and allowed to re stabilise, after which a three segment scan was done from 0 to +300, +300 to 0 and then 0 to -300 mV with E_{CORR} as the zero point.

13.2 RESULTS

13.2.1 Carbon Manganese Steel in Rich Gas

Polarisation curves were drawn at 20°C, 50°C and 80°C after pressurising to 18 bar total pressure. Additional curves were drawn at 20°C, for 18, 10 and 5 bar total pressure. All curves were characterised by increasing anodic and cathodic polarisation with time, a movement of E_{CORR} through a potential range of approximately 100 mV, and a time dependent breakdown potential for anodic passivation. Figures 86 to 91 show curves drawn in rich gas.

After 2 hours (Figure 86) the cathodic current density was significantly less than the film free condition and E_{CORR} was about 10 mV more negative. The corresponding anodic curve after 2 hours showed a slight hump due to inhibition of the anodic reaction. After a slightly longer exposure the size of the anodic hump had increased and the line for the cathodic reaction had moved further to the left (Figure 86). At a longer exposure time of 8 hours (Figure 87), little additional cathodic polarisation occurred but the anodic current was significantly reduced and the stability range of passivation was extended to a breakdown potential of about -425 mV. The increase in anodic passivation was accompanied by a slight positive movement of E_{CORR} . The pattern was followed by a 24 hours exposure, after which the range of anodic passivation had extended further (Figure 88). Figure 89 contains all the curves drawn at 20°C superimposed to show the time dependence of the anodic and cathodic polarisation.

In Figure 90, the effect of scanning rate is shown. The curve drawn at the higher scan rate (1000 mV/min compared with 20 mV/min) was similar to that obtained by reverse scanning to obtain a film free surface, except that the cathodic currents were higher suggesting that some absorption and inhibition of the cathodic reaction might have occurred during the course of the reverse scan.

The effect of carbon monoxide and carbon dioxide partial pressures was assessed by adjusting the total pressure of the autoclave. The group of curves shown in Figure 91 drawn after similar exposure times, shows the effect of changing partial pressures. The shape of the curves was virtually independent of partial pressure and in each case E_{CORR} was close to -590 mV.

A similar set of polarisation curves were drawn for lean gas to show the effect of time. These are shown in Figures 92 to 95. The results resembled those from rich gas except that inhibition of the cathodic reaction occurred sooner than inhibition at the anode, with the result that the cathodic curve moved sharply to the left and E_{corr} moved 30 mV more negative to the film free condition (Figure 92). With longer exposure times up to 50 hours there was little change in the cathodic curve but the anodic polarisation was slowly increased, (Figures 93, 94 and 95) and E_{corr} moved to more positive values, eventually stabilising at around -570 mV. The film breakdown potential corresponding to this condition was close to -400 mV. The low CO partial pressure in lean gas did not significantly affect the rate of cathodic inhibition, but inhibition of the anodic reaction occurred at a much slower rate than in rich gas.

13.2.3 Effect of Temperature

Polarisation curves drawn at 50°C for rich gas and lean gas (Figures 96 and 98) resembled those at 20°C showing increased polarisation with longer exposure times. The anodic inhibition process however proceeded at a much slower rate, with E_{corr} and breakdown potentials, respectively more negative than -600 and -450 mV recorded after a 10 hours exposure period. Once again anodic passivation was much slower in lean gas than in rich gas, presumably due to its much lower CO partial pressure.

Polarisation curves drawn in rich gas at 80°C (Figure 97) followed a similar pattern, relatively high anodic currents were recorded compared to a similar exposure time at 50°C and 20°C however the inhibited zone was stable up to higher potentials showing a plateau around -400 mV.

13.2.4 3½ Ni Steel In Rich Gas

The electrochemical behaviour of 3½ Ni steel in rich gas was similar to that of carbon steel, showing the start of anodic and cathodic passivation after short exposure times (Figure 101). The curves do not indicate a benefit from the use of this material in wet CO-CO₂ service.

13.2.5 9Cr-1Mo Steel in Rich Gas

The polarisation curve for 9Cr-1Mo resembled that obtained using a carbon steel electrode. Except that the anodic passivation occurred much faster (Figure 99) and there was no plateau at -400 mV due to breakdown of passivity. A slight inflection at this potential was however observed. Increased exposure times did not significantly alter the polarisation characteristics of 9Cr-1Mo (Figure 100). A superimposed fast scan (done at 1 000 mV/min) showed only a slight deviation from the slow scan curve and did not indicate any particular susceptibility to stress corrosion cracking (Figure 99).

13.2.6 Rich Gas Plus Inhibitors

The effect of various inhibitors added to condensate pressurised with rich gas was assessed by the polarisation curves drawn in Figures 102 to 107. KD-40, KXO-63 and Petrotec 1420 at 10 and 100 ppm all gave similar plots that were variations on the family of curves shown earlier for uninhibited rich gas (Figure 89). The results suggested that these inhibitors only slightly affect the kinetics of the anodic and cathodic reactions due to CO and CO₂. The eventual outcome however is the same.

The two inhibitors AO-003 and Petrotec 1430 prevented film breakdown at -400 mV (Figure 103) and a large addition of Petrotec 1420 (5 000 ppm) moved the corrosion potential more positive than the breakdown potential (Figure 105).

The behaviour of Reomet was interesting as it delayed the development of anodic and cathodic polarisation (Figures 106 and 107).

During the early experiments it was noticed that the initial corrosion potential after pressurising with gas was near to -500 mV and moved more negative to about -600 mV after the passage of rich gas. Following, prolonged exposure the open circuit potential moved to slightly more negative values and eventually stabilised near to -560 mV. Tests made after longer periods of degassing did not show a large initial downward shift and E_{corr} was usually close -600 mV soon after pressurising. Curves drawn for both cases are in Figure 108. This result is not unlike the behaviour in Reomet (Figure 107) and is considered to be due to the presence of oxygen which allowed the oxygen reduction reaction to take place at the cathode. The oxygen was eventually purged from the system with further passage of gas from the plant with the result that E_{corr} moved to potentials measured after more thorough degassing.

13.2.8 Movement of Corrosion Potential after Holding Above the Anodic film Breakdown Potential

Carbon steel electrodes were polarised to -300 mV which was of the order of 100 mV more positive than the breakdown potential for the anodic film and the open circuit potential was measured as soon as the polarising current was switched off. It was found that the recorded value of E_{corr} immediately fell to around -630 mV and over a period of 15 to 10 minutes recovered to -560 mV. Since there was a 1 to 2, minute delay switching from one instrument to another the potential could not be measured immediately after removing the polarising current so it is likely that it moved more negative than the -630 mV measured.

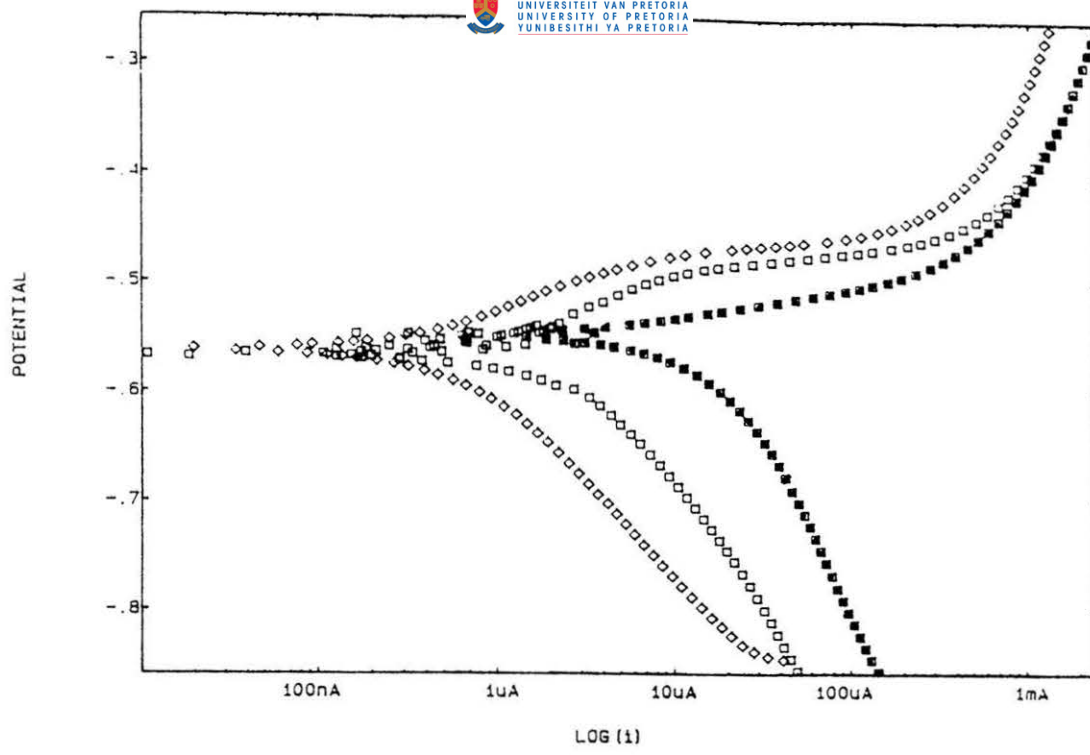


FIGURE 86 Carbon steel scanned in rich gas 18 bar, 20°C, ■ film free, □ 2 hours, ◇ 4 hours.

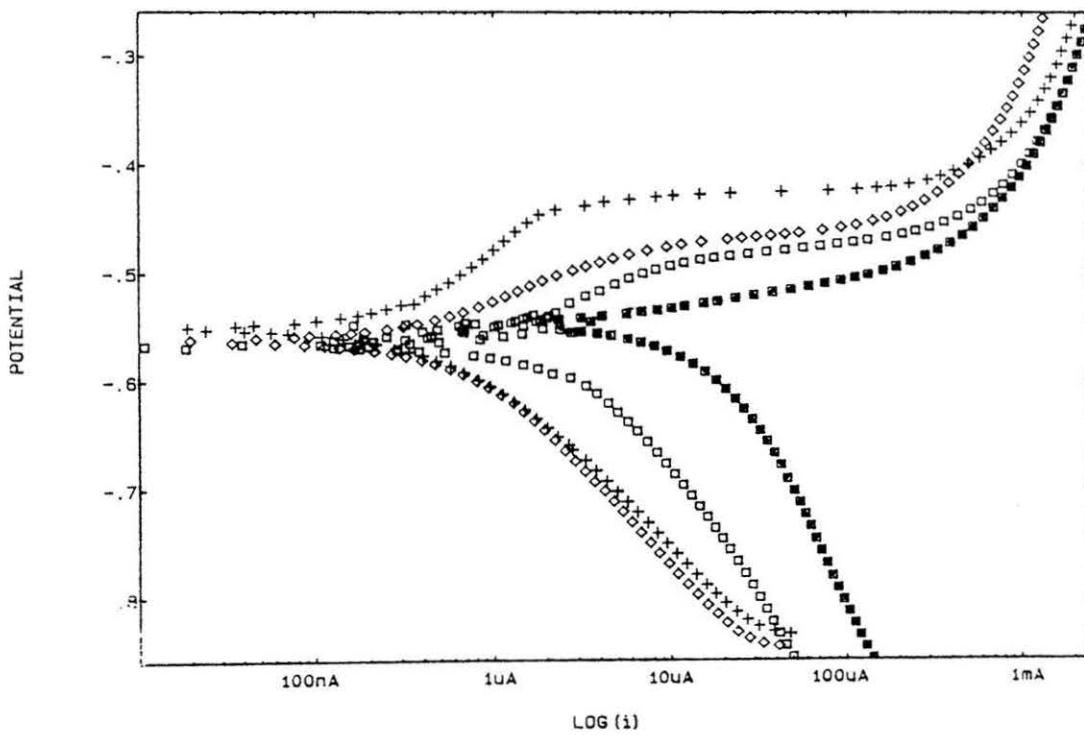


FIGURE 87 Carbon steel scanned in rich gas 18 bar, 20°C, ■ film free, □ 2 hours, + 8 hours.

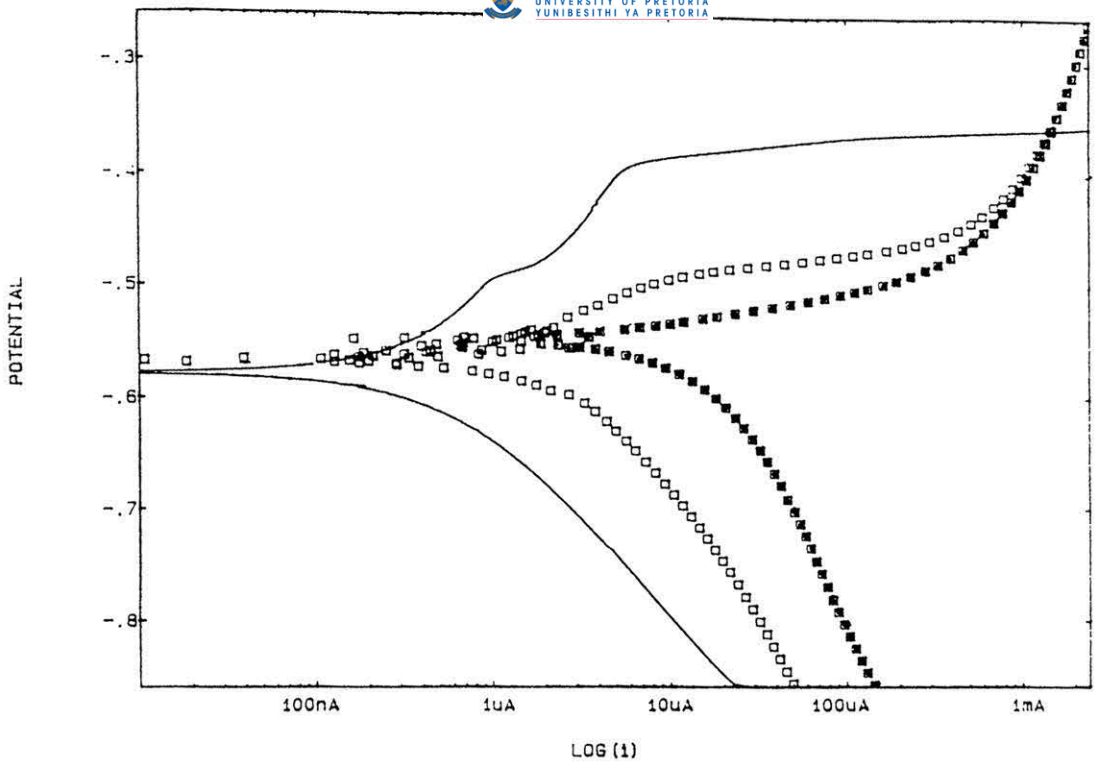


FIGURE 88 Carbon steel scanned in rich gas 18 bar, 20°C, ■ filmfree, □ 2 hours, - 10 hours.

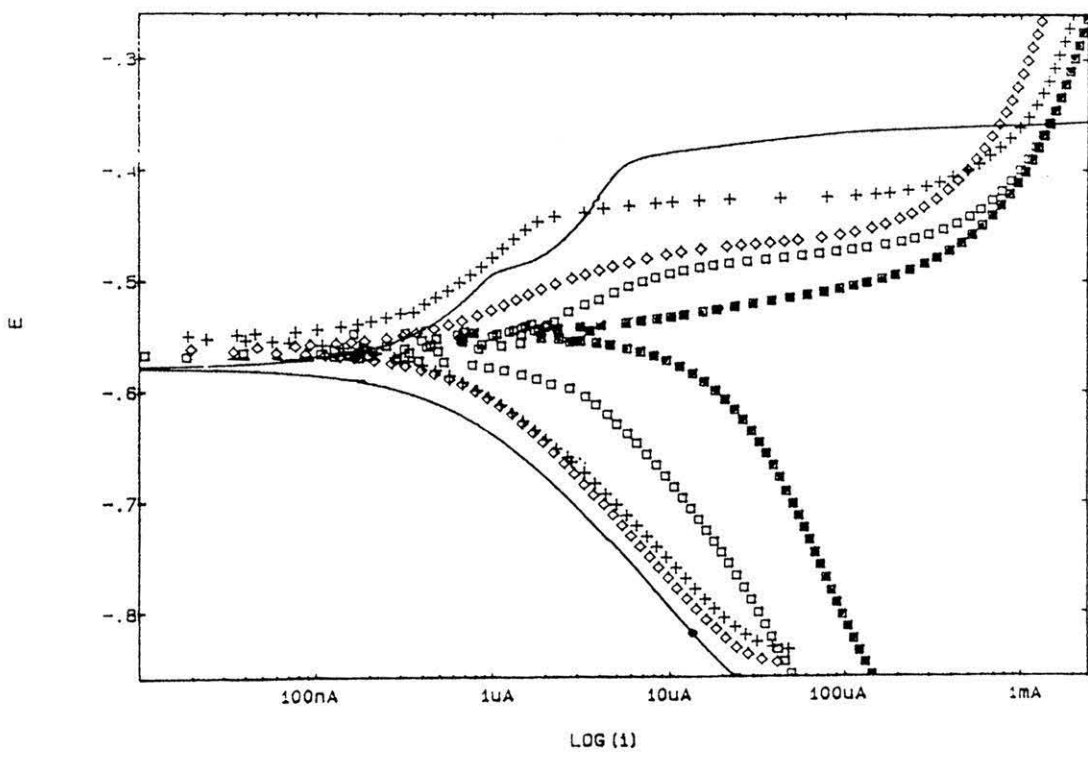


FIGURE 89 Carbon steel scanned in rich gas 18 bar, 20°C.
■ film free, □ 2 hours, ◇ 4 hrs, + 8 hours, - 10 hours.

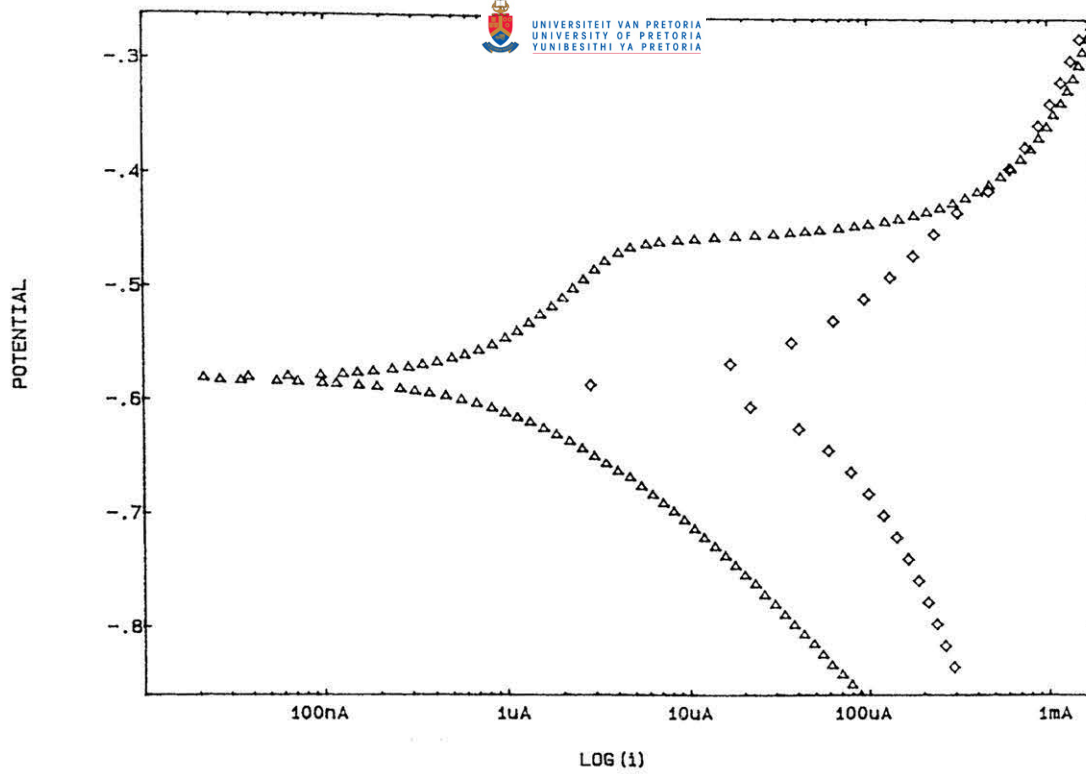


FIGURE 90 Fast (1 000 mv/min, \diamond) and slow scan (20 mV/min, Δ) for carbon steel, in rich gas at 18 bar, 20°C.

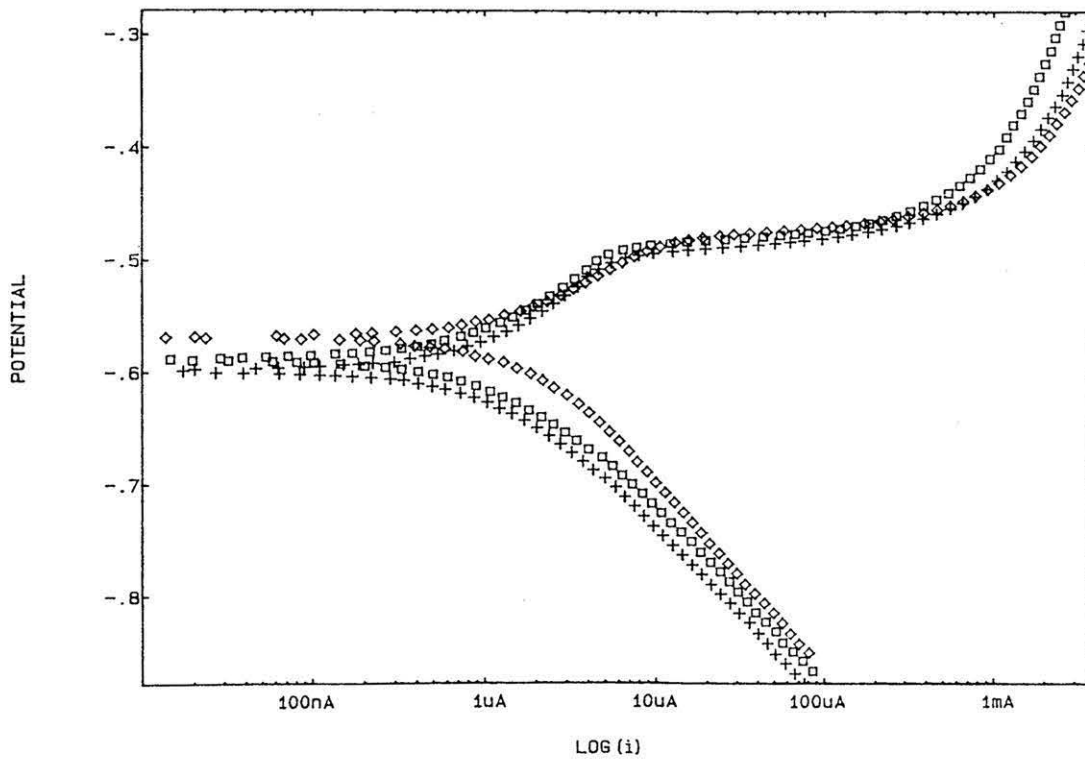


FIGURE 91 Carbon steel in rich gas scanned after 4 hrs at 20°C at various total pressures. + 5 bar, \square 10 bar, \diamond 18 bar.

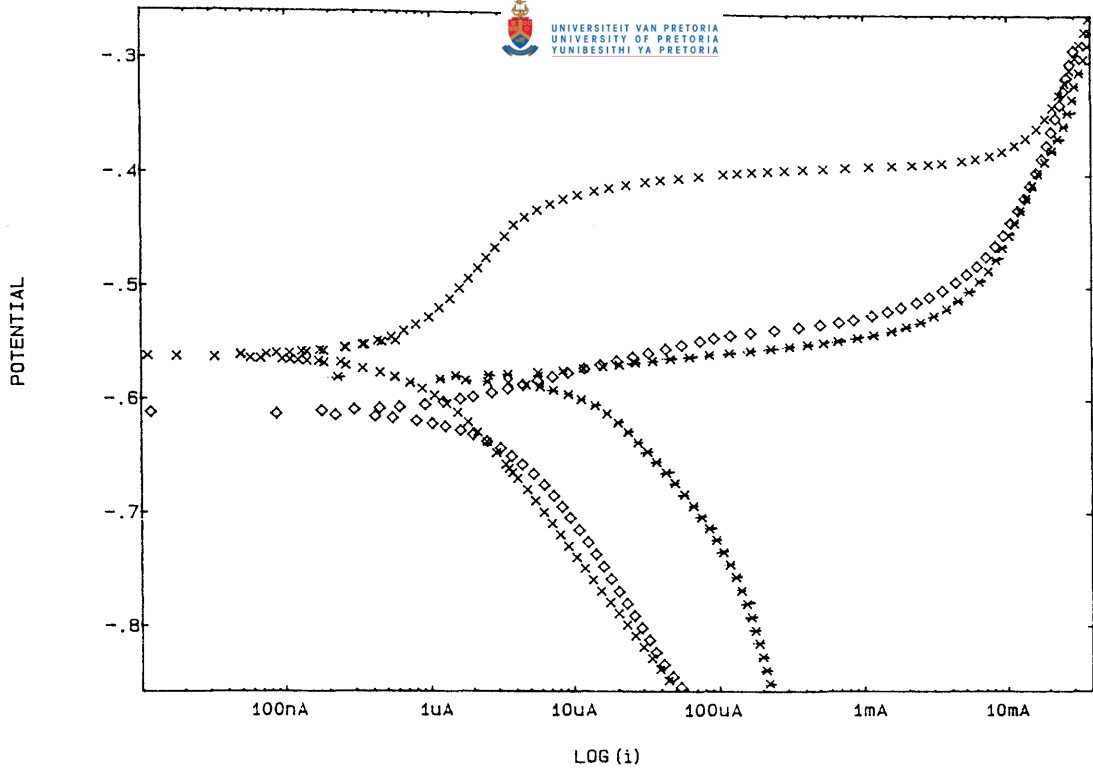


FIGURE 92 Carbon steel scanned in lean gas 20°C, 18 bar. x film free, o 2 hours, + 24 hours.

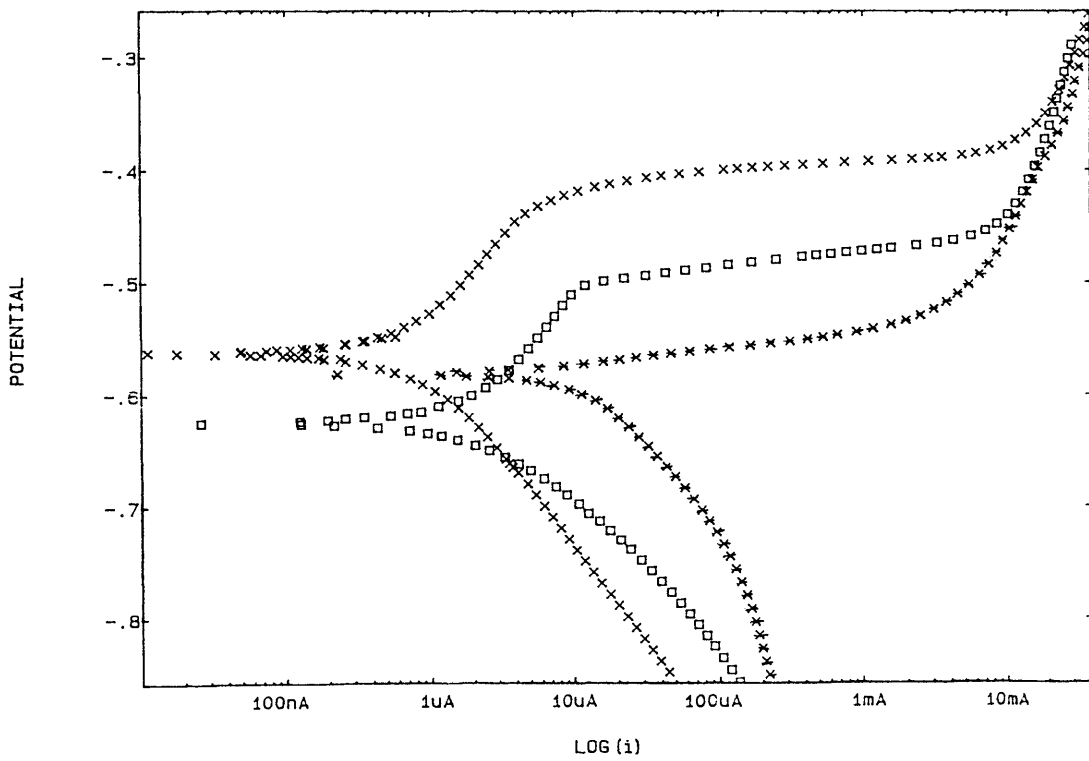


FIGURE 93 Carbon steel scanned in lean gas 20°C, 18 bar. x film free, □ 10 hours, + 24 hours.

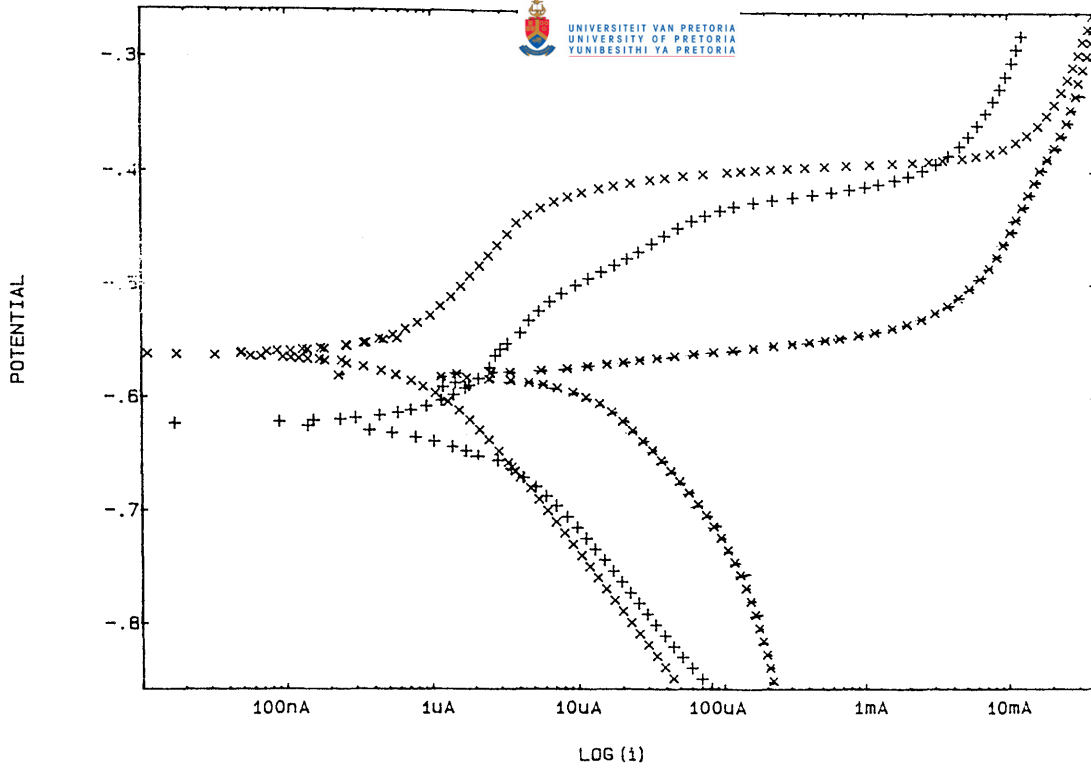


FIGURE 94 Carbon steel scanned in lean gas 20°C, 18 bar, * film free, + 12 hours, x 24 hours.

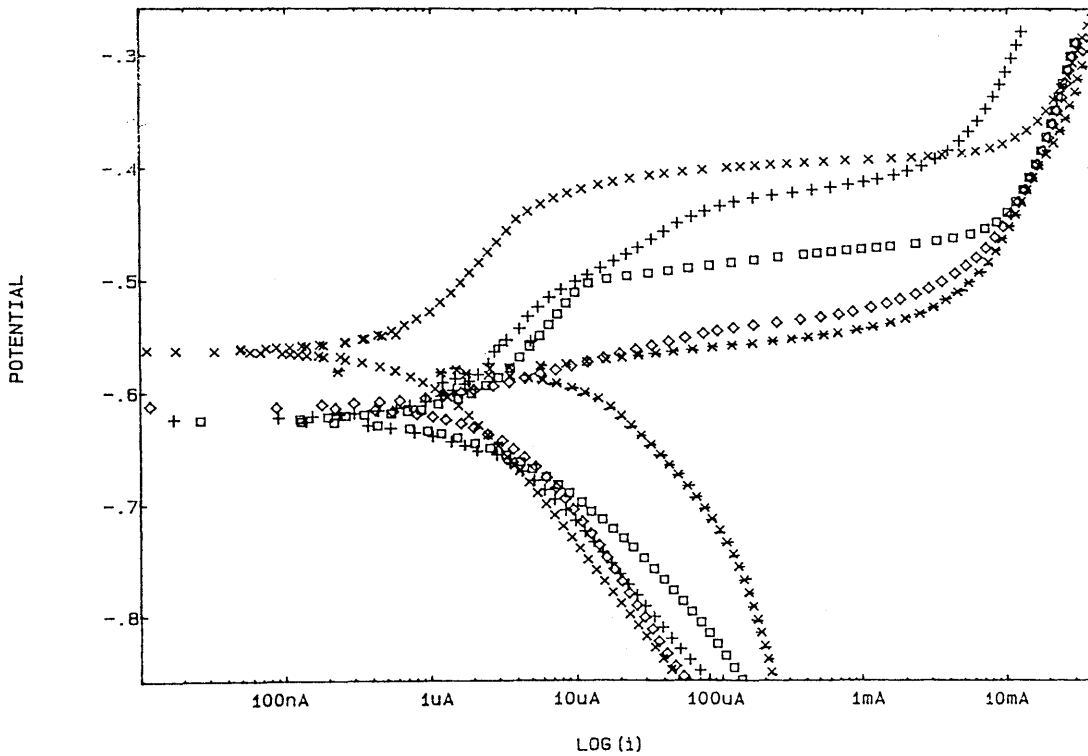


FIGURE 95 Carbon steel scanned in lean gas 20°C, 18 bar,
* film free, \diamond 1 hour, \square 10 hours, + 12 hours, x 24 hours.

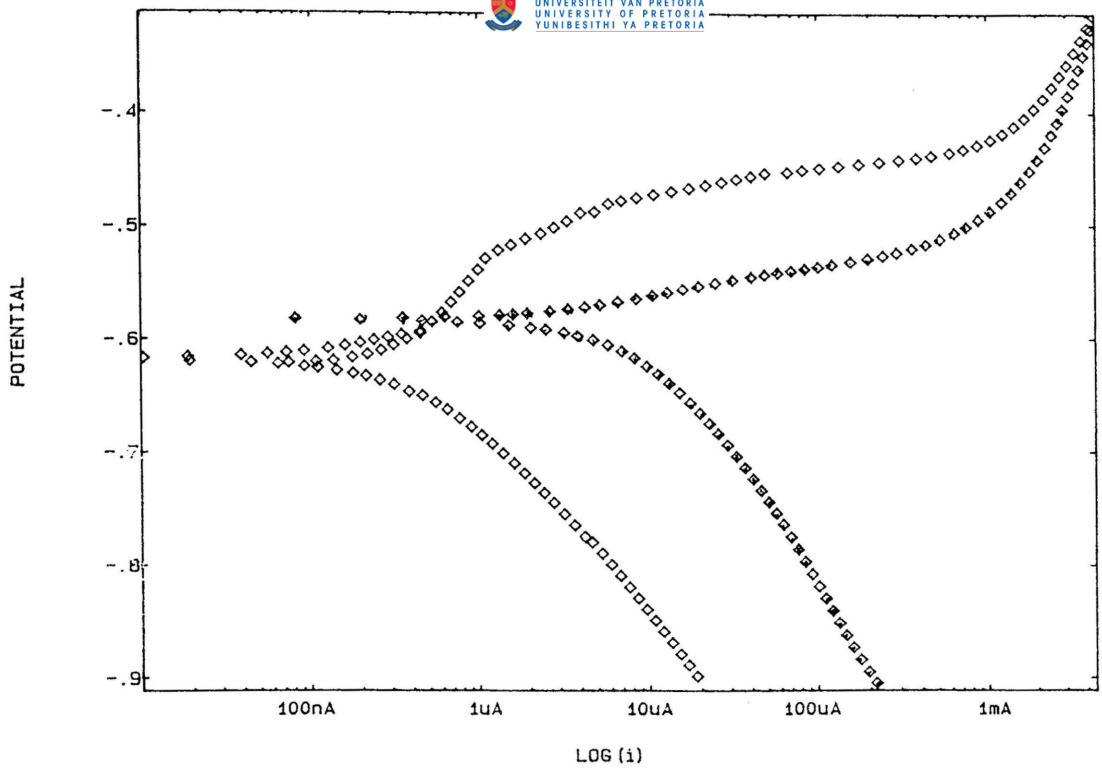


FIGURE 96 Carbon steel scanned in rich gas 50°C 18 bar, \diamond film free, \diamond 10 hours.

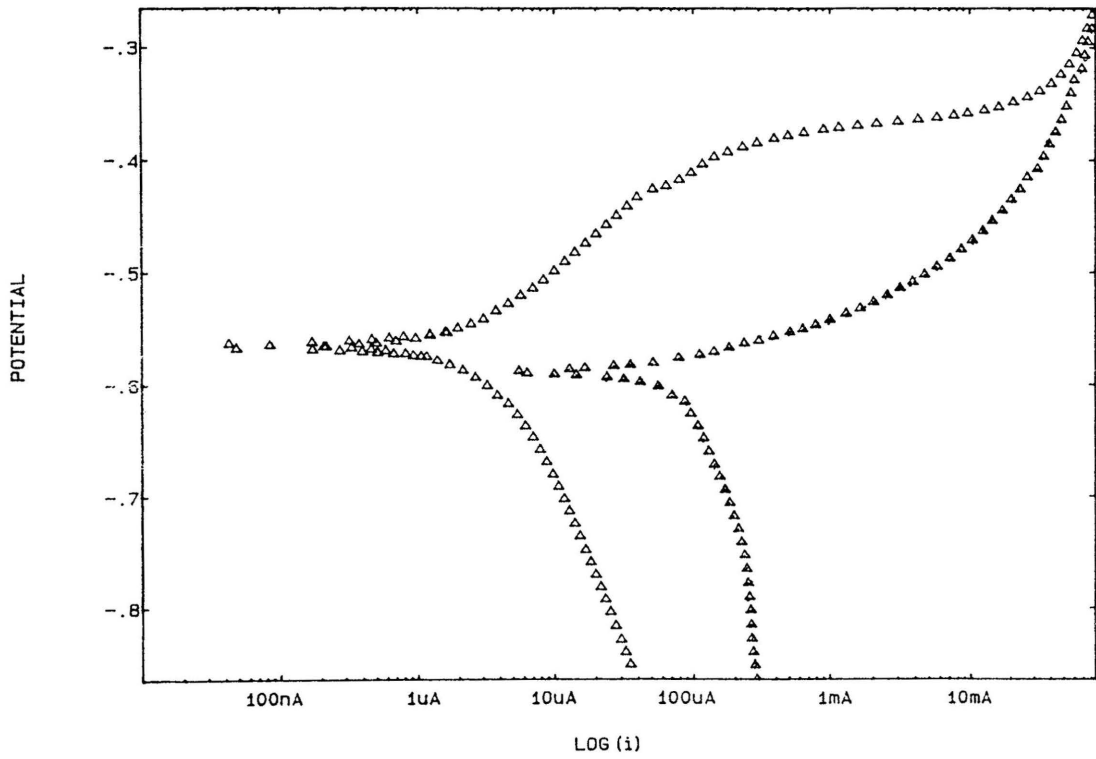


FIGURE 97 Carbon steel scanned in rich gas 80°C 18 bar, \blacktriangle film free, \blacktriangle 10 hours.

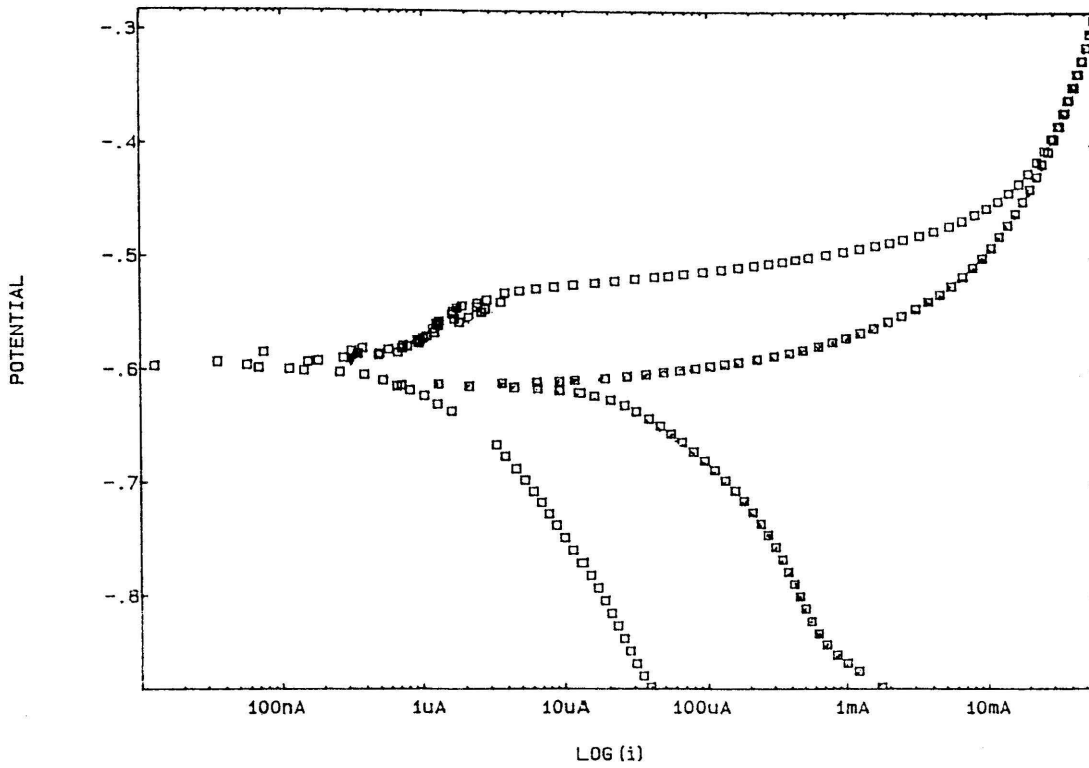


FIGURE 98 Carbon steel scanned in lean gas 50°C, 18 bar. ■ film free, □ 30 hours.

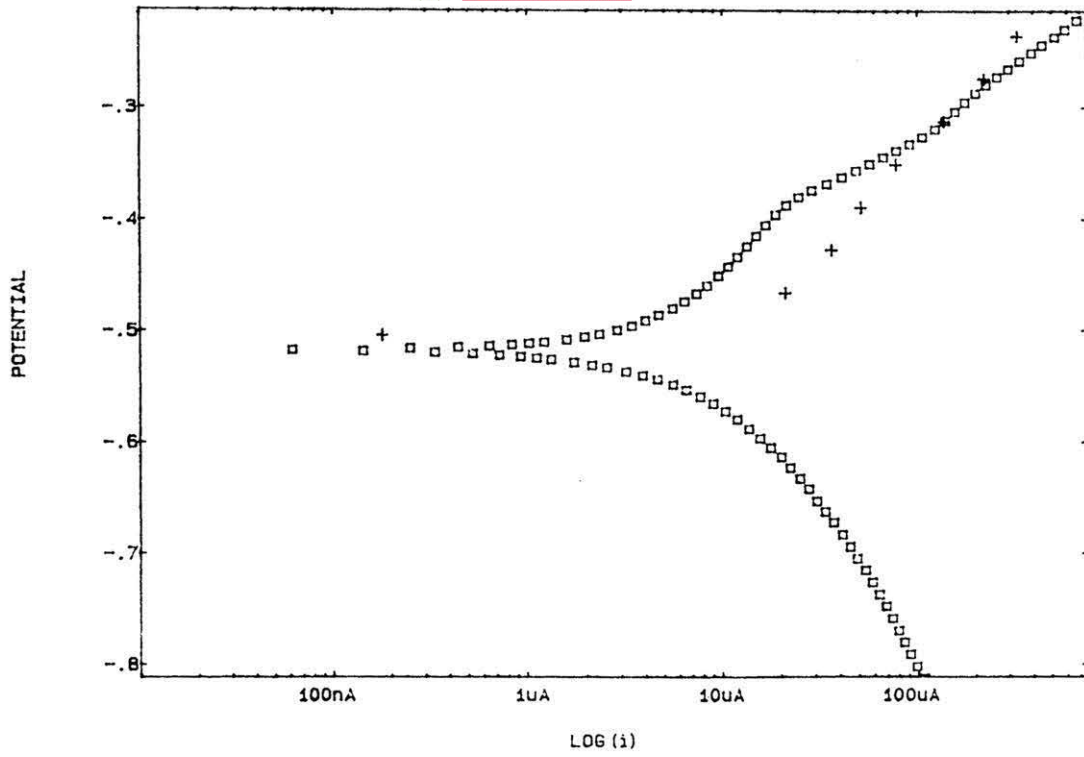


FIGURE 99 9Cr-1Mo steel in rich gas 50°C, 18 bar, 1 hour.

□ scan rate 20 mv/min, + 1000 mv/min.

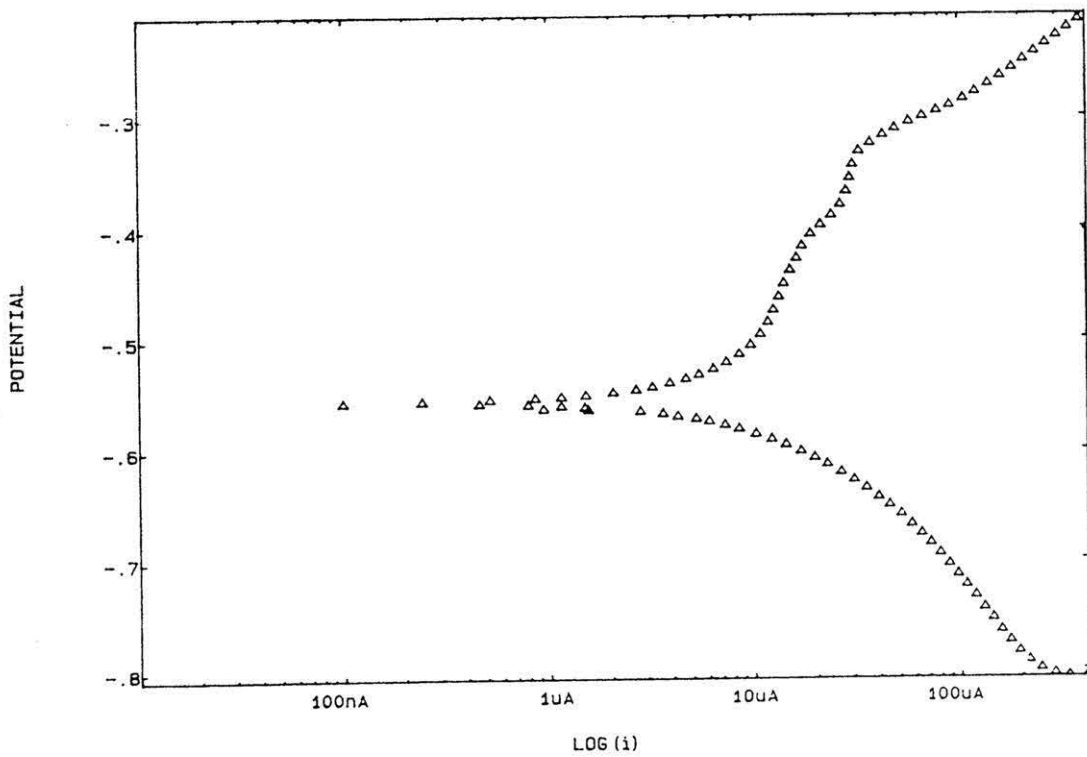


FIGURE 100 9Cr-1Mo steel in rich gas 50°C, 18 bar, 30 hours.

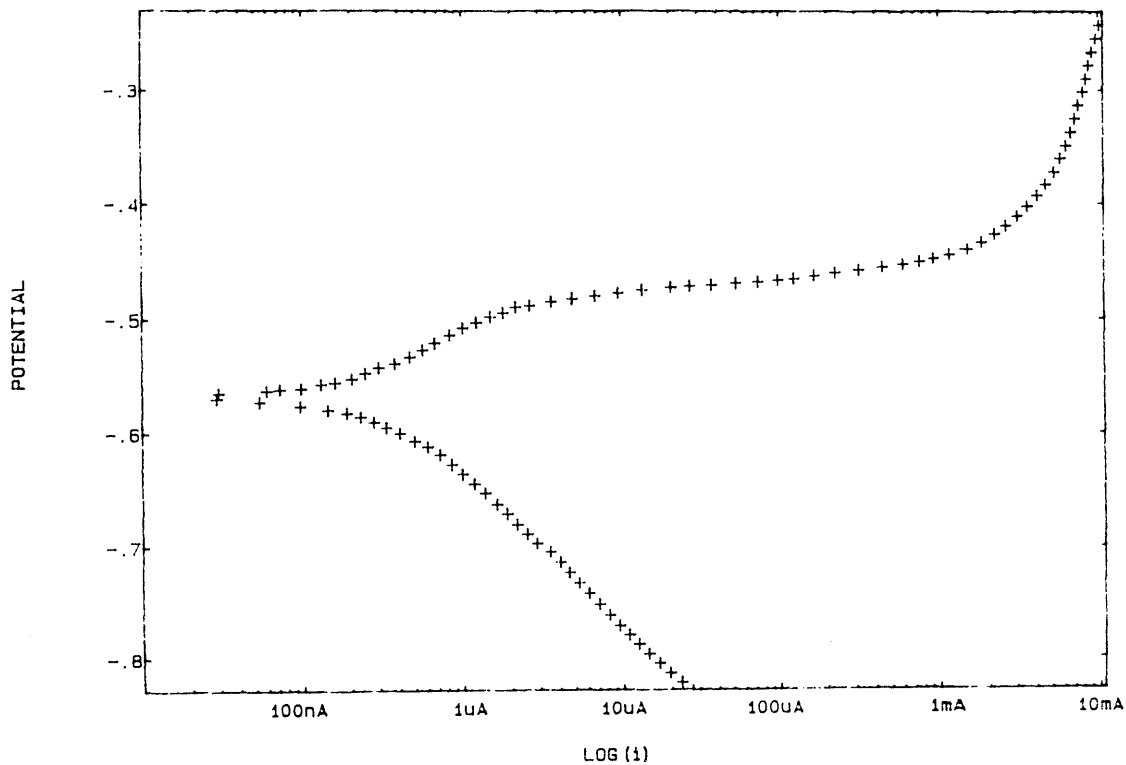


FIGURE 101 3½ Ni steel rich gas, 50°C, 18 bar, 3 hours.

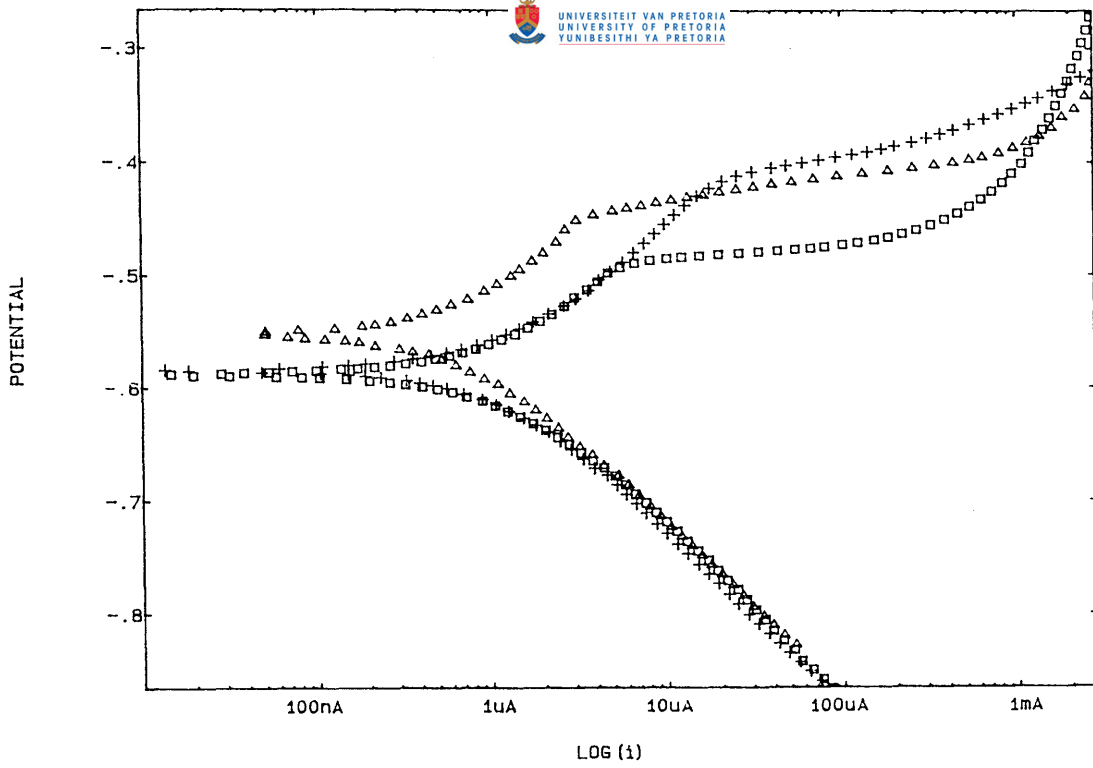


FIGURE 102 Carbon steel, addition of 100 ppm inhibitors to rich gas 50°C, 18 bar, 3 hours
 + KXO - 63, Δ KD - 40, □ rich gas.

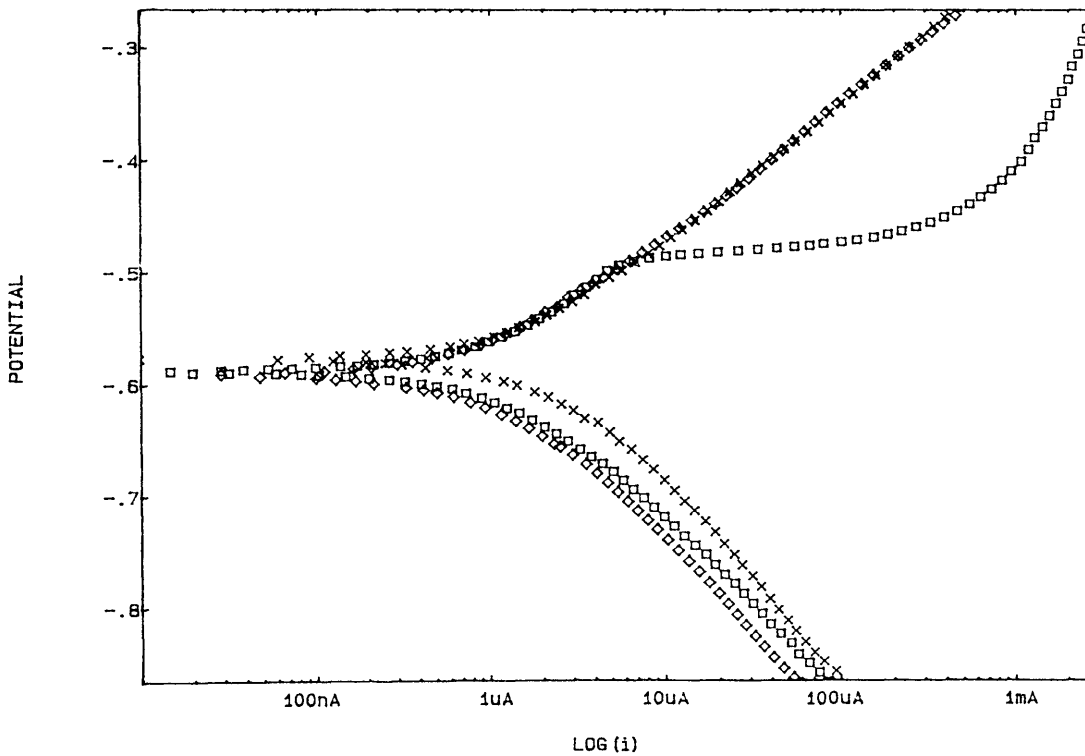


FIGURE 103 Carbon steel, addition of 100 ppm inhibitors to rich gas 50°C, 18 bar, 3 hours
 x AO-003, ◊ Petrotec 1430, □ rich gas.

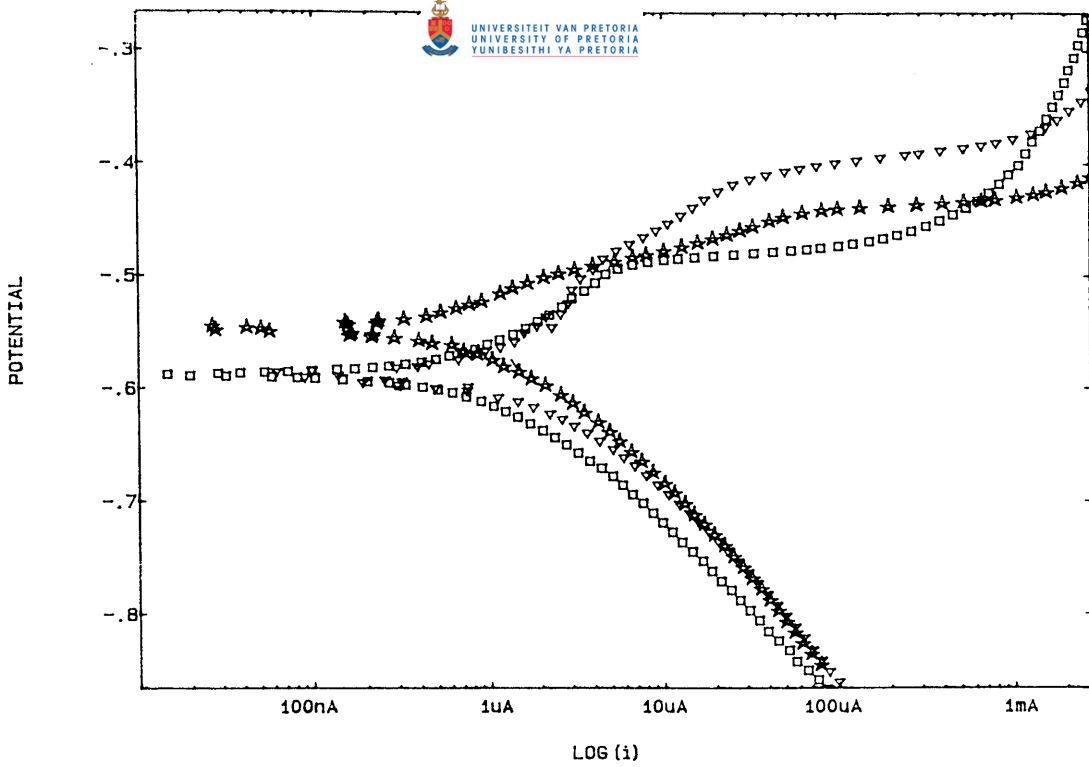


FIGURE 104 Carbon steel, addition of various strengths of Petrotec 1420 to Richgas 50°C, 18 bar, 3 hours
▽ 10 ppm, * 100 ppm.

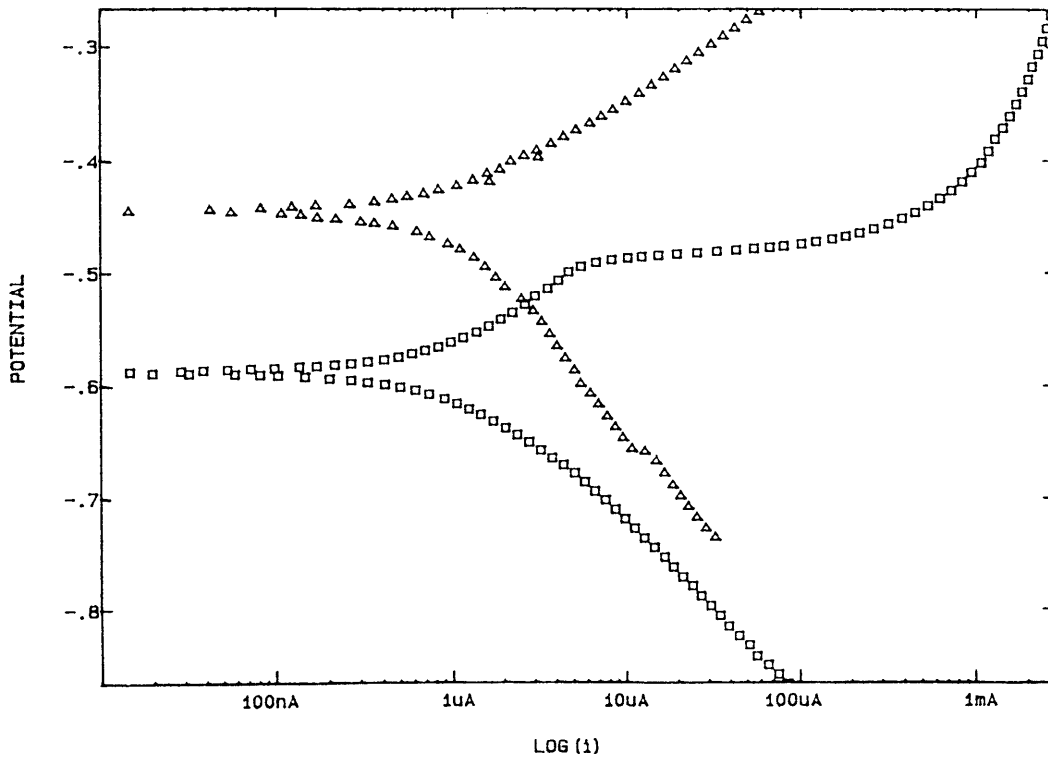


FIGURE 105 Carbon steel, addition of 5000 ppm Petrotec 1420 to Rich gas, 50°C 18 bar, 3 hours
△ Petrotec 1420, □ rich gas

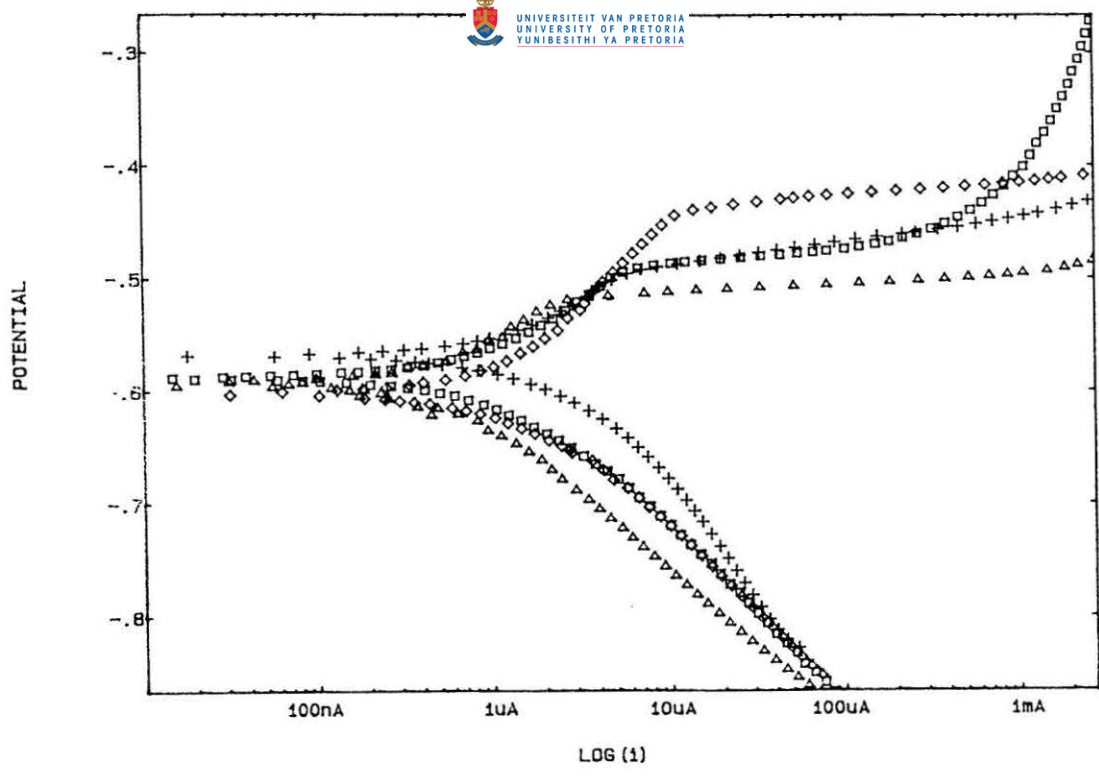


FIGURE 106 Carbon steel, addition of various amounts of Reomet 42 to rich gas 50°C, 18 bar, 3 hours
 □ 10 ppm, ◇ 100 ppm, + 1000 ppm, □ rich gas.

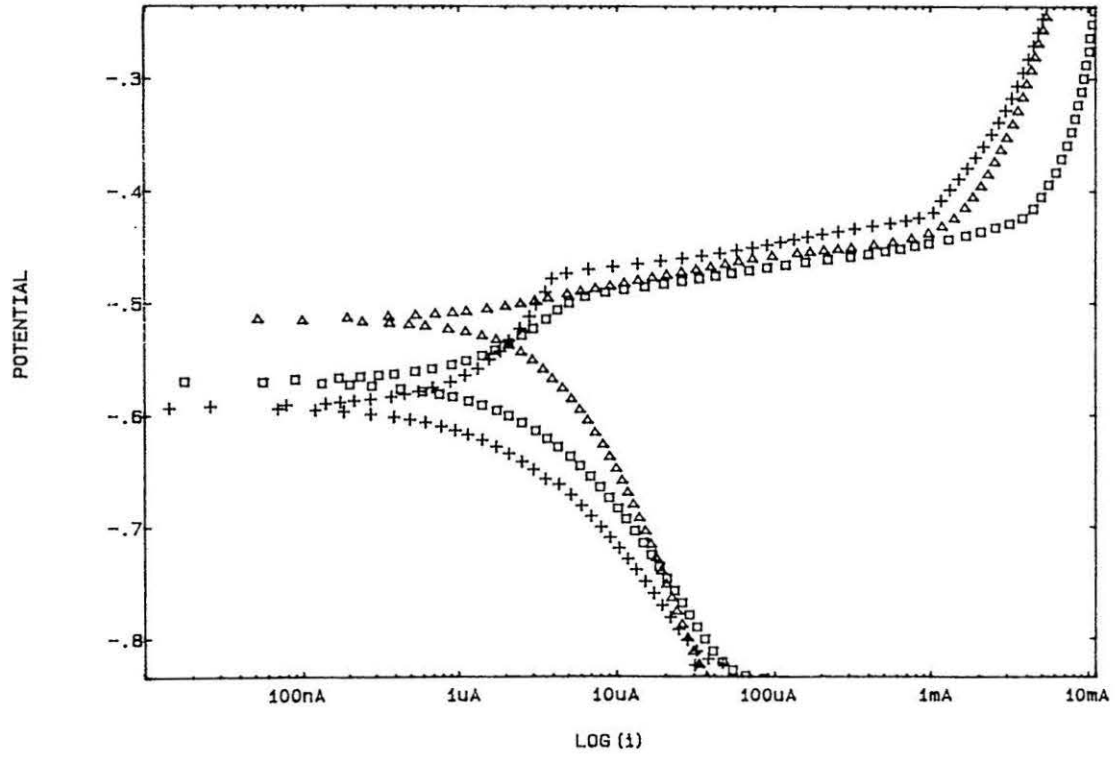


FIGURE 107 Carbon steel. Effect of exposure time after additions of Reomet 42 to rich gas 50°C, 18 bar.
 Δ 5 hours, □ 20 hours, + 30 hours.

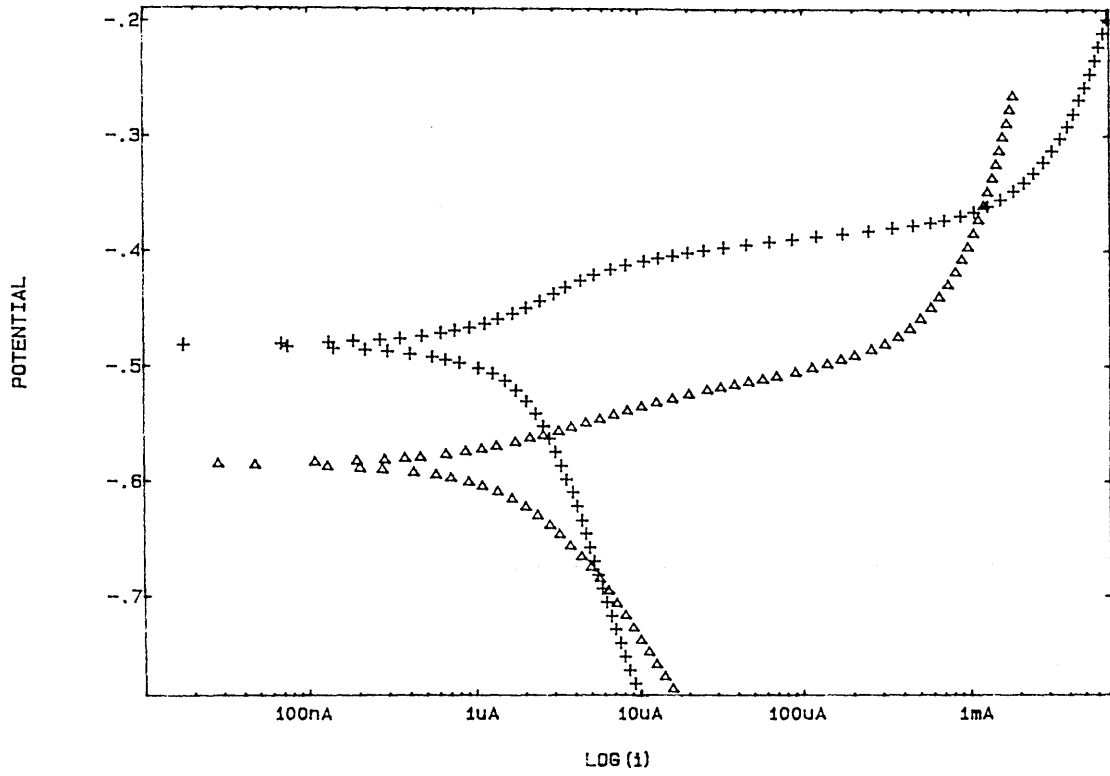


FIGURE 108 Carbon steel. Effect of deoxygenation, Rich gas 20°C, 18 bar, 1 hour Δ oxygen free, + oxygen.

14.1 APPLICATION OF ELECTROCHEMICAL NOISE MONITORING TO CO-CO₂-H₂O SYSTEMS

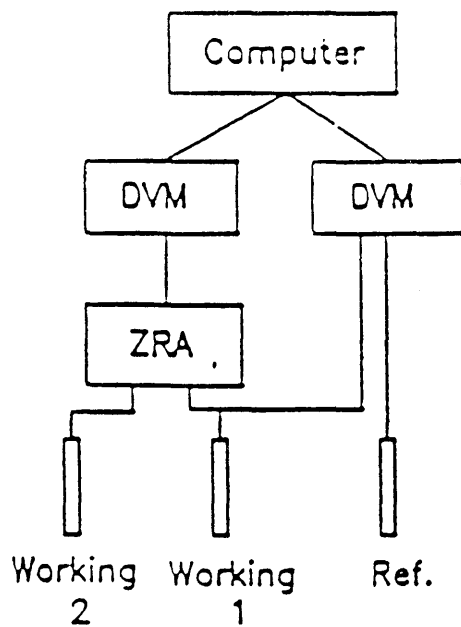
During studies to characterise electrochemical noise (ECN), it has been noted that the amplitude of low frequency potential or current noise is related to the rate of the corrosion process and that the frequency is influenced by the nature of the process. Metals exhibiting passivity give low coupling currents and noise levels. Initiation of localised corrosion events increases the potential noise level whilst propagation of localised types of corrosion increases the mean current and current noise.^(63,64) This ability of the noise technique to distinguish corrosion processes has led to an interest in its use to identify SCC. It might be expected that SCC would give rise to characteristic ECN especially if cracking is occurring by film rupture and subsequent anodic dissolution. Lotto and Cottis⁽⁶³⁾ report that the noise technique can be used to monitor SCC processes in alpha brass⁽⁶²⁾ and high strength aluminium alloys.⁽⁶¹⁾ In most cases cracking was indicated by the highest noise amplitude and by the highest standard deviation peaks. More recently ECN associated with SCC of sensitised stainless steels in room temperature thiosulphate solutions and in oxygenated high temperature water was studied at Harwell Laboratories.⁽¹¹⁴⁾ In a slow strain rate test, crack initiation was indicated by numerous current transients which later fell dramatically as the crack initiation rate reduced. At large strains the noise level increased again as stable cracking set in by coalescence of small cracks.

Eden⁽¹⁰²⁾ reported that potential and current transients symptomatic of stress corrosion cracking could be detected by monitoring electrochemical noise (ECN) generated on stressed carbon steel specimens immersed in water pressurised under mixtures of carbon monoxide and carbon dioxide. The noise traces obtained were characterised by anodic (positive going) potential transients associated with negative current events. The potential transients were of the order of 0,5 mV with corresponding current transients in excess of 6 μ A. The mean currents were usually negative indicating that the stressed electrode was more cathodic than the unstressed counter electrode. Increasing the carbon monoxide concentration from 5% to 15 % resulted in a lowering of the mean corrosion current and a reduction in the amplitude and frequency of the transients, all indicative of more efficient inhibition by CO.

Observation of ECN characteristic of SCC in the CO-CO₂-H₂O system can be exploited in two ways. One by monitoring the plant on line to determine if SCC is periodic and if so establish if the periodicity is linked to process fluctuations. Secondly, ECN can be used either on line or in the laboratory to establish if alterations to the environment, for instance additions of inhibitor are successful in preventing SCC. The following sections describe the results of bench tests and plant monitoring to establish if ECN can be used to identify when the environment supports SCC.

14.2 ELECTROCHEMICAL NOISE MONITORING SYSTEM

A commercially available system was used to monitor electrochemical potential noise (EPN) and electrochemical current noise (ECN) in a laboratory set up and on line in the plant. The instrument was connected to a three-element probe comprising of a stressed carbon steel electrode coupled to an instrument electrode of similar material. The mean coupling current the current noise were logged continuously. At the same time, potential noise was monitored between the couple comprising of the stressed and unstressed electrode and a third electrode used as a reference. In this case the reference electrode was fabricated from type 304 stainless steel. Figure 109 shows a schematic of the instrumentation arrangement used. The three electrodes were interrogated sequentially, measuring potential and current at intervals of typically 1 or 2 seconds. Appropriate software was used for data analysis in which mean, standard deviation and root mean square (RMS) were calculated for potential and current. Noise resistance was calculated by dividing the standard deviation of the potential noise by the standard deviation of the current noise, which gives a term analogous to polarisation resistance which can be used to obtain an estimate of corrosion rate. Information is also obtainable from the ratio of the standard deviation and RMS of the current noise which indicates whether the corrosion is general or localised, or if the system has passivated. For general corrosion the ratio is less than 0,1 and for localised forms of corrosion it is normally between 0,1 and 1. Passivation also results in a ratio below 0,1 and can be distinguished from general corrosion by comparing the mean currents and noise amplitude.



- DVM - Digital voltmeter
- ZRA - Zero resistance ammeter
- Ref - Reference electrode

FIGURE 109 Schematic of the instrumentation arrangement for digital analysis.

14.3 PROBE DESIGN

The arrangement shown in Figure 110 was initially used for the laboratory tests. The electrodes were fabricated from SA 516 Gr70 carbon steel and the stainless steel autoclave body was used as the reference electrode. This arrangement gave poor results and was later replaced with smaller electrodes, each with an electrode area of 1.5 sq cm, mounted closer together and sealed to eliminate crevices. Where previously the autoclave body was used as a reference, a reference electrode was introduced and placed close to the two working electrodes, more closely reproducing the electrode arrangement that was to be used during the plant monitoring. The whole arrangement was located in a glass container that fitted inside the autoclave so that the monitored environment was isolated. Probes similar to that shown in Figure 111 were used in the plant and were also sometimes used for laboratory tests.

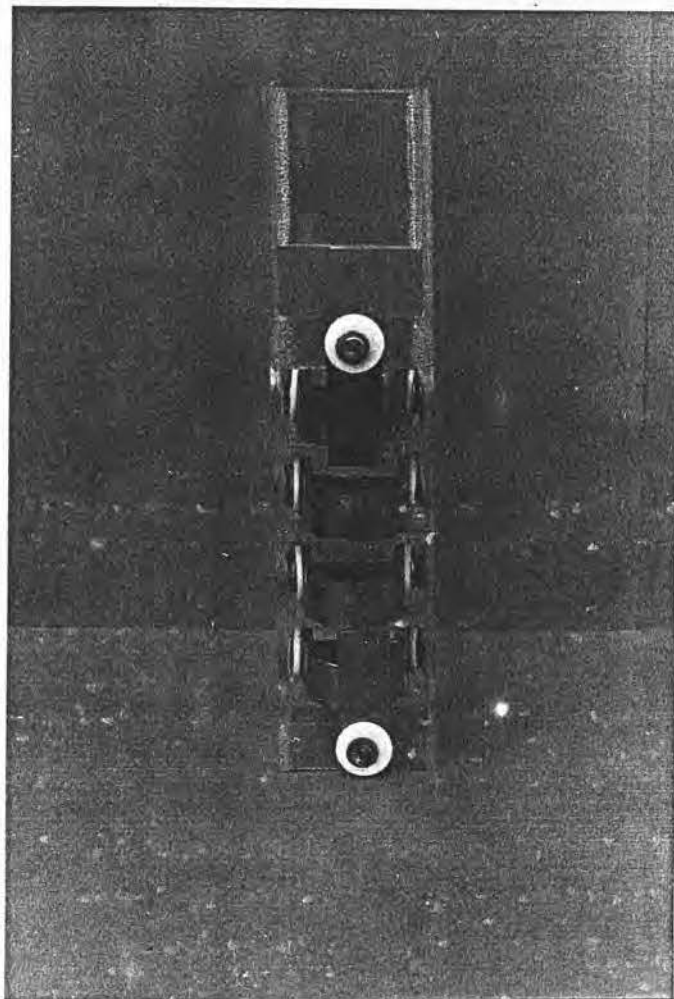


FIGURE 110 Probe used for the laboratory tests

For plant monitoring the probe arrangement shown in Figure 111 was used. The stressed element was fabricated from a small modified U-bend specimen. The reference electrode included in the probe was fabricated from 300 series austenitic stainless steel. A similar arrangement was used in later laboratory tests.

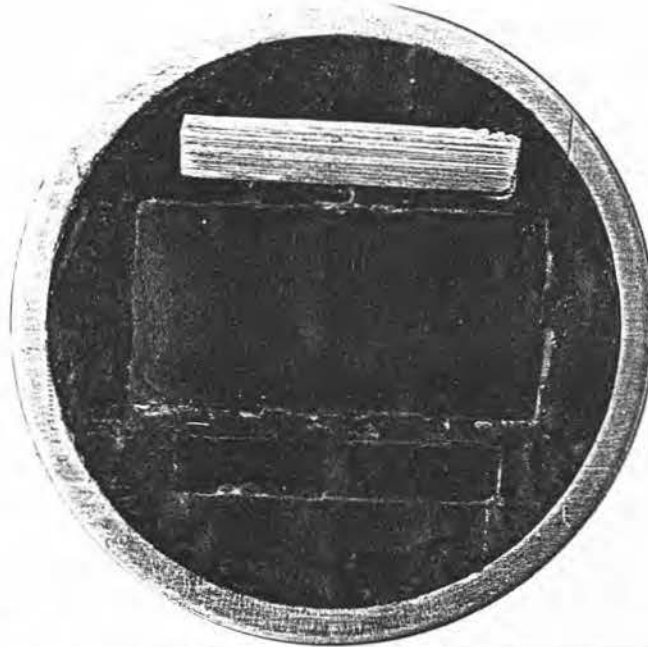


FIGURE 111 Probe used for plant monitoring.

Top - Reference electrode, total area 1.0 sq cm

Centre - Stressed electrode, total area 3.5 sq cm

Bottom - Un-stressed electrode, total area 1.0 sq cm

14.4 TEST ENVIRONMENT

14.4.1 Laboratory Tests

The noise data was generated by placing the probe in a 600 ml capacity autoclave that was subsequently filled with condensate and pressurised with gas in the manner described for the potentiodynamic polarisation studies. Monitoring was usually continued for a period of about six weeks, after which the samples were removed and examined for physical evidence of cracking.

14.4.2 Plant Monitoring

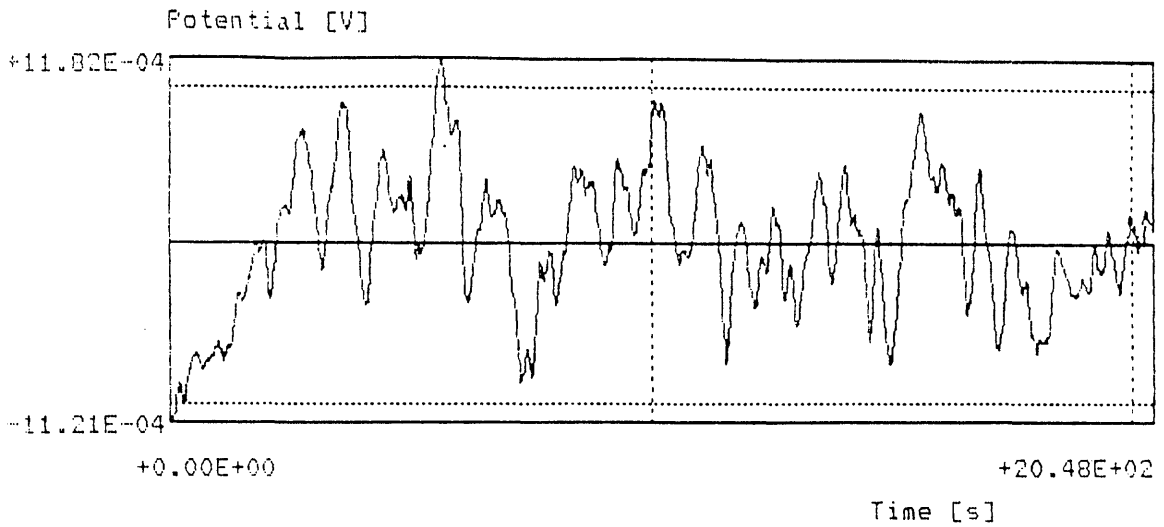
Probes were installed in rich and lean gas having PCO and PCO₂ partial pressures of 210 and 230, and 34 and 266 kPa respectively. After exposure the plant probes were also examined for cracks.

14.5 RESULTS

14.5.1 Laboratory Tests

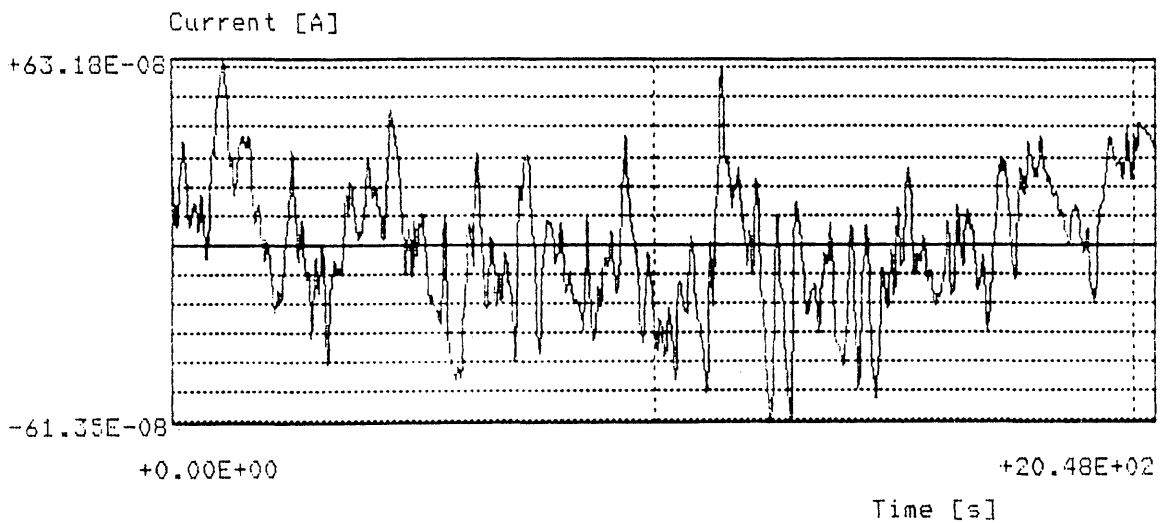
Shortly after pressurising, the noise traces obtained were similar to those shown in Figure 112 and contained no sharp transients. The main current was low at a value of $3,19E-06$ A and the noise resistance recorded was $1,88E+03$ A. After about 20 hours, the current noise stabilised and was characterised by discreet packets of transients (Figure 113). At this time, the mean current decreased slightly and the noise resistance increased, showing a greater tendency toward passivation. This was supported by a degree of localisation below 0,1. The observation of increased passivity with longer exposure times is in keeping with the results of the polarisation studies which identified a time dependence for CO absorption. The discreet bursts of transient activity observed at this time, may be associated with SCC, but since they were evenly distributed between the stressed and unstressed electrode as indicated by more or less equal numbers of positive and negative going transients, it is considered more likely that they were caused by stochastic surface adsorption and desorption of carbon monoxide. The predominantly negative going current transients observed in Figure 115, are more promising and are in agreement with Eden's ⁽¹⁰²⁾ observation of positive potential transients and negative going current transients in the system when SCC is occurring.

Figure 116 shows noise traces typical of those obtained from plant monitoring in rich gas. The traces were characterised by positive going potential transients of the order of 9,0 mV and corresponding very small current transients measuring around 5 nA. In lean gas (Figure 117) similar traces were obtained with potential transients of the order of 0,7 mV with corresponding current transients around 3 nA. The segmented appearance noted in the laboratory tests was discernable in the traces obtained in rich gas (Figures 116 and 117). The very low mean currents and high noise resistance were indicative of passivation. The difference in the magnitude of mean current values, noise resistance and transient amplitude, when comparing plant data to laboratory data, may be explained by different electrochemical characteristics of a condensed film (plant data) compared to bulk solutions. Electrolyte thickness, availability and composition are all variables that will affect the magnitude of transients recorded in a condensing system. The ECN monitoring is able to clearly differentiate between passive and corrosive conditions that might prevail at different times in the plant. Transient behaviour, however, is more difficult to identify. When the monitoring programme was initially conceived, it was believed the SCC occurred at potentials in a range of transition from active to passive behaviour. The noise results did not indicate that movement in and out of this zone of susceptibility could be identified with confidence. However, polarisation studies showed that there is no "transition" type behaviour in the CO-CO₂-H₂O system but rather SCC susceptibility is due to a slow time dependent passivation process. The passivation is the result of CO adsorption and occurs below a well defined breakdown potential. Therefore, any carbon or low alloy steel showing CO passivation in the CO-CO₂-H₂O system will be at risk from SCC. In order to determine if plant fluctuation change the ability of the environment to promote SCC, it is necessary to only monitor for a change from active to passive behaviour. This can easily be achieved using ECN. Similarly, ECN monitoring can be used to identify fluctuations above and below the dew point which can also be used as a SCC controlling mechanism.



=====

Current Noise



=====

Potential and Current Raw Data
 File started at 5.31 on 03 June 1992
 (92F03E31.01F)

Trend removal : First

< Raw Data Statistics >

Potential [Volts]

Current [Amps]

mean : 7.11E-03

mean : -3.19E-06

sdev : 4.39E-04

sdev : 2.33E-07

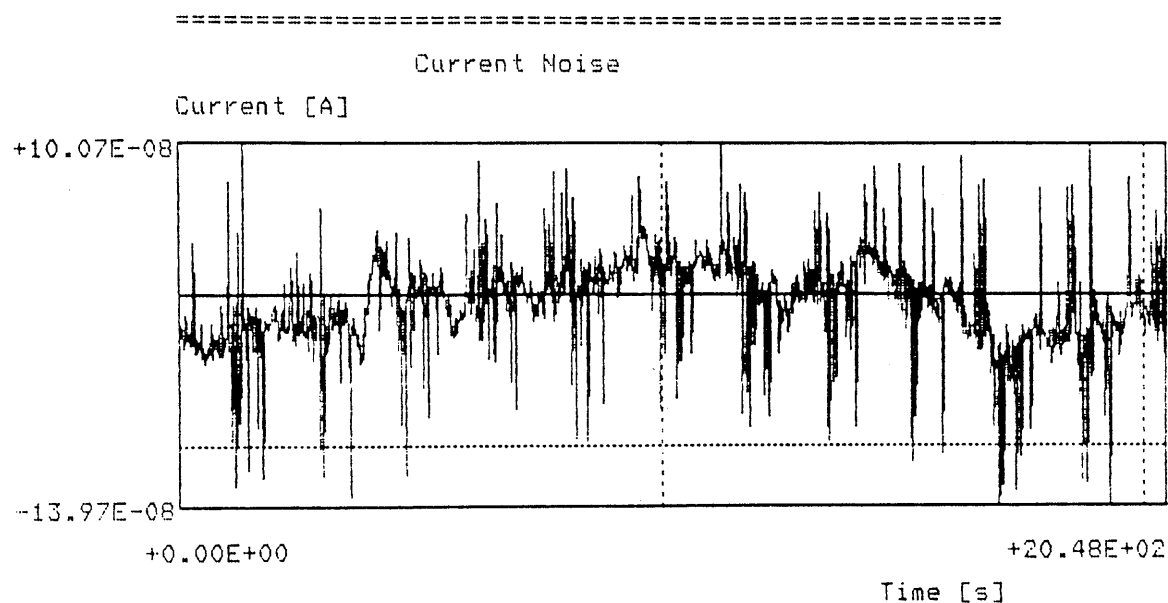
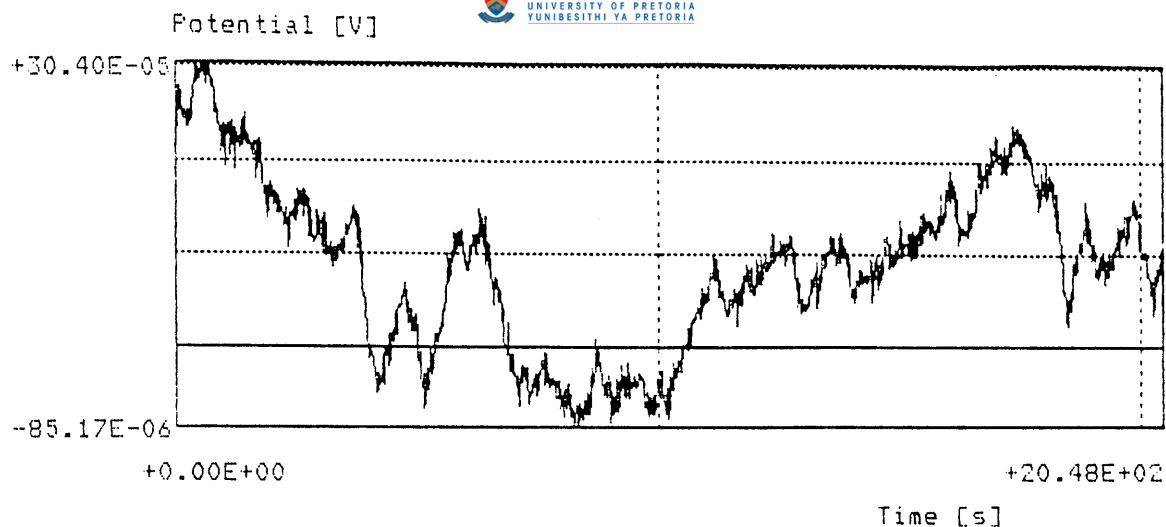
rms : 7.13E-03

rms : 3.20E-06

Res. Noise (j): 1.88E+03

Fitting Index : 7.29E-02

FIGURE 112 Noise traces obtained immediately after pressurising



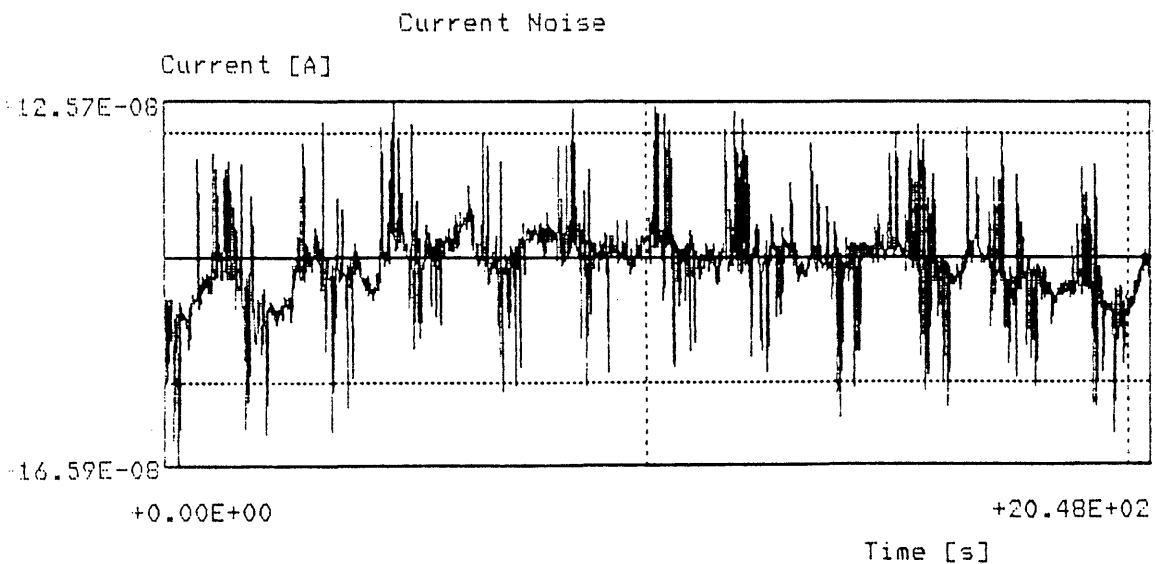
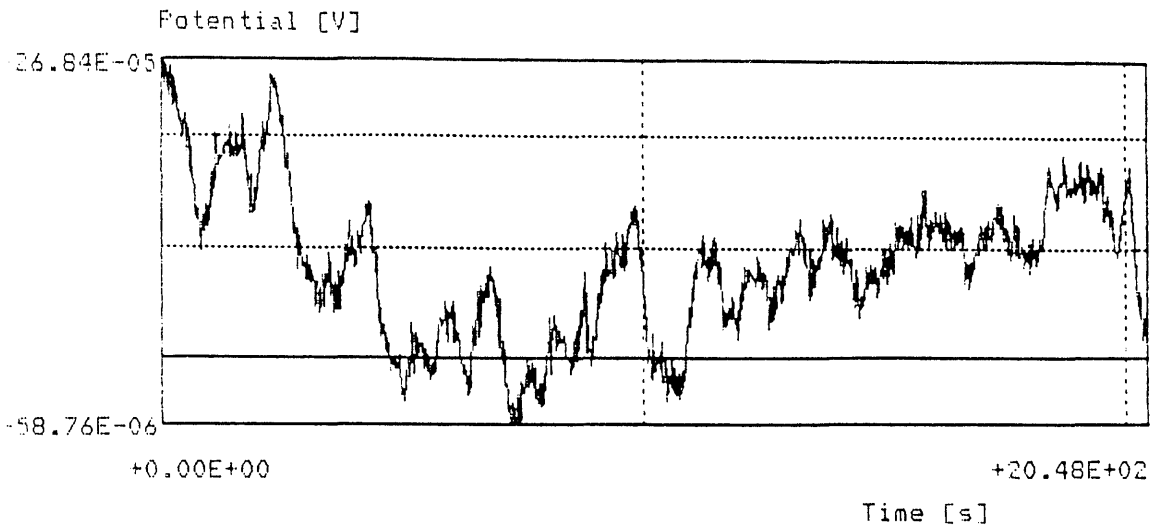
=====
Potential and Current Raw Data
File started at 3.44 on 04 June 1992
(92F04C44.01F)

Trend removal : First

< Raw Data Statistics >

<u>Potential [Volts]</u>	<u>Current [Amps]</u>
mean : 4.42E-02	mean : -2.81E-06
sdev : 1.05E-04	sdev : 3.23E-08
rms : 4.42E-02	rms : 2.81E-06
Res. Noise (j): 3.25E+03	
Fitting Index : 1.15E-02	

FIGURE 113 Noise traces obtained 20 hours after pressurising



Potential and Current Raw Data
File started at 0.52 on 04 June 1992
(92F04@52.01F)

Trend removal : First

< Raw Data Statistics >

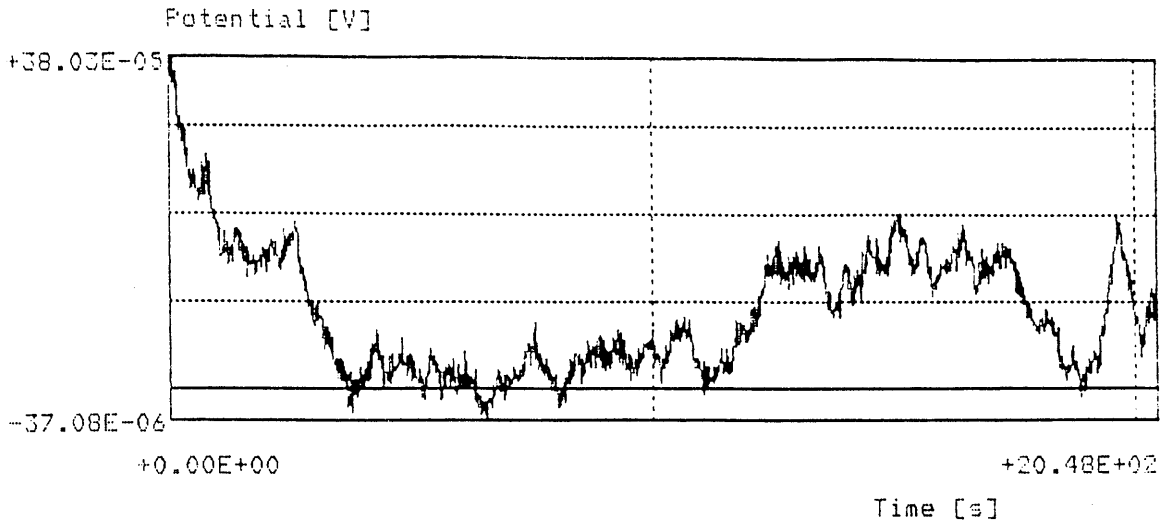
Potential [Volts]	Current [Amps]
mean : 4.33E-02	mean : -2.86E-06
sdev : 1.04E-04	sdev : 3.66E-08
rms : 4.33E-02	rms : 2.86E-06

Res. Noise (j): 2.83E+03

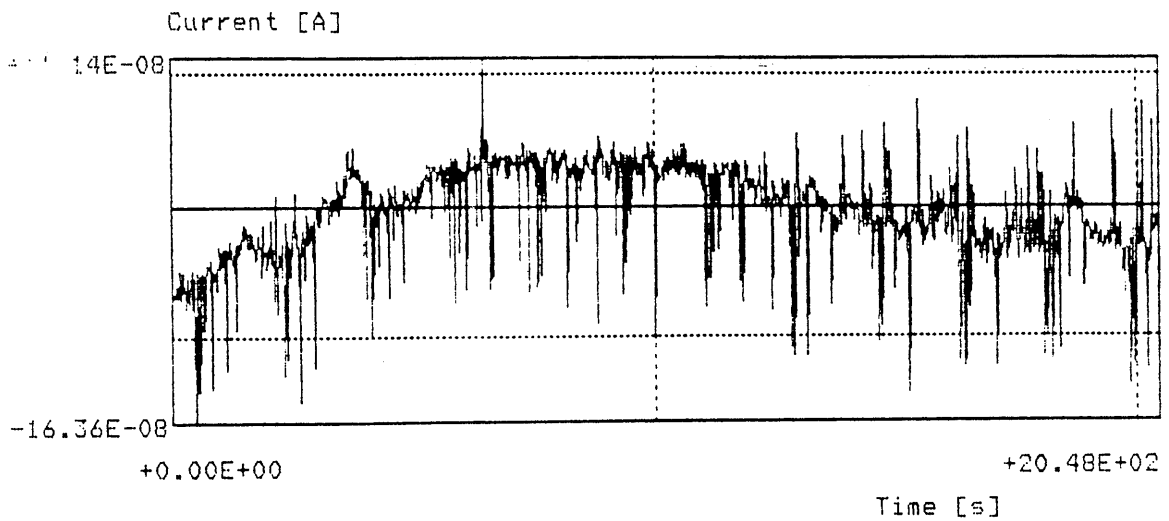
Pitting Index : 1.28E-02

FIGURE 114 Noise traces 17 hours after pressurising

Potential Noise



Current Noise



Potential and Current Raw Data

File started at 6.37 on 04 June 1992

(92F04F37.01F)

Trend removal : First

< Raw Data Statistics >

Potential [Volts]

Current [Amps]

mean : 4.49E-02

mean : -2.76E-06

sdev : 1.79E-04

sdev : 4.26E-08

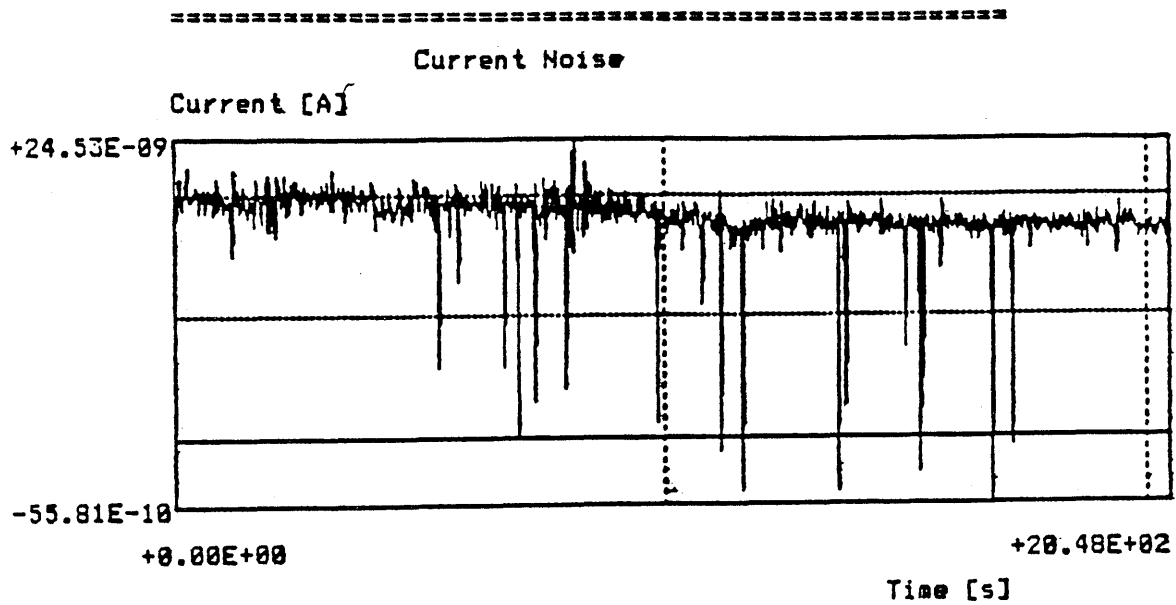
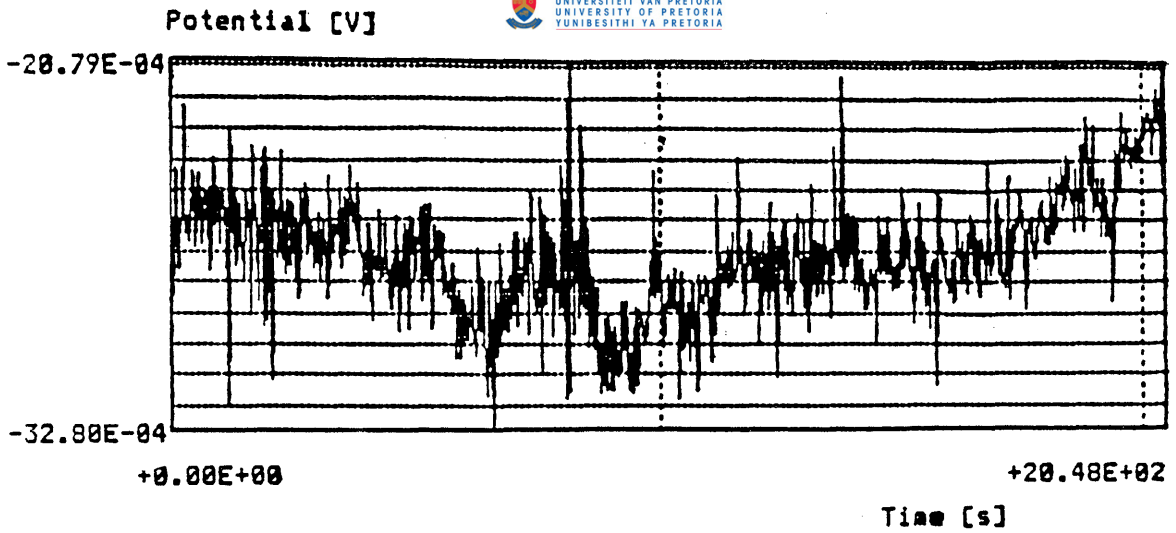
rms : 4.49E-02

rms : 2.76E-06

Res. Noise (j) : 4.21E+03

Pitting Index : 1.55E-02

FIGURE 115 Noise traces obtained during the bench experiment



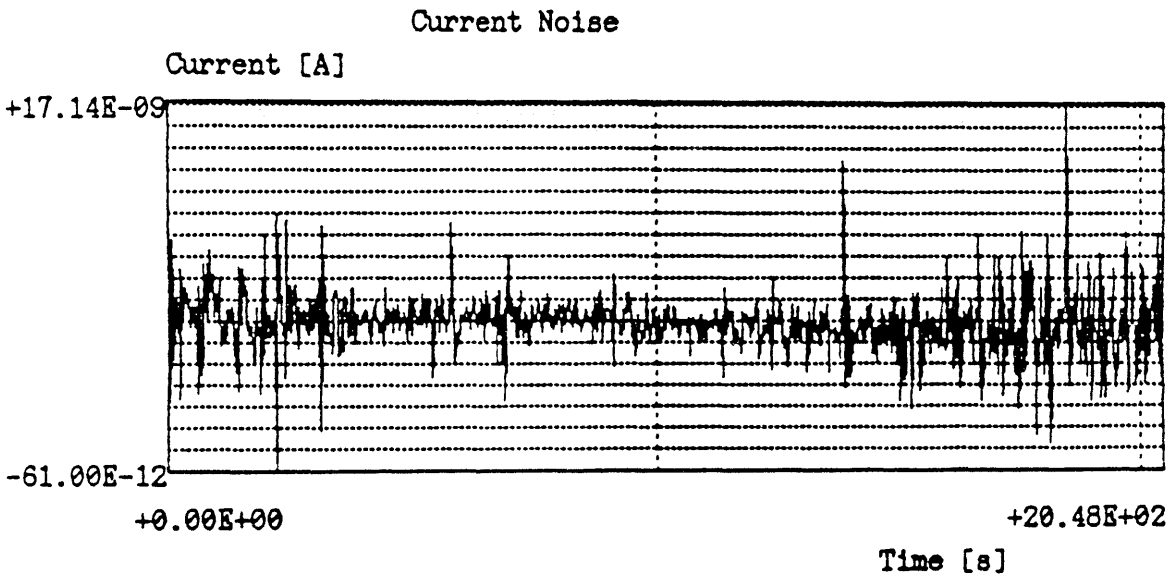
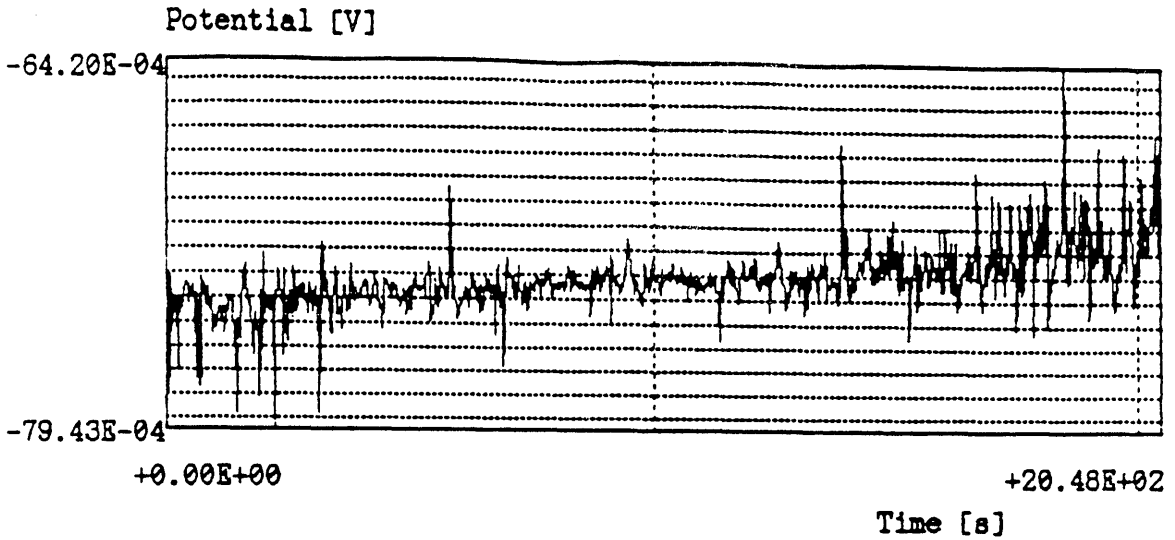
Potential and Current Raw Data
File started at 6.34 on 26 July 1991
(91626F34.01F)

Trend removal : None
< Raw Data Statistics >

Potential [Volts]	Current [Amps]
mean : -2.71E-03	mean : 1.81E-08
sdev : 1.86E-04	sdev : 2.50E-09
rms : 2.72E-03	rms : 1.83E-08

Res. Noise (Ω) : 7.43E+04
Degree of Localization : 1.37E-01

FIGURE 116 Noise traces typical of those obtained monitoring rich gas on line



=====
Potential and Current Raw Data
File started at 0.23 on 06 August 1991
(91H06@23.02F)

Trend removal : None

< Raw Data Statistics >

Potential [Volts]	Current [Amps]
mean : -7.31E-03	mean : 6.85E-09
sdev : 1.32E-04	sdev : 1.32E-09
rms : 7.32E-03	rms : 6.97E-09

Res. Noise (Ω): 1.00E+05

Degree of Localization : 1.89E-01

FIGURE 117 Noise traces obtained on line in lean gas

15.1 CHARACTERISATION OF CRACK MORPHOLOGY

Metallography of sections of cracked piping removed from various locations at industrial gas processing plants revealed an apparent dependence of crack appearance on the prevailing carbon monoxide partial pressure. At low partial pressures (PCO - kPa 34) found in the low pressure lean gas, the conditions favoured pitting, although limited SCC was also observed at the base of pits (Figure 36). At higher partial pressures (PCO - kPa 51) found in high pressure lean gas, pitting still occurred but stress corrosion cracking was more prevalent (Figure 36). For both lean gas conditions significant widening of the crack was noticed due to breakdown of passivation on the crack wall and subsequent corrosion. Stress corrosion cracks observed in the rich gas system (PCO - kPa 199) were extremely fine and generally showed more branching than cracks in lean gas piping. Very few corrosion pits were found on the metal surface.

The absence of significant corrosion on the crack walls and lack of pitting in this system suggested that conditions in rich gas, compared to lean gas, favoured passivity. This was in agreement with the higher prevailing carbon monoxide partial pressure (PCO - kPa 199). Figure 46 summarises how crack appearance is correlated with carbon monoxide partial pressure.

The cracks found in samples from the Pilot plant showed a greater tendency towards pitting than would be expected for the prevailing partial pressure of carbon monoxide, however the temperature at the location they were taken from was slightly higher (60°C) compared with other systems. A higher temperature would be expected to lower carbon monoxide adsorption and increase wet carbon dioxide corrosion rates. This condition would therefore tend to favour pitting and more general corrosion.

At all the carbon monoxide partial pressures investigated the cracking was transgranular and multibranching. Cracking could either be transverse or longitudinal to the weld axis and occurred with equal frequency in the welds and heat affected zones. However, cracking was not always restricted to weldments and could sometimes be found in parent metal remote from any welding.

Hardness values adjacent to cracks were almost without exception below 240 Hv which indicated a low susceptibility to hydrogen embrittlement. This result suggested that the cracking mechanism was more likely anodic SCC than hydrogen embrittlement due to cathodic charging.

In contrast to the results obtained from samples removed from the plant, the morphology of cracks produced in laboratory tests showed no relationship to the prevailing carbon monoxide partial pressure. The cracks were always extremely fine and showed no evidence of significant uniform corrosion on the crack walls. Also missing from the laboratory tests was localised subsurface penetration by corrosion from the crack wall into base metal.

It was concluded that widening of the stress corrosion cracks observed in gas systems containing low carbon monoxide partial pressures does not occur concurrent with crack propagation but occurs after the crack has arrested. The initial crack appearance is independent of carbon monoxide partial pressure although subsequent corrosion of the crack walls, resulting in either wide cracks or pits, is more likely at low carbon monoxide partial pressures, probably due to the difficulty in maintaining passivity in the crevice formed by an arrested crack.

15.2 DETERMINATION OF STRESS CORROSION CRACK GROWTH RATES IN CO-CO₂-H₂O SYSTEMS USING PRECRACKED SPECIMENS (DCB)

Few codes or standards recognise any limited tolerance for stress corrosion cracks, or for that matter tolerance of other crack-like defects. BSI PD6493 : 1991 'Guidance on Methods for Assessing the acceptability of Flaws in Fusion Welded Structures' however, in Section 4 Paragraph 25.3 describes how environmentally assisted cracking might be approached. The applied stress intensity factor is first estimated taking into account flaw size and primary and secondary stresses including residual stress. The applied stress intensity factor K_I is then compared with the threshold stress intensity for stress corrosion cracking K_{ISCC} , using an appropriate safety factor (f). If K_I is less than $f K_{ISCC}$, the stress corrosion cracks will not grow under the specific combination of flaw size, environment and metal assessed. PD6493 warns against the sensitivity of K_{ISCC} to small changes in test conditions and refers to ISO 7539-1 for detailed guidance on determination of K_{ISCC} .

If the applied value of K_I exceeds $1/FP K_{I,SCC}$, PD6493 : 1991 indicates that the possibility of SCC growth should be recognised and that remedial action, such as modifying the environment, or changing to a non-susceptible material or stress relief is taken. As an alternative the document (PD6493) describes how an assessment may be made to determine whether the flaws would grow to an unacceptable size within the design life of the structure or within an appropriate inspection interval. The method uses the observation, that once initiated, stress corrosion cracks usually attain an approximately uniform velocity which is dependent on the metal and environment and is largely independent of stress intensity. The crack velocity (da/dt) is plotted against stress intensity factor K_I . Once the applied stress intensity factor is known the appropriated growth rate can be established from a relationship of the type $da/dt = CK^n$ where C and n are constants, and K is the stress intensity. Integration of this expression will give the anticipated amount of SCC growth during the design life or appropriate inspection period. As mentioned earlier, ISO 7539-6 is referred to for suitable methods to establish $K_{I,SCC}$ and da/dt values. Without exception the methods require the use of fatigue precracked plane strain fracture mechanics specimens to establish $K_{I,SCC}$ and da/dt .

For the assessment reported here DCB specimens were chosen, however after numerous exposures both in a laboratory and in the plant no crack extension was recorded even though smooth specimens exposed at the same time cracked due to stress corrosion.

It is considered that whilst the potential at the surface of smooth specimens settled to within the range where SCC occurs, as demonstrated by the failure of C-ring, ring weld and U-bend specimens, the potential at the crack tip of the DCB's did not fall inside the SCC susceptible range (-475 to -685 mV SCE) and therefore no crack extension took place. A similar behaviour was reported by Parkins⁽¹⁰⁴⁾ in carbonate-bicarbonate systems where cracks grew from the smooth surface of a cantilever beam specimen rather than from the tip of the pre-fatigue crack, indicating a stronger dependence on the micro environment (local potential) than on stress intensity. Nyborg and Linde⁽¹⁰³⁾ reported that fatigue pre-cracked compact tension specimens tested in anhydrous ammonia, also did not crack. In this case severe crevice corrosion was found in the outer part of the fatigue crack. It was concluded that the presence of crevice corrosion prevented SCC. Significantly SCC susceptibility in anhydrous ammonia is also sensitive to potential.

It appears therefore that precracked specimens may not be suitable for study of SCC systems where there is a marked dependence on a narrow range of potentials.

As an alternative to stress corrosion testing precracked specimens and using the procedures given in ISO 7539-6 to generate growth rate data, PD6493 suggests that it may be possible to conservatively estimate crack velocity by appropriate inspection of equipment at suitable intervals. It would seem reasonable to add values of crack velocity obtained on smooth specimens to data collected in situ to obtain a reliable and representative expression for growth rate. In order to determine if limited cracking can be tolerated, growth rate expressions are integrated to predict the amount of crack growth during the relevant inspection period. If, as a result of the anticipated growth, the stress corrosion cracks do not reach the maximum tolerable crack size for other failure mechanisms (brittle or ductile fracture or leak if the substance is flammable) then cracking can be tolerated within the limits established. If the integration predicts that the crack size will exceed the tolerable crack size before the end of the inspection period, then assessed flaws cannot be tolerated. Clearly there are many uncertainties. The environment may fluctuate, there may be dynamic stresses present, the materials will not be homogeneous. All of which can significantly affect stress corrosion growth rates. Additionally growth rates obtained from smooth specimens inevitably include an incubation period. The end result after all these uncertainties are taken into account is usually a stress corrosion crack growth rate that is overly conservative.

This is illustrated by giving consideration to Table 25 which contains growth rates for CO/CO₂ stress corrosion cracks. The crack velocity varies from 50 mm/year to 1,0 to 1,5 mm after 10 years.

Taking the worst case condition it is predicted that it will take a 1 mm deep stress corrosion crack that lies transverse to a girth seam just over 2 months to penetrate a 8 mm thick pipe to produce a leak and another 2 months to reach a critical length of 40 mm calculated for a longitudinal through thickness crack, assuming K independent SCC growth and no crack interaction.

Despite the detection of numerous SCC cracks on the plant, leaks have seldom been reported. Clearly the growth rates are too conservative. It is concluded therefore that a formal determination of the tolerance of limited cracking and the adoption of a fail-safe concept of life prediction is impractical due to uncertainties of crack growth data. This is compounded by the inability to produce crack extension in precracked specimens, exposed to the CO-CO₂-H₂O environment.

Rather, the approach to complicated piping and vessel systems should be to prevent initiation (safe-life concept) and where cracks are found they should be ground out before the material is returned to service so that the initiation growth cycle has to be repeated.

TABLE 25 GROWTH RATES FOR CARBON STEEL IN VARIOUS CO-CO₂ GAS MIXTURES

CONDITION / SOURCE	GROWTH RATE mm/year
CERT, rich gas and lean gas	50 mm
Brown et al ⁽⁴²⁾ plateau growth rates in CO-CO ₂ -H ₂ O systems	10 to 30 mm
Laboratory autoclave. Rich gas. Ringweld specimens	4,3 mm
Laboratory autoclave. Rich gas. C-rings	1,0 to 1,7 mm
Laboratory autoclave. Lean gas. C-rings	2 to 5,8 mm
Base metal, plant equipment. Lean gas	1,0 to 1,5 mm after 10 years
Piping. Lean gas	5 mm after 10 years
Piping. Rich gas	Leaks (8 to 10 mm) after 10 years

15.3 EVALUATION OF INHIBITOR ADDITIONS TO CO-CO₂-H₂O SYSTEMS USING CONSTANT EXTENSION RATE TESTS

15.3.1 CERT Without Inhibitor Additions

The results of CERT tests made to obtain baseline values for reduction of area also allowed a brief assessment to be made of the effect of temperature and gas composition on the severity of the interaction between carbon steel and a wet CO/CO₂ environment. In rich gas, reducing the temperature from 50 to 20°C had little effect on the severity of SCC. Similar reduction of areas were recorded for both temperatures. Testing at 50°C and 20°C in lean gas also gave a comparable result with values of 27% and 25% recorded for 20 and 50°C respectively.

However one test made at 20°C exhibited a high ductility ratio of 0,83 and a corresponding reduction of area of 54% which represented a considerable improvement over tests made at 50°C. No secondary cracks were found in the specimen. A wide spread of values for reduction of area (54 to 27%) is taken to indicate that the test condition 20°C, PCO 54 was close to the boundary condition for cracking in wet CO-CO₂-H₂O.

The CERT tests recorded no influence of PCO when temperature was kept constant, similar reduction of areas and ductility ratios were recorded in both media, indicating that lean gas (PCO 54) and rich gas (PCO 210) were equally severe when assessed by a short term test such as CERT. It would appear that provided there is sufficient carbon monoxide to create and maintain a passive layer, further additions do not substantially affect the speed and efficiency with which film ruptures are repaired at the crack tip such that above a minimum CO partial pressure for SCC, further increases in CO concentration have little effect on crack velocity.

15.3.2 CERT With Inhibitor Additions

The inhibitors tested had all been used successfully in gas and oil production or in refineries to control corrosion by wet CO₂. The CO-CO₂-H₂O stress corroded system is in effect a wet CO₂ environment inhibited by carbon monoxide that has absorbed onto the carbon steel surface. It was therefore considered that an inhibitor addition might be successful in two ways, either by absorbing more efficiently than CO so that anodic dissolution at film ruptures could be prevented or by absorbing in preference to CO, eliminating the critical balance required at film ruptures for SCC. The first CERT tests made in rich gas using 10 ppm additions of Petrotec 1420, Petrotec 1430 and Reomet 42 inhibitor produced very little change in the fracture properties of the test specimens. The ductility ratios showed little improvement over specimens tested in uninhibited rich gas. The test concentration was subsequently increased to 100 ppm to ensure that excess inhibitor was present for the duration of the test. A test was also done at 1000 ppm. Although it was conceded that the latter is an unrealistic dosage rate, it represented a go-no-go test for the inhibitor. In most cases the reduction of area was not changed by inhibitor concentrations over 100 ppm.

The ductility ratio calculated for uninhibited rich gas was close to 0,53 which represented a small improvement over uninhibited rich gas which gave a ductility ratio close to 0,30. A large addition of Petrotec 1420 was the only inhibitor that significantly retarded SCC and this was reflected by a high ductility ratio (0,89). The success of this particular inhibitor at high concentrations was undoubtedly due to its neutralising ability and SCC was prevented by the amine component neutralising the dissolved carbon dioxide. The addition of Reomet 42 gave an interesting result. Increasing the concentration of inhibitor from 10 ppm to 100 ppm increased the ductility ratio from 0,38 to 0,60, however a further increase to 1000 ppm caused the ductility ratio to drop to 0,28. Polarisation studies are required to confirm the reason for this result but it is probable that the different inhibitor concentrations behaved like a chemical potentiostat and were shifted in and out of the SCC susceptible region.

By and large inhibitor additions to lean gas gave a similar result to the rich gas tests and ductility ratios of the order of 0,5 were recorded. Two of the inhibitors tested improved the measured ductility ratios to 0,73 which represented an improvement over the value of ca 0,30 recorded in uninhibited lean gas. However stress corrosion cracking was not entirely prevented.

The laboratory test results indicated that none of the inhibitors evaluated would successfully prevent stress corrosion cracking in rich gas. Some success was demonstrated by large additions of Petrotec 1420, however the practice of neutralising the carbon dioxide is unacceptable for process reasons. Such high dosage rates would also be eliminated for economic reasons. Parkins⁽¹⁸⁾ warns against using inhibitors that work by shifting the rest potential outside the range of potentials for SCC. These he terms "unsafe" as other agents can shift the potential back within the cracking range even with the inhibitor still present. For this reason the encouraging result obtained using Reomet 42 cannot be utilised as the inhibitor appears to work by shifting the potential.

The results of the tests made in lean gas were more encouraging. The dosage of inhibitors to prevent SCC can be expected to be at least twice that required to prevent corrosion but not necessarily as high as the levels tested in the CERT. The effectiveness of plant scale inhibitor dosing to prevent SCC will depend on how efficiently the inhibitor is transported to where it is needed in the system. In the gas phase sufficient inhibitor transport is difficult. As inhibitor addition is unlikely to arrest SCC cracks once they nucleate, continuous dosing, together with verification by on-line monitoring, would be required.

15.4 EVALUATION OF ALTERNATIVE MATERIALS

15.4.1 U-bend Tests

The results of the U-bend tests are summarised in Table 22. Carbon steel specimens cracked regardless of the surface finish; cracking occurred in both liquid phase and the gas phase although in lean gas the cracks found in specimens exposed to the gas phase were more severe than those in samples immersed in condensate. None of the alloy steels tested suffered SCC indicating that 3CR12 type 410, SAF 2205 and type 304 stainless steel are all satisfactory materials for exposure to low temperature wet CO-CO₂-H₂O systems. Additionally no cracks were found in 3CR12 welded with 309L austenitic stainless steel.

Type 304 austenitic stainless steel was found to be fully resistant to the environment even after a severe sensitising heat treatment. Clad vessels that require post weld heat treatment for the base metal can therefore be safely stress relieved without the lining losing its resistance to SCC in wet CO-CO₂.

Dissimilar joints between carbon steel and type 304 stainless steel that had been post weld heat treated suffered disbonding at the fusion line of the joint. The cracks were intergranular and propagated through a region of high local hardness (460 to 500 Hv10) at the high alloy side of the fusion line. No cracks were found in as-welded specimens. This type of SCC is without question hydrogen induced and demonstrates the ability of the wet CO-CO₂ environment to promote cathodic SCC if susceptible material is present. It is likely that the cracks found in the repair welds shown in Figure 45 are further examples of cathodic SCC in this environment.

15.4.2 CERT

Table 23 summarises the results of CERT made in rich gas and lean gas environments at 50°C. The most resistant material was 3CR12. No evidence of secondary stress corrosion cracks were found in the samples tested. The specimen tested in rich gas failed with a small reduction of area which resulted in a low ductility ratio. The behaviour of 3CR12 during tensile tests in air was rather variable. The reduction of areas fluctuated from 44 to 51 which gave an average of 48 that was subsequently used to determine the ductility ratios. If the worst value is used for the calculation, the ductility ratio only increased to 0,61.

It therefore seems likely that the low reduction of area and correspondingly low ductility ratio measured for 3CR12 in rich gas represented an environmental influence and was not the result of a mechanical property variation.

The next best test result was recorded by the 9Cr-1Mo low alloy steel. A few shallow secondary SCC were found in the necked region indicating that although the material has a high resistance to CO-CO₂-H₂O SCC it is not immune.

In comparison to carbon steel, large reduction of areas were recorded when 3½ Ni steel was tested in rich gas and lean gas. This gave correspondingly high ductility ratios suggesting that the material possessed good resistance to stress corrosion cracking in both environments and was significantly better than carbon steel. The secondary cracking was limited to the necked regions of the specimen, a characteristic of hydrogen embrittlement rather than stress corrosion. Although this result indicated a degree of environmental influence, the cracking would probably not occur in practice. It is therefore considered that the material should be examined further as a candidate for the containment of wet CO-CO₂ gas mixtures.

15.5 POST WELD HEAT TREATED CARBON STEELS

A survey of post weld heat treated carbon steel piping and equipment after several years' service in rich and lean gas was carried out at two operating plants. It was revealed that stress relief did not prevent SCC of vessels operating in lean gas. In contrast, piping operating in lean and rich gas showed no evidence of stress corrosion cracking at weldments following stress relief. Shallow parent metal craze cracking was however observed in lean gas service. The cracks showed a marked tendency to corrode, eventually forming benign, sub-surface cavities.

It is believed that there are two reasons for the different behaviour of piping and vessels. Firstly the piping was heat treated at a slightly higher temperature than the vessels and this, together with the thinner wall, would be expected to result in lower residual stresses in piping compared to vessels. Secondly, since the piping wall thickness is usually determined by pipe schedule rather than the minimum thickness needed to contain the service pressure, the service stress in piping is often a lot lower than vessels. This would be more so for vessels designed to ASME Division 2 which utilises significantly higher allowable stress values than Division 1.

It is likely that the parent metal craze cracking found in the lean gas system is due to shallow surface stresses near to yield point and that crack arrest occurred once the cracks ran out of the surface zone of high stress. After arrest the cracks proceeded to corrode by crevice corrosion and blunted to form sub-surface corrosion cavities. The origin of surface stress is unclear but may be due to "settling in" during initial pressurisation since the cracks normally lie perpendicular to the direction of the hoop stress.

15.6 POTENTIODYNAMIC POLARISATION

The polarisation curves obtained in condensate saturated with carbon dioxide and carbon monoxide gas revealed that the system was virtually independent of carbon monoxide partial pressure and that given sufficient time the anodic and cathodic curves settle to the same shape and current densities regardless of the original gas mixture. However at very low carbon monoxide partial pressures this process can be quite slow, and there is a greater tendency towards free corrosion. Anodic and cathodic polarisation in the CO-CO₂-H₂O system shows a marked time dependence and is characterised by the following features:

1. Significant early cathodic inhibition shifts to cathodic curve leftwards to significantly lower current densities. This is accompanied by a movement of E_{corr} to more negative values.
2. Slower inhibition of the anodic reaction shifts the uninhibited virtually horizontal anodic curve towards the vertical plane. This is accompanied by an upward shift in E_{corr} . When anodic and cathodic passivation occur simultaneously there is little change in E_{corr} .
3. The anodic passivation is typified by a "breakdown" potential which is time dependent and moves to more positive values after longer exposure times. Above the breakdown potential small changes in potential gave rise to high current densities.
4. In the presence of oxygen E_{corr} is located at significantly higher potentials than when oxygen is absent.

These basic features are best explained by reference to an Evans diagram (Figure 118). Inhibition of the cathodic reaction will result in a slightly downward movement of E_{corr} from E_1 to E_2 if the anode remains film free. By the same token anodic passivation will shift the corrosion potential from E_1 to more positive values at E_3 should the cathode stay film free. However if the cathode is simultaneously passivated E_{corr} will eventually settle at E_4 . By adding the oxygen reduction reaction to the Evans diagram it can be seen that even after anodic passivation, E_{corr} will be located at relatively positive values in the presence of oxygen.

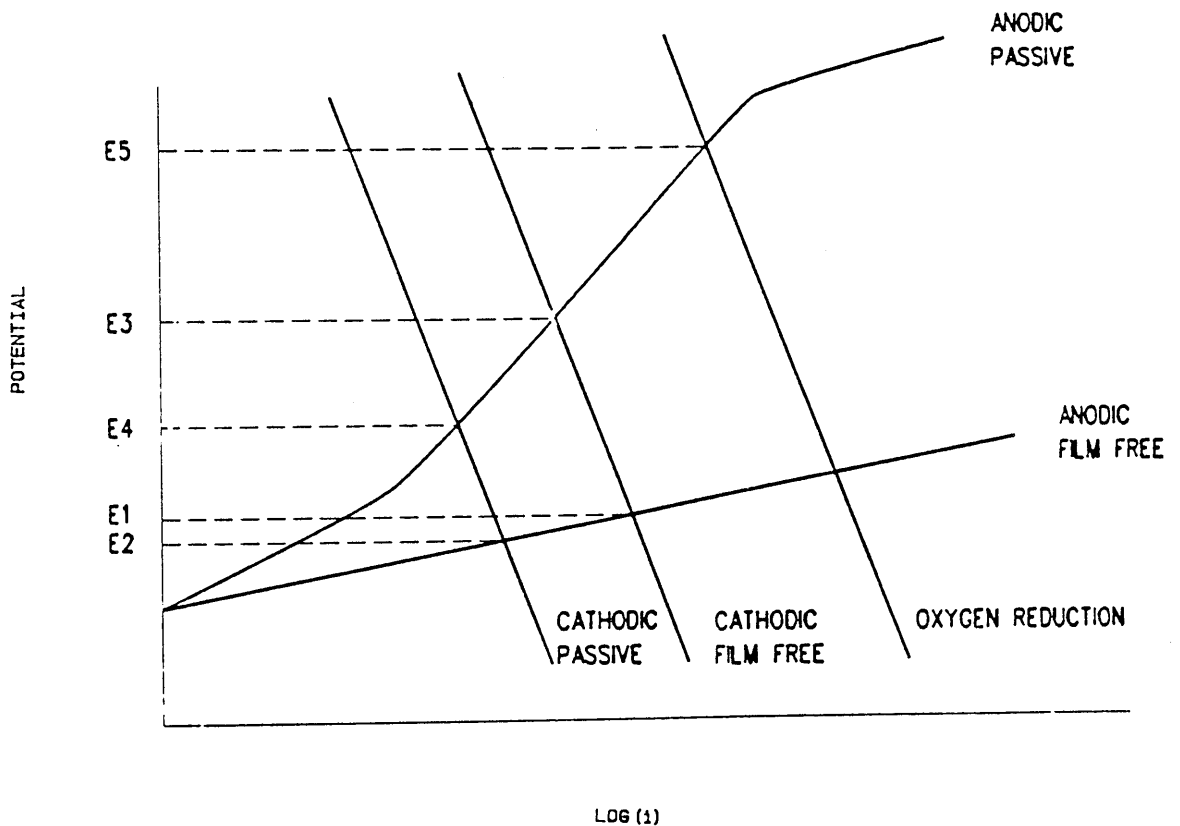
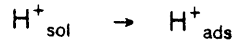


FIGURE 118 Evans diagram showing the effect of anodic and cathodic inhibition on E_{corr}

It is worth briefly considering carbon dioxide corrosion. The corrosion rates observed in solutions saturated by carbon dioxide cannot wholly be accounted for in terms of protons formed from the dissociation of carbonic acid. It can be shown that three distinct mechanisms contribute hydrogen ions to the cathodic reaction: ^(109,113)

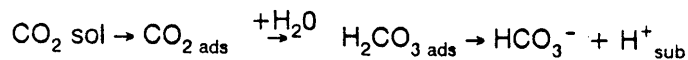
1. Direct diffusion of H^+ , as in any acid.



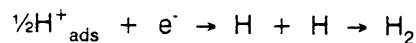
2. diffusion of carbonic acid



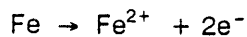
3. adsorption and hydration of CO_2



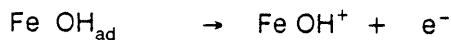
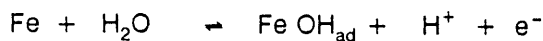
Each reaction participates in the cathodic current and in each case leads to hydrogen evolution via.



The anodic reaction



proceeds through intermediate reactions involving absorption of hydroxyl ions according to



Clearly adsorption of carbon monoxide on the iron surface will block both the anodic and cathodic reactions and give rise to the time dependent pseudo passivity that is apparent in the polarisation curves for iron in $CO-CO_2$ mixtures. The SCC sensitivity extends across the full range of the "passivity" resulting from CO absorption and is considered to arise from the kinetics of the re-passivation process. The behaviour compares to the active-passive transition zone of more conventional passivating systems (stainless steels) and supports the view that SCC requires a critical balance between the corrosion rate at the tip and the re-passivation process. At low partial pressures where CO adsorption is slow, particularly at the anode, the tendency is toward localised corrosion rather than SCC. An important factor in CO/CO_2 SCC can be the adsorption of hydrogen into the base metal. Carbon dioxide absorption at the cathode increases hydrogen entry into the metal by inhibiting the hydrogen recombination reaction in much the same way as hydrogen sulphide does in sour systems.^(109,112) This can be assessed by measuring the hydrogen permeation current. Carbon monoxide further increases the rate of hydrogen entry by between 4 and 10 times over that due to CO_2 supporting a hydrogen embrittlement mechanism.⁽¹¹²⁾

The study of CO passivation was extended to higher temperatures where the main effect appeared to be a reduced rate of anodic passivation due to less CO adsorption coupled to a slightly lower breakdown potential.

None of the inhibitors tested prevented CO adsorption although there was evidence that the rate of adsorption was altered slightly. Two of the inhibitors AO-2 and Petrolite 1430 prevented the appearance of a film breakdown potential. A large addition of Petrolite 1420 shifted the open circuit potential to above the breakdown potential.

The polarisation characteristics of nickel steel were similar to those of carbon steel. This was in contrast to 9Cr-1Mo steel which passivated rapidly and did not show a plateau on its anodic polarisation curve from film breakdown. However a superimposed fast scan suggested that CO adsorption did have a slightly inhibiting effect.

15.7 CORROSION MONITORING USING ELECTROCHEMICAL NOISE

The results of the potentiodynamic polarisation studies indicated that the open circuit potential is determined by the relative amounts of anodic and cathodic inhibition due to carbon monoxide adsorption. Positive and negative going transients might be expected to accompany this process. From the observed time dependence of the adsorption process and initially high frequency and amplitude of transients accompanied by a slow drift in the mean potential might be anticipated just after pressurisation. The size and frequency of the transient would be expected to diminish once CO was fully adsorbed. This was not observed in practice. Additionally stripping the carbon monoxide film by holding above -400 mV during the polarisation study resulted in a sharp move to negative potentials followed by a slow recovery to -560 mV. It would seem reasonable to expect a similar movement in potential due to mechanical disruption of the protective carbon monoxide film. This also was not observed in practice although the segmented appearance of the potential trace accompanied by sharp bursts of current activity in Figures 113 to 115 might be a manifestation of this process. However the results remain unconvincing and do not provide a reliable method for detecting the onset of CO/CO₂ stress corrosion. However ECN should be capable of detecting film breakdown occurring above -400 mV if this was adopted as a method of control. In this case the distinction would merely be between passive behaviour and general corrosion which is easily achievable by ECN monitoring.

SCC in the CO-CO₂-H₂O system is characterised by time dependent adsorption of carbon monoxide onto the anodic and cathodic surfaces. The adsorbed carbon monoxide inhibits both reactions by a blocking mechanism. Cathodic inhibition proceeds at a slightly higher rate and is near completion after a few hours. The anodic passivation takes longer and results in a near vertical line on the polarisation curve and a plateau that signifies film breakdown near to -400 mV depending upon temperature. The extent of the vertical portion on the polarisation curve defines the region of SCC susceptibility. The behaviour in this area compares to the active-passive transition zone of more conventional passivating systems where passivation may also be quite slow and exhibit a marked time dependence. CO-CO₂-H₂O SCC is virtually independent of the partial pressure of the two gases provided there is a sufficient "reservoir" of CO for adsorption and sufficient CO₂ to drive the corrosion reaction. At low CO partial pressure the anodic passivation is quite slow and there is a greater tendency towards corrosion, which not surprisingly resembles "mesa" or "ringworm" attack associated with CO₂-H₂O systems. Apart from anodic SCC, promoted by a critical balance between the crack tip corrosion rate and the re-passivation process, the CO-CO₂-H₂O system will also support a hydrogen embrittlement mechanism. Both CO₂ and CO block the hydrogen recombination reaction and promote hydrogen entry into the base metal. CO does this between 4 and 10 times more effectively than CO₂. It is suggested that in low strength steels the cracks are initiated by an anodic SCC mechanism but proceed by hydrogen embrittlement due to migration of cathodic hydrogen to the plastic zone at the crack tip. This would explain the appearance of the SCC fracture surface which resembles quasi cleavage. In high strength steels (Hardness >240 Hv10) exposed to CO-CO₂-H₂O the crack proceeds directly by hydrogen embrittlement.

The inhibitors tested were ineffective in blocking CO adsorption with the result that SCC still took place. The inhibitors did work better in lean gas where CO inhibition of the anodic process is anyway slower and was probably made even slower by the presence of inhibitor, competing for and blocking adsorption sites on the metal surface. Only gross additions of Petrotec 1420 which moved the corrosion potential above the film breakdown potential, prevented SCC as tested by the slow strain rate test. Petrotec 1430 and AO-2 prevented the appearance of film breakdown potential but SCC was nevertheless observed in the slow strain rate test. It is possible that these inhibitors extend the potential range over which SCC is observed.

The good performance of thicker steel is considered to be the result of its deformation characteristics since electrochemically it was very similar to carbon steel. Nickel steels exhibit a restricted zone of first stage plastic deformation, were the conditions suit film rupture and anodic SCC. Instead the material moves quickly to gross localised necking which favours hydrogen embrittlement and would anyway quickly promote high strain rates that prevent an environmental influence of any kind. Additionally nickel steels are extremely notch tough so high reduction of areas might still be recorded even with anodic cracks present on the specimen surface. Consequently it is difficult to predict how this material will perform in practice. Crack initiation will probably occur but crack growth may be retarded.

The electrochemical results and constant extension rate test for 9Cr-1Mo steel were in agreement; no SCC was predicted and non occurred. The material would need to be used with some caution due to its high hardenability which can easily promote hard heat affected zones and welds that would be susceptible to hydrogen embrittlement when exposed to CO-CO₂-H₂O. The same goes for austenitic-ferritic joint used to join 3CR12. Whether or not the corrosion rates of these materials would be sufficient to generate enough hydrogen to cause embrittlement remains a matter for conjecture.

Materials selection for fabricated piping and equipment is presently a choice between post weld heat treated carbon steel and 300 series stainless steel. There remains some doubt over the performance of the former particularly for vessels, although the results obtained in piping are better.

16

CONCLUSIONS

The CO-CO₂-H₂O system is characterised by a time dependent adsorption of carbon monoxide onto anodic and cathodic sites. The adsorption produces a critical balance between crack tip corrosion rate and the repassivation process and is comparable to the behaviour at the active-passive transitions zone of more conventional passivating systems.

The anodic passivation exhibits a breakdown potential that defines the zone of SCC susceptibility. The breakdown potential is time and temperature dependent and occurs near to -400 mV at 20°C.

The inhibition of the anodic and cathodic reactions by CO is virtually independent of CO partial pressure provided there is a sufficient "reservoir" of CO to provide a source for adsorption. At low partial pressures the anodic passivation is quite slow and there is a tendency towards corrosion rather than SCC.

Likewise SCC is virtually independent of the partial pressure of the two gases, provided there is sufficient CO to adsorb and sufficient CO₂ to promote the corrosion reaction.

The morphology of cracks in sections removed from the gas processing plant revealed an apparent dependence upon the prevailing carbon monoxide partial pressure. At low partial pressures the cracks were widened by corrosion on the crack walls and often resembled pits. At high partial pressures the cracks were extremely fine. This result was not repeated in short term tests, where the cracks were always found to be fine. It was concluded that initial crack appearance is independent of carbon monoxide partial pressure, although subsequent corrosion of the crack walls resulting in either widened cracks or pits is more likely at low carbon monoxide partial pressures, probably due to difficulty in maintaining passivity in the crevice formed by an arrested crack. It is possible that at low CO partial pressures the progress of the SCC crack is self limiting.

Fatigue pre-cracked specimens did not show crack extension after numerous plant and laboratory exposures, even though smooth specimens exposed at the same time cracked due to stress corrosion. A similar behaviour has been reported by other workers in environments where SCC shows a dependence on a narrow range of potentials. It is concluded that, unless the crack tip potential can be controlled, pre-cracked specimens are not suitable for study of these systems.

The growth rates calculated from smooth specimens exposed in rich and lean gas was ca 4 and 6 mm/year respectively. A value of 50 mm/year was calculated from the slow strain rate test. It has proved impractical to determine a tolerance for limited cracking due to uncertainty of growth rates.

CERT carried out at two gas compositions did not reveal an influence of carbon monoxide partial pressure. It would appear that above a minimum CO partial pressure for SCC, further increases have little effect on crack velocity.

Reducing the temperature from 50°C to 20°C has little effect on susceptibility of carbon steel to SCC in CO-CO₂ environments. This is surprising as a similar temperature reduction would be expected to lower the general corrosion rate in wet CO₂ by about one-fifth.

Inhibitors that are used successfully to control corrosion by wet CO₂ in gas and oil production do not prevent carbon monoxide adsorption and do not prevent SCC in CO-CO₂ when assessed by CERT. U-bends exposed to the same inhibited environments did not crack, indicating that they might be used successfully in equipment that does not experience plastic strain during service.

Electrochemical noise monitoring was unconvincing as a tool for detecting SCC in CO-CO₂-H₂O but could be used indirectly to show if film breakdown was occurring.

Type 304 austenitic stainless steel is resistant to cracking in wet CO-CO₂ systems even when it is severely sensitised. The duplex stainless steel SAF 2205 is also resistant and might be used in CO-CO₂ systems where the presence of chlorides precludes the usage of 300 series austenitic stainless steel.

The 12% and 11% chromium steels, 410 and 3CR12 were both resistant to CO-CO₂ SCC but difficulties in welding usually precludes the use of these materials for fabricated pressure piping and equipment. The latter requires welding with an austenitic filler. Although 3CR12 welds did not crack, tests made with carbon steel/austenitic stainless steel joints revealed that dissimilar welds are susceptible to hydrogen induced disbonding in wet CO-CO₂ systems. Careful consideration would therefore be needed before installing ferritic/austenitic joints in this service.

CERT on 9Cr-1Mo steel confirmed the high resistance of this material to CO-CO₂ SCC and is considered to be a candidate for service in environments that contain mixtures of these gases. However precautions will be necessary to ensure the low hardness values needed to preclude hydrogen embrittlement.


A low alloy 3½ Ni steel performed very well in the CERT and its possible use in CO-CO₂ should be evaluated further as it has several engineering advantages over 9Cr-1Mo.


In piping post weld heat treatment was successful in preventing transverse and longitudinal SCC caused by residual weld stresses. However shallow stress corrosion cracks that manifested as craze cracking were still encountered in systems that were lean in CO. The depth of craze cracking was less than 1 mm and more often below 0,5 mm. The majority of craze cracks had subsequently corroded to form subsurface cavities that resembled "mesa" corrosion associated with CO₂-H₂O. Some deep SCC cracks >1 mm were found at hard weld repairs.


Post weld heat treatment was unsuccessful in preventing SCC in vessels, possibly due to the lower heat treatment temperatures used and higher service stresses.


- (1) TÜV Rheinland (SA) (Pty) Ltd : Occasional paper No 1 "The origin of failures in service".
- (2) NACE : TPC Publication No 5 - "Corrosion control in Petroleum Production", 1979.
- (3) Lancaster, J., International Metal Reviews, 1976 No 3 - p.101.
- (4) Leslie, William C., The Physical Metallurgy of Steels - Ch.1 p.1. Mc Graw-Hill, 1982.
- (5) ASM Metals Handbook, Ninth Edition, Vol 13 p.18, 1987.
- (6) Turner, M., What every chemical engineer should know about stress corrosion cracking. The Chemical Engineer. May 1989.
- (7) Kупpa, J., Erhart, H. and Grabke, H., Corr Sci. Vol 2, 1981, p.217.
- (8) Bandyopadhyay, N., Newman, R.C. and Sieradzki, K., Proceedings of the Ninth International Congress on Metallic Corrosion (Toronto, Canada), NACE, 1984.
- (9) Pickering, H.W. and Swann, P.R., Corrosion, Vol 19, No 3, 1963, p.373.
- (10) Pugh, E.N., On the propagation of transgranular stress corrosion and JR Pickers, Ed Plenum Press, 1983, p.994.
- (11) Pickering, H.W. and Swann, P.R., Corrosion, Vol 19, No 3, 1963, p.373.
- (12) Swann, P.R. and Embury, J.D., High strength materials, Zackay, V.F., Ed. Wiley New York (1965), p.327.
- (13) Silcock, J.M. and Swann, P.R., Environment-sensitive fracture of engineering materials. Forouli, Z.A. Ed. The Metallurgical Society 1979 p.133.
- (14) Kaufman, M.J. and Fink, J.L., Evidence for localised ductile fracture in the "brittle: transgranular stress corrosion cracking of ductile FCC alloys. Acta Metall Vol 36, No 8, 1988, p.2213-2228.
- (15) Staehle, R.W., "Predictions and experimental verification of the slip dissolution model for stress corrosion cracking of low strength alloys". Stress Corrosion Cracking and Hydrogen Embrittlement of Iron Based Alloys. NACE 1977, p.180.


- (16) Engle, H.J., Theoretical aspects of stress corrosion cracking in alloys. NATO 1971.
- (17) Scully, J.C., Corrosion Sci, Vol 15, 1975, p.207.
- (18) Parkins, R.N., Br Corros, J., Vol 14, 1979, p.5.
- (19) Forty, A.J. and Humble, P., Philos Mag, Vol 8, 1963, p.247.
- (20) Pugh, E.N., In Stress Corrosion Cracking and Hydrogen Embrittlement of Iron Based Alloys. NACE, 1977, p.37.
- (21) Sieradzki, K. and Newman, R.C., Philos Mag A, Vol 51 (No.1), 1985, p.95.
- (22) Paskin, A., Sieradzki, K., Sonn, D.K. and Dienes, G.J., Acta Met, Vol 31, 1982, p.1253.
- (23) Pugh, E.N., Progress toward understanding the stress corrosion problem.
Corrosion - NACE, Vol 41, No.9, September 1985, p.517.
- (24) Forty, A.J., Physical Metallurgy of stress corrosion fracture. TN Rhodin Ed. Interscience 1959, p.99.
- (25) Uhlig, Herbert H., New perspectives in the stress corrosion problem. Physical Metallurgy of stress corrosion. Interscience Publishers, 1959 (TMS of AIME) p.1.
- (26) Stoloff, N.A., Environment-sensitive Fracture of Engineering Materials. Foroulis, Z.A. Ed. The Metallurgical Society, 1979, p.485.
- (27) Petch, N.J. and Stables, P., Delayed Fracture of Metals under Static Load. Nature, Vol 169, 1952, p.842.
- (28) Griffith, A.A., "The phenomena of rupture and flaw in solids." Transactions, Royal Society of London, A-221, 1920.
- (29) Oriani, R.A., A mechanistic theory of hydrogen embrittlement of steels. Berichte der Bunsen - Gesellschaft für Physikalische Chemie, Vol 76, 1972, p.301.
- (30) Beachem, C.D., A new model for hydrogen-assisted cracking (Hydrogen "Embrittlement"). Metallurgical Transactions, Vol 3, Feb 1972. The Metallurgical Society of AIME/ASM, p.259.
- (31) Tien, J.K., Nair, S.V. and Jensen, R.R., "Dislocation sweeping of hydrogen and hydrogen embrittlement", Hydrogen effects in metals. MS AIME Pittsburgh, 1980 p. 37-56.


- (32) Pressouyre, G.M.  I.M., A Quantitative analysis of hydrogen trapping. Metall Trans, Vol 94, 1978, p.1571.
- (33) Gahr, S., Grossbech, M.L. and Birnbaum H.K., Acta Metall, Vol 25, 1977, p.125.
- (34) ASTM G39-79. Practice for preparation and use of bent beam SCC specimens.
- (35) ASTM G38-73/1984. Practices for making and using C-ring SCC coupons.
- (36) ASTM G49-85. Recommended practice for preparation and use of direct tension stress corrosion test specimens.
- (37) ASTM G30-79. Practice for making and using U-bend stress corrosion test specimens.
- (38) ASTM G58-83. Practice for the preparation of stress corrosion test specimens for weldments.
- (39) Ugiansky, G.M. and Payer, J.H. Ed., Stress corrosion cracking - The slow strain-rate Technique, STP 665. American Society for Testing and Materials, 1979.
- (40) Parkins, R.N., Development of strain-rate testing and its implications in stress corrosion cracking - The slow strain rate technique, STP 665./ Ugiansky, G.M. and Payer, J.H. Ed. American Society for Testing and Materials, 1979.
- (41) Payer, J.H., Berry, W.E. and Boyd W.K., Constant strain rate technique for assessing stress - corrosion susceptibility, in stress corrosion - New approaches STP 610, Craig, H.L. Jr. Ed. American Society for Testing and Materials, 1976, p.82-93.
- (42) Brown, B.F. and Beacham, D.C., "A study of the stress factor in corrosion cracking by the use of the precracked Cantilever-Beam Specimen". Corrosion Science, 1965.
- (43) Novak, S.R. and Rolfe, S.T., "Modified WOL specimen for K_{ISCC} environmental testing". Journal of Materials, JMLSA ASTM. Philadelphia G, No 3, September 1969.
- (44) Hyatt, M.V., Use of precracked specimens in stress corrosion testing of high strength aluminium alloys. Corrosion, Vol 26 (No 11), 1970, p.487-503.
- (45) Wei, R.P. and Novak, R.P., Interlaboratory evaluation of K_{ISCC} and da/dt determination procedures for high strength steels. The American Society for testing materials, 1987. ASTM Committee E-24.

- (46) ASTM G35-73.  d practice for determining the susceptibility of stainless steels and related nickel chromium alloys to SCC in Polythionic acid.
- (47) ASTM G36-73. Recommended practice for performing stress-corrosion tests in a boiling magnesium chloride solution.
- (48) ASTM G41-81. Test method to determine cracking susceptibility of metals exposed under stress to a hot salt environment.
- (49) ASTM G44-75. Recommended practice for alternate immersion stress corrosion testing in 3,5% sodium chloride solution.
- (50) NACE TM-01-77. Testing of metals for resistance to sulfide stress corrosion cracking at ambient temperatures, NACE, Houston, Texas.
- (51) ASTM G37-85. Test method for use of Mattsson's solution of pH 7,2 to evaluate SCC susceptibility of copper-zinc alloys.
- (52) ASTM G47-49. Test method to determine susceptibility to stress corrosion cracking of high strength aluminium alloy products.
- (53) ASTM G64-85. Classification of resistance to stress corrosion cracking of high strength aluminium alloys.
- (54) Parkins, R.N., Predictive approaches to stress corrosion cracking failure. Corrosion Science, Vol 20, 1980, p.147-166.
- (55) Parkins, R.N. and Fessler, R.R., Materials in Engineering applications, Vol 1, 80-90 (1978).
- (56) Newman, R.C., Ph.D Thesis, University of Cambridge (1980).
- (57) Yu J., Ph.D Thesis, University of Newcastle upon Tyne, (1984).
- (58) Dawson, J.L., Cox, W.M., Eden, D.A., Hladky, K., John, D.G., Corrosion monitoring in plants using advanced electrochemical techniques. il Giornale de Prove non Distruttive 2/86, p.49.
- (59) Hladky, K., Dawson, J.L., Corrosion Science 22, 231. (1982).
- (60) Zanki, A.L., Gill, J.S., Dawson, J.L., Electrochemical noise measurements on mild steel in 0,5M sulphuric acid. Electrochemical methods in corrosion research. Duprat, M., Ed., Materials Science Forum Vol 8, 1986. p.463-476.
- (61) Lotto, C.A. and Cottis, R.A., Electrochemical noise generation during stress corrosion cracking of the high strength aluminium AA 7075-T6 Alloys. Corrosion Vol 45 No 2, February 1989, p.136.

- (62) Lotto, C.A. and C  Electrochemical noise generation during stress corrosion cracking of alpha-brass. Corrosion - NACE Vol 43, No 8, August 1987, p.499-504.
- (63) Lotto, C.A. and Cottis, R.A., Electrochemical noise generation during SCC of a high strength carbon steel. Corrosion - January 1990, p.12-19.
- (64) Roberge P.R., Beaudoin, R. and Sastri, U.S., Electrochemical noise measurements for field applications. Corrosion Science, Vol 29, No 10, 1989, p.1231-1233.
- (65) Fontana, M.G. and Green, N.D., Corrosion Engineering, 2nd Edition, Mc Graw-Hill, 1982.
- (66) Richardson, J.A. and Fitzsimmons, T., "Use of aluminium foil for prevention of stress corrosion cracking of austenitic stainless steel under thermal insulation." ASTM STP 880. Pollock, W.I. and Barnhart, J.M. Eds. American Society for testing and Materials. 1985, p.188-189.
- (67) McIntyre, D., "Factors affecting the stress corrosion cracking of austenitic stainless steels under thermal insulation." ASTM STP 880. Pollock, W.I. and Barnhart, J.M. Eds. American Society for Testing and Materials. 1985, p.24-41.
- (68) Kalis, J.W. Jr., "Using specifications to avoid chloride stress corrosion cracking." ASTM STP 880. Pollock, W.I. and Barnhart, J.M. Eds. American Society for Testing and Materials. 1985, p.199-203.
- (69) Cragnolino, G., McDonald, D.D., Intergranular stress corrosion cracking of austenitic stainless steels at temperatures below 100°C. A review "Corrosion", Volume 38, No 8, 1982, p.406-424.
- (70) Samans, C.H., "Stress corrosion cracking susceptibility of stainless steels and nickel base alloys in polythionic acids. Corrosion Vol 20 No 8, 1964, p.256-261.
- (71) Piehl, R.L., "Stress corrosion cracking by sulphur acids." Proc API, 44, 1964, p.189-197.
- (72) Heller, J.J. and Prescott, G.R., "Cracking of stainless steels in wet sulphide environments in refinery units." Materials protection, Vol 4 No 9, 1965, p.14-18.
- (73) Couper, A.S. and McConomy, H.F., "Stress corrosion cracking of austenitic stainless steels in refineries. Proc API, 46, 1966, p.321-326.

- (74) NACE recommen  RP-01-70. "Protection of austenitic stainless steel in refineries against stress corrosion cracking by use of neutralising solutions during shutdowns".
- (75) Beirne, W.J., "Investigation of the effects of stress corrosion on high strength tubular goods", Humble Oil and Refining Company Proprietary Report, September 1963.
- (76) NACE standard MR-01-75 Sulphide stress cracking resistant metallic materials for oil field equipment.
- (77) Tuttle, R.N., Guidelines aid in designing for H₂S service. The Oil and Gas Journal -December 11, 1978, p.99.
- (78) Richard, Sivalls C. Hydrogen sulphide service dictates special equipment design above requirements. Oil and Gas Journal, July 8 1985, p.56.
- (79) Parker, JG and Sadler MA "Stress corrosion cracking of a low alloy steel in high purity steam." Corrosion Science, 15, (1975) p.57-63.
- (80) Bandopadhyay, N. and Briant, C.L., "Caustic stress corrosion cracking of NiCrMoV rotor steels - The effect of impurity segregation and variation in alloy content." Metallurgical Transactions A. 14A (1983), p.2005-2019.
- (81) Cracknell, A., Proc. Institution of Chemical Engineers. Conference on "Advances in Petrochemical Technology", London May 1977, p.47-56.
- (82) Loginow, A.W., A review of stress corrosion cracking of steel in liquefied ammonia service. Materials Performance, December 1986, p.18.
- (83) Towers, O.L., SCC in welded ammonia vessels. Metal Construction, August 1984, p.479.
- (84) Code of Practice for the storage of anhydrous ammonia under pressure in the United Kingdom. Spherical and cylindrical vessels. Publ. Chemical Industries Association Ltd, January 1980.
- (85) Cracknell, A., "Stress corrosion cracking of steels in ammonia: Proc Institution of Chemical Engineers Conference on "Advances in petrochemical technology", London, May 1977, p.47-56.
- (86) International Nickel Company. Publication number 14M 2-58 336 9 B-141.
- (87) Minutes of NACE Fall Committee meeting - 23 September 1984, NACE, Houston, Texas.

- (88) Garwood, G.L., A  Corrosion. The Oil and Gas Journal, 27 July 1953, p.334.
- (89) Hughes, P.G., Stress corrosion cracking in a MEA Unit: Case Study. UK National Corrosion Conference, 1982, p.87.
- (90) Ishimaru Hel al., Preventing stress corrosion cracking in the carbon dioxide absorber of ammonia plants. American Institute of Chemical Engineers Ammonia Safety Conference, 1980, p204.
- (91) Parkins, R.N. and Usher, R., The stress-corrosion cracking of mild steel in Coal Gas Liquors. J appl Chem, 9 September 1959, p.445.
- (92) Eiji Sato and Tomoni Murata., Stress corrosion cracking of mild steel in Coal Gas Liquid Transactions ISIJ Vol 24, 1984.
- (93) Parkins, R.N., Alexandridou, D. and Majumdar, P., Stress corrosion cracking of C-Mn steels in environments containing carbon dioxide. Materials Performance, October 1986, p.20.
- (94) Brown, A., Harrison, J.T. and Wilkins, R., Electrochemical investigations of stress corrosion cracking of plain carbon steel in the carbon dioxide-carbon monoxide water system. Conf. Stress Corrosion Cracking and Hydrogen Embrittlement of Iron Base Alloys, June 12-16, 1973. Unieux-France, p.686-695.
- (95) Grafen, H., Schlecker, H., "Stress corrosion cracking (SCC) of unalloyed steels exposed to CO-CO₂-H₂O systems. Int. Report, Bayer, Leverkusen, 1985.
- (96) Berry, W.E. and Payer, J.H., Internal stress corrosion cracking by aqueous solutions of CO and CO₂. 6th Symposium on line pipe research. American Gas Association, Houston Texas, October 29 - November 1, 1979, p.251-268.
- (97) Schmitt, G. and Schlerkmann, G., "Corrosion cracking of steel in the system CO₂/H₂O. Proceedings of the Eighth International Congress on Metallic Corrosion, 1981, p.282.
- (98) Dunlop, A.K. and Olson, E.E., Inhibition of stress corrosion cracking of steel in aqueous CO/CO₂ environments. Proceedings of the Sixth International Congress on Metallic Corrosion, 1975, p.332-342.
- (99) Bowmann, R.W., Dunlop, A.K. and Trales, J.P., CO/CO₂ cracking in inert gas - Miscible flooding. Materials Performance, April 1977, p.28-32.
- (100) Kowaka, M. and Nagata, S., Stress corrosion cracking of mild and low alloy steels in CO-CO₂-H₂O. Corrosion 32 (1976) 10 395/401.

- (101) Hannah, I.I.  C. and Procter, R.P.M., Environmental cracking of C-Mn steels in aqueous CO-CO₂ environments, Proc of the 4th International Conference on the effect of hydrogen on the behaviour of materials. Edited by NR Moody and AW Thompson. September 12-15 1989, p.965.
- (102) Eden, D.A., Rothwell, A.N. and Dawson, J.L., Electrochemical noise for detection of susceptibility to stress corrosion cracking. Corrosion '91, Paper 444.
- (103) Nyborg, Rolf and Linde, Liv R., Integrity of ammonia storage vessels - life prediction based on SCC experience. Materials Performance, November 1991, p.61.
- (104) Tarimura, M., Nishimura, T. and Nakazawa, T., "Stress corrosion cracking of high strength steels in CO-CO₂ gas". Nippon Kokai Technical Report Overseas No 19, December 1974.
- (105) Saegusa, F., "Effect of carbonaceous gas environments on the corrosion of AISI-4330 high-strength steel". Watervliet Arsenal Report R-WV-T-X-Z-73, January, 1973.
- (106) Sato Keiji, Yamamoto Katsumi, Kagawa Noahiko, "Prevention of CO₂ corrosion in gas gathering systems". Corrosion '83, paper 56.
- (107) De Berry, D.W., Shelton, Clark W., Yost, A., "Corrosion due to use of carbon dioxide for enhanced oil recovery". Carbon dioxide, September 1979, p.7.
- (108) Schmitt, G. and Rothman, B., "Studies on the corrosion mechanism of unalloyed steel in oxygen-free carbon dioxide solutions". Werkstoffe and Korrosion, Vol 28, 1977, p.816.
- (109) Schmitt, G. and Rothman, B., "Corrosion of unalloyed and low alloyed steels in carbonic acid solutions". Werkstoffe and Korrosion, Vol 29, 1978, p.237.
- (110) Berry, W., "How carbon dioxide affects corrosion of line pipe". Oil and Gas Journal, March 21, 1983, p.160.
- (111) Murata Tomomi, Sato Eiji, Matsushashi Ryo, "Factors controlling corrosion of steels in CO₂ saturated environments". Corrosion '83, paper 53.
- (112) Schmitt, G., "Fundamental aspects of CO₂ corrosion". Corrosion '83, paper 43.
- (113) Ikeda, A., Mukai, S and Ueda, M., "Prevention of CO₂ corrosion of line pipe and oil country tubular goods". Corrosion '84, paper 289.

- (114) Stewart, J., Scocellato, D.E., Wells, D.B., Harwell Report No. AERE R12889, UKAEA, Harwell Lab, (1987).
- (115) Newman, J.C. and Raju, I.S., Stress intensity factor equation for cracks in three-dimensioned finite bodies subjected to tension and bending loads. NASA Technical Memorandum 85793 National Aeronautics and Space Administration, Langley Research Center, Virginia, April 1984.
- (116) Corrosion data survey 1974, NACE p.274-277.
- (117) LaQue and Copson "Corrosion resistance of metal alloys", 1963.

APPENDIX 1.

COMPOSITION OF TEST MATERIALS

Appendix 1. Composition of test materials

Material Specification	Generic Type	Composition Wt%								
		C	Mn	P	S	Si	Ni	Cr	Mo	N
SA 516 Gr70	C-Mn	0.15	0.90	0.013	0.002	0.21	-	-	-	-
SA 203 GrE	3.5Ni	0.15	0.5	0.010	0.003	0.20	3.5	-	-	-
SA 387 Gr91	9Cr-1Mo	0.10	0.4	0.006	0.002	0.21	-	9.10	1.1	-
3CR12	12Cr	0.02	1.1	0.010	0.010	0.4	1.2	11.5	-*	
SA 240 type 410S	12Cr Martensitic ss	0.08	1.0	0.004	0.003	1.0	-	12.0	-	-
SA 240 type 304L	18-8 Austenitic ss	0.04	2.0	0.004	0.003	1.0	9.0	19.0	-	0.10
SAF2205	Duplex ss	0.03	1.7	0.003	0.003	0.8	5.5	22.0	3.0	0.4

* Titanium 0.25